Trends in Nuclear Explosion Monitoring Research & Development

- A Physics Perspective -

Los Alamos National Laboratory
Monica Maceira, Philip S. Blom, Jonathan K. MacCarthy, Omar E. Marcillo, Garrett G. Euler, Michael L. Begnaud

Lawrence Livermore National Laboratory
Sean R. Ford, Michael E. Pasyanos

Naval Research Laboratory
Gregory J. Orris

Pacific Northwest National Laboratory
Michael P. Foxe

Sandia National Laboratories
Stephen J. Arrowsmith, B. John Merchant, Megan E. Slinkard

LA-UR-17-21274 June 2017 DOI:**10.2172/1355758**

Document Availability

Online Access:

U.S. Department of Energy (DOE) reports produced after 1991 and a growing number of pre-1991 documents are available free via DOE's SciTech Connect (http://www.osti.gov/scitech).

"Trends in Nuclear Explosion Monitoring Research & Development - A Physics Perspective" is available online at http://www.osti.gov/scitech/10.2172/1355758. This electronic version of the document is recommended to the reader to take advantage of the internal and external links to references and other information sources.

Reports not in digital format may be purchased by the public from the National Technical Information Service (NTIS):

U.S. Department of Commerce
National Technical Information Service
5301 Shawnee Rd
Alexandria, VA 22312
www.ntis.gov
Phone: (800) 553-NTIS (6847) or (703) 605-6000
Fax: (703) 605-6900
Email: orders@ntis.gov

Reports not in digital format are available to DOE and DOE contractors from the Office of Scientific and Technical Information (OSTI):

U.S. Department of Energy
Office of Scientific and Technical Information
P.O. Box 62
Oak Ridge, TN 37831-0062
www.osti.gov
Phone: (865) 576-8401
Fax: (865) 576-5728
Email: reports@osti.gov

Disclaimer

Abstract

This document entitled “Trends in Nuclear Explosion Monitoring Research and Development – A Physics Perspective” reviews the accessible literature, as it relates to nuclear explosion monitoring and the Comprehensive Nuclear-Test-Ban Treaty (CTBT, 1996), for four research areas: source physics (understanding signal generation), signal propagation (accounting for changes through physical media), sensors (recording the signals), and signal analysis (processing the signal). Over 40 trends are addressed, such as moving from 1D to 3D earth models, from pick-based seismic event processing to full waveform processing, and from separate treatment of mechanical waves in different media to combined analyses. Highlighted in the document for each trend are the value and benefit to the monitoring mission, key papers that advanced the science, and promising research and development for the future.

Preface

It is useful for the reader to keep in mind several unique and/or notable features of this document:

- This literature review features selected references that are linked directly to the source papers. This allows readers of the electronic version of this document to explore in depth the research in their area of interest.
- The reader's experience of the electronic version of the document is purposefully enhanced by utilization of both internal and external links. Specifically:
  - The "Bookmarks" PDF feature has been set up to mirror the Table of Contents providing easy navigation in the document. To open the bookmarks, click on the "ribbon" icon at the upper left corner of the document.
  - The summary bullets in the last chapter are internally linked to the associated trend's "Future R&D" box.
  - The trend titles are linked to associated roadmap R&D themes.
  - Finally, and arguably most importantly, the citations in the text are linked to the source paper through the full reference.
    - › To find a source paper, click on the citation abbreviation in contrasting font color in the text which will jump to the full reference citation in the back of the document. From here you can either click on the digital object identifier (DOI) or specified universal resource locator (URL) to go to the source document, or *return to the page where the reader left off (click the Alt and left-arrow key on a PC; click the Command and left-arrow on a Mac)*.
- The writing seeks to provide individual subject matter experts with insight into other disciplines and encourage multi-disciplinary research relevant to nuclear explosion monitoring.
- A clear aim of this review is to spark renewed readership of previously published papers by placing them into the context of broader technology development trends.
- This document takes inspiration from an earlier paper entitled Trends in Nuclear Explosion Monitoring (Anderson et al., 2004).
- While the review presented here is intended to be representative of trends occurring in the broad international community, it is recognized that the lead authors are mostly from the U.S. national laboratories and the document reflects their interests and expertise.
- The document was authored by a team of writers and editors. The lead authors 1) have published peer-reviewed journal articles relevant to the subject matter; 2) are early career geophysicists and nuclear physicists representative of the next generation of researchers; and 3) were nominated by their management. See the Acknowledgments for a complete list of authors, contributors and reviewers.
- Future fruitful research is suggested that would continue nuclear explosion monitoring improvements. The suggested research is presented as a natural extension of trend analysis. The trends are also keyed to the research themes (summarized in the R&D Themes appendix) from the U.S. National Nuclear Security Administration (NNSA) Ground-based Nuclear Detonation Detection (GNDD) Technology Roadmap (Casey, 2014).

Acknowledgments

Creation of "Trends in Nuclear Explosion Monitoring Research & Development - A Physics Perspective" required and benefited from the contributions and varied expertise of many people. While the lead authors are responsible for any of the document's shortcomings, they gratefully acknowledge contributions of others. Lead authors and contributors are listed here.

Lead Authors

Dr. **Monica Maceira**, LANL, for expertise in seismology.
Dr. **Phillip S. Blom**, LANL, for expertise in infrasound.
Dr. **Jonathan K. MacCarthy**, LANL, for expertise in seismology.
Dr. **Omar E. Marcillo**, LANL, for expertise in infrasound.
Dr. **Michael L. Begnaud**, LANL, for expertise in seismology.
Dr. **Garrett G. Euler**, LANL, for expertise in seismology and infrasound.
Dr. **Sean R. Ford**, LLNL, for expertise in seismology.
Dr. **Michael E. Pasyanos**, LLNL, for expertise in seismology.
Dr. **Greg J. Orris**, NRL, for expertise in hydroacoustics.
Dr. **Michael P. Foxe**, PNNL, for expertise in radionuclides.
Dr. **Stephen J. Arrowsmith**, SNL, for expertise in infrasound.
Mr. **B. John Merchant**, SNL, for expertise in seismic and infrasound instrumentation.
Ms. **Megan E. Slinkard**, SNL, for expertise in seismology.

Mentors, Program Managers, Peer Reviewers and Other Contributors

Dr. **Dale N. Anderson**, LANL, for mentoring early career researchers and expertise in event categorization.
Dr. **Marie D. Arrowsmith**, SNL, for peer review.
Dr. **G. Eli Baker**, AFRL, for seismology peer review.
Dr. **Sanford (Sandy) Ballard**, SNL, for seismology review.
Dr. **Steven Biegalski**, University of Texas at Austin, for radionuclide expertise and peer review.
Mr. **V. Mark Bitter**, AFTAC, for peer review.
Dr. **Robert R. Blandford**, AFTAC Emeritus, for seismology peer review.
Dr. **David Bowers**, AWE Blacknest, for seismic expertise and peer review.
Dr. **Augustine (Gus) J. Caffrey**, INL, for expertise in nuclear physics and peer review.
Ms. **Leslie A. Casey**, NNSA, for orchestration.
Mr. **Marvin D. Denny**, LLNL Emeritus, for seismology peer review.
Dr. **Marco DiCapua**, NNSA, for peer review.
Mr. **John J. Dwyer**, AFTAC, for seismic review and expertise.
Mr. **Timothy G. Evans**, NNSA, for peer review.
Mr. **Joel B. Forrester**, PNNL, for radionuclide expertise and bibliographic assembly.
Dr. **Lance M. Garrison**, NNSA, for radionuclide tutorials.
Dr. **Steven J. Gibbons**, NORSAR, for seismology peer review.
Dr. **David Green**, AWE Blacknest, for infrasound expertise and peer review.
Dr. **James C. Hayes**, PNNL, for mentoring early career researchers and radionuclide expertise.
Dr. **Bahman (Ben) Heshmatpour**, DTRA, for peer review.
Dr. **Ross Heyburn,** AWE Blacknest, for seismic expertise and peer review.
Ms. **Emilee R. Jones**, LANL, for graphic design assistance.
Dr. **Robert C. Kemerait**, AFTAC, for seismology expertise and peer review.
Dr. **Rosara F. Kephart**, AFTAC, for radionuclide expertise and peer review.

Dr. **Thomas E. Kiess**, NNSA, for peer review.
Dr. **Keith D. Koper**, University of Utah, for seismology peer review.
Dr. **Tormod Kvaerna**, NORSAR, for seismology peer review.
Dr. **Charles A. Langston**, University of Memphis, for seismology peer review.
Dr. **Thorne Lay**, University of California at Santa Cruz, for seismology peer review.
Mr. **John C. Lucas**, AFTAC, for radionuclide expertise and peer review.
Dr. **Kevin G. Mackey**, Michigan State University, for seismology expertise and peer review.
Dr. **Justin I. McIntyre**, PNNL, for radionuclide expertise.
Mr. **Kevin S. Muhs**, AFTAC, for peer review.
Dr. **Stephen C. Myers**, LLNL, for mentoring early career researchers and expertise in seismology.
Dr. **Michael J. Newman**, NNSA, for nuclear treaty and nuclear physics expertise.
Dr. **Stuart Nippress**, AWE Blacknest, for seismic expertise and peer review.
Dr. **Paul A. Nyffenegger**, Kegman, Inc., for geophysical expertise and peer review.
Dr. **Jessica N. Paul**, LLNL, for radionuclide tutorials.
Dr. **James J. Peltz**, NNSA, for peer review.
Dr. **W. Scott Phillips**, LANL, for text on high frequency amplitude, discrimination, and yield estimation.
Prof. **Sara Pozzi**, University of Michigan, for peer review.
Dr. **Anil Rao**, AFTAC, for peer review.
Dr. **Denis M. Reidy**, Kegman, Inc., for peer review.
Dr. **Paul G. Richards**, Columbia University, for geophysics expertise and peer review.
Dr. **Anders Ringbom**, Swedish Defence Research Agency, for radionuclide peer review.
Dr. **William L. Rodi**, MIT, for seismology expertise and peer review.
Dr. **David R. Russell**, Weston Geophysical Corporation, for seismology peer review.
Dr. **George C. Rybicki**, Florida Institute of Technology, for radionuclide peer review.
Mr. **Pete A. Sandford**, LANL, for graphic design.
Mr. **Gilbert (Gil) C. Sateia**, U.S. Department of State (Emeritus), for peer review.
Dr. **James A. Scoville**, AFTAC, for radionuclide peer review.
Dr. **B. Scott Sears**, AFTAC, for peer review.
Dr. **Yang Shen**, University of Rhode Island, for seismology peer review.
Dr. **Calvin L. Shipbaugh**, DTRA, for peer review.
Mr. **Craig T. Sloan**, NNSA, for peer review.
Dr. **Gary M. Stange**, Nonproliferation Graduate Fellow, for radionuclide peer review.
Dr. **Jeffry L. Stevens**, Leidos, for seismology peer review.
Dr. **Brian W. Stump**, Southern Methodist University, for seismology and infrasound peer review.
Dr. **Neill P. Symons**, SNL, for mentoring early career researchers.
Dr. **Curt A. L. Szuberla**, University of Alaska Fairbanks, for infrasound peer review.
Dr. **Carl Tape**, University of Alaska at Fairbanks, for seismology peer review.
Dr. **William J. Tedeschi**, SNL, for peer review.
Dr. **Suzan van der Lee**, Northwestern University, for seismology peer review.
Dr. **Gerard A. Vavrina**, DTRA, for peer review.
Dr. **William R. Walter**, LLNL, for seismology expertise and peer review.
Dr. **Rodney W. Whitaker**, LANL, for infrasound expertise.
Dr. **Donna S. Wilt**, NNSA, for peer review.
Dr. **Mark T. Woods**, AFTAC, for peer review.
Dr. **Xiaoning Yang**, LANL, for reviews regarding surface-wave and noise attenuation in signal propagation.
Dr. **John P. Ziagos**, LLNL Retired, for seismology peer review.
Dr. **John J. Zucca**, LLNL, for peer review.

*Table of Contents**

** The "Bookmarks" PDF feature has been set up to mirror the Table of Contents providing easy navigation in the PDF file. To open the bookmarks, click on the "ribbon" icon at the upper left corner of the file.*

Acronyms and Abbreviations

1D	one-dimensional
2D	two-dimensional
3D	three-dimensional
AFTAC	Air Force Technical Applications Center (operator of the U.S. National Data Center)
Ar-37	Argon-37 ($T_{1/2}$ = 35.04 d) radioisotope is produced by a secondary reaction of neutrons on calcium in soil and has potential to be a delayed signature of underground nuclear explosions (notation also appears with a superscript, ^{37}Ar)
ARIX	Analyzer of Radio-Isotopes of Xenon
ARSA	Automated Radioxenon Sampler-Analyzer
ATM	atmospheric transport modeling
BGSim	Beta-Gamma Simulation tool
BISL	Bayesian Infrasonic Source Localization
Bq	becquerel, a measure of radioactivity (one becquerel equals one nuclear disintegration per second)
CART	classification and regression trees
coda	part of a waveform forming a "tail" immediately before or after the dominant event
CFD	computational fluid dynamics
CMT	centroid moment tensor
CTBT	Comprehensive Nuclear-Test-Ban Treaty
CTBTO	Comprehensive Nuclear-Test-Ban Treaty Organization
dB	decibel, a logarithmic measurement unit
DOA	direction of arrival
DOE	U.S. Department of Energy
DOI	digital object identifier
DPRK	Democratic People's Republic of Korea (i.e., North Korea)
ECM	event categorization matrix
FACT	Facility for Acceptance, Calibration and Testing at SNL
FF	finite-frequency
FM	first motion
FMM	fast marching method
GF	Green's function
GNDD	Ground-based Nuclear Detonation Detection
HPC	high performance computing
HPGe	high-purity germanium
Hz	hertz, a unit of frequency in the International System, equivalent to one cycle per second (the middle C note on a piano is at 262.6 Hz)
IDC	International Data Centre
IFE	integrated field exercise
IMS	International Monitoring System
INGE	International Noble Gas Experiment
INL	Idaho National Laboratory
InSAR	Interferometric Synthetic Aperture Radar
JVE	Joint Verification Experiment
keV	kiloelectron volt, an energy unit (medical radiography equipment typically produces 40 keV X-rays)
kt	kiloton (nuclear explosion yields are typically expressed in kilotons of TNT equivalent)
LANL	Los Alamos National Laboratory
LDA	linear discrimination analysis
LEB	late event bulletin

LIDAR	LIght Detection And Ranging
LLNL	Lawrence Livermore National Laboratory
LP	long-period (surface energy)
LTBT	Limited Test Ban Treaty
M	magnitude, undifferentiated
MARDS	Movable Argon-37 Rapid Detection System
mb	body-wave magnitude
mBq	millibecquerel (one-thousandth of a becquerel)
MCMC	Markov-Chain Monte Carlo
MDA	minimum detectable activity
MDAC	magnitude and distance amplitude correction
MDC	minimum detectable concentration
MEMS	micro electro mechanical system
ML	local magnitude, commonly referred to as "Richter magnitude"
MLE	maximum likelihood estimation
Mo	moment
Ms	surface-wave magnitude
Mw	moment magnitude
NDC	National Data Center
NEM	nuclear explosion monitoring
NIST	U.S. National Institute of Standards and Technology
NNSA	National Nuclear Security Administration
NPE	Non-Proliferation Experiment
NTM	national technical means
NTS	Nevada Test Site (now named the "Nevada National Security Site")
OFIS	optical fiber infrasound sensor
OSI	on-site inspection
OSIRIS	On-Site Inspection RadioIsotopic Spectroscopy
PNNL	Pacific Northwest National Laboratory
PREM	Preliminary Reference Earth Model
Q	"Quality Factor" which quantifies energy loss per cycle, and is dimensionless, $Q = 2\pi$ x Stored Energy/Energy Dissipated per cycle
QDA	quadratic discrimination analysis
RASA	Radionuclide Aerosol Sampler/Analyzer
RDA	regularized discrimination analysis
REB	reviewed event bulletin
ROC	receiver operating characteristic
RSA	Radionuclide Signal Analysis (R&D theme designator)
RSE	Radionuclide Sensors (R&D theme designator)
RSO	Radionuclide Source Physics (R&D theme designator)
RSP	Radionuclide Signal Propagation (R&D theme designator)
RSTT	Regional Seismic Travel Time model
RT	ray-theoretical
SAUNA	Swedish Automatic Unit for Noble-gas Acquisition
SCM	standard cubic meters (e.g., volume of air)
sec	seconds
SEM	spectral element method
SNL	Sandia National Laboratories
SNR	signal-to-noise-ratio

SODAR	SOnic Detection And Ranging
SOFAR	SOund Fixing And Ranging
SPALAX	Système de Prélèvement Automatique en Ligne avec l'Analyse du Xénon
SPE	Source Physics Experiment(s)
$T_{1/2}$	half-life of a radioisotope
TNT	trinitrotoluene (The explosive yield of TNT is considered to be the standard measure of the energy released by a chemical/conventional explosion. TNT is not the same as dynamite, which is a special formulation of nitroglycerin for use as an industrial explosive.)
TTBT	Threshold Test Ban Treaty
URL	uniform resource locator
U.S.	United States (of America)
USGS	U.S. Geological Survey
USNDC	U.S. National Data Center
USSR	Union of Soviet Socialist Republics
UTTR	Utah Test and Training Range
VSM	virtual seismometer method
WNRS	wind noise reduction systems
WSA	Waveform Signal Analysis (R&D theme designator)
WSE	Waveform Sensors (R&D theme designator)
WSO	Waveform Source Physics (R&D theme designator)
WSP	Waveform Signal Propagation (R&D theme designator)
WWSSN	World Wide Standardized Seismograph Network
Xe-135	Xenon-135 ($T_{1/2}$ = 9.14 hr), the shortest-lived radioxenon isotope (notation also appears with a superscript, ^{135}Xe)
Xe-133	Xenon-133 ($T_{1/2}$ = 5.24 d), the second longest-lived radioxenon isotope and most commonly observed (notation also appears with a superscript, ^{133}Xe)
Xe-133m	metastable Xenon-133 ($T_{1/2}$ = 2.19 d), which decays into Xenon-133 by emitting a conversion election (notation also appears with a superscript, ^{133m}Xe)
Xe-131m	metastable Xenon-131 ($T_{1/2}$ = 11.84 d), the longest-lived radioxenon isotope (decays to Xe-131 with the emission of a conversion electron) (notation also appears with a superscript, ^{131m}Xe)

Introduction

Starting in the late 1940s, the United States (U.S.) developed a capability to monitor atmospheric nuclear explosive tests and was successful in detecting the first Soviet nuclear explosion in August 1949 by routine air sampling over the Pacific Ocean. Over the next decade, systems for improved air debris sampling and infrasound detection were developed, and an initial network of seismic stations was established to monitor anticipated underground nuclear explosive testing. The Limited Nuclear-Test-Ban Treaty (LTBT, 1963) (banning signatories from nuclear explosive testing underwater, in the atmosphere, and in space) did not establish an international monitoring system, but depended on the many LTBT signatories' independent national technical means, which were directed at keeping track of each other's nuclear programs and possible nuclear explosive testing by non-signatories of the LTBT (NAS, 2002).

The majority of nuclear explosive tests were conducted by the United States (50%) and the Soviet Union (35%), where the average rate of testing was approximately once a week during the Cold War and peaked at 175 tests in 1962 (see Figure 1), the year prior to the LTBT. Most of these nuclear explosive tests were between 20 and 150 kt (DOE, 2015; Sykes and Davis, 1987), although some were much larger, with the largest being the Tsar Bomba in 1961 (57 megatons). In 1974, the U.S. and the Soviet Union signed a bilateral Threshold Nuclear-Test-Ban Treaty (TTBT, 1974), banning underground nuclear explosive tests of yield greater than 150 kt, which involved extensive, close cooperation between the two countries (NAS, 2002). Throughout the course of nuclear explosive testing, atmospheric measurements of carbon-14 have been used to track the impact of nuclear weapons on the environment (Figure 2). The amount of radioactivity in the environment peaked as atmospheric tests were being performed, and slowly began to return to pre-testing levels as nuclear testing transitioned to underground explosions.

Figure 1. Number of nuclear explosive tests per year. Note the change to underground testing and the start of the CTBT signature process (from ctbto.org). For updates to the information in this chart go to https://www.ctbto.org/nuclear-testing/history-of-nuclear-testing/nuclear-testing-1945-today/.

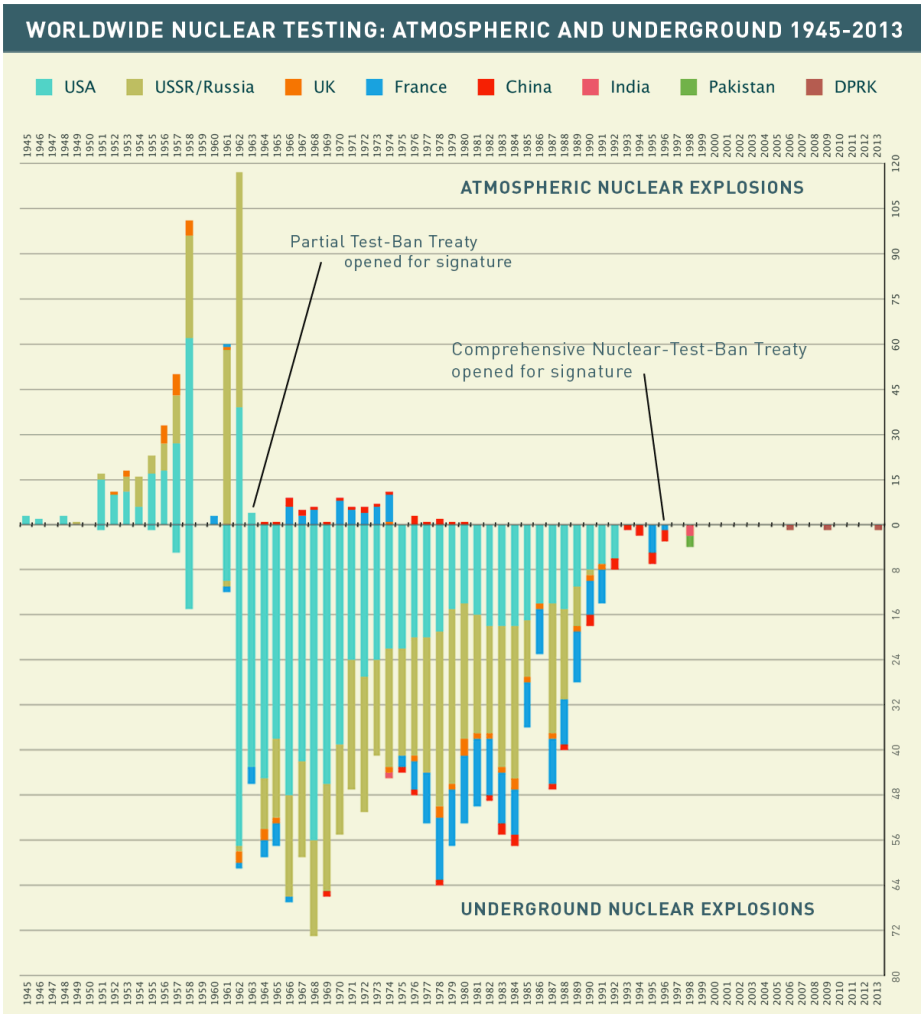

Since 1980, after China conducted the last atmospheric nuclear explosion, all declared nuclear explosive tests have been conducted underground, in effect making seismic waves the principal means for prompt detection, location, identification of source type (e.g., earthquake, explosion), and yield estimation.

This emphasis on seismic waves raises the important task of discrimination between nuclear and chemical (e.g., conventional explosives such as TNT) explosions (Denny and Zucca, 1994). For underground explosions, radionuclide monitoring is increasingly focused on capturing the delayed radioactive noble gases and radionuclide particulates or aerosols that vent or seep from an underground triggering event, and is the principal means in establishing whether or not an explosion is nuclear.

During negotiations (Mallin, 2017) of a comprehensive nuclear-test-ban in the mid-1990s, the international community was no longer satisfied to rely on the capabilities of the nuclear weapon states (primarily the U.S.) to monitor the proposed new treaty, but wanted it to be based on a truly internationally operated system with information available to all parties (NAS, 2002).

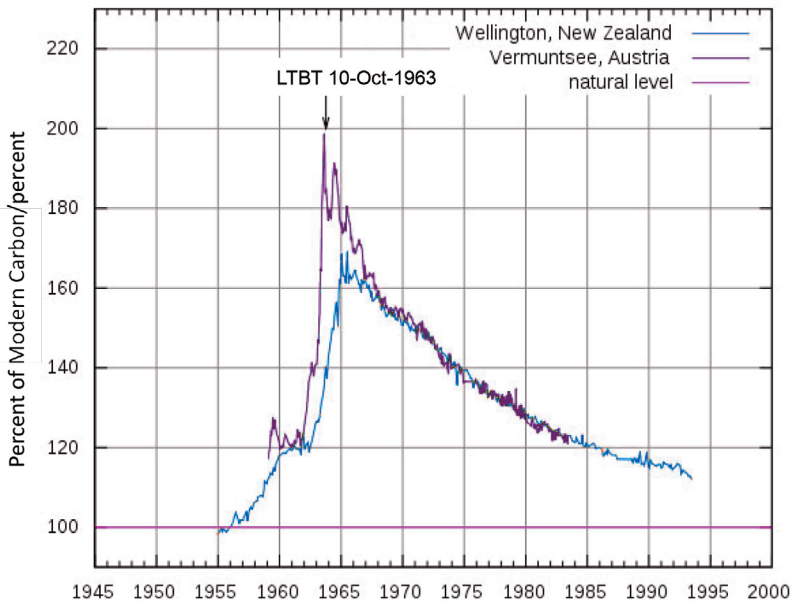

Figure 2. Radioactivity in the environment throughout the course of nuclear explosive testing, with the peak being the signing of the LTBT (from the CTBTO website, http://tinyurl.com/z299zf4).

Tutorial: History of Nuclear Science

While the age of nuclear weapons began in the 1940s, radioactivity was first discovered in 1896. Around 1900, scientists performed experiments confirming the existence of radiation, and characterizing the alpha decay, beta decay, and gamma decay processes (Becquerel, 1896 and 1900; Curie, 1904; Rutherford and Royds, 1908; Rutherford, 1911). Each of these decay mechanisms results in a distinct signature that is presently used to help identify when a nuclear explosion occurs. In 1938, the world started its shift into the nuclear age with the discovery of nuclear fission (Hahn and Strassman, 1939; Meitner and Frisch, 1939). In 1939, a number of prominent physicists around the world suggested (both proposing and warning) that a nuclear weapon could be produced. In 1942, the Chicago Pile (CP-1) showed the capability for a nuclear chain reaction (Fermi, 1946). While the first nuclear explosion occurred in 1945 (Trinity), nuclear weapon testing was at its peak between the 1950s and 1980s. With the increase in nuclear weapons testing arose the era of monitoring nuclear weapons tests. Early monitoring of nuclear weapons tests arose for national security, environmental, and diagnostic reasons. Monitoring technologies, while available, were not initially refined for relatively small amplitude, and potentially ambiguous signatures that are increasingly commonplace today. Present day monitoring now focuses on these relatively small signatures for treaty verification.

Timelines

There are several timelines of nuclear testing that have been published and are available through the internet. Examples are the timeline on the CTBTO website, the Nevada Test Site Oral History Project website, and the timeline in the March 2009 issue of Scientific American (Richards and Kim, 2009).

Efforts to slow the development of more sophisticated weapons culminated in the CTBT, which forbids all nuclear explosions, including the explosive testing of nuclear weapons. Even though the CTBT has not yet come into force, every nation that signed it—including those that have not yet ratified—has maintained a moratorium on nuclear explosive testing at least since the United Nations voted to adopt it and opened it for signature in 1996. The three nations that have conducted nuclear explosive tests since 1996 - India, North Korea (DPRK), and Pakistan—have not signed the treaty (Richards and Kim, 2009). The announced nuclear explosive tests from those countries were all underground. Based on the measured seismic magnitude (mb=3.94, Selby et al. (2012)), the DPRK test in 2006 was an order of magnitude smaller than initial nuclear explosive tests by other nuclear weapons states. It was still detected and confidently identified as an explosion via seismic means and identified as nuclear via radionuclide sampling.

Research and development relevant to nuclear explosion monitoring underpins what can be accomplished with the CTBT's global verification regime, enabling both CTBT state-signatories and other states to monitor the near-worldwide moratorium on nuclear explosive testing. This document reviews research trends related to the significant technological and scientific advances relevant to nuclear explosion monitoring. The organization of the document follows a physics-based approach with chapters on source physics, signal propagation, sensors, and signal analysis. The research and development trends within each chapter are summarized in the Table of Contents as section headings.

This document focuses on roughly the period from 1993 to 2016, which included the creation of the Preparatory Commission for the Comprehensive Nuclear-Test-Ban Treaty Organization (CTBTO) and the near completion and technical maturation of its associated International Monitoring System (IMS), International Data Centre (IDC), and on-site inspection (OSI) framework. During this timeframe, there have been significant technical advances of the core monitoring technologies (seismic, infrasound, hydroacoustic, and radionuclide) specified by the CTBT for the IMS. These core technologies largely bound the review areas in this document. The CTBT also allows a wide range of technologies for use in on-site inspections to clarify whether a nuclear weapon test explosion or any other nuclear explosion has been carried out in violation of the Treaty, and, to the extent possible, to gather any facts which might assist in identifying any possible violator. However, OSI is distinct from the monitoring function and OSI technologies are largely not addressed in this document. Technological advances have occurred amid an increasing number of treaty signatures and ratifications, as well as some continued nuclear explosive testing by non-signatory states.

This document does not speak to policy issues but rather addresses the significant technological and scientific advances relevant to nuclear explosion monitoring. The primary audience for this document is the next generation of research scientists that will further improve nuclear explosion monitoring, and others interested in understanding the technical literature related to the nuclear explosion monitoring mission.

A body of literature - in the form of journal articles, conference proceedings (as listed in the references at the end of this document), topical review papers (e.g., DOE, 1994), and books (e.g., Dahlman and Israelson, 1977; Blandford, 1977; Aki and Richards, 2002; NAS, 2002; Romney, 2009; NAS, 2012; Douglas, 2013) - has been emerging that documents the successes and challenges of the individual nuclear explosion monitoring technologies. For the next generation of researchers interested in monitoring issues, this document is intended to be an important starting point to gain an introduction to the field, as well as a guide to avoid future research duplication. Furthermore, the document is intended to help sustain the international conversation regarding the CTBT and nuclear explosive testing moratoria while simultaneously acknowledging and celebrating research to date.

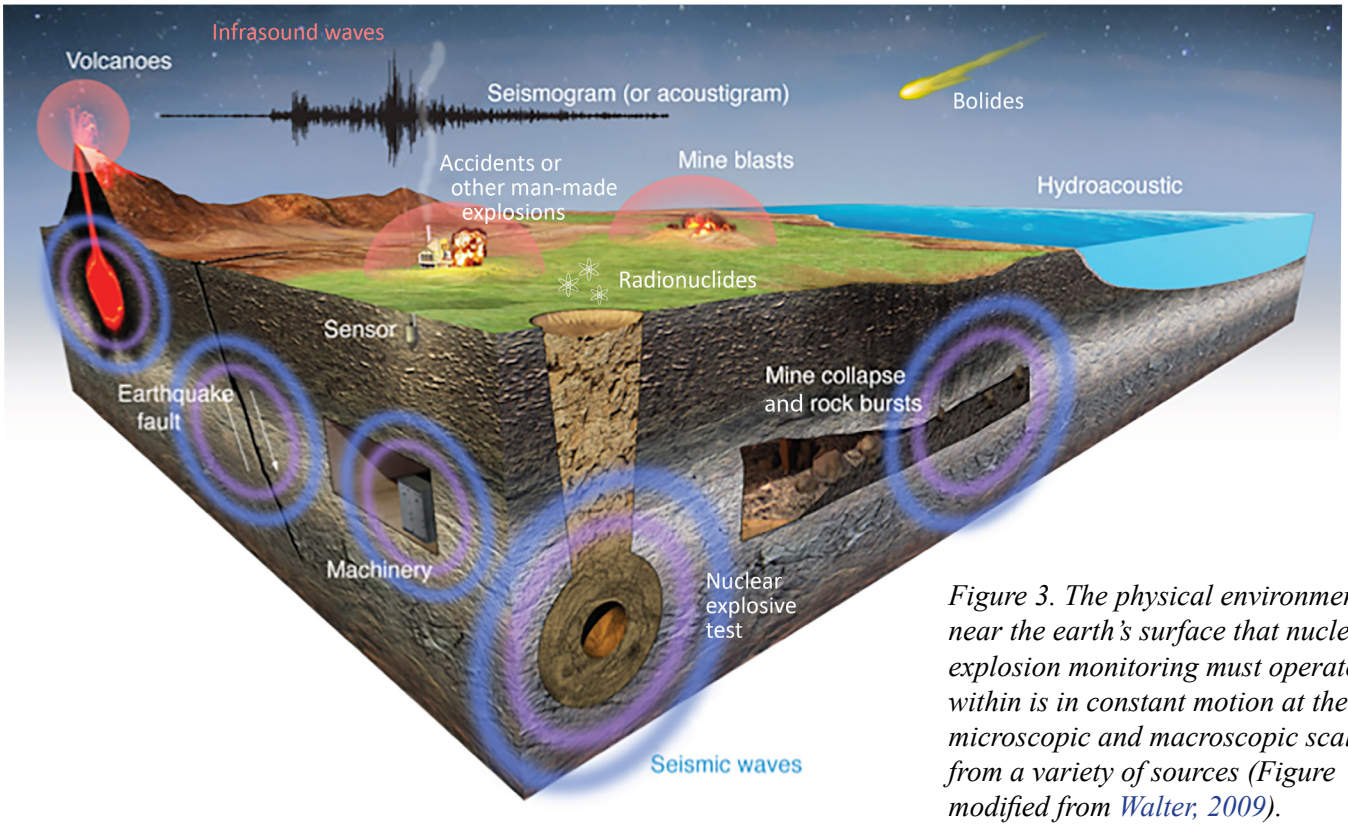

Figure 3. The physical environment near the earth's surface that nuclear explosion monitoring must operate within is in constant motion at the microscopic and macroscopic scales from a variety of sources (Figure modified from Walter, 2009).

Figure 3 shows the physical environment where sources of interest for nuclear explosion monitoring occur, which is predominately near the earth's surface or slightly into the crust. This environment is rich with confounding natural sources of seismic, hydroacoustic, and acoustic signals, such as earthquakes, volcanic activity, bolides, pounding of the surf on shorelines, mine collapses and rock bursts, and human-engineered events such as mine blasts, reactor accidents, or other man-made explosions.

All these sources generate seismic, infrasonic (including acoustic waves along the surface of the earth), and hydroacoustic waves that can be recorded at large distances with today's ultra-sensitive sensors. Each individual source recorded at a particular sensor location has a unique signature. Advanced signal analysis seeks to distinguish the signature of a nuclear explosion from background noise and other non-nuclear events.

The most commonly used waveform signals are seismic waves with periods of several milliseconds up to thousands of seconds, infrasonic waves above 0.05 seconds, and hydroacoustic waves between 0.01 and 1 seconds, as illustrated in Figure 4. These ranges contain the strongest signals that are generated by explosions and that effectively propagate through earth, air, and water, respectively, enabling remote detection. Seismic signals are comprised of many seismic phases, which describe whether the waves are primary (compression) or secondary (shear) and what path they take through the earth. While there are hundreds of seismic phases used in global seismology (Storchak et al., 2003), only a relatively small subset (~10-20) of the phases produce the most discernible signals of nuclear explosions at remote monitoring stations. See the Guide to Seismic Waves and Phases at the end of this document for an introduction to the nomenclature.

The waveform sensors used in nuclear monitoring are required to operate between 0.02 and 16 Hz for seismic sensors, 0.02 and 4 Hz for infrasound sensors, and 1 and 100 Hz for hydroacoustic sensors. In addition, the instruments used operate over a wide range of expected amplitudes that spans more than 120 dB for seismic, 108 dB for infrasonic, and 120 dB for hydroacoustic.

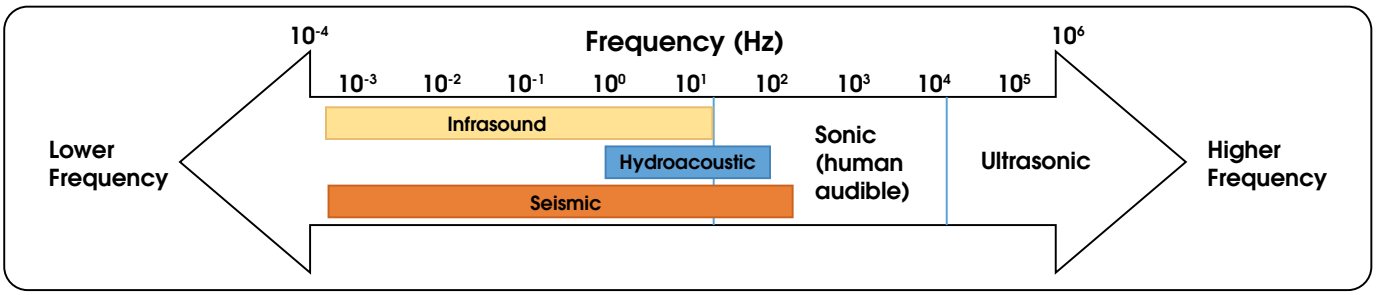

Figure 4. The segments of the acoustic (waveform) spectrum that are useful for event detection using infrasonic, hydroacoustic, and seismic technologies.

Although seismic, hydroacoustic, and infrasound monitoring can identify an explosive event, in general radionuclide detection is required to confirm that the event is nuclear. A nuclear explosion produces many isotopes, including radioactive noble gases such as isotopes of xenon (from fission reactions) and argon (through interactions with the surrounding environment). An atmospheric event releases these radioactive gases, along with fission product particles, into the atmosphere where they can be detected. If an event occurs underground or in the ocean, the amount of these isotopes dispersed into the atmosphere is significantly decreased, but detection is still potentially achievable. When an underground event vents, particulates and gases containing radionuclides are released directly into the atmosphere. Without venting, particulates are usually no longer quickly detectable at a distance, but over time noble gas fission products and activation products can still escape the ground through fractures assisted by barometric pumping. The four radioxenon isotopes that historically have been of most interest [^{135}Xe, ^{133m}Xe, ^{133}Xe, and ^{131m}Xe (See Acronyms and Abbreviations for definitions of each isotope)] were selected for measurement because they are produced in sufficient quantities; they are chemically inert, increasing the likelihood of escaping the underground environment to disperse effectively in the atmosphere; and their relatively long half-lives (days) allow time for atmospheric transport prior to complete decay of the signal. These four isotopes are created directly from fission or from the beta decay of fission product iodine isotopes. Comparing relative concentrations of these radioxenon isotopes provides insight into the time and type of a nuclear event (e.g., nuclear explosion vs. nuclear reactor release).

Researchers seek to enhance and improve operational monitoring systems. There are several classical perspectives that apply to nuclear explosion monitoring. The systems perspective focuses on the monitoring networks, stations and instrumentation. The technology perspective focuses on what different technologies (seismic, infrasound, hydroacoustic, and radionuclide) can do to detect and analyze the signals. The functional or operational perspective is particularly useful for waveform monitoring operations as it deals with the near-real-time collection of waveforms and the reduction of this voluminous raw "data" into useful information on a timescale that is helpful to monitoring organizations. This is broken into processing steps of event detection, association, location, discrimination, and magnitude/yield estimation. To elaborate further, as data are obtained, they are processed for signal detections which are then associated to a common event. The associated signals are used to calculate an event location, and algorithms are employed to discriminate between an explosion and other event types. In some cases, additional processing steps are performed with regard to the magnitude/yield of the event if discrimination tests suggest an explosive event occurred. For research purposes it is useful to realize that much of the operational or functional improvement relies on improving understanding of the science behind the generation, propagation, recording, and interpretation of seismic, infrasound, hydroacoustic, and radionuclide signals. Therefore, a physics-based perspective, based on a source-to-receiver flow, provides a full scope representation of nuclear explosion monitoring processes. Describing the research in terms of what part of the physics rubric is being addressed provides helpful orientation for the reader and researcher.

A simplified physics-based operational monitoring schematic is illustrated in Figure 5. Starting from the left, an event occurs (Source Physics); the signals from that source move away from the source (Signal Propagation); these signals are detected, measured, and stored as data (Sensors); and those data are processed by the monitoring authority to generate a list of all sources of interest as well as other derived information (Signal Analysis). These elements provide a framework capable of capturing the full scope of nuclear explosion monitoring processes, and can be thought of as a simplified amalgamation of nuclear explosion monitoring physical environments, along with a generalization of the operational systems.

Research and development in nuclear explosion monitoring plays a central role in developing and incorporating methods of detection, location, and discrimination of potential nuclear events, and has resulted in significant monitoring improvements. Functional operational monitoring metrics draw on advances in source physics, signal propagation, sensors, and signal analysis. Although this physics-based framework provides a useful way to visualize and understand nuclear explosion monitoring, the very nature of R&D means that few research projects fit neatly into one research area, nor are the paths often simple from R&D to operational use. Most products take several years to develop and progress from an idea to operational assimilation.

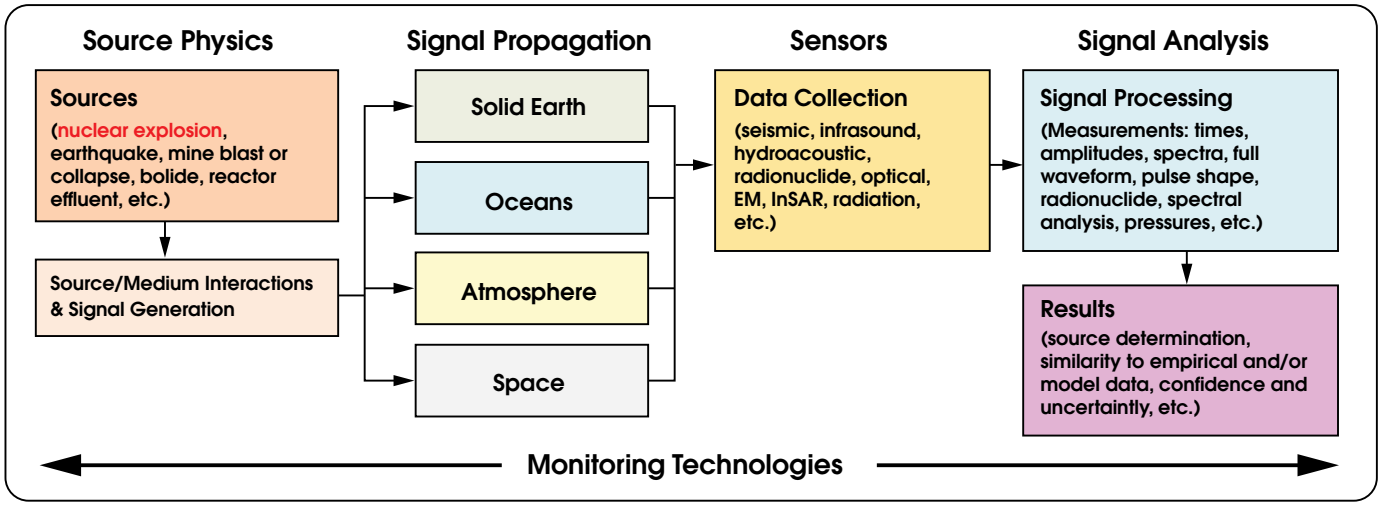

Figure 5. Physics-based research areas were chosen as a full scope representation of nuclear explosion monitoring processes and are shown in a context of operational data and process flow.

Contextual Trends

A few trends cut across the physics-based framework. These include external drivers that influence the direction and shape of research and development pursuits.

From large atmospheric to small underground explosions

In the event of an atmospheric or above-ground nuclear explosion, there is an immediate release of most of the radionuclides into the atmosphere. For such above-ground explosions, nearly 100% of the radionuclides (particulate and gaseous) are released into the environment. Effects of this release can be seen in the amount of radionuclides in the environment during the period of atmospheric nuclear explosive testing (Figure 2).

The shift from atmospheric to underground nuclear explosive testing following the signature and entry into force of the LTBT significantly changed the radionuclide monitoring regime. One consequence of nuclear explosive testing going underground is the potential for the radionuclide signals to be diminished, leaving only the signatures of the most mobile radionuclides. The waveform data are used as a flag that a suspected nuclear event has occurred, and radionuclide data is used to add insight into the interpretation of the observed waveform data. With the transition to underground nuclear explosive tests, the radionuclide monitoring community has concomitantly transitioned from measuring data from easily observable atmospheric nuclear explosive tests, to monitoring fewer signatures (notably radioxenons) from underground nuclear explosions (Bowyer et al., 1997; Bowyer et al., 2002).

From large signals to those hidden in the noise

A major trend that has a focusing effect on the research is the transition from large to small signal-to-noise ratios, which requires pulling signals out of noisy background measurements. In the early days of nuclear explosive testing, there were large explosions and relatively few background sources of relevant sizes (both for radionuclide and waveform technologies).

The current monitoring regime must deal with the long-term trend of searching for increasingly low-amplitude signals amongst other natural and anthropogenic (human-made) signals, which are often not of interest to the monitoring mission. A few factors have contributed towards monitoring for smaller signals. Firstly, nuclear explosive tests have become smaller in recent years. Secondly, when searching for smaller signals, one must also deal with more background signals associated with operations throughout the world, both for waveform signals and radionuclide releases. These background signals arise from a wide variety of sources, from mining operations to medical isotope releases, and occur throughout the world in both rural and urban environments.

In general, the development of signal detectors operates in a continuous cycle in which detectors become more sensitive, opening the door for new backgrounds that were not previously visible. Once those backgrounds are either eliminated or understood through analysis, the sensitivity of the detector systems is modified to improve, starting the development cycle over again.

The need to detect smaller amplitude signals while maintaining acceptable false alarm rates is likely to drive research toward the fusion of different phenomenologies for monitoring purposes.

From paper to high-performance computing

Prior to the 1960s, global seismology science was handicapped by the small number of seismic stations around the globe. But in 1961 the World Wide Standardized Seismograph Network (WWSSN), consisting of 120 well-calibrated short- and long-period seismographs, was deployed around the world (Figure 6), providing a high-quality dataset of analog records that allowed for significant advances in research on earthquake locations and mechanisms, the structure of the earth's interior, as well as plate tectonics.

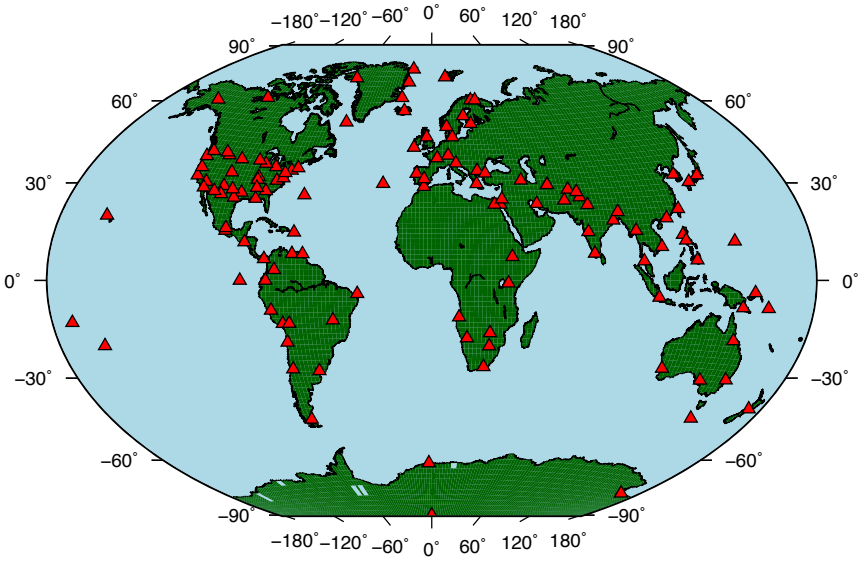

Figure 6. World Wide Standardized Seismograph Network, created in 1961.

Digital seismograms were introduced in the early 1970s. Rapid advances in computer technology allowed analysis of increasing volumes of data and observational seismology to leap ahead of theoretical understanding. Still, early applications were challenged by what would probably today be regarded as breathtakingly limited hardware. For example, in the late 1970s, the cutting edge in computing power was Cray I that was capable of a peak performance of 250 million FLOPS (floating point operations per second), while present computers using a single Intel Core i7 processor can expect performance of around 40+ billion FLOPS. Increases in computing power following the Moore's Law (Moore, 1965) trajectory led to improved data processing techniques and increased capabilities in monitoring, which, in turn, begged for more data from more densely spaced seismometers. Thus, the value of computer resources must be considered in the context of the new challenges faced by the monitoring mission, along with the proliferation of regional and local seismic networks that provide vast quantities of high-quality digital seismic data to be processed. It is also now commonplace to have continuous seismic and infrasound waveform data available in real and near-real time thanks to the introduction of satellite telemetry. The recorded data are digitally telemetered to processing institutions with minimum latency, improving remote monitoring capabilities of events around the globe.

Signal analysis capabilities have advanced over the last decades with computational processing. For the signals of real concern, this area is changing from a human intensive endeavor toward a much more automated one with expert analysts supported by computer-aided tools. The increase in the number of available sensors combined with advances in signal processing is driving down monitoring thresholds (e.g., minimum magnitude of event that will be detected). However, each major reduction in monitoring threshold comes with a significant increase of the background signals. Thus when decreasing the threshold, overall capabilities, particularly discrimination, must advance to keep the monitoring operational burden manageable.

Tutorial: Data Archives

There are many worldwide seismic databases. A large amount of seismic data are available publicly and electronically via the Internet, in large part due to the importance of the data to earthquake prediction and hazard mitigation.

- The National Earthquake Information Center (NEIC) (https://earthquake.usgs.gov/contactus/golden/neic.php), a part of the Department of the Interior, U.S. Geological Survey, has three main missions. One of them is to be the national data center and archive for earthquake information. As such, the NEIC collects and provides to both scientists and the public an extensive seismic database that serves as a solid foundation for scientific research. The data collected by the NEIC are published in a variety of formats (e.g., the Preliminary Determination of Epicenters (PDE) bulletin) and are available electronically (http://earthquake.usgs.gov/data/).
- The Incorporated Research Institutions for Seismology (IRIS) Data Management Center (DMC) (http://ds.iris.edu/ds/nodes/dmc/) archives and distributes data to support the seismological research community in general. The facilities of IRIS Data Services, and specifically the IRIS DMC, can be used to access seismic and infrasound waveforms, related metadata, and/or derived products. IRIS Data Services are funded through the Seismological Facilities for the Advancement of Geoscience and EarthScope (SAGE) of the National Science Foundation.
- ORFEUS (Observatories & Research Facilities for European Seismology) (http://www.orfeus-eu.org) is a non-profit foundation that coordinates and promotes digital, broadband seismology in the European-Mediterranean area. ORFEUS provides access to seismological data such as waveforms through the European Integrated Data Archive (EIDA, http://www.orfeus-eu.org/data/eida/index.html) infrastructure.
- The International Seismological Center (ISC) (http://www.isc.ac.uk/) provides full access to data (e.g., hypocenter locations, focal mechanism solutions) within the ISC Bulletin (http://www.isc.ac.uk/iscbulletin/search/), which is considered the definitive record of earth's seismicity. Many other geophysical and seismological institutions and organizations in several other countries also provide seismic catalogs and data, such as the Instituto Geográfico Nacional (IGN) of Spain (http://www.ign.es/ign/layoutIn/sismoFormularioCatalogo.do), or the GEOFON earthquake monitoring system (http://geofon.gfz-potsdam.de), located at Postdam, Germany, and which acts as a key node for rapid global earthquake information for the European-Mediterranean Seismological Centre (EMSC).

Techniques for handling large data sets are advancing rapidly together with easier access to high-performance computing. In addition, data storage costs are decreasing. The net result is that much of the historical monitoring archive can be kept online and used to automatically compare the incoming data stream to the archive in ways that were simply not possible until recently. As an example, researchers are taking the lead on using new computational power to investigate waveform template matching in both the frequency and time domains as a means to improve monitoring capabilities (e.g., Harris and Dodge, 2011; Slinkard et al., 2014, Shumway and Stoffer, 2017). Recent and present work is focused on ways to utilize commercial big data techniques to greatly improve processing speeds (e.g., Addair et al., 2014). Initial applications of large-scale calculations show that a significant fraction of the earth's seismic signals is amenable to automated template processing (e.g., Dodge and Walter, 2015), opening up new and much more efficient methods for monitoring data pipeline processing.

Similar to the progress in signal processing, physics-based simulation codes have advanced significantly in recent years, greatly aided by progress in high performance computing. The capability now exists to model an explosion from the device, through the non-linear shock region, then couple the model into the

Tutorial: Historical Seismology

Large accomplishments and solutions to scientific challenges related to key monitoring research areas (source physics, signal propagation, signal analysis, and sensors) are inextricably linked with the rapid advances in digital computing and microprocessor technology that began in the 1960s. Before then, and even before the instrumental era (refer to Dewey and Byerly, 1969, for an introduction to early seismometry), theory was significantly ahead of observation. In the early 1800s Cauchy (1828), Poisson (1828), Stokes (1845, 1849), Rayleigh (1877, 1885), and Love (1888, 1892), among others, developed the theory of elastic wave propagation in solid materials. They found the major waves that pass through a solid and described primary (P) and secondary (S) body waves as well as surface waves. Nevertheless, the first serious attempt at observational seismology did not come until Mallet (1859), an Irish engineer, traveled to Italy to study the damage caused by an earthquake near Naples; he pointed out the need to establish observatories to monitor earthquakes. However, the first time-recording mechanical instruments (undamped and very inaccurate) were not developed until the last quarter of the 19th century; and it was not until the early 1900s when the first electromagnetic seismographs appeared and seismic station networks were established. Availability of seismograms from many earthquakes recorded at many distances during the first decades of the 20th century promoted many new first-order discoveries about the earth's interior and earthquake sources: Mohorovičić (1909) identified the seismic velocity boundary between the crust and the mantle (Moho); Oldham (1914) identified P, S, and surface waves in earthquake records and detected the earth's liquid core; Richter (1935) developed the first quantitative measure of relative earthquake size (the Richter magnitude scale); Lehmann (1936) discovered the earth's solid inner core; Jeffreys and Bullen (1940) published the final version of their travel-time tables for many seismic phases; and Gutenberg (1951, 1959) published travel-time tables, that include core phases and estimated the depth of the fluid core, which are accurate enough to still be used today. These discoveries are even more remarkable considering that all of them were made before the digital era and at a time when measurements were made slowly by careful and meticulous observation of analog paper seismograph recordings and the information derived from these original recordings.

long-range elastic propagation codes, to better simulate how the waves carry out to the standoff distance where monitoring occurs. The rise of seismic tomography is also inextricably linked with the rapid advances in digital computing and microprocessor technology. This branch of seismology would simply not be feasible without the ability to make millions of calculations per second. To properly accommodate the large quantities of high quality seismic data that are now being recorded and archived, it is important to represent the earth by many parameters and, therefore high performance computing is needed for tomographic studies. New computer capabilities today enable solutions that were previously intractable.

The following chapters on Source Physics, Signal Propagation, Sensors, and Signal Analysis discuss these and other trends in greater detail. The final chapter on Research Potential for Further Performance Improvements synthesizes and summarizes promising future research.

Source Physics - Understanding Signal Generation

Source physics research focuses on improving our ability to understand what happened at the source, based on the observed signals recorded by sensors. Of critical importance is our ability to deduce whether an event was a nuclear explosion, chemical explosion, or earthquake. Although, in tectonic regions of the world, earthquakes are usually the dominant form of observed seismic signal, in stable regions, mining and industrial explosions can be most prominent. In certain regions of the world, anthropogenic sources can be the primary source of radionuclide signals. Such circumstances present monitoring challenges and comprehensive models provide insight into understanding how an event of a particular type interacts with the surrounding medium (Evernden, 1976; Leith, 2000; Adushkin and Leith, 2001) and creates the signatures seen at sensors.

Source physics R&D activities advance our understanding of nuclear and conventional (i.e., chemical) explosions, earthquakes, mine collapses, and other sources of waveform and radionuclide signals. Research emphasis is on developing models that best simulate the pertinent physics of a nuclear detonation as it interacts with the surrounding local environmental medium, and how it differs from a conventional detonation. These models need to be developed and validated (typically with experiments) for new kinds of emplacement conditions that go beyond historical nuclear explosive testing conditions to anticipate future ones.

From natural to anthropogenic radioxenon background sources (RSO1[1])

Radioxenon background is ever-present with levels continuously fluctuating throughout the world, both from natural and anthropogenic (human-made) sources. The presence of radionuclide particulates or gases can be indicative of a nuclear explosion, but must be distinguished from natural backgrounds. Prior to the production of radioxenon through anthropogenic sources, primordial uranium and thorium decay were some of the dominant production mechanisms (Wetherill, 1953; Kuroda, 1956).

Radionuclides have always been present in the soil and atmosphere, partly from the decay of uranium and thorium within the earth. In the Precambrian era (600 million years ago), a local concentration of uranium was so high at Oklo in Gabon, Africa, that it reached criticality, effectively resulting in a natural nuclear reactor (http://www.ans.org/pi/np/oklo/). In addition to the decay of primordial uranium and thorium, cosmic ray production of isotopes of interest was also a primary source for backgrounds. In more recent times, human-made nuclear reactors became one of the primary sources of radionuclide signatures. As nuclear reactors exploit a fission process, many observable radioisotopes from a nuclear explosion can also originate in a nuclear reactor. The Fukushima nuclear reactor meltdown (Le Petit et al., 2014) provided environmental release of radionuclides on a much larger scale than what is seen from normal operations of a nuclear reactor. As the containment was lost, the radionuclides from the nuclear reactor were dispersed across the globe. More recently, releases from nuclear reactors around the world have decreased through efforts to reduce emissions, and medical isotope production has become one of the key anthropogenic backgrounds for the radionuclide detection community. In medical isotope production the target is processed after irradiation (to extract the medical isotopes), resulting in a significant portion of the radioxenon generated (for fission-based production) being released into the atmosphere, creating a background for radioxenon detectors throughout the world. There were 450 nuclear power reactors throughout the world in 2016 (https://www.nei.org/Knowledge-Center/Nuclear-Statistics/World-Statistics). As of 2010 there were 15 fission-based medical isotope production facilities throughout the world, which release an average of approximately $1x10^{13}$ Bq/day of radioxenon into the atmosphere (Saey et al., 2010a,b). In order for the medical isotope backgrounds to have minimal impact on the radioxenon detectors utilized by the CTBTO

[1] *The trends are keyed and linked to the R&D Themes from the GNDD Technology Roadmap.*

Preparatory Commission within the IMS, the emission rate from any given plant should be less than $5x10^9$ Bq/day (Figure 7). With an emission rate of $5x10^9$ Bq/day (Bowyer et al., 2013), the release from a medical isotope facility would be on par with that of a nuclear reactor.

In 2009, scientists met with medical isotope production (MIP) companies around the world to discuss the potential impact of radioxenon releases from MIP facilities. This began a series of meetings (now known as the Workshop on Signatures of Man-Made Isotope Production, http://wosmip.pnnl.gov/) and collaborations between scientists and companies interested in producing isotopes (Matthews et al., 2012). The goal of the collaborations is to reduce the radioxenon releases from all current and future MIP facilities to no more than $5x10^9$ Bq/day without unacceptable impact on medical isotope production.

Techniques to distinguish a nuclear explosion from natural backgrounds have been demonstrated, but these techniques must become more sophisticated to distinguish a nuclear explosion from anthropogenic background sources.

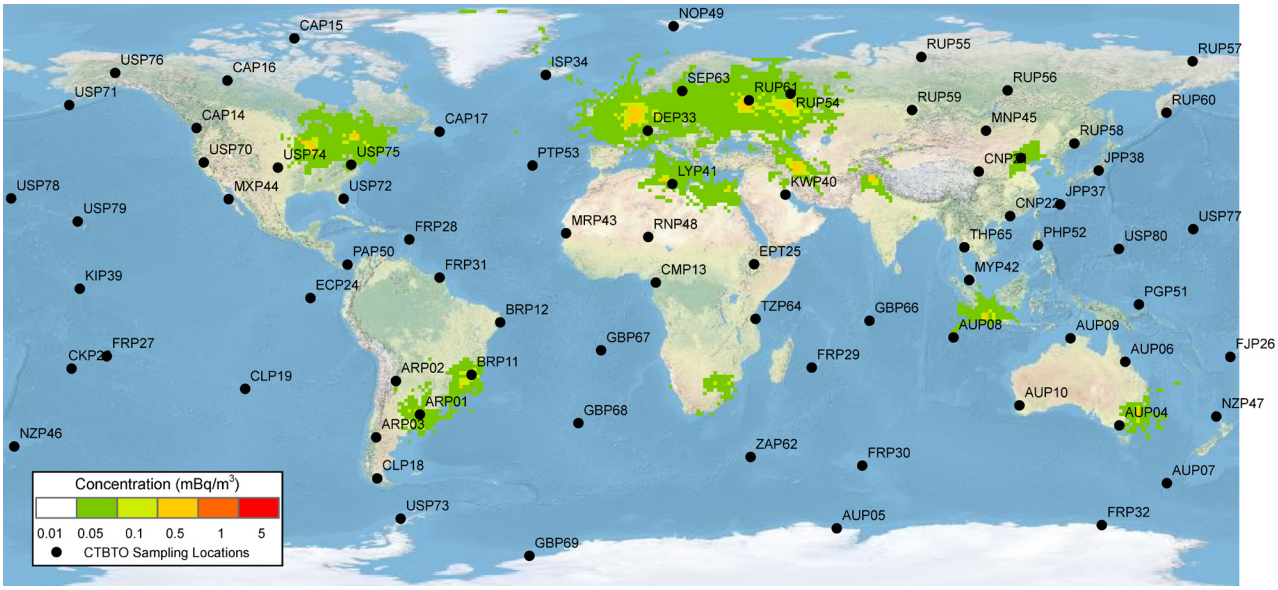

Figure 7. Plot of the IMS radionuclide stations with the global maximum radioxenon backgrounds present from a $5x10^9$ Bq/day release from medical isotope facilities in operation as of 2013.

Future R&D

Discrimination techniques for anthropogenic sources are an important step in furthering our ability to monitor for nuclear explosions. Additional means of accounting for anthropogenic radiological backgrounds will be required to understand signals for monitoring purposes.

From detection of single to multiple isotopes (RSO1)

From the 1960s until the 1980s nuclear explosion monitoring measurements focused on the detection of ^{133}Xe (Bolmsjo and Persson, 1982). In the early days of the atomic age, it was a fair assumption that the detection of ^{133}Xe was indicative of a nuclear explosion, but as more anthropogenic sources of radioxenon became present in the world (i.e., nuclear reactors and medical isotope production facilities) the background levels of ^{133}Xe increased. With the additional anthropogenic backgrounds, a means of discriminating a nuclear explosion from a nuclear reactor or medical isotope facility was needed. Fortunately, detection sensitivities improved with the Automated Radioxenon Sampler-Analyzer (ARSA) (Bowyer et al., 2002), Swedish Automatic Unit for Noble gas Acquisition (SAUNA) (Ringbom et al., 2003), Système de Prélèvement Automatique en Ligne avec l'Analyse du Xénon (SPALAX) (Fontaine et al., 2004), and Analyzer of Radio-Isotopes of Xenon (ARIX) (Dubasov et al., 2005), and the measurement of multiple xenon isotopes (^{135}Xe, ^{133}Xe, ^{133m}Xe, ^{131m}Xe) became possible and traditional.

Tutorial: Radioxenon Decay - A simplified list of radioxenon isotopes and an abbreviated decay chain for at least one isotope, highlighting both its genesis and progeny.

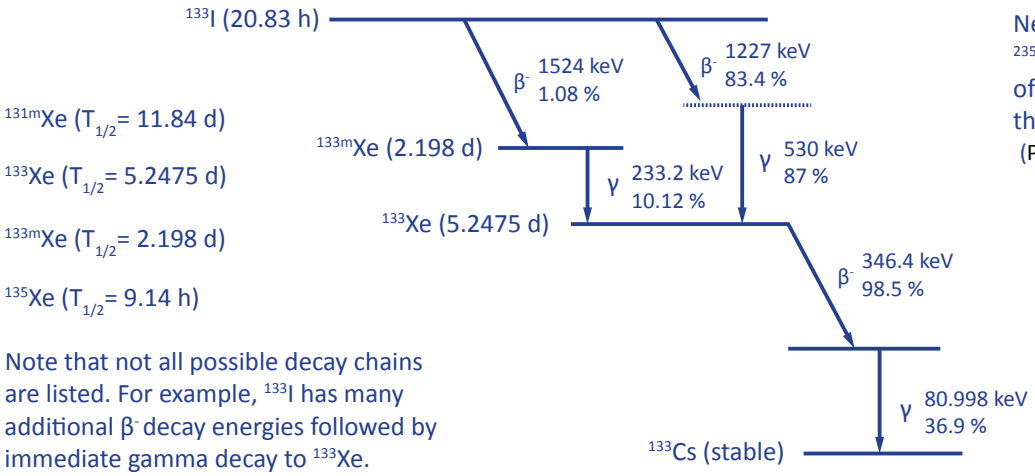

Neutron induced fission of ^{235}U produces a greater ratio of ^{133m}Xe/(^{133m}Xe+^{133}Xe) than the decay of ^{133}I. (Perjarvi et al., 2010)

Note that not all possible decay chains are listed. For example, ^{133}I has many additional β⁻ decay energies followed by immediate gamma decay to ^{133}Xe.

Due to the extended period of time between release and measurement, it was initially thought that ^{135}Xe would decay away prior to any radioxenon detection, but the near-real-time radioxenon detection systems proved that this was not the case. In 2006, soon after the development of systems capable of measuring the four radioxenon isotopes, analysis methods were developed capable of determining if the source of radioxenon was indeed a nuclear explosion rather than a nuclear reactor or a medical isotope production facility (Kalinowski and Pistner, 2006). By taking the ratio of various xenon isotopes (^{135}Xe, ^{133}Xe, ^{133m}Xe, and ^{131m}Xe), it is possible to constrain the source of the radioxenon as detailed in Figure 8. In recent years the IMS has demonstrated the ability to detect and discriminate nuclear explosions as in the case of the DPRK nuclear explosive tests (Ringbom et al., 2014).

More recently, there has been research into the production and detection of more exotic non-traditional xenon isotopes such as ^{125}Xe and ^{127}Xe (Klingberg et al., 2015). These non-traditional radioxenon isotopes are considered to be exotic for their relatively complex decay schemes compared to the traditional radioxenon isotopes (Figure 9). The non-traditional radioxenon isotopes are of interest for two reasons: they have the potential to be a background for traditional radioxenon isotopes, and they could serve as an additional detection signal. In the future, it is possible that the nuclear explosion monitoring community may turn to the more exotic radioxenon isotopes to help discriminate a nuclear explosion from anthropogenic backgrounds as anthropogenic backgrounds increase.

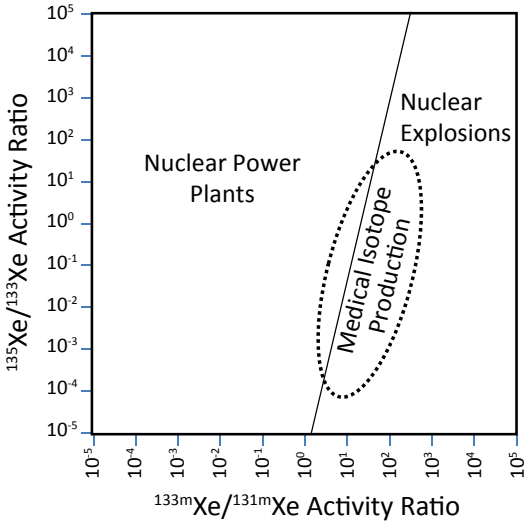

Figure 8. By taking the ratio of activities between the radioxenon isotopes, it is possible to discriminate between nuclear reactors (left side), medical isotope production facilities (center) and nuclear explosions (right side).

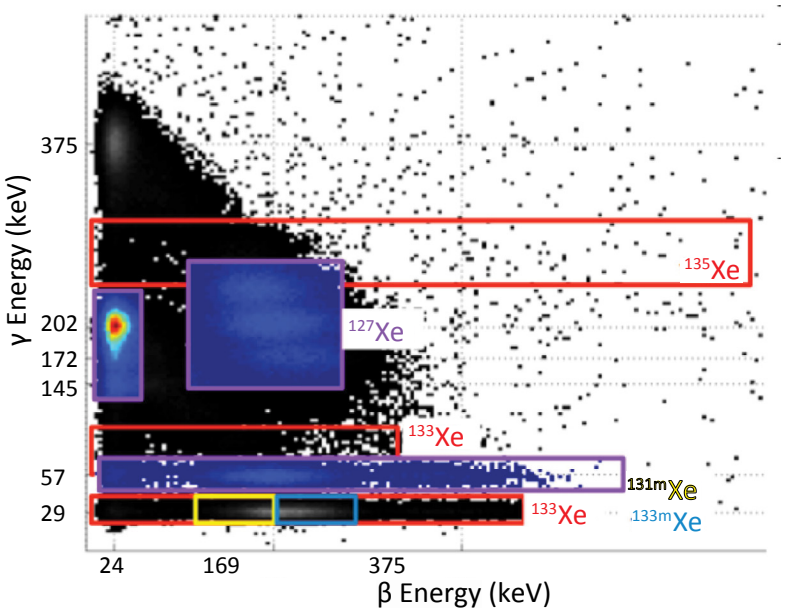

Figure 9. A beta-gamma coincidence spectrum with the spectral regions-of-interest (ROIs) of the four traditional radioxenon isotopes (framed in red, blue, and yellow) and the new ROI for ^{127}Xe (highlighted in color and framed in purple) (Klingberg et al., 2015).

In addition to measurements of radioxenon, measurements of radioactive particulates have been one of the primary techniques utilized to monitor for nuclear explosions. There are a number of radioactive isotopes of interest that are measured through gamma spectroscopy that can be used to verify whether a nuclear explosion occurred. It is often the case that the particulate signatures have a noble gas precursor, which may or may not be detectable. Through the correlation of particulate and noble gas signatures, it has been shown that additional information can be obtained from the radionuclide signals, which serve to help better discriminate from anthropogenic sources (Kalinowski, 2011; Kalinowski and Becker, 2014). To monitor for nuclear explosions, it is important to be able to distinguish the radionuclide signature of a nuclear explosion. For this reason, the list of radionuclides of interest has gradually expanded to better discriminate radioxenon from an explosion from that of background sources. For example, the addition of ^{37}Ar as a secondary delayed relevant radionuclide has helped to provide better discriminating power to radionuclide measurements. Since ^{37}Ar is produced via neutron activation and not as a direct result of the fission process and has a much longer half-life than the xenon isotopes (35.04 day half-life), it provides additional information in a similar manner as the radioxenon-particulate correlation. Due to the greater abundance of non-radioactive argon in air, less air need be processed compared to xenon, but higher sample purity is required.

Future R&D

In coming years, research should be focused on both better ratio measurements for the four traditional radioxenon isotopes, and how to measure and quantify non-traditional radioxenon isotopes.

From simple analytical models to phenomenological numerical calculations for radionuclides (RSO2)

In the event of an underground nuclear explosion, it is advantageous to know the impact of geologic structures on delaying the release of radioactive noble gases and aerosols into the environment for detection. Without knowledge of the physical parameters of the geologic media, there is increased uncertainty associated with the simulations used to predict signals that will be available for detection.

When an underground nuclear explosion occurs, it is well known that not all radionuclide signatures will escape to the earth's surface and be detected at an IMS station or during an on-site inspection (OSI). The exact amount to escape to the earth's surface will vary on a case-by-case basis and must be estimated at the time of measurement, taking into account the many delay factors such as migration time, chemical sorption, radioactive decay, etc.

In 1996, when the sampling period of weeks to months after an explosion was suggested for OSI (Carrigan et al., 1996), it was based on simulations and the observation of tracer gases (Figure 10). With the observations and transport times, it was determined that the transport could not be produced by diffusion alone, but required another more macroscopic transport mechanism. It was suggested that sampling along fault lines would allow for chromatographic-type transport of radioxenon and radioargon.

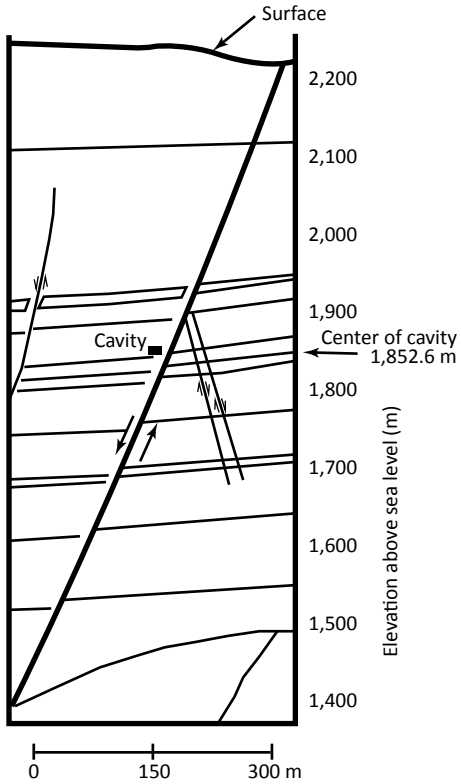

Figure 10. Noble gases can migrate out of fractures in the earth, as observed during an experiment at Rainier Mesa (Carrigan et al., 1996).

When nuclear explosions are conducted closer to the earth's surface, and eventually shift from above ground to underground, the neutrons created during the fission process have a higher chance of interacting with soil. Calcium, of which ^{40}Ca is the primary naturally occurring isotope, is one of the abundant elements within the earth's crust. As the neutrons are captured by ^{40}Ca, the calcium undergoes an (n,α) reaction that produces ^{37}Ar (See the tutorial on ^{37}Ar). With nuclear explosive testing performed underground in an effort to contain the blast and the radioactive material, there is often ample calcium within the rock to be irradiated by the neutrons produced in an explosion. The fraction of ^{37}Ar to escape from the rock and from the underground environment has only recently started to be studied as a potentially important delayed signature of nuclear explosions.

For years, SF_6 (sulfur hexafluoride) was used as a tracer gas and a surrogate for xenon in gas transport models and gas transport experiments. The use of SF_6 allowed for gas transport models to be based on physical data with underlying assumptions (Carrigan et al., 1997). In 2011, measurements were performed injecting both radioxenon and SF_6 into an underground bore hole, then pumping them out and measuring them at a later time (Olsen et al., 2016). If xenon and argon migrated at the same rate as SF_6, the ratio of dilution factors would be on the 1:1 line. While these results generally agreed with the simulations (Figure 11), there were some differences observed in dilution factors. The use of Freon instead of SF_6 has also been investigated recently as an improved surrogate (Carrigan et al., 2016).

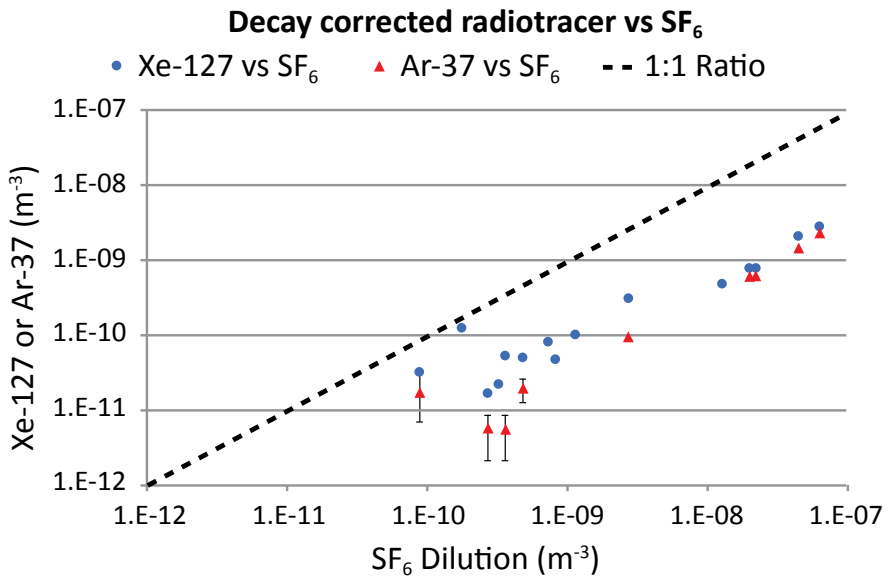

Future R&D

Further development of the measurement of real transport parameters, or the correlation between xenon or argon isotopes and their surrogates, will be required for accurate predictions of the radionuclide signals present from a nuclear explosion.

Figure 11. Both Xe and Ar show increased dilution (falling below the 1:1 ratio line) as compared to the common migration surrogate (SF_6) (Olsen et al., 2016).

Work performed by PNNL and the University of Texas in 2015 demonstrated distinct differences between the transport of xenon and SF_6 under both dry and wet soil conditions (Lowrey et al., 2015). These measurements were the first step in utilizing models with measured physical parameters (i.e., diffusion coefficients in wet and dry conditions) for the species of interest. The measurement of these parameters will likely require modifications to the transport models to incorporate additional variations that may occur in experiments or measurement campaigns.

From narrow-band magnitude estimates to full spectral estimates of the seismic source (WSO3)

Size is a fundamental property of seismic events, and magnitude is an attempt to quantify the size of earthquakes and related events. Magnitudes are estimated from the amplitude of the ground shaking that is generated by the specific event, taking into account the distance of the measuring point from the event. There are different ways to make the measurement, leading to various magnitude scales discussed in the paragraphs below. Event magnitudes are used in a variety of explosion monitoring tasks, including discrimination between earthquakes and explosions (See "From surface-to-body-wave magnitude ratios to corrected regional phase amplitude ratios"). These include the mb:Ms (body-wave magnitude to surface-wave magnitude) discriminant and magnitude corrections for regional high-frequency P/S discrimination (See terminology of seismic phases in Guide to Seismic Waves and Phases). Magnitudes can also be used to estimate yield (See "From narrow-band teleseismic explosion size estimates to full-spectral estimates of coupled explosion size and depth"). Over the years our understanding of earthquake size has evolved from narrow-band magnitude estimates to low-frequency estimates of seismic moment and moment magnitude on to full spectral estimates of the source.

The original Richter magnitude (Richter, 1935), known as the local magnitude (ML), measured the largest amplitude (usually the S-wave) on the horizontal components near the dominant period (0.8 s) of signals recorded on a Wood-Anderson seismometer. Embedded in the public's consciousness as the "Richter scale," the original formula is technically only applicable to local and near regional earthquakes in southern California. The formula was adopted for other regions of the world by empirically determining parameters which account for regionally-varying source and propagation effects. Other narrow-band magnitude

formulas were developed to be more generally valid and applicable for teleseismic events. The body-wave magnitude (mb) is a short-period (~1 second) teleseismic P-wave magnitude (Gutenberg and Richter, 1956). The surface-wave magnitude (Ms) is a long-period (~20 seconds) teleseismic surface-wave magnitude (Gutenberg, 1945). The combination of mb:Ms has become one of the most established discriminants between explosions and earthquakes. Other formulas, such as mbPn (Evernden, 1967) and mbLg (Nuttli, 1973), were developed to be applicable to regional events.

The variable period surface wave magnitude formula (aka Ms VMAX) (Russell, 2006; Bonner et al., 2006) was developed to broaden the range of applicable periods for surface-wave magnitude from a narrow-band 20-second measurement to 8-25 seconds, making it applicable to both teleseismic and regional events.

Aki introduced the concept of seismic moment (Aki, 1966) where the long period of the source spectra in the far field can be represented by the seismic moment Mo = μAD where μ is the shear modulus, A is the rupture area, and D is the average displacement. This was followed by the introduction of moment tensors (Gilbert, 1971; Randall, 1971) which take into account the orientation of the slip. The moment is typically estimated using the longest period waves that an earthquake generated. The scalar seismic moment can be converted to a moment magnitude Mw (Kanamori, 1977; Hanks and Kanamori, 1979), where Mw=(2/3) $\log_{10}$Mo -10.7 and Mo is in dyne-cm (10^7 dyne-cm = 1 N-m). Because it is not measured at a single frequency, and moment is tied to physical parameters, Mw is generally considered to be the best magnitude for estimating the size of a seismic event.

Starting in 1976, the Harvard Centroid Moment Tensor (Harvard CMT) project started systematically calculating moment tensors for large (M>=5.0), teleseismically recorded events (Dziewonski et al., 1981). Since 2006, this has continued at Lamont-Dougherty Earth Observatory as the Global Centroid Moment Tensor (Global CMT) project (Ekström et al., 2012; www.globalcmt.org). These projects have provided the community with thousands of moment tensor solutions (see Figure 12).

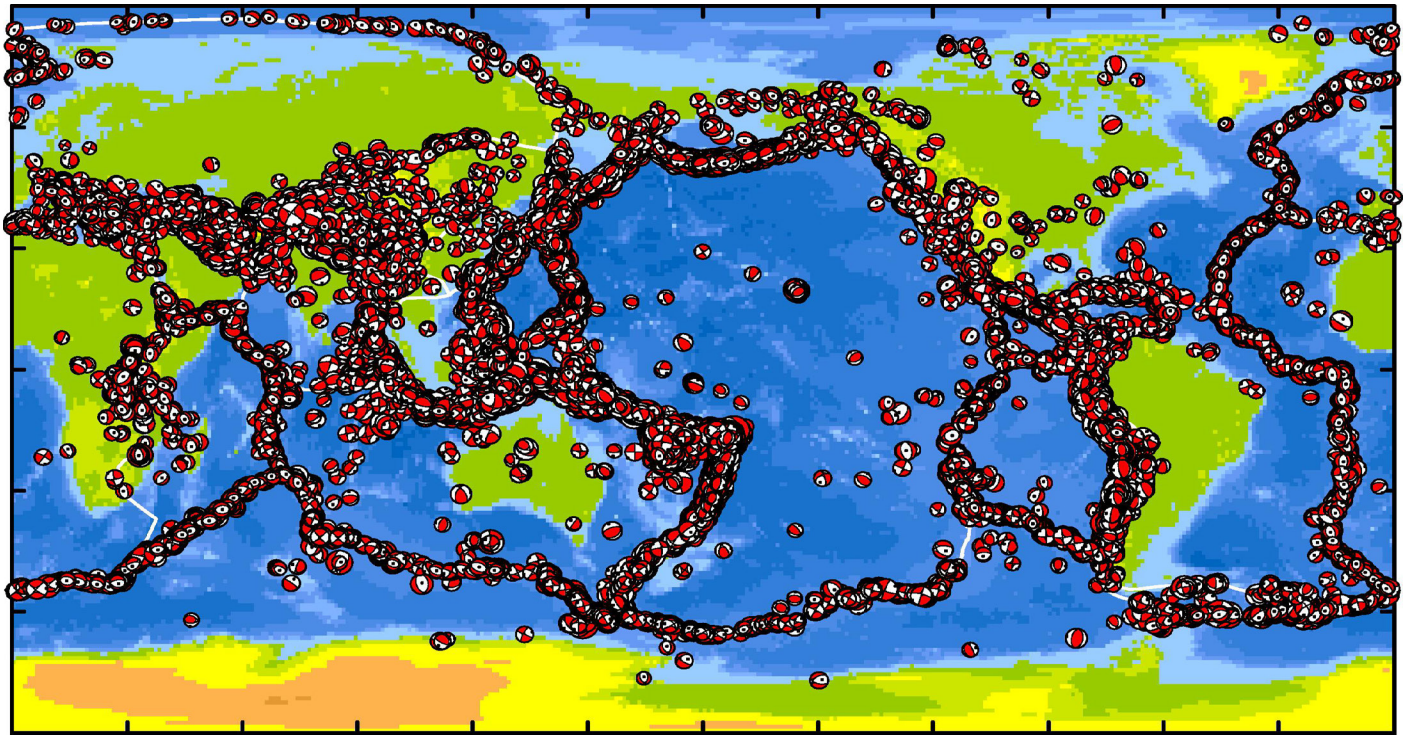

Figure 12. Map of shallow earthquakes with CMT solutions from 1976-2005 (from www.globalcmt.org)

In the 1990s, these methods were being applied to smaller (M>=3.5) events only recorded regionally using shorter periods (10-50 seconds). Many methods were developed in California including those by Romanowicz et al. (1993), Dreger and Helmberger (1993), Thio and Kanamori (1995), Ritsema and Lay (1995), and Pasyanos et al. (1996), then applied in other regions of the world.

In the meantime, methods were developed to take advantage of the stable shape and amplitudes of the waveform coda (Mayeda and Walter, 1996; Mayeda et al., 2003; Phillips et al. 2008). Coda is comprised of later arriving reverberating waves which have been delayed by scattering. The observed coda amplitude levels were empirically tied to regional and global moment tensors, providing a coda-based moment magnitude estimate. This allowed the determination of seismic moment for much smaller events (M<3.5).

Ultimately, however, even seismic moment is a limited concept and does not take into account the rupture characteristics of an event, often distinguished by its rupture area, source time, and stress drop, which can have a large effect on high-frequency observations and ground motions. Ideally, one would like to determine the source spectra of an event, which is the moment-rate from the low-frequency moment level through the corner frequency to the high-frequency rolloff. This can account for variations in stress that can produce different amplitudes for the same magnitude event.

The waveform coda can be used to reliably estimate source spectra for a wide range of events. More recent work has focused on making 2D propagation corrections (e.g., Phillips et al., 2008; Pasyanos et al., 2016). With 2D corrections, one can extend the stability of coda to higher frequencies, allowing one to determine the full spectra even for smaller events. An example is shown in Figure 13. One can then couple the observed spectra for the whole frequency band to earthquake and explosion models.

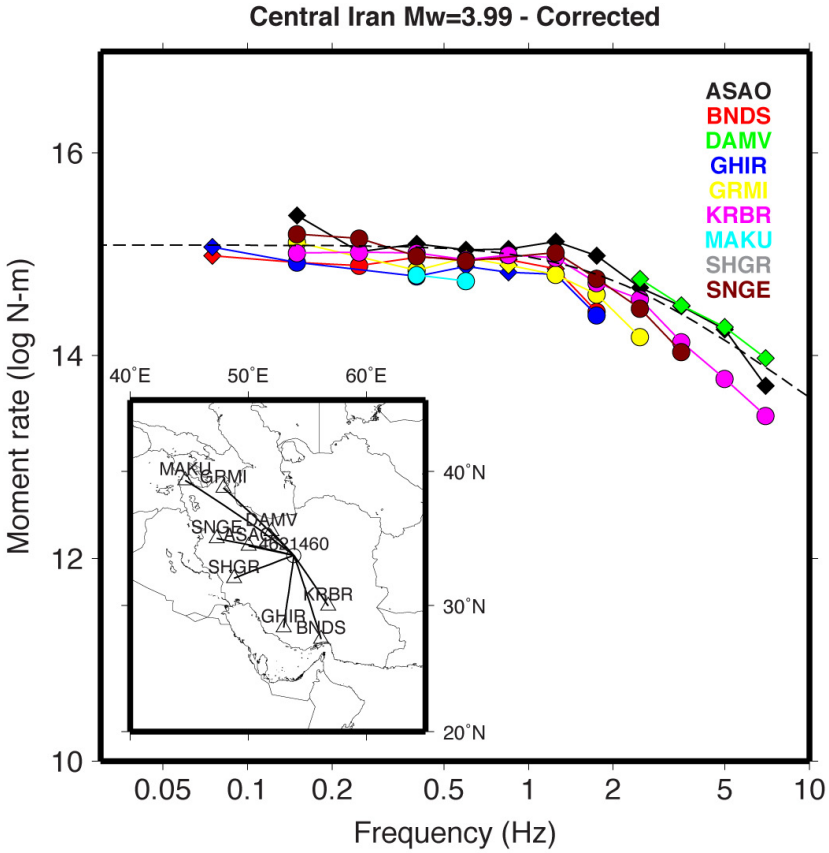

Figure 13. Source spectra from S-wave coda for an event in central Iran recorded at a number of stations using 2D propagation (from Pasyanos et al., 2016).

Future R&D

Improved estimates of the source size can be achieved by coupling the observed event spectra for the whole frequency band to existing and next generation earthquake and explosion models.

From surface-to-body-wave magnitude ratios to corrected regional phase amplitude ratios (WSO1)

Near the beginning of the atomic age a key challenge was distinguishing seismic waves caused by underground nuclear explosions from those of earthquakes (Leet, 1962). Combining teleseismic amplitude measurements made at variable frequencies initially solved the discrimination problem. The most effective of these measures was the ratio of long period surface-wave amplitudes to short period body-wave amplitudes (e.g., Evernden, 1969; Liberman and Pomeroy, 1969; Marshall and Basham, 1972; McEvilly and Peppin, 1972). These amplitudes were converted to standard magnitudes of Ms for long period Rayleigh waves and mb for short period body waves (see Figure 14), leading to the shorthand Ms:mb to describe the discriminant. Its success at separating explosions from earthquakes led Evernden (1969) to optimistically state: "The basic problem for differentiating earthquakes and underground explosions of magnitude 4 ¾ and greater by seismic criteria has been solved." Physical explanations in terms of depth and source time function and mechanisms differences came later, most notably in Stevens and Day (1985). Current assessments and historical background of Ms:mb by Selby et al (2012) show that the North Korean declared nuclear events did not separate particularly well, so the slope of the screening line was improved to agree with theory. However, small earthquakes still remain difficult to screen out and are the subject of current research.

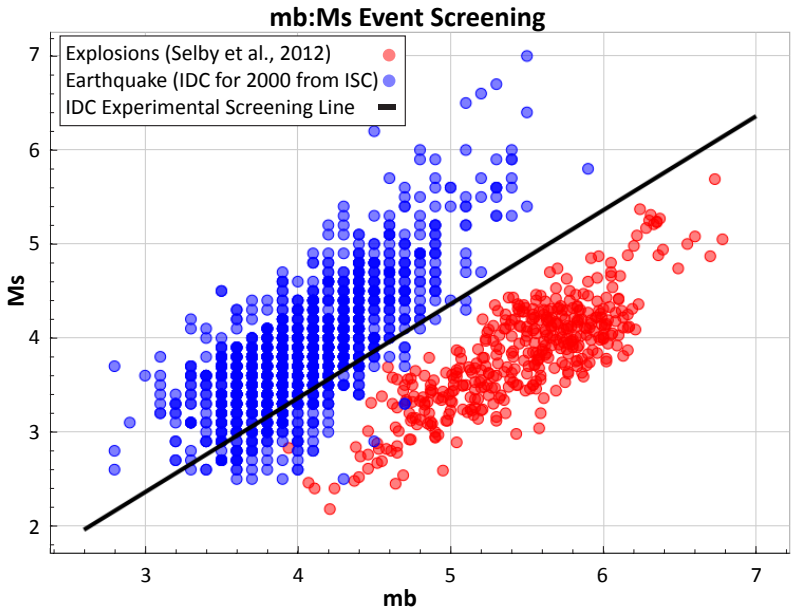

Figure 14. mb:Ms of earthquakes from the IDC Reviewed Event Bulletin (REB) and of explosions from Selby et al. (2012).

Because explosive sources are expected to produce significantly less shear wave energy than earthquakes, the ratios of compressional (P) to shear (S) wave energy is a straightforward and theoretically sound way to discriminate, as introduced by Willis et al. (1963). However, early attempts using analog seismic stations were disappointing (cf. Pomeroy et al., 1982). With the advent of digital recording in the 1980s, P/S values at a variety of frequencies were investigated and good performance was found at regional distances for frequencies generally above about 2-4 Hz (e.g., Baumgardt and Young, 1990; Kim et al., 1993; Walter et al., 1995; Taylor, 1996; Hartse et al., 1997). This approach was improved by a number of scientists by adding better site and path corrections, first 1D and then 2D, which is the current state-of-the-art (Phillips, 1999; Rodgers et al., 1999; Pasyanos and Walter, 2009).

The regional discriminants were formalized in the Magnitude and Distance Amplitude Correction (MDAC) technique (e.g., Taylor and Hartse, 1998; Walter and Taylor, 2001; Taylor et al., 2002). An error model and hypothesis tests for regional discriminants were developed in Anderson et al. (2009). MDAC corrects each regional phase (e.g., Pn, Pg, Sn, and Lg) amplitude as a function of frequency in an attempt to make amplitudes independent of distance, magnitude, and station.

Tutorial: Measurements for Event Screening

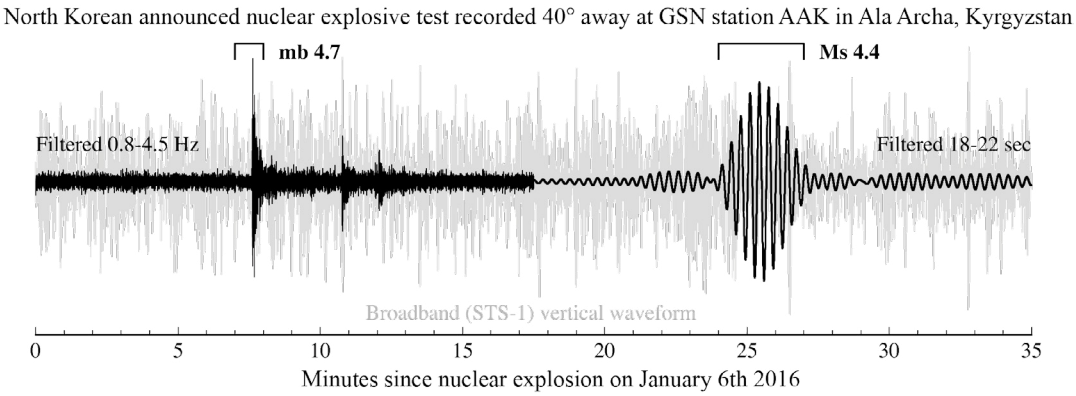

The relative amplitudes of compressional and surface waves gives insight into the type of source event, which is used in event screening. Explosions direct energy into compressional P-waves, thus the amplitude of the P-waves is high relative to the amplitude of the surface waves. Two magnitudes are commonly applied to distant events: mb is measured using the first few seconds of a teleseismic P-wave and Ms is derived from the maximum amplitude Rayleigh wave. Shown above is a recording of an announced North Korean nuclear explosive test with sections of the waveform bracketed that are used to calculate the mb and Ms. The raw waveform is shown in the background in gray. The waveform amplitudes are measured to obtain an mb of 4.7 and Ms of 4.4.

Current efforts to improve the MDAC approach aim to impart a physics-based model correction for the P/S amplitude ratios. The first practical step in this research was taken by Fisk (2006), who observed consistent differences between the corner frequencies of the different phases. Additional efforts have been made to explain the lack of discriminatory power for regional phase ratios at low frequency (1-4 Hz). Day et al. (1983) propose that this discrepancy is due to spall effects and Goldstein (1995) suggests that it is due to a propagation effect, where the higher modes of a shallow explosion are trapped in near-surface highly-attenuating layers so that at distance this energy is no longer observable. O'Rourke et al. (2016) support this mechanism with experimental observations at local and regional distance.

A more theory-focused approach is to use the full description of the seismic source provided by the seismic moment tensor as was done by Dreger and Woods (2002) and applied to nuclear explosive tests, earthquakes, and mine collapses in Ford et al. (2009). The discriminant can now test against a theoretical explosion or earthquake, thereby decreasing the possibility of surprise events that do not fit the empirical models as happened for Ms:mb with the 2006 explosion in North Korea (Kim and Richards, 2007), though regional P/S worked well (Hong, 2013). Hudson et al. (1989) and Tape and Tape (2012) have proposed ways to view these multidimensional discriminants for ease of understanding the explosion hypothesis.

Future R&D

Improvements to the explosion and earthquake source models, including uncertainty calculations, will make it possible for an explosion discriminant to be applied to an event in a new location. This enables event identification with a calculated confidence interval.

From narrow-band teleseismic explosion size estimates to full-spectral estimates of coupled explosion size and depth (WSO2)

Along with detection, location, and discrimination, the determination of explosive size, or yield, is a core function of nuclear explosion monitoring. Probably one of the most commonly employed methods of estimating explosion size is from teleseismic mb-derived yield. This usually takes the form of mb = A + B log W, where W is the yield in kilotons, A and B are empirically determined parameters, and mb is the body-wave magnitude. It is normally assumed that the explosion is fully coupled into rock. For example, using data from the Joint Verification Experiment (JVE), Murphy (1981a, 1996) (Figure 15) assigned the following formulas to the former U.S. nuclear explosive test site in Nevada and the former U.S.S.R. test site in Semipalatinsk, Kazakhstan:

$$mb = 3.92 + 0.81 \log W \text{ (NTS)}$$
$$mb = 4.45 + 0.75 \log W \text{ (Semi)}$$

Once mb has been calculated, one can solve for the yield W. The numerical values in the above equations are empirically based and attempt to simultaneously account for the material properties for the region, nominal containment depths, and an appropriate upper mantle attenuation along the path for the site. Similar relationships have been developed for Ms/yield (Stevens and Murphy, 2001), but these are generally regarded to be not as reliable as body-wave derived yields.

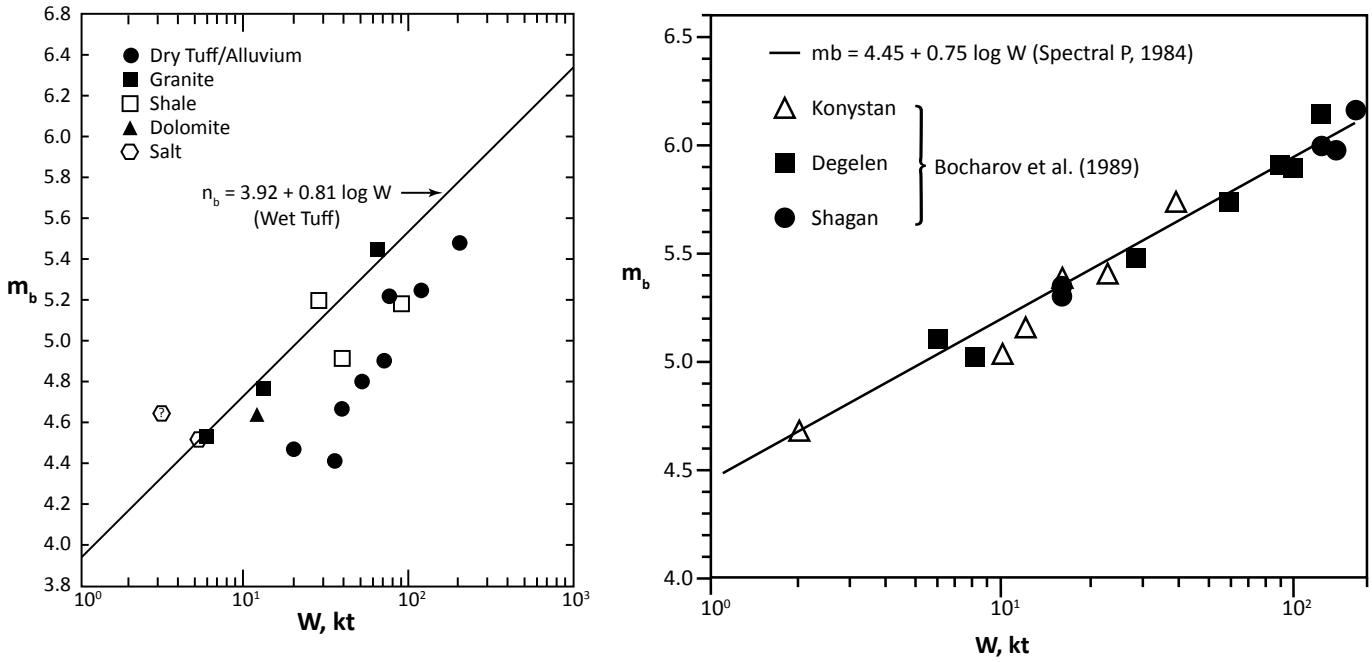

Figure 15. Regressions of mb and yield for events at NTS and Semipalatinsk (figures from Murphy 1981a, 1996).

The positive aspects of the method are its simplicity and its applicability to many events and test regions. One of the major downsides is that it is only applicable to events large enough to be recorded teleseismically, limiting its use on low yield events. Also, as an empirical method, the values of A and B need to be determined by regressing observed values of mb for events with known yields. In addition, hidden assumptions about the method and any changes to the material properties, scaled depth-of-burial, or attenuation properties from the calibration dataset can introduce errors.

All published magnitude-yield relationships (e.g., Mueller and Murphy, 1971; Denny and Johnson, 1991) have been calibrated using primarily data from events buried according to established containment rules. Consequently, there is an inherent tradeoff between yield and depth (e.g., Koper et al., 2008). An effort to determine the effect of depth-of-burial [h] on cavity radius and on observed seismic moment resulted in two proposed depth corrections both from Denny and Johnson (1991). They found that the size of the cavity radius decreases as -0.7875log[h] while the seismic moment decreases as -0.4385log[h]. The difference in rate was attributed to the damage zone around the cavity. Patton and Taylor (2011) introduced damage models to quantify this difference and found that the effects are minimized as the inherent strength of the emplacement material increases with depth. This topic is the subject of current research.

Magnitude-derived yield methods have been extended to regional magnitudes using mb(Lg), mb(Pn), etc. which can make it suitable to smaller events, but many of the same downsides (calibration, assumed depth, etc.) remain. A further extension and improvement of regional magnitudes are coda magnitudes (e.g., Mayeda et al. 2003; Murphy et al., 2009). These magnitudes are based on the highly stable waveform coda, which is less variable than the direct phases, making them suitable for single station estimates of yield (Figure 16). Usually performing with broadly applicable 1D coda calibrations, more recent work has focused on 2D propagation corrections (Phillips et al., 2008; Pasyanos et al., 2016).

Most recently, efforts have focused on making use of the broader spectra to estimate the coupled yield and depth, both of which affect the spectral shape. One such method is the waveform envelope method (Pasyanos et al., 2012). An example is shown in Figure 17. Because the method is physics-based, coupling parametric explosion source models to regional propagation models, the method can be applied to test sites which are not necessarily empirically calibrated and have potentially different shot points, propagation characteristics, and scaled depths.

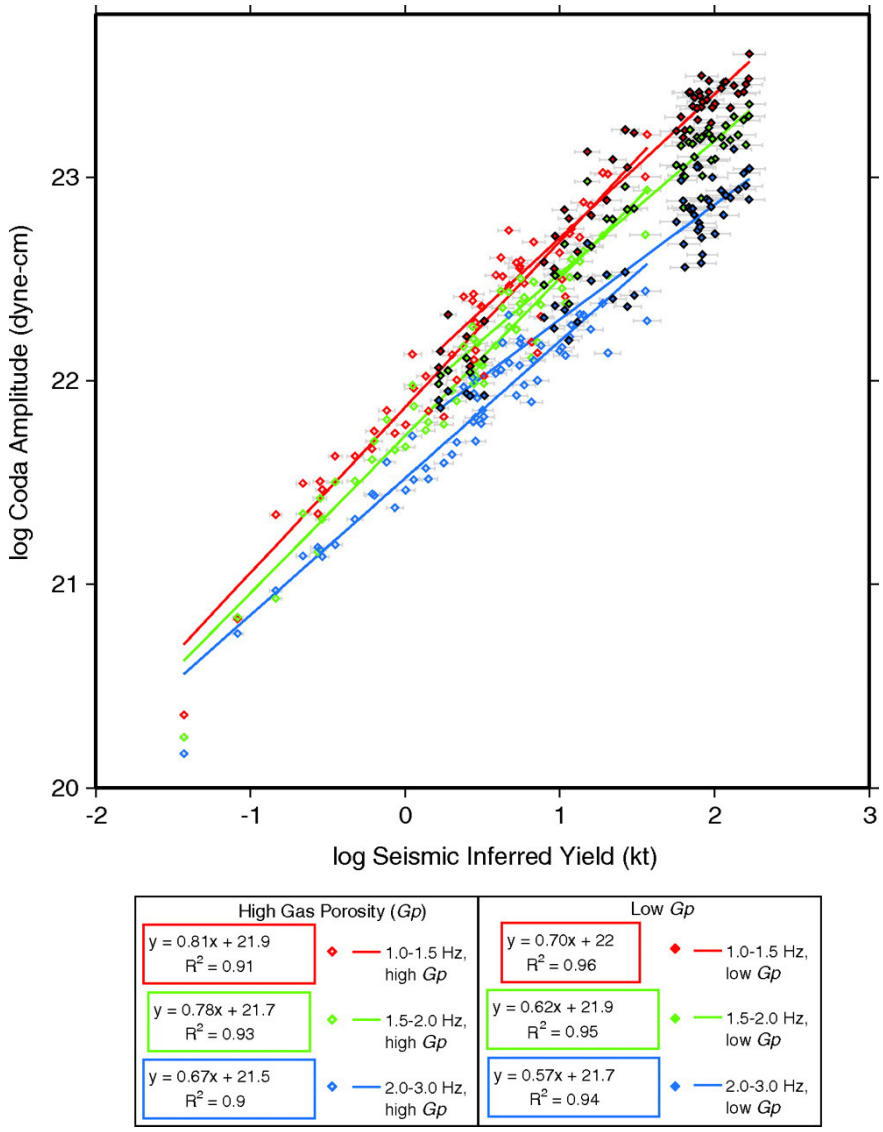

Figure 16. Coda amplitudes in various frequency bands (1-1.5, 1.5-2, 2-3 Hz) plotted as a function of observed yield (figure from Murphy et al., 2009).

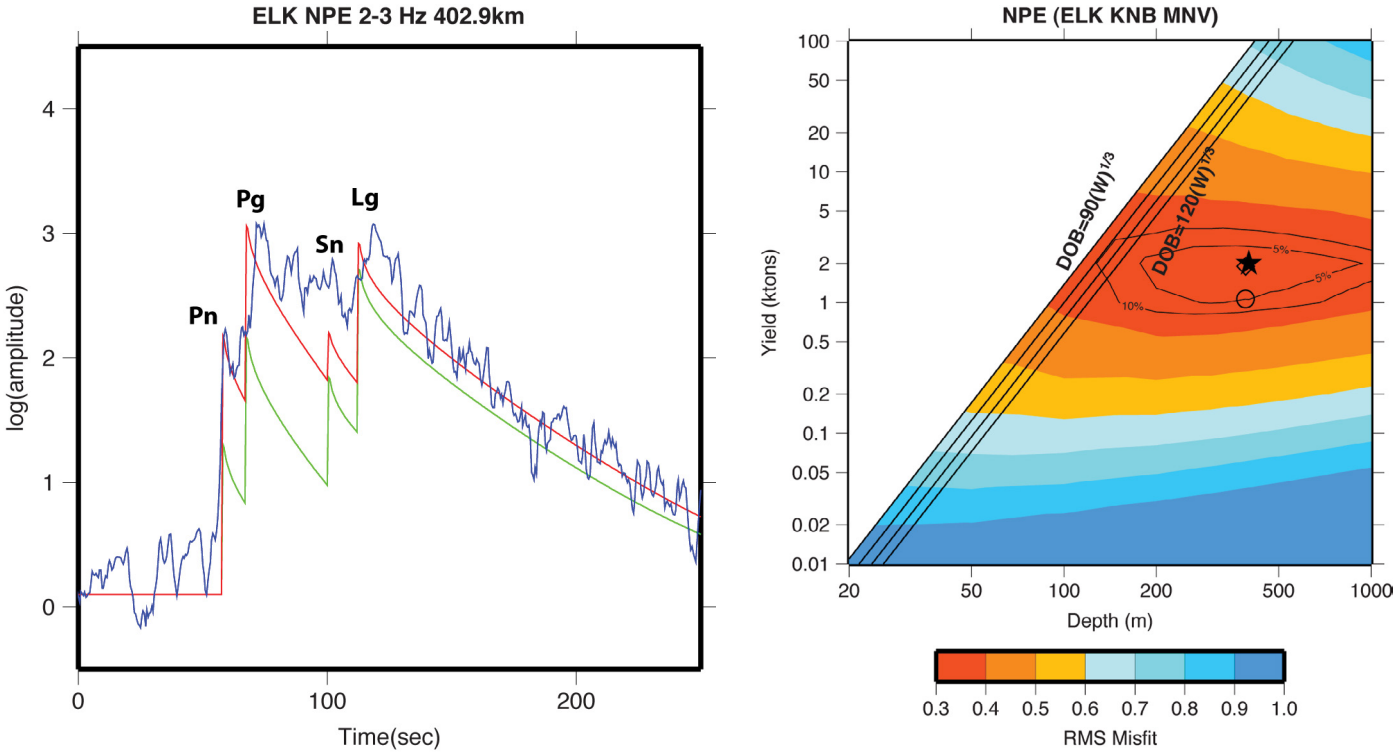

Figure 17. The panel on the left shows waveform envelopes for the Non-Proliferation Experiment (NPE), also known as the chemical kiloton experiment (Denny, 1994; Denny and Zucca, 1994). Data is in blue and lines show envelopes for earthquake (green) and explosion (red) source models. The panel on the right shows the root-mean-square misfit between synthetic envelopes and data for a range of yields and depths. The star shows the minimum misfit which matches the true yield of the event (Figures from Pasyanos, 2013).

The waveform envelope method has also proven applicable to events near the earth's surface where the loss of seismic coupling is taken into account (Pasyanos and Ford, 2015). Coupling issues have also been addressed in studies of explosions in low-coupling media (e.g., Murphy and Barker, 2009). Future work in this area of research will focus on extending explosion source models to be relevant to more earth materials, more emplacement conditions, and a wider range of yields and depths.

Numerous field experiments over the last three decades have provided data to answer R&D questions in nuclear explosion monitoring (NEM). On the next page is a table of NEM-relevant field experiments with key R&D results, remaining R&D questions, as well as selected references. Non-nuclear experiments can provide high fidelity data that may be used in place of historical nuclear datasets that typically were not recorded or archived for monitoring purposes.

Future R&D

Field experiments will continue to provide NEM-relevant datasets for improving explosion source models, making them applicable in a wide variety of geologic media and a wide range of yields and depths.

Seismoacoustic R&D Field Experiments Relevant to Nuclear Explosion Monitoring.

Year - Experiment Name (Acronym) - Location	R&D Results Obtained	Selected References	Remaining R&D Questions
1988 - Joint Verification Experiments (JVE) - Nevada Test Site, USA & Semipalatinsk Test Site, USSR	(1) Test site geology significantly biased traditional seismic yield estimates and that Ms & mb(Lg)-based estimates have less bias than mb-based estimates. (2) An improved model of the tectonic release was developed that improved accuracy of yield determination.	Douglas & Marshall, 1996; Walter & Patton, 1990; Walter & Priestley, 1991	- Are there seismic yield estimation techniques that are test site agnostic? - How does one reconcile the high corner frequency for P-wave spectra observed from the Soviet JVE compared to source models developed from nuclear explosions at the Nevada Test Site?
1993 - Non-Proliferation Experiment (NPE) - Nevada Test Site, USA	(1) Seismic waveforms from chemical explosions were found to be similar to, but higher in amplitude than, those produced by nuclear explosions at the same depth. (2) Chemical explosions may be used as a surrogate for nuclear explosions at the frequencies of interest to local and regional seismic explosion monitoring. (3) Seismic identification of mine blasts depends upon the quarries operational practices.	Denny & Zucca, 1994; Olsen & Peratt 1994; Stump et al., 1999	- Can the seismic wavefield be used to discriminate between nuclear and chemical explosions and if so, at what frequecies and distances?
1997 - Kazakhstan Depth of Burial Experiment (DOB) - Semipalatinsk Test Site, Kazakhstan	(1) Source depth had a positive influence on regional discrimination suggesting underground nuclear tests may be distinguished from industrial explosions. (2) A sparse regional seismic monitoring network was capable of locating low-yield underground explosions. (3) An improved model of spall was developed that is more consistent with near-field recordings of Rg waves. (4) S wave generation may occur by Rg-to-S scattering as evidenced by Rg & Lg amplitude consistency.	Phillips et al., 2001; Patton et al., 2005; Hartse et al., 2012	- What discriminants are most effective at separating undergound nuclear explosions from industrial explosions?
1999 - Arizona Cast Blast Experiment - Black Mesa, Arizona, USA	(1) Confirmed that variations in blasting practices have a significant impact on regional seismic waveforms and therefore limit the effectiveness of correlation-based detectors. (2) Modeling of cast blasts identified Rg azimuthal variation caused by horizontal spall. (3) Surface waves were primarily generated by ground impact of spalled material.	Bonner et al., 2003	- Are Rg radiation patterns an effective discriminant of cast blasts?
2003 - Arizona Source Phenomenology Experiment (SPE) - Black Mesa, Arizona & Southeast Arizona Copper Mine, USA	(1) Lack of confinement (e.g., surface rupture) reduced Rg amplitudes by up to a factor of 10. (2) The vertical blast wall introduced azimuthal variation in Rg with highest amplitudes behind the wall. (3) Regional and teleseismic ratio-based discriminants were effective at local distances when calibrated for local geology.	Hooper et al., 2006; Zeiler & Velasco, 2009	- Can Rg spectral ratios be exploited to discriminate between unconfined and confined explosions?
2006 - Alaska Frozen Rock Experiment (FRE) - Goldstream Valley, Alaska, USA	(1) Seismic amplitude spectra from explosions in frozen rock did have an increased corner frequency compared to those in unfrozen rock. (2) Frozen rock exhibited reduced shear wave generation that impacted high-frequency P/S discriminants. (3) In-situ velocity measurements were obtained for future modeling of explosions in frozen rock. (4) Parabolic equation models of infrasound propogation underpredicted amplitudes behind terrian features.	Bonner et al., 2009; McKenna et al., 2012	- What is the physical mechanism behind reduced shear wave generation in frozen rock? - What improvements can be made to infrasound propagation modeling to better account for amplitude variations introduced by topographic scattering?
2008, 2013 - New England Damage Experiments (NEDE) - Rock of Ages Quarry, Vermont, USA	(1) Detonation velocity had a notable influence on peak ground motion and the amount of fracturing and thus shear wave generation. (2) Rock damage caused a frequency-independent reduction in seismic amplitudes. (3) Shear-wave generation appeared to be largely driven by spallation. (4) Cavity radius in hard rock scaled as the cube root of yield and was independent of explosion type.	Leidig et al., 2010; Stroujkova et al., 2012; Stroujkova et al., 2015a,b; Stroujkova et al., 2016	- What are the physical mechanisms driving reduced shear wave generation from explosives with high detonation velocities?
2009, 2011 - Sayarim Infrasound Experiments - Sayarim Military Range, Israel	(1) Showed seismic and acoustic data can be combined to significantly better constrain yield, and height or depth, for near surface explosions. (2) Second shock delay time provided a stable and reliable estimate of yield. (3) Long-range infrasound propagation models were validated.	Bonner et al., 2013; Fee et al., 2013; Gitterman & Hofstetter, 2014	- Can long-range infrasound measurements provide accurate location and yield estimates? - Are there measurements that can be used to improve atmospheric models of the mesosphere?
2011, 2012, 2015, 2016 - Source Physics Experiments (SPE) - Nevada National Security Site, USA	(1) Explosion source models were revised to accommodate discrepancies observed over a wider range of yields and emplacements in hard rock. (2) Cavity radius measurements indicated a factor of 2 difference between the observed radii and that predicted from nuclear tests, which may be due to bulking of the surrounding material. (3) Shear-wave generation appeared to be largely driven by opening of tensile fractures and spallation.	Ford & Walter, 2013; Snelson et al., 2013; Rougier & Patton, 2015; Pitarka et al., 2015; Sammis & Rosakis, 2015; Steedman et al., 2016; Yang 2016; Saikia, 2017	- Will explosions emplaced in soft rock require additional adjustments to new chemical explosion source models? - Do new explosion source models predict the behavior of the seismic wavefield from explosions at the depths of earthquakes? - Does near-field source model match near-field raw spectral data?

From simple explosion source analytical models to physics-based numerical seismic calculations (WSO2)

A description of the explosion source underlies every aspect of nuclear explosion monitoring. It defines the type of waves that are received for use in location determination, it states how the hypothesis is formulated for discrimination, and it is a direct link to estimate explosive energy from seismic observables.

The explosion source was first described theoretically by Kawasumi and Yosiyama (1935). They considered the simplest physical system used to model seismic wave radiation from explosions, which is a spherical cavity in a homogeneous, isotropic, infinite elastic solid. Sharpe (1942) used their work to propose the solution for any arbitrary source-time function acting on a sphere, which he called the equivalent cavity (and later the elastic radius by Toksöz et al. (1964)).

The theoretical formulations were put to the test during World War II when many nations looked to seismology to understand explosions both in solid and liquid media. World War II was also the beginning of nuclear explosion seismology. Gutenberg (1946) described the far field acoustic and seismic waves of the first nuclear explosion.

Nuclear explosive test data of near-field and far field recordings could now be used to parameterize the existing theoretical models, which had been expanded by the work of Haskell (1967), von Seggern and Blandford (1972), and Helmberger and Harkrider (1972). An attempt at physical parameterization of the models was by Mueller and Murphy (1971), so that now the explosion source could be predicted based on source and medium properties. Recent attempts have been made to express the significance of the near-field source contribution (Saikia, 2017). An alternative approach taken by Denny and Johnson (1991) was to use regression to infer explosion source parameters from seismically-derived parameters like moment and corner frequency. The empirical parameters in these relationships continue to be refined as more data are analyzed. The current and future approach to improving understanding of the explosion source is to combine historical understanding with empirical analysis and numerical capabilities as was done by Rougier et al. (2011) and Xu et al. (2014).

Theoretical work on the explosion source continues due to an observed difference in long- and short-period derived source functions. Early work by Archambeau (1972) focused on the impact of tectonic strain release, which can explain much of the observed discrepancy (Day et al., 1987). Additionally, Patton and Taylor (2011) proposed that late time damage can account for such a discrepancy.

The theoretical explosion source modeled as a vibrating sphere, which is the system used as a basis for most far field approaches, does not produce shear waves, yet these waves are observed on far field seismograms from underground explosions. Therefore, this simple treatment of the explosion source is incomplete and unsatisfactory, especially since the ratio of compressional to shear energy is the basis of regional seismic explosion identification. An excellent review of shear wave mechanisms is provided in Baker et al. (2012ab).

Current and future work attempts to describe the full source process within the elastic sphere, which leads to the anisotropic, anelastic effects described by, for example, Vorobiev et al. (2015). This is pursued both experimentally by projects like the Source Physics Experiment (Snelson et al., 2013) and theoretically, as is done in Pitarka et al. (2015) and Yang (2016).

Future R&D

The effects of tectonic stress and joints on the explosion source need to be experimentally verified with observations of large explosions at great depths. This direct shear generation mechanism can then be compared with transfer mechanisms outside the elastic volume like topographic scattering and P and Rg transfer mechanisms.

From simple analytical models to physics-based numerical infrasound and overpressure calculations (WSO1)

Infrasound signals carry information about above-ground and shallowly-buried explosions. Explosion source models are important for discriminating events of interest from background signals, and for quantifying the energy content of explosive sources. Infrasound source models are important for nuclear explosion monitoring because they provide a means to functionally relate measured infrasound observations at receivers to source explosion properties.

A significant amount of research has been conducted with the aim to develop means of estimating various characteristics of an above-ground explosive source using the properties of the observed overpressure and infrasound wave. During the 1960s, 70s, and 80s, thermo- and hydrodynamic methods and the limited computing capabilities of the time were used to construct simple, 1-dimensional, numerical models for shock fronts in the atmosphere. These models led to physical scaling laws for the various characteristics of blast waves produced by explosions (Korobeinikov, 1971; Baker, 1973; Kinney and Graham, 1985). In the 1980s and 90s, data sets became more extensive and parametric blast wave models were developed using semi-empirical models informed by physical theory (ANSI, 1983; Douglas, 1987). More recently, high performance computing (HPC) capabilities including graphics processing unit (GPU)-based simulation frameworks have allowed for the development of high fidelity computational fluid dynamics (CFD) codes, which can model the propagation of blast waves in complex environments (e.g., Waltz et al., 2014). The current state-of-the-art methods for modeling blast wave propagation through complex environments leverage thermo- and hydrodynamics methods as well as damage models to account for interactions with the ground surface and structures in the source region. In addition to better understanding the near-source overpressure signal, more realistic modeling and physical understanding of the generation of the acoustic signal is needed for continued development and improvement of infrasonic yield estimation methods using observations hundreds or thousands of kilometers from the source (Pierce et al. (1971), Stevens et al. (2002), Whitaker and Mutschlecner (2008), Le Pichon et al. (2012)).

The scaling law methods and parametric models used for explosive infrasonic sources have proven to be useful in analysis of explosive yield (e.g., Koper et al., 2002). However, complications arise in cases such as a shallowly buried explosion or when emplacement of the explosion results in a radiation pattern inconsistent with the point-source assumption made by most models. Because of these complications, additional research is required to better account for the complicated radiation pattern of energy from the source when emplacement conditions are more complex. Of particular interest to such studies is the case of a near-surface explosion for which the energy is partitioned between the atmosphere and solid earth. In such a case, improved models will assist in estimating depth-of-burial or height-of-burst; however, preliminary studies have shown that the specific partitioning ratios are strongly dependent on the ground lithology (Ford et al., 2014).

Future R&D

Advancing high performance computing and computational fluid dynamics capabilities will allow increasingly accurate modeling of the propagation of the blast wave from an explosion through complex environments in the near-source region. Further from the source, these predictions can be handed off to linear infrasonic and seismic modeling methods to account for propagation to larger distances.

From separate treatment of mechanical waves in different media to combined analyses (WSO6)

Events near boundaries between the solid-earth, water, and air can generate waves that propagate in different media. Historically, these waves have been researched and analyzed separately by experts on the respective type of wave, leading to a somewhat artificial boundary between research areas. A separate treatment of these waves is appropriate in many cases, especially at long distances where many effects associated with coupling of energy across earth-water-air interfaces can usually be neglected. The combination of disparate data types provides an opportunity to more accurately discriminate and estimate the yield of explosive sources, especially at local distances. Modeling waves across the strong boundary in material properties that separates the solid earth and fluids remains a challenge that is being actively explored (e.g., Collins and Siegmann, 2015). Coupling of energy across solid/fluid interfaces is a complex problem, especially for sources that occur near the interface. For example, shallow-buried explosions can generate acoustic waves via a variety of processes that include gas-venting as well as excitation of the atmosphere by surface pumping (Vortman, 1965). The use of the Rayleigh integral to model the transfer of seismic to acoustic energy via surface pumping has recently been used to successfully model explosions (Jones et al., 2015), although improvements are needed for modeling high-frequency effects in the near-field. Coupling of energy from the atmosphere into the solid earth can generate seismic waves through direct loading of the surface by the overpressure from an incident acoustic wave. Simplifying equations for the transfer from acoustic to seismic wave motion at the surface have been developed (Murphy, 1981b) and successfully applied in several studies, however they are based on very simple fluid/solid half-space models and need to be extended for more realistic models. As a first step in this direction, recent work has applied the method of Murphy to layered media (Bonner et al., 2013).

The importance of future work on coupling effects is demonstrated by recent work on yield estimation for explosions near the solid-earth/atmosphere boundary (Ford et al., 2014). This work has developed empirical curves for seismic displacement and acoustic impulse as a function of the scaled height-of-burst from explosions. The use of these curves with equations relating overpressure and seismic waves to explosion yield has been shown to provide combined estimates of the yield and the height-of-burst (Pasyanos and Ford, 2015). Further numerical and experimental work is needed on characterizing wave coupling effects for a range of different surface geologies.

Future R&D

Through combined experimental and numerical research on the coupling of waves between the solid earth and atmosphere, improved discrimination and yield estimation of events should be made possible, especially at local distances.

From expert system to model-based event discrimination (WSO1, WSO3, WSO4, WSO5)

Under the Threshold Test Ban Treaty (TTBT), seismology was the core science for underground explosion monitoring and initially involved a seismic analyst processing large amplitude seismic waves that propagate largely through the mantle (as teleseismic events). With the moratorium on nuclear explosive tests, and with increasing capability to monitor small explosions, the integration of regional and teleseismic discriminants became necessary for seismic event screening. However, this teleseismic discrimination system could not be used in conjunction with newly developed regional discriminants, because there was no technical basis to judge relative confidence between the teleseismic/regional results. The Event Categorization Matrix (ECM) system overcomes this by combining all discriminants in an objective, statistically defensible framework. This early discrimination system, used to monitor the TTBT, was designed to emulate the analysis procedures of an experienced seismic analyst. It uses six seismic discriminants to identify explosions and earthquakes and additionally offers a technically defensible indeterminate decision. Initial development of an extensible screening framework (ECM) began with four of these discriminants mathematically formulated in Anderson et al. (2007): depth from traveltime (TT, p-value Y_{TT}), presence of long-period surface energy (LP, p-value Y_{LP}), depth from reflective phases (PP, p-value Y_{PP}), and polarity of first motion (FM, p-value Y_{FM}). The ECM system is constructed to be extensible; additional teleseismic, regional, or local discriminants can be readily included into the framework.

The developed framework consists of two fundamental components. First, for each discriminant – teleseismic, regional, or local – a probability model is formulated under a general null hypothesis. The veracity of this null hypothesis for each discriminant is measured with a p-value calculation that ranges between zero and one. A value near zero is inconsistent with an explosion. The p-value calculation is analogous to a sigmoid activation function utilized in neural network discrimination, however in the ECM system the p-value is strongly tied to physical basis interpretation through the formulated hypothesis. To illustrate, the teleseismic discriminants formulated for the initial development of ECM are summarized in Figure 18 in terms of an explosion characteristics null hypothesis and associated physical basis interpretation.

A p-value is not the probability that the null hypothesis is correct -- in fact, it is calculated assuming the null hypothesis is true. Assuming the null hypothesis is true and before observing data, a p-value is calculated as the probability of observing a discriminant as extreme or more than the p-value. After observing data, a p-value is conceptually a measure of evidence against the null hypothesis. This is the case when presenting the analysis of several discriminants in one ensemble table. Because a p-value is derived from an observed discriminant, it is also a discriminant. A statistical test of hypothesis is essentially inference by contradiction. A null hypothesis is assumed true and remains true unless data contradicts the hypothesis.

The mathematics of constructing a formal hypothesis test requires that an alternative hypothesis also be defined. For example, the null hypothesis for a depth discriminant might be that the event depth is less than or equal to 10 km, and the alternative hypothesis is an event depth greater than 10 km. The mathematics of hypothesis test construction provides a test statistic, that is, a numerical calculation of the data that

Future R&D

Reducing the detection false-alarm rate, while maintaining an extremely low probability of missed events, can be achieved with ECM extensions. Examples of future ECM advances include shallow crust discriminants and additional source types. New discriminants can be integrated into the framework as follows: 1) the seismic theory of the discriminant must be incorporated into an appropriate probability model, 2) a hypothesis test must be formulated, and 3) the result of the test must be summarized as a p-value calculation. The mathematics does not need to change when new discriminants and/or source types are added.

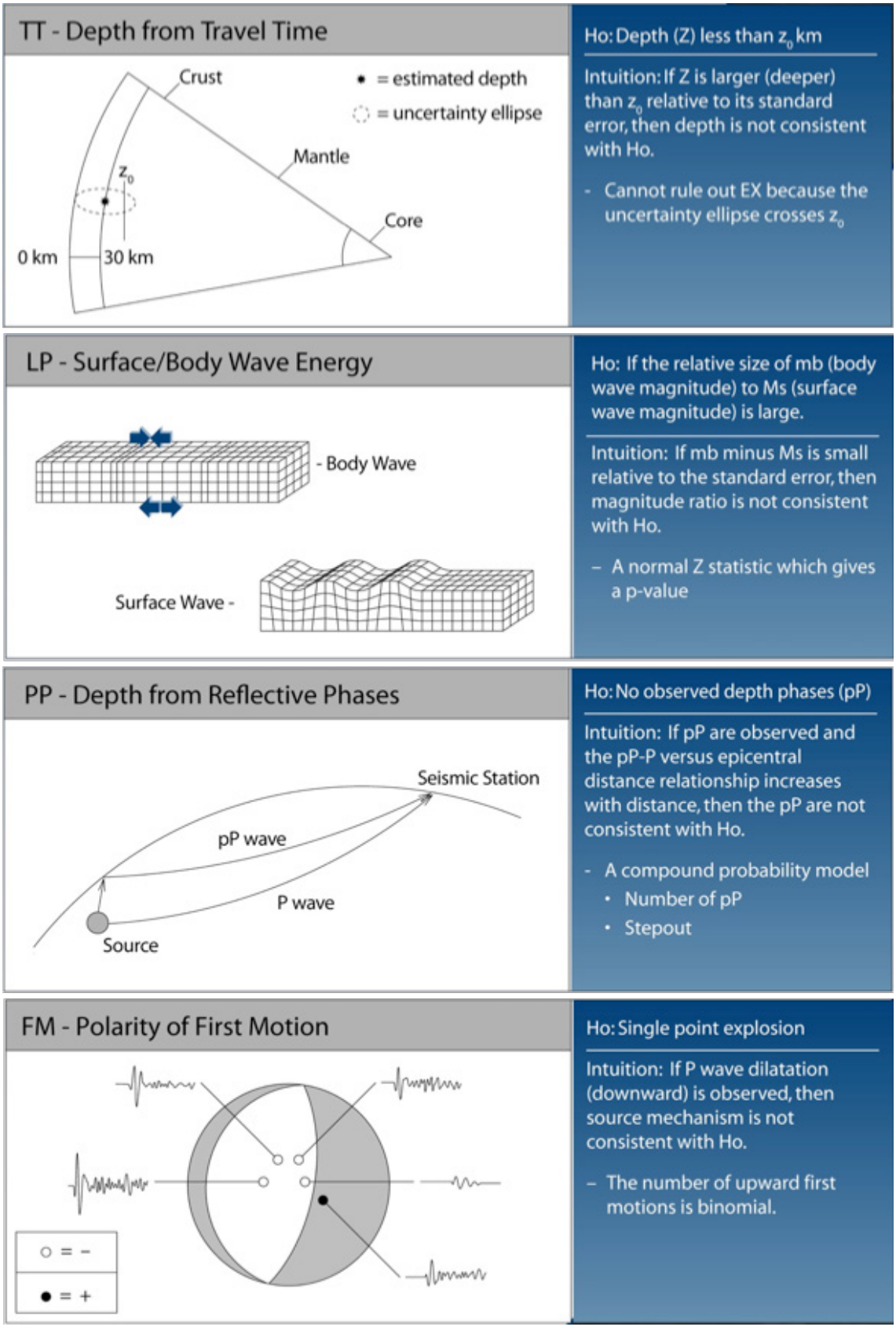

Figure 18. In the ECM system, discriminants are formulated as a hypothesis (Ho) test that an event has explosion characteristics. The statistical and physical basis for teleseismic discriminant hypothesis tests is summarized in this figure.

can be used to assess the veracity of the null hypothesis. A p-value is computed with the null hypothesis probability model, and it is the probability of observing a test statistic equal to, or more than, the observed test statistic. For example, if an estimated depth, standardized by its associated standard error, is inconsistent with event depth less than or equal to 10 km, then the p-value is small and the alternative hypothesis is rejected.

In the second component, individual p-values are combined to formulate a unified decision with statistical classification (categorization) methods (McLachlan, 2004; Dumbgen et al., 2008; Anderson and Taylor, 2002; Anderson et al., 1997, 1999, 2007, 2010a, 2014), and an event can be declared:

- consistent with historical explosions,
- not consistent with historical explosions,
- consistent with an explosion and at least one other source (Indeterminate), or
- not consistent with all sources (Unidentified).

The declarations "Indeterminate" and "Unidentified" are technically defensible and provide the basis for further analysis. With the ECM system formulated with teleseismic discriminants, it was extended to include regional discriminants (Anderson et al., 2009).

Some categorization methods to combine individual p-values include Regularized Discrimination Analysis (RDA) including Linear (LDA) and Quadratic Discrimination Analysis (QDA), sequential Classification and Regression Trees (CART), Kernel Discrimination, Logistic Discrimination, and Fisher's Linear Discrimination. Transparency is of key importance to both the enhancements of individual discriminants and the mathematics of combination. A critical requirement for ECM was that it retains, in every respect, the physical basis of discriminants. A study of several important selection criteria for each of the methods revealed that no one method is best on all issues. For example, an aggregation method must appropriately compensate for missing discriminants. Missing discriminants are quite common in seismic signal processing and must be addressed in a multivariate discrimination system. Missing data can occur if a station is offline or the signal is simply not measurable, e.g., surface-wave seismic signals for extremely deep earthquakes. An important aspect of future discrimination research is the construction of discriminants in cases where the energy signal is clipped by the seismometer or when knowledge of a signal to noise threshold can be reasonably exploited (Elvers, 1974; Anderson et al., 1999). The ECM system can fully utilize these advanced discriminants by formulating the discriminant as a test statistic for a hypothesis test. Seismic measurements can be missing from calibration samples used to build and test the discrimination rules as well as at the operational stage when unknown events are analyzed. RDA and CART effectively mitigate the issue of missing discriminants in an operational setting. All of the methods are sophisticated enough to achieve essentially equivalent performance (Hand, 2006).

The ECM system is modular, and the mathematics to aggregate standardized discriminants is operationally independent of the construction of new discriminant hypothesis tests. This extensibility is an important advance for the future to resolve fundamental monitoring questions: Where is the seismic event located? What is the source type for the event? If an explosion, what is the event size? ECM meets the operational requirement of year-to-year consistency from the model in treaty monitoring operations and reporting, which are critical to defensibility and credibility.

Signal Propagation - Accounting for Changes through Physical Media

The main value to nuclear explosion monitoring of studying waveform signal propagation is elucidating how it impacts event detection and location, as well as how it provides insight into event discrimination and magnitude/yield estimation and improves waveform prediction. Understanding radionuclide signal propagation is mostly useful for estimating uncertainties related to source and location. The event source is generally not directly observable. Consequently, in the observed signal, one must account for degradation as it propagates before it is observed at recording stations. A description of signal propagation research trends as they relate to seismic, infrasound, hydroacoustic, and radionuclide signals follows.

From global to local seismic models (WSP3)

Accurate knowledge of the earth's 3D structure is essential to successfully fulfill the nuclear explosion monitoring mission. This involves, at a minimum, the detection and location of seismic events around the world to identify non-natural events. Central to this endeavor are accurate seismic and atmospheric models for the correction of propagation effects on seismic and infrasonic waves.

The seismic and acoustic signals observed by monitoring stations undergo complicated evolution as they propagate from the source to the observer's location. When an earthquake or underground explosion occurs, the seismic waves that are generated propagate through the earth, reflecting and refracting at different interfaces and illuminating its 3D structure, while also carrying the signature of the source. Similarly, the acoustic waves propagate in the atmosphere and are influenced by changes in the speed of sound, which vary with altitude, temperature, and the speed and direction of the winds. The seismic wavefield recorded for many events at many stations around the world can be used to image the structure of the earth using tomographic approaches. Seismic tomography, first introduced 40 years ago (Aki et al., 1977; Dziewonski et al., 1977), is still a rapidly developing field, and provides important insights into unraveling our planet's present and past dynamics and the driving forces for plate tectonics.

Accurate location of seismic events requires minimizing the difference between observed and predicted arrival times and waveforms. While a location error of tens of kilometers can be adequate for plate tectonics studies, a smaller error is required to guide an on-site inspection, such as under the Comprehensive Nuclear-Test-Ban Treaty (CTBT) which allows a maximum inspection area of 1,000 km^2. The better and more comprehensive the model used to predict the arrival times, the more accurate the location of the event and the smaller the associated error will be. On the other hand, accurate seismic event locations also feed back to other forms of tomographic studies such as amplitude and waveform, which are essential to other aspects of the nuclear monitoring mission. Reducing location error and providing proper uncertainty estimates are critical for input to tomographic algorithms for higher-dimensional earth models. There are many seismic location methods available, summarized by existing review articles (e.g., Bondár et al., 2014 and references therein), from standard single-event location to relative relocation, as well as methods using waveform cross-correlation (Richards et al., 2006).

Since the first adaptation of tomographic methods to seismology, extensive theoretical, experimental, and computational work has been done in the general geophysical community as well as the monitoring research community, such that tomography is now a standard procedure for imaging properties of the earth and atmosphere. For further details on different aspects of tomography, please refer to the trends "From ray theory to full waveform" and "From regular to irregular parameterization."

Signal Propagation - Accounting for Changes through Physical Media

Until recently, most studies have relied on only a small fraction of the information contained in an observed seismogram, i.e., the traveltimes and amplitudes of seismic phases that are well separated in the time domain, and many researchers have generated compressional (P) and/or shear (S) wave velocity and attenuation models at global and regional scales that have been used for our monitoring mission (e.g., Phillips et al., 2000, 2007; Li et al., 2008; Myers et al., 2010; Simmons et al., 2012; Ballard et al., 2016b).

The use of full waveforms was introduced early on in global seismology (Woodhouse and Dziewonski, 1984; Li and Romanowicz, 1995), but the simplified theoretical assumptions on wave propagation used put strong limitations on acceptable lateral variations in structure, which were particularly inadequate for the earth's crust and uppermost mantle. Indeed, the depth to the crust-mantle discontinuity, the Moho, can vary laterally by a factor of 10 or more, hardly a situation where quasi-linear "crustal corrections" should apply. Still, several generations of 3D shear wave velocity models of the earth's mantle at the global and continental scale have been developed, and there is now good agreement on the longest wavelength structure (e.g., Trampert, 1998; Romanowicz, 2008). However, structure at finer scales needs to be better constrained, including lateral gradients across structural boundaries and amplitudes of lateral variations. Fine scale structure needs to be known accurately for physical interpretation as well as for accurate propagation corrections.

The shift in the monitoring community from global to regional and even local tomographic models, was partly supported by the realization of the need for representing the earth's structure at finer scales.

In the last ten years, new horizons have opened up in earth structure imaging, with the advent of powerful numerical methods to compute the seismic wavefield in realistic 3D elastic structures with unprecedented accuracy. In particular, two theoretically equivalent methods now make it possible to exploit all of the information contained in regional and teleseismic seismograms. The Spectral Element Method (SEM) (Komatitsch and Vilotte, 1998; Komatitsch and Tromp, 1999) is a numerical method, recently introduced in global seismology, which solves the wave equation in its integral form without any assumptions on the characteristics of the structure. The first local (Tape et al., 2009), regional (Fichtner et al., 2009), and global (Bozdag et al., 2016; Afanasiev et al., 2016) models based on SEM and derived from adjoint tomography have been published. Because of its relative simplicity in implementation, the finite-difference (FD) method, which also solves the complete wave equation, has also been widely used in seismology (e.g., Virieux, 1986;, Zhang et al., 2012). By calculating the Green's tensors from the receivers using the FD method, the scattering integral method (Zhao et al., 2005; Zhang et al., 2007; Zhang and Shen, 2008) differs from the adjoint method in its computational approach – refer to Chen et al. (2007a) for a comparison of both methods. Crustal (e.g., Chen et al., 2007b; Lee et al., 2014) and upper mantle (e.g., Gao and Shen, 2014a; Covellone et al., 2015) models following the scattering integral method have also been recently published. Nevertheless, challenges remain due to the heavy computations involved, imposing limitations on the frequency range, size of region studied, representation of the crust in the case of mantle imaging, and/or means to compute the kernels for the inverse step of the imaging procedure. Another important remaining question is that of sensitivity of the solution to the starting model. While the Bayesian framework provides estimates of errors in the model, there is no simple way to compute them in inversions that are based on an adjoint formalism (e.g., Fichtner and Trampert, 2011).

Recognizing the need for regional accurate probabilistic 3D crust and upper mantle models, a well-known class of algorithms adopted and used within the nuclear explosion monitoring community is Monte Carlo Markov Chains (MCMC). The MCMC approach allows researchers to broadly sample the elastic and inelastic parameter space and construct families of models that provide satisfactory fits to a combination of geophysical parametric datasets (e.g., Sambridge et al., 2006; Pasyanos et al., 2006; Bodin and Sambridge, 2009a; Hauser et al., 2011). One of the advantages of these stochastic approaches is that they provide a way to estimate uncertainties in the model parameters. A major limitation is that they restrict the number of parameters to be considered, due to computational considerations, making them impractical for problems with many free parameters, such as 3D global tomography models.

The deterministic counterpart to these stochastic models is the recently adopted tendency of combining disparate datasets into a simultaneous joint inversion to better constrain the crustal and upper mantle seismic structure. As discussed above, tomography is typically performed with a single data type (either traveltime or surface-wave dispersion, for example), and this results in incomplete retrieval of earth properties due to sensitivity limitations inherent in each of the data types. In the last fifteen years, more attention has focused on simultaneous inversion of two or more seismic data types whose sensitivities are complementary, resulting in improved resolution. Julià et al. (2000) first combined teleseismic P-wave receiver functions with surface-wave dispersion measurements to improve the shear-wave structure underneath a seismic station. This technique has been applied in many other studies. Motivated by the shortcomings of single-parameter inversion methods in accurate prediction of both seismic waveforms and other geophysical parameters, Maceira and Ammon (2009) developed a method to jointly invert surface-wave dispersion measurements and gravity observations for shallow seismic structure. They also showed its application to improving our monitoring capabilities for short period surface waves at regional scales. Since then, many models resulting from a combination of different datasets have been developed at global (e.g., Simmons et al., 2010), regional (e.g., Kgaswane et al., 2009; Chang et al., 2010; Tokam et al., 2010; Syracuse et al., 2016) (Figure 19), and local (e.g., Zhang et al., 2014; Syracuse et al., 2015) scales.

Future R&D

Traditional traveltime tomography still has many limitations and, in the future, these tomographic results need to be interpreted jointly with other types of geophysical data. Full waveform approaches overcome this difficulty, but for better imaging of crustal heterogeneities required for local monitoring, we need higher frequency full waveform models and/or more sophisticated and improved joint inversion techniques.

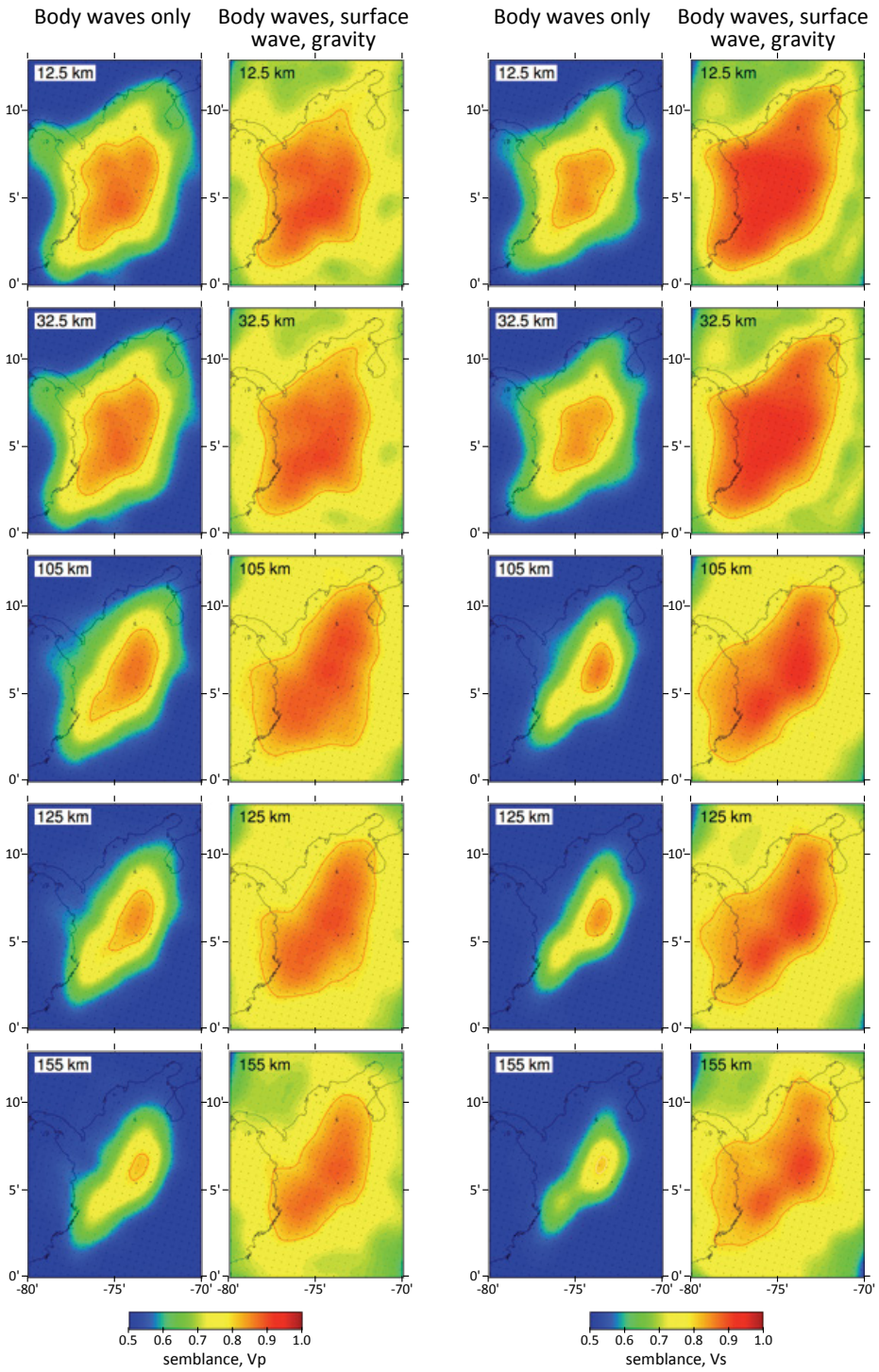

Figure 19. Joint inversions of multiple geophysical data types improve model recovery in comparison to inversions using a single data type. Synthetic data were created for 100 random velocity models, the data were inverted, and the semblance between each recovered and input velocity model was calculated (semblance=1 if recovery is perfect; semblance=0.5 if nothing is recovered). For each model, two inversions were conducted, one using only body wave data, and one using body wave, surface wave, and gravity data. For each of the two sets of inversion, the results of the 100 tests were averaged and are shown here as horizontal slices at the indicated depths. The left two columns show the results for Vp, the right two columns show the results for Vs. The higher semblance values, indicated by warmer colors, show the drastic improvement in velocity recovery when multiple data types are jointly inverted, as opposed to one data type. The red line indicates a semblance value of 0.8, which delineates the well-recovered regions of the velocity models (Syracuse et al., 2016).

From limited to broadband, multi-parameter surface-wave dispersion and attenuation models (WSP1, WSP3)

One significant trend is major improvements in the quality and resolution of surface-wave dispersion and attenuation models, driven by enhancements in data type, coverage, and quality, and advances in measurement and inversion methods. Previously, these models were limited by resolution, bandwidth, phase, and dispersion type.

In contrast to body waves, surface waves travel along the surface of the earth. Love and Rayleigh waves are produced from waves of the SH (horizontally-polarized S) and P-SV (P and vertically polarized S) systems, respectively, interacting with the free surface or slow velocities found near the earth's surface. As dispersive waves, their velocities are a function of frequency. These velocities can be characterized by the velocity of the peaks and troughs (phase velocity) or the velocity of the energy (group velocity). Amplitudes of surface waves decay with propagating distances reflecting the attenuation properties of the shallow earth structure.

The importance of surface-wave dispersion and attenuation models in explosion monitoring is multi-fold, including event discrimination and mathematical representation of the earth structure. The surface-wave magnitude Ms (discussed under the Source Physics trend "From narrow-band magnitude estimates to full spectral estimates of the seismic source") is one component of the long-established mb:Ms seismic discriminant. Surface waves are also quite effective in characterizing earth structure, particularly shallow earth structure (crust and upper mantle) that can be difficult to characterize broadly using body waves. The sensitivity variation of kernels for different frequencies and different wave types allows for excellent depth resolution. For example, longer-period (lower-frequency) waves are sensitive to deeper structure, and Love waves are sensitive to shallower structure than Rayleigh waves. They are also typically a component of joint inversion models (discussed in the trend "From global to local seismic models").

Early surface-wave analysis (e.g., Oliver, 1962) focused on its dispersive characteristics, noting, for example, generally faster velocities at longer periods (lower frequencies) and noting major differences between Love and Rayleigh velocities (Figure 20). Large differences were also observed between oceanic and continental crust due to the significant differences in crustal thickness and lithospheric thickness between them. Mathematical methods were developed to calculate fundamental and higher-mode surface waves in layered elastic media (Harkrider, 1964; Harkrider, 1970), making observed dispersion easier to interpret.

With time, measurements of dispersion for both Love and Rayleigh waves were numerous enough to tomographically invert them for 2D variations in either phase or group velocity. These models were event-based, that is, dispersion was measured along a path from an earthquake to recording stations, normally for a wide period band. These models were first regional, then continental, and finally global in extent, with models increasingly improving in quality and resolution.

Future R&D

Accurate knowledge of surface waves properties, such as velocity and attenuation, is crucial for monitoring missions (e.g., seismic discrimination). While surface wave velocity tomography has evolved considerably in the last years, knowledge of surface wave attenuation is much more limited. Taking advantage of new computational capabilities and theoretical developments, and the vast amount of available data, researchers should focus on improving and obtaining global surface wave attenuation models that fully account for elastic effects such as focusing and defocusing.

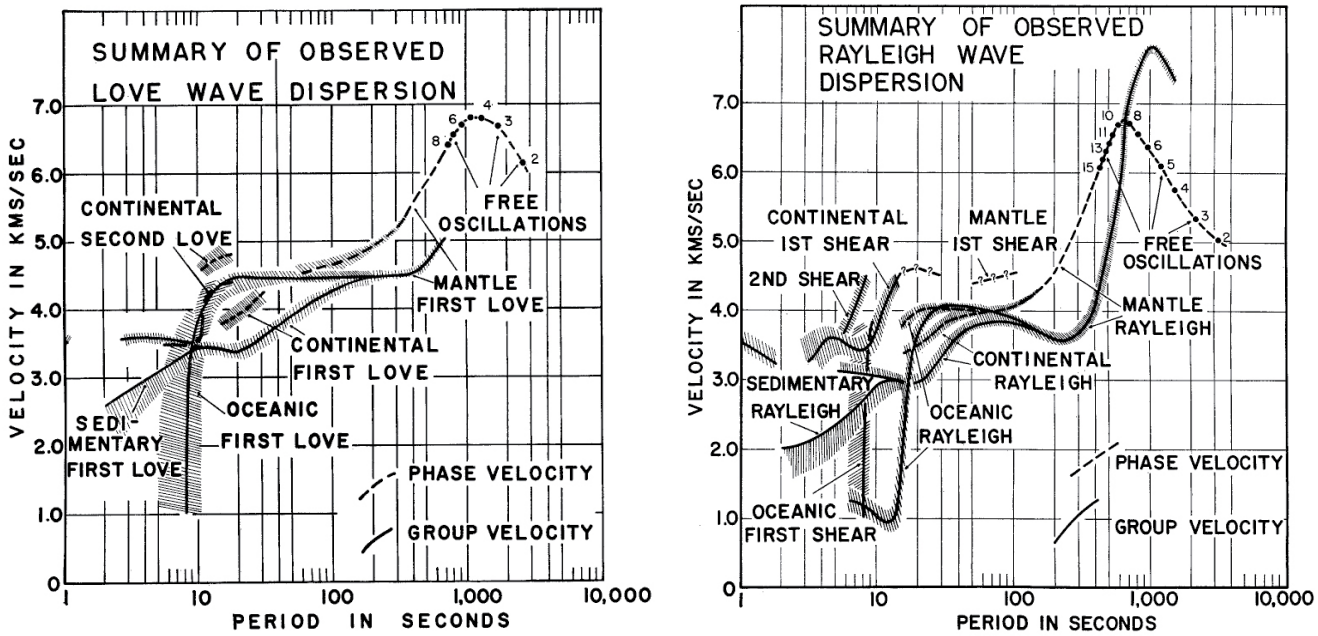

Figure 20. 1D Love (left) and Rayleigh (right) group velocity dispersion curves for oceanic and continental regions (from Oliver, 1962)

There have been many of these models, but some that were developed for explosion monitoring purposes were the dispersion models of Ritzwoller and Levshin (1998), Stevens and McLaughlin (2001), Maceira et al. (2005), Pasyanos et al. (2001), and Pasyanos (2005). An example of 20 second Rayleigh wave group velocities from the LLNL model is shown in Figure 21. At this frequency, Rayleigh waves are sensitive to the upper 20 km of the earth, so they reveal crustal thickness differences between oceanic (faster velocities in blue) and continental crust as well as deep sedimentary basins (slower velocities in red).

These dispersion maps are a key component in building surface-wave-derived models, including those in Eurasia (Pasyanos and Walter, 2002; Tkalcic et al., 2006; Gok et al., 2007; Di Luccio and Pasyanos, 2007; Pasyanos et al., 2007; Maceira and Ammon, 2009; Gok et al., 2011) and Africa (Benoit et al, 2006; Pasyanos and Nyblade, 2007; Tokam et al., 2010), but also in testing *a priori* models (Pasyanos et al. 2004), to determine lithospheric thickness (Pasyanos, 2010), and in stochastic models (Pasyanos et al., 2006; Hauser et al., 2011).

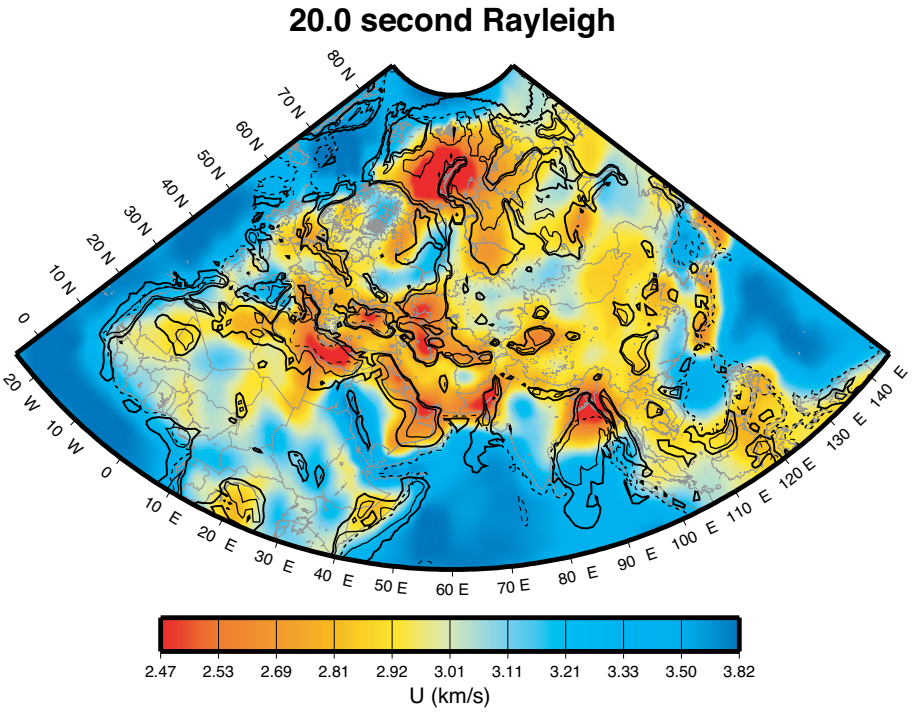

Figure 21. 20 second group velocity model for Eurasia and North Africa (from Pasyanos, 2005)

The most recent models have been driven by several new techniques. The first is the use of ambient noise to estimate the dispersion between stations rather than event-based ("ballistic") measurements between source and station (Weaver and Lobkis, 2001; Sneider, 2004; Shapiro et al., 2005). This results in better coverage of aseismic regions like northern Africa, and well-instrumented regions like the United States, as well as providing complementary coverage to ballistic measurements. Ambient noise techniques are also better able to provide coverage for shorter periods that are more difficult to measure using event-based measurements.

The second technique uses cluster analysis to make many dispersion measurements (e.g., thousands of stations recording the same event) simultaneously for a narrow frequency band (Ma et al., 2014). Envelopes are computed for the narrow-band filtered signals, and the functions are then grouped by similarity and used to identify outliers and make group velocity measurements. A comparable method allows measurements of phase velocities (Ma and Masters, 2014). This results in unprecedented path coverage (Figure 22).

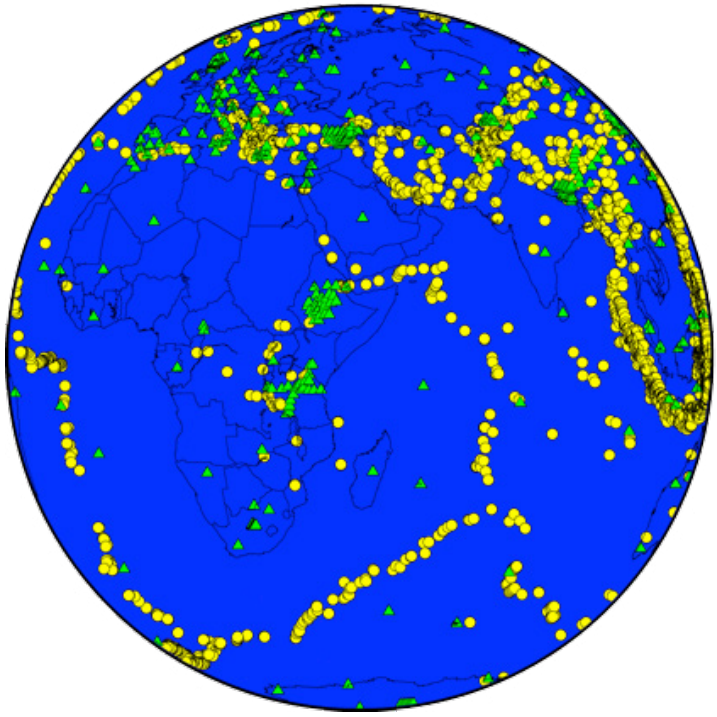

Figure 22. Path coverage of surface waves for 50 s Rayleigh wave group velocity with events (yellow circles), stations (green triangles), and paths (blue lines) which due to their exceptional coverage appear solid blue (from Pasyanos et al., 2014).

Due to the sensitivity of surface-wave attenuation to elastic heterogeneities, accurate surface-wave attenuation models are more difficult to constrain, particularly for shorter periods. Mid- and short-period models, which are more relevant to explosion monitoring, have been developed only for certain regions of the earth. These models include a 20 second Rayleigh-wave attenuation model for Asia (Yang et al., 2004b), mid-period attenuation models for Eurasia (Levshin et al., 2010), and an attenuation model for the Middle East (Pasyanos, 2011). Figure 23 shows the Rayleigh-wave Q model of Levshin et al. (2010) at multiple frequencies.

The use of ambient noise and cluster analysis, along with significantly improved station coverage, result in high-resolution global dispersion models. These models consist of group and phase velocity, both Love and Rayleigh waves, over a broad frequency band. For surface-wave attenuation models, the main challenge is focusing, defocusing, and multipathing caused by elastic heterogeneities (Lin and Ritzwoller, 2011; Lin et al., 2012; Ma et al., 2016). When developing their attenuation models, Yang et al. (2004b) employed certain measures such as phase-match filtering in an attempt to alleviate the elastic effects. Future research will be focused on new inversion methods, such as the wave-equation-based method (Lin et al., 2012), to formally account for elastic effects and on using additional data types, such as ambient noise (Zhang and Yang, 2013), to develop surface-wave attenuation models.

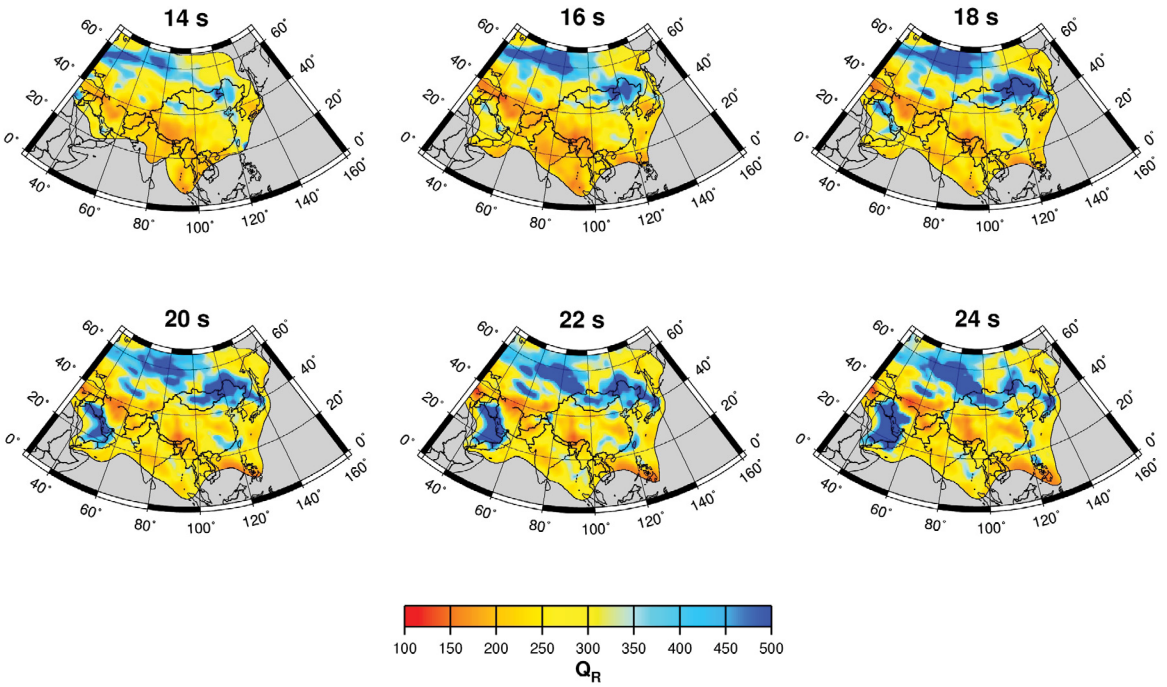

Figure 23. Tomographic maps of Rayleigh-wave Q across Asia and surrounding regions at indicated periods (from Levshin et al., 2010).

From low-resolution *a priori* crustal models to high-resolution data driven crustal models (WSP1, WSP3)

Crustal models are essential for a number of explosion monitoring goals. Accurate crustal models are needed in the development of global 3D tomography models, such as LLNL-G3D (Simmons et al., 2011, 2012, and 2015) and SALSA3D (Ballard et al., 2016b), which are being developed to produce the best event locations. Models are also used to generate Green's functions for moment tensor analysis. There have been significant advances in the lateral and vertical resolution of baseline crustal models, evolving from low-resolution models completed by geophysical analogy to higher-resolution data-driven models. Global tomography of the mantle requires the use of a crustal model, and imperfect crustal models are a significant source of error in tomography results. There are currently many global tomography models in development for science and monitoring applications which will benefit from more accurate crustal models.

The CRUST5.1 model (Mooney et al., 1998) was an early model developed specifically for tomography purposes (Figure 24). Crust models are hard to develop globally in a broad sense, so other methods such as geophysical analogy were used to fill in the large holes of the model. In this technique, it is assumed that any unsampled craton (a large stable portion of a continent), for instance, is similar to other cratons, any unsampled orogenic zone is similar to other orogenic zones, etc. This technique has since been shown to be

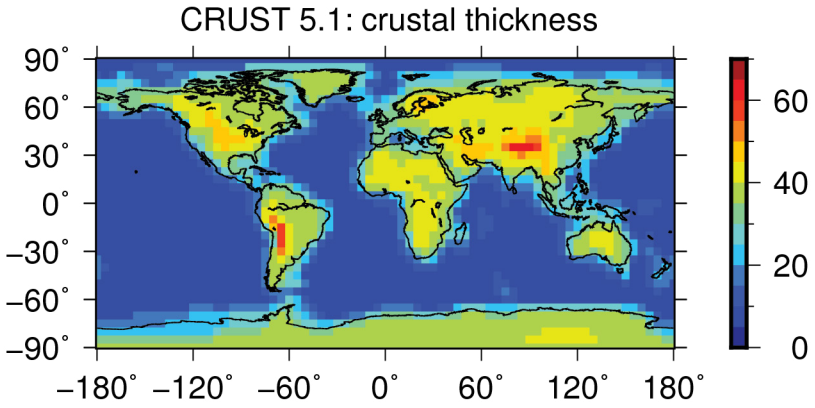

Figure 24. Crustal thickness (in km) from the CRUST5.1 model.

of only limited utility, and there are large differences in major lithospheric parameters (e.g., crustal thickness and upper mantle velocity) within these broadly defined regions.

While the 5-degree resolution of the model was sufficient for the tomography models of the time, increasing seismic data and path coverage have demanded higher resolution crustal models. This basic method was taken to higher-resolution with the 2-degree CRUST2.0 model (Bassin et al., 2000) and the 1-degree CRUST1.0 model (Laske et al., 2013). A 1-degree three-layer sediment model (Laske and Masters, 1997) was developed for the shallow earth. Specific *a priori* models were built for Western Eurasia and North Africa (Pasyanos et al., 2004) and eastern Eurasia (Steck et al., 2004), which were brought together to become a unified model which was used, for instance, as the starting point for the RSTT (Regional Seismic Travel Time) model (Myers et al., 2010), a 2½-D model for predicting regional travel times.

The LITHO1.0 model is an attempt to go in a slightly different direction by selecting among plausible models by comparing model prediction to surface-wave data (Pasyanos et al., 2014). The LITHO1.0 model also dove deeper into the solid earth by including the lithospheric lid, the portion of the upper mantle where the rheology is, such that it acts as a coherent tectonic plate with the crust. Lid velocity and thickness (Figure 25) can have a large effect on regional traveltimes.

While great progress has been made, these models can continue to be improved upon in the future. For instance, all of the models discussed in this section have been isotropic models. Anisotropy is known to exist and be strong, particularly in the upper mantle, and can be inverted for using a combination of Love and Rayleigh waves. While the LITHO1.0 model was specifically built using global surface-wave models that exist at all locations, including oceanic basins, this limited the frequency band of the dispersion data used.

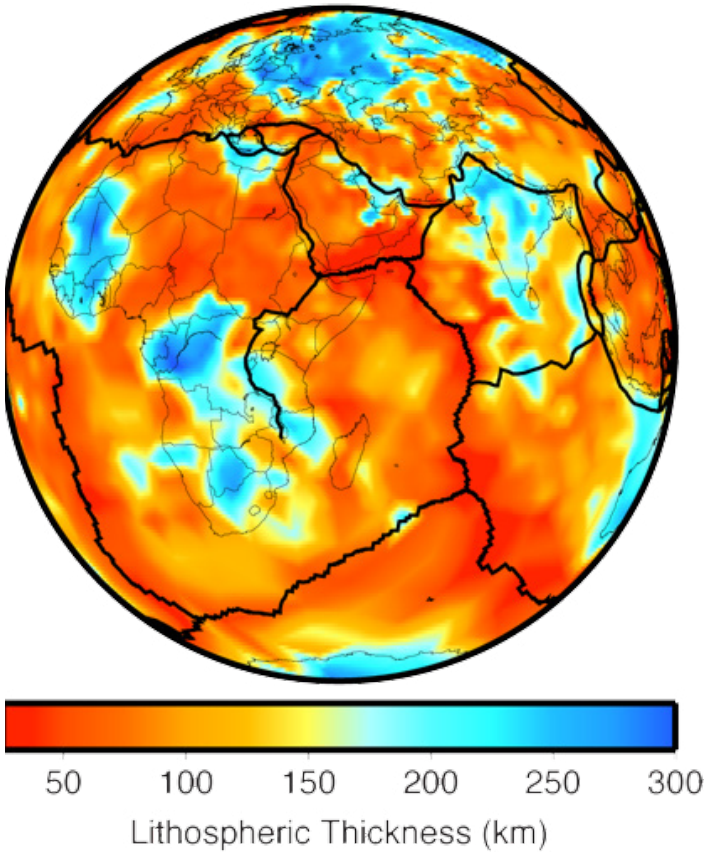

Figure 25. Lithospheric thickness estimates from the LITHO1.0 model (from Pasyanos et al., 2014).

Future R&D

Several explosion monitoring tasks (e.g., event location, moment tensor analysis) require accurate seismic models. The crust, being the most heterogeneous layer of all, is very difficult to model accurately, and imperfect crustal models can introduce significant errors in global seismic models. Therefore, it is important to develop improved, high resolution, crustal models, including models with ultra–high resolution regions embedded where data availability allows, and models that account for seismic properties like anisotropy.

From adapted to infrasound-specific propagation tools (WSP1, WSP2)

Infrasound propagation modeling is a major component in nuclear explosion monitoring because large above- and below-ground explosions generate infrasonic signals by direct deposition of energy into the atmosphere or through the displacement of the ground surface by seismic waves, respectively. The resulting infrasonic signals attenuate very slowly as they propagate through the atmosphere and some very energetic sources have produced signals that circled the earth multiple times. To utilize infrasonic signals to estimate the location, magnitude/yield, and other characteristics of the source, a thorough understanding of propagation effects is required.

Atmospheric and underwater acoustics have been active areas of research in the scientific community for over a century. However, methods specifically intended for modeling the propagation of low frequency sound waves into the middle- and upper atmosphere have been an intermittent focus of research. In the pre-satellite, atmospheric testing era, infrasonic studies and simulations were conducted to better understand the observed signals (Pierce, 1967; Donn & Rind, 1971). When satellite observations became more feasible and testing shifted from atmospheric to underground, infrasonic observations and the related physics became of less interest to much of the scientific community. Much of the continued research in acoustic propagation modeling focused on higher frequency signals in the near-ground layer of the atmosphere and underwater applications. Initial investigations into underwater acoustics included methods to detect icebergs and other submerged objects and atmospheric acoustics typically focused on military and civilian use involving noise control and other applications (Embleton, 1996). In 2000-2010, infrasound modeling became more relevant to a number of fields including detonation detection, atmospheric sounding, and volcano monitoring. In general, the modeling methods developed for underwater and atmospheric acoustics can be utilized for lower frequency signals (Jensen et al., 2011; Salomons, 2001). Ray tracing methods have been found to accurately predict propagation times for infrasonic arrivals from the stratosphere and thermosphere, while finite frequency methods such as the parabolic equation and normal mode expansions are applicable to infrasonic signals in the lower- and middle atmosphere (Garcés et al., 1998; Waxler et al., 2015).

The continued study of infrasound has led to the identification of a number of challenges in applying the methods developed in other acoustic propagation modeling regimes. The dynamic and poorly constrained nature of the atmosphere introduces significant uncertainty in the propagation of infrasound in the middle- and upper atmosphere, which must be included in propagation modeling applications. Gravity waves in the atmosphere due to buoyancy forces, and turbulence from interaction of the wind with near-ground structures, can create small-scale structures in the atmosphere that produce scattering of signals into predicted shadow zones and increased multi-pathing, which complicates the structure of observed waveforms (Ostashev et al., 2005; Chunchuzov et al., 2011). At high altitudes, the decreasing density of the atmosphere forces the propagation out of the linear regime and signals undergo non-linear propagation effects that can lead to wave stretching and the formation of N- and U-waves due to finite-amplitude effects (Norris et al., 2008; Lonzaga et al., 2015; deGroot-Hedlin, 2016), as discussed in the following tutorial. The wave stretching introduced in the high atmosphere results in coupling between acoustic and gravity waves. The inclusion of these effects is crucial in propagation modeling applications for infrasound, and future simulation tools will need to incorporate the effects of scattering from topographical and fine-scale atmospheric structures, non-linear propagation, and acoustic-gravity wave coupling to fully describe the physics of infrasonic propagation.

Future R&D

Infrasound propagation simulation capabilities can be further improved by accounting for fine scale structure, high flow velocities, rarefication, earth curvature, and a number of other unique challenges of acoustic propagation in the middle and upper atmosphere.

Tutorial: An overview of infrasound propagation

Modeling infrasound propagation requires knowledge of the atmospheric state, which is dynamic and constantly changing. However, some features of the atmosphere have consistent structure and are frequently present. For this example, a polynomial fit to the US Standard Atmosphere (Lingevitch et al., 1999) is used with a single wind jet near the stratopause to represent the stratospheric jet (also termed the circumpolar vortex) to identify "typical" propagation paths in the atmosphere. In the left panel of Figure 26, the solid line denotes the adiabatic sound speed defined as $c=\sqrt{\gamma RT}$, where γ is the specific heat ratio, R is the molar gas constant, and T is the absolute air temperature. Note that in the case of acoustic propagation, the propagation velocity increases with temperature, which is the reverse of the propagation velocity for elastic waves in the earth. The dashed line denotes the effective sound speed for propagation to the east as defined by the sum of the adiabatic sound speed with the winds in that direction. The propagation paths up- and downwind of this stratospheric jet are shown in the right panel of Figure 26.

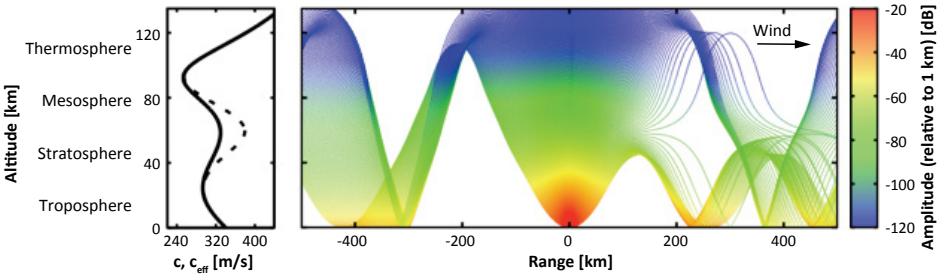

Figure 26. Propagation paths up- and downwind of the stratospheric jet in the US Standard Atmosphere. Stratospheric propagation paths are present for propagation downwind due to the combined influence of thermal and wind gradients.

Differences in propagation velocity (whether due to temperature, wind, or some other variation) cause a wavefront to bend because the portion of the wavefront in the faster region of the medium moves ahead and turns or refracts the wavefront into the region with slower propagation speed. In the case of acoustic waves, this refraction is into regions of colder temperatures. Because the temperature maximum at the stratopause (boundary between stratosphere and mesosphere) is typically lower than the ground temperature, infrasonic energy is only refracted back to the ground by the combined effects of the thermal and wind gradients at the stratopause. This produces anisotropic (azimuthally varying) propagation paths that vary depending on the relative wind and propagation directions. Stratospheric arrivals are predicted for propagation downwind of the source. A thorough discussion of stratospheric arrivals is available in Waxler et al., 2015. Upwind of the source, the energy propagates into the upper atmosphere and is refracted back towards the ground by the increasing temperatures in the thermosphere.

The infrasonic arrivals from high altitudes have a further complication due to the rarefication of the atmosphere at high altitude and finite-amplitude effects. Non-linear propagation effects due to the decreased density in the meso- and thermosphere produce waveform steepening that generates high frequency energy as well as waveform stretching that shifts the dominant frequency to lower values. This effect is shown in Figure 27 for a simple model impulse waveform. In the first panel the impulse has some initial shape as it propagates through the lower- and middle atmosphere. In the second and third panels, the positive and negative phases of the impulse shift due to finite amplitude effects and produce an "N-wave". Lastly, during the refraction from the increasing temperatures of the thermosphere, a phase shift is encountered along the propagation path that changes the "N-wave" into a "U-wave". Observations of "U-waves" are common for thermospheric paths and are occasionally observed in stratospheric arrivals for sources with high initial energy.

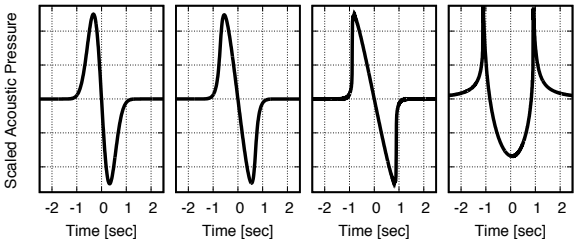

Figure 27. Non-linear effects lead to waveform steepening and the formation of an N-wave during propagation in a themospheric waveguide. The phase shift near the turning point produces a phase shift that changes the N-wave into a U-wave.

From generalized climatology-based models to statistical infrasound propagation models (WSP1, WSP2, WSP3)

The construction of infrasound models is complicated by the dynamic and poorly constrained nature of the atmosphere and the large variations that this produces in propagation predictions. Despite this complication, temporal shifts can be identified in the atmospheric state and related to variations in infrasonic propagation characteristics (Drob et al., 2010; Green and Bowers, 2010; Le Pichon et al., 2012).

Propagation medium models are important tools in nuclear explosion monitoring because they provide a means to quantify uncertainties in estimates of source location, magnitude/yield, and various other characteristics.

Currently, infrasound data are primarily used in underground test monitoring to help discriminate between quarry blasts and possible nuclear explosive tests. While the presence of a strong infrasound signal can be a very strong indicator of a surface event, the absence is challenging to use and requires propagation modeling. The state of the atmosphere varies dramatically and dynamically so that propagation paths observed at any given time may be distinct from those observed at another time. Therefore, seismic tomography methods utilizing a large number of historic events to characterize the earth structure are not applicable to infrasonic tomography. However, for infrasound, there are seasonal and diurnal (24-hour) trends in the atmospheric state that can be studied to identify those propagation paths that are more probable to be observed for a given location and time of year. While the thermal structure of the atmosphere can be directly characterized and is relatively stable, the winds vary by a significant amount and, due to direct measurements being sparse and expensive, result in large uncertainties for predictions of the propagation of infrasound. Typically, infrasonic signals are refracted back towards the ground from altitudes near the tropopause (10 – 12 km), stratopause (45 – 60 km), or lower thermosphere (110 – 140 km). Refractions from the thermosphere are produced by rapidly increasing temperatures, but the tropospheric and stratospheric waveguides are dependent on the wind structure near the refraction altitudes (Drob et al., 2003).

The tropospheric winds can often be well characterized from numerical weather prediction and ground-based observations (SODAR, LIDAR, etc.); therefore, the presence and directionality of a tropospheric waveguide can be identified and the related propagation effects are easily and accurately predicted. However, current technologies are unable to provide high quality, continuous measurements of the winds in the middle atmosphere, which results in large uncertainties for the wind structures in this region. It has been shown by a number of infrasound studies that, consistent with climatology models, the winds near the stratopause (often termed the stratospheric jet or circumpolar vortex) are typically oriented westward in the summer months and eastward in the winter months in the northern hemisphere, and this is reversed in the southern hemisphere. Figure 28 shows the atmospheric state as reported by the Ground-2-Space (G2S) tool at a mid-latitude location in the northern hemisphere over the entirety of 2014. The upper panel shows the temperature structure of the atmosphere, while the middle and lower panel show the zonal (east/west) and meridional (north/south) components of the wind, respectively. Although the exact wind speed and direction is variable and difficult to predict or specify, the larger scale seasonal trend for the winds in the middle atmosphere seen in the figure is consistently observed and well understood. Because these winds strongly influence the ducting of infrasound, the seasonal variations in wind direction and strength produce a correlated trend in the presence and directionality of a stratospheric waveguide for infrasonic signals (Drob et al., 2010; Le Pichon et al., 2006). One current area of research in infrasonic propagation aims to extend the identification of such trends to construct statistical models for propagation based on seasonal and diurnal trends. Recently, infrasound scientists have utilized historical archives of atmosphere specifications and numerical propagation tools to construct statistical models for infrasound propagation (Marcillo et al., 2014; Morton and Arrowsmith, 2014). These propagation-based, stochastic models have been found

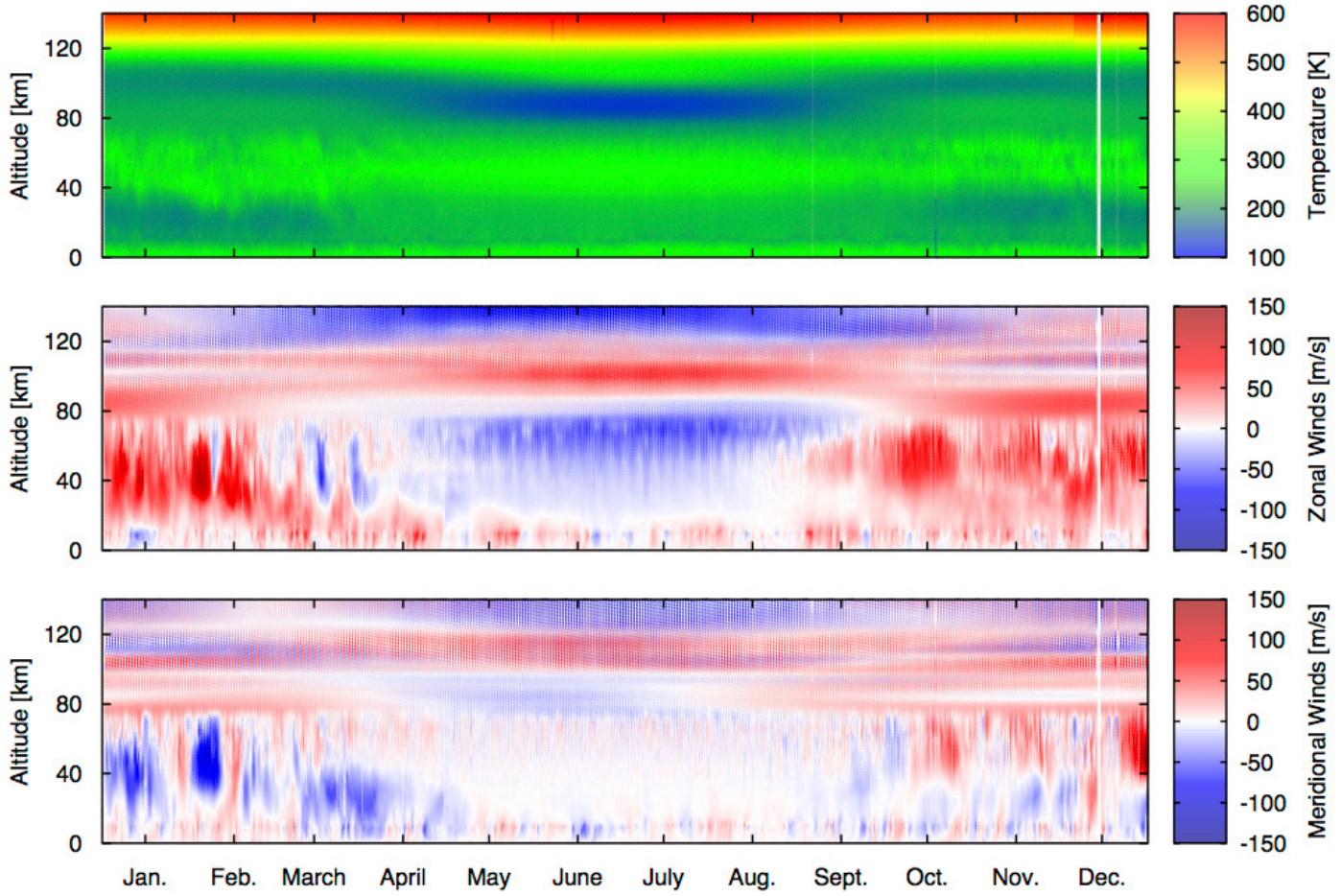

Figure 28. Temperature and wind fields in the atmosphere as specified by the Ground-2-Space (G2S) tool for a location representative of the northern hemisphere during 2014. The temperature maximum at the stratopause is clearly observed at an altitude of 40 – 60 kilometers. This temperature structure and the seasonal variations of the zonal winds produce a stratospheric waveguide with seasonally varying direction. Zonal wind is the component of wind in an east-west direction and is positive to the east while meridional wind is the component in a north-south direction and is positive to the north.

to significantly improve the results of source location estimates for infrasonic signals observed at distances of hundreds of kilometers (Blom et al., 2015).

Because of the dynamic nature of the atmosphere, it is highly unlikely that a high-precision, accurate, near-real-time model of the global atmosphere will be attainable. Therefore, uncertainties in the atmospheric state will always need to be identified and quantified in infrasound research. Continued work will require extending the construction of stochastic models to be semi-empirical via the inclusion of ground-truth data sets to validate and improve the results in cases where the archived atmosphere specifications are inaccurate. Current studies have focused on traveltime and direction of arrival variations, which improve applications of location estimation; however, estimation of the source magnitude/yield or other characteristics may require the use of more robust and computationally expensive

Future R&D

Hybrid simulation- and empirical-based models for infrasound propagation characteristics should be developed over a global grid of virtual sources to quantify the influence of the dynamic nature of the propagation medium. Additionally, acoustic tomography methods are applicable for improvement of atmospheric specifications used to analyze events of interest.

propagation modeling methods to estimate transmission loss and other waveform features relevant to source characterization. Further, a large-scale simulation campaign will be required to construct and investigate the performance of statistical propagation models for a global grid of virtual sources. Understanding and properly utilizing the resulting propagation models should greatly improve the quality of infrasound contributions to nuclear explosion monitoring.

From seismic noise to seismic signal (WSP1, WSP2, WSA2)

Seismic velocity models are critical for accurate seismic phase arrival prediction and event location, which have direct bearing on monitoring and on-site inspection (OSI) applications. Traditionally, models derived from surface waves used signals generated from earthquakes, which were filtered to remove background noise such as global microseisms (Berger et al., 2004). Following seminal work by Shapiro and Campillo (2004) and Shapiro et al. (2005), however, it was realized that seismic wave propagation models could be derived by using only the ambient wavefield in the absence of data from earthquakes. In fact, removal of earthquake signals was part of the data processing (Bensen et al., 2007) and, thus, what was previously seismic "noise" became seismic "signal."

Many seismic velocity models derived from surface waves used only earthquake sources, and the resolution of the models was constrained by the spectral content of the sources and the event-station geometries. Earthquakes large enough to have a good signal-to-noise ratio (SNR) typically contain energy at lower frequencies, which results in models without a lot of information about the shallow structure of the crust. Additionally, natural sources are not uniformly distributed in the earth, restricting the usable paths between sources and stations. Ambient noise tomography (ANT) uses the stacked cross-correlations of inter-station noise to recover information about the velocity structure between stations. Thus, lateral resolution is not limited to paths between stations and natural sources, but instead uses paths between station pairs. The frequency content of ambient noise generally is higher than that of natural sources, and so velocity models derived from ANT are better able to resolve crustal structure.

The application of ANT has led to improved lateral and depth resolution in regional and global velocity models. Yao et al. (2005), for example, used 110 paths of high-quality surface-wave dispersion data from earthquakes to produce Rayleigh wave dispersion maps of western China at periods of 20-120 seconds and ~7-degree lateral resolution. A more recent study by Zheng et al. (2008), using the ambient noise wavefield, produced Rayleigh wave group velocity maps for periods of 6 to 60 seconds, which include much more information at shorter periods, translating to increased resolution at shallower depths. Finally, comprehensive lateral and depth resolution can be achieved when traditional earthquake-based methods are combined with those based on ambient noise (e.g., Bao et al., 2015).

More recently, the ambient noise field has been used to extract information about amplitude and attenuation in the earth. Zhang and Yang (2013) correlated the coda of seismic noise correlations to extract stable and accurate estimates of attenuation along the paths between stations pairs, using the "C3" method of Stehly et al. (2008). This method is promising, but has proven to be highly sensitive to the uneven distribution of seismic noise sources, which tends to result in biased attenuation estimates.

Future R&D

The suitability of the ambient noise field for retrieval of amplitude information continues to be explored numerically and theoretically, and is a future growth area for research using seismic noise.

In a somehow similar way to ANT where seismic stations could be considered as virtual sources to compute the impulse response using Green's functions (GF) between a couple of stations, one could think of sources becoming virtual seismometers. The Virtual Seismometer

Method (VSM) is an interferometric technique that provides precise estimates of the GF between seismic sources (Hong and Menke, 2006; Curtis et al., 2009). The technique isolates the portion of the wavefield that is sensitive to the source region and dramatically increases our ability to see into tectonically active features where seismic stations either cannot be or have not been located, such as at depth in fault zones. In simple terms, VSM involves correlating the record of a pair of events recorded at an individual seismometer and then stacking the results over all elements of the seismic network to obtain the final waveform. In the far field, when most of the stations in a network fall along a line between the two events, the result is an estimate of the GF between them, modified by the source terms. In this geometry, each source is effectively a "virtual seismometer" recording all the others. When this alignment is not met, one also needs to address the effects of the geometry between the two events relative to each seismometer. The technique is quite robust, and highly sensitive to tectonically active regions, especially in areas where there may be hundreds to thousands of events.

From 1D to 3D earth models (WSP1, WSP3)

Tasks of monitoring agencies include the detection, location, and discrimination of seismic activity. Event location accuracy is crucial to these tasks, as location itself can provide insight about the event.

Traditionally the earth models used to predict P and S traveltimes for seismic event locations have been one-dimensional (1D), radially symmetric models where seismic velocities and density vary only as a function of depth. Examples of such models are the Preliminary Reference Earth Model (PREM) (Dziewonski and Anderson, 1981), *iasp91* (Kennett and Engdahl, 1991), or *ak135* (Kennett et al., 1995). Even though traveltimes predicted using these models vary only as a function of source-receiver distance and source depth, these simple 1D models predict significant complexity of the wavefield due to reflections and conversions of wave energy at sharp discontinuities such as the core mantle boundary (e.g., Garnero, 2000). 1D models have worked fairly well for teleseismic P arrivals, and it is still current practice for most monitoring agencies to rely on 1D model predictions and to account for large-scale 3D effects through source specific station corrections. Therefore, for seismically active areas with good ground-truth event coverage, inaccurate and simple models can be corrected by interpolating results from nearby archived events (e.g., Schultz et al., 1998; Phillips, 1999; Myers and Schultz, 2000) and, consequently, it is possible to detect, locate, and identify large events even with limited resolution models. However, this is not necessarily the case for smaller events, and it is even more of a challenge for aseismic regions.

As a result of a workshop, Zucca et al. (2009) outlined a plan to develop and implement 3D models in an operational system, and several models of earth structure have been subsequently developed with a focus on improving regional and teleseismic traveltime predictions and event locations (e.g., Phillips et al., 2007; Myers et al., 2010; Simmons et al., 2011, 2012 and 2015; Ballard et al., 2016b) (Figures 29 and 30). It has also been shown that global and regional 3D models improve traveltime prediction and, therefore, event location over 1D models for broad areas (e.g., Ritzwoller et al., 2003; Yang et al., 2004a; Bondár et al., 2014; Myers et al., 2015) (Figure 31). Figure 32 shows relocation results using a 3D model from joint inversion of seismic and gravity observations for the area of Iran showed in the inset plot. This type of study aims to answer the question of "Can multi-parameter tomography address crustal heterogeneities in areas of limited coverage and improve traveltime predictions?" For the particular case shown in Figure 32, as well as for other tested earthquake sequences, the 3D joint inversion model always performs as well or better than the body-wave-travel-time-only model. Despite advancements in the development of 3D models, 1D models remain the standard for routine travel-time computation at most monitoring centers due to the expensive cost of traveltime computation through 3D models as well as poor ray-path approximations at certain distances.

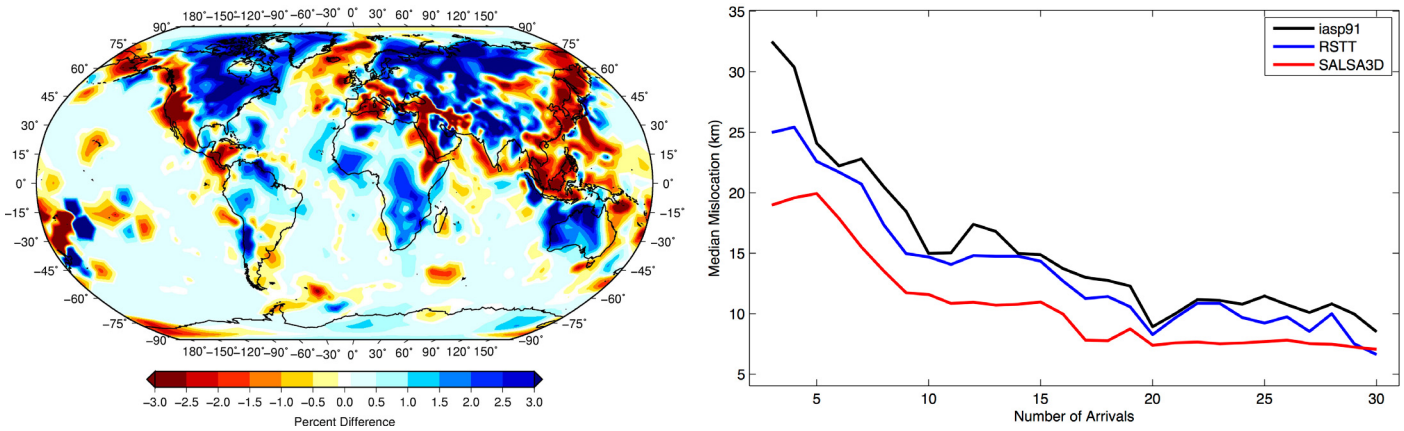

Figure 29. (left) SALSA3D model image of percent P-wave velocity change from the ak135 model at 100 km depth. (right) Mislocation of ground-truth (GT) validation events with the number of IMS Station P/Pn arrivals for iasp91, RSTT, and SALSA3D models.

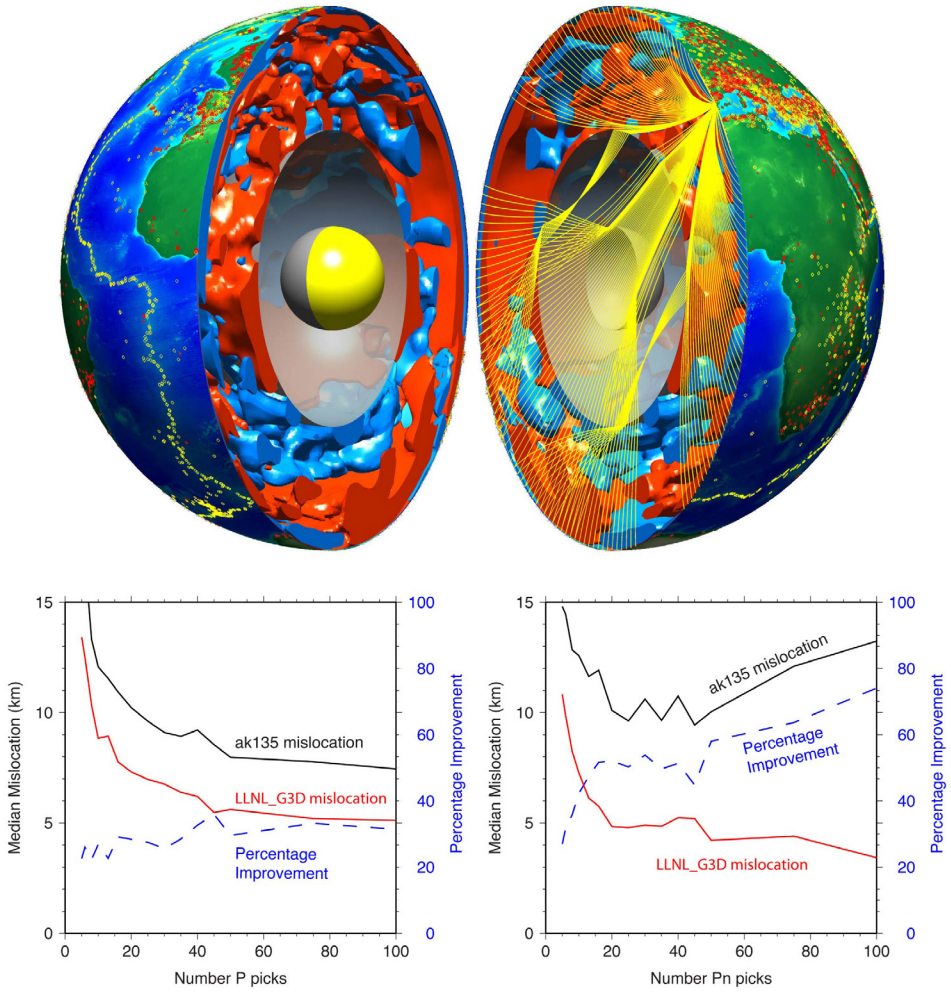

Figure 30. (top) A 3D view of the LLNL-G3D-JPS seismic tomography model (Simmons et al., 2015) showing contoured fast (blue) and slow (red) shear-wave anomalies in the mantle. The model is the result of simultaneous inversion of millions of P- and S-wave arrivals including a broad suite of seismic phases and full 3D ray tracing (example 3D ray paths shown in yellow). (bottom) The results of a seismic location validation study (Myers et al., 2015) using an LLNL-G3D P-wave model (Simmons et al. 2012) with various amounts of teleseismic P (left) and regional Pn (right) arrivals. With sufficient data, the median event mis-location error reaches the 4-5 km range with this global model.

During development of these 3D seismic models for the monitoring mission, the focus has always been on improving seismic phase traveltime predictions and event locations. Routinely, this improvement has been quantified by comparing the model predictions to ground-truth (GT) event parameters (Bondár et al., 2004; Bondár and MacLughlin, 2009). The GT coverage, however, is not ideal, and there are many areas around the world that lack this information. In recent years, the monitoring community has been optimistically looking at the results from interferometric synthetic aperture radar (InSAR) as a potential surrogate for GT events as well as an aid to understanding underground explosions.

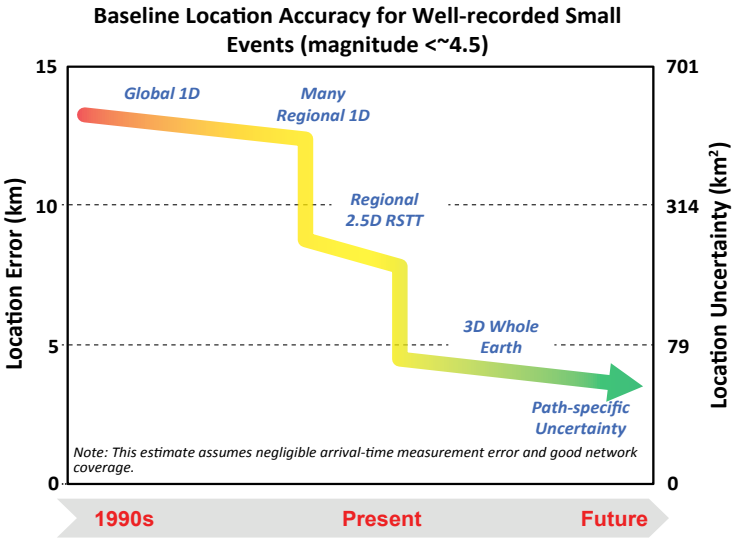

Figure 31. Time progress of improvement in location error and location uncertainty by moving from 1D to 3D models.

InSAR from earth-orbiting spacecraft provides a tool to map global topography and deformation of the earth's surface. Radar images taken from slightly different viewing directions allow the construction of digital elevation models of meter-scale accuracy. These data sets aid in the analysis and interpretation of tectonic and volcanic landscapes. If the earth's surface deformed between two radar image acquisitions, a map of the surface displacement with tens-of-meters resolution and subcentimeter accuracy can be constructed (Bürgmann et al., 2000).

As Bürgmann et al. (2000) state, although the deformation measurement capabilities of InSAR had been demonstrated earlier, it was the successful measurement of deformation associated with the 1992 Landers earthquake that demonstrated the revolutionary nature of the technique. Using interferometric images of ERS-1 satellite radar data collected before and after the Landers earthquake, scientists were able to image the deformation surrounding the rupture in astounding detail (Massonnet et al., 1993).

InSAR has been used extensively to measure the complex deformation fields associated with intruding dikes, inflating or deflating magma chambers, and geothermal systems, as well as faulting and slumping of volcanic systems. The theoretical developments needed to understand volcanic systems are directly applicable to underground explosions. Since both types of

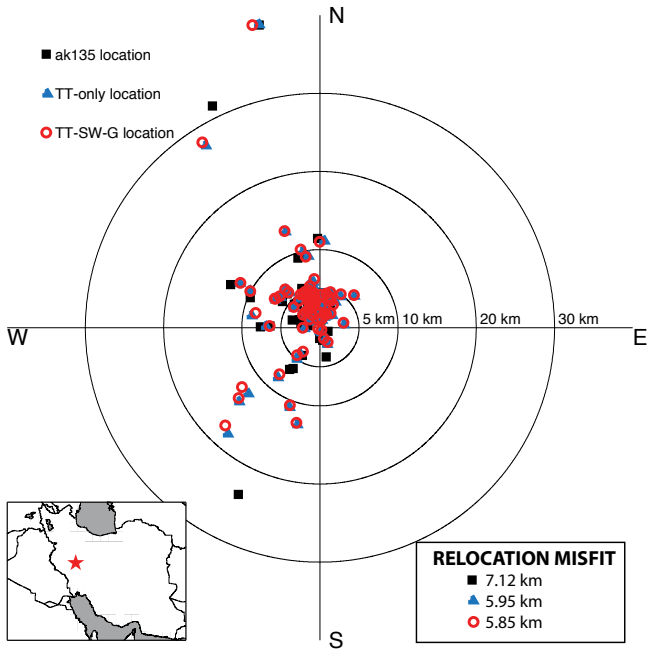

Figure 32. Polar plot showing the relocation misfit between different models (ak135 1D model as black squares, body wave traveltime only 3D model for the Iranian region as blue triangles, joint inversion – body wave traveltimes, surface-wave dispersion, and gravity observations - model for the Iran region as open red circles) for the 2006 M6.1 Silahour earthquake sequence in western Iran (red star in inset plot, and center of main plot). Contours indicate misfit in ground distance between the location provided by different models and the ground-truth location for the earthquake sequence. The joint model shows the smallest relocation misfit.

deformation are accompanied by significant vertical displacements, InSAR is particularly useful for these investigations.

Vincent et al. (2003) detected and measured coseismic crater formation from two underground nuclear explosive tests at the Nevada Test Site using InSAR. A smaller magnitude test also occurred during the time that the radar satellite was operating, but no ground deformation was detected. Carluccio et al. (2014) claimed a detection of the 2009 DPRK event that was about 10 km away from a seismic location, though they added that it could be due to landsliding in the region. Finally, Hartmann et al. (2016) and Wei (2017) reported the detection of the January 2016 DPRK explosion using InSAR (Figure 33). This shift in usage of InSAR analysis of large earthquakes to small explosions has promise to be complementary to other waveform event location technologies.

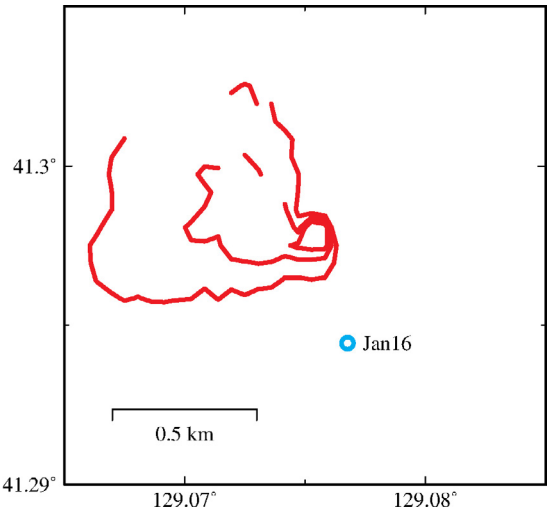

Figure 33. Contours of ground displacement (red lines) based on InSAR show that the probable location of the January 2016 announced nuclear test is approximately 0.5 km north northwest of the epicenter based on relative seismic locations and the absolute reference frame of Wen and Long (2010).

Predicting regional and local phase amplitudes as well as coda and full envelopes began with empirical correction surface methods, similar to regional traveltimes, showing that laterally varying corrections reduced scatter in discriminant ratios for earthquake populations (Phillips et al., 1998). This development was expected to improve discrimination coverage as lower frequencies (e.g., 2-4 Hz) are especially amenable to correction and propagate longer distances than the bands then deemed most effective for discrimination (e.g., 6-8 Hz). However, empirical methods only allowed corrections to be applied to events within a specified distance of previous events, which motivated the use of tomographic techniques to image regional phase attenuation. Two-dimensional attenuation models have been used for years by seismologists (e.g., Campillo, 1987), and applications to monitoring problems have been plentiful since Phillips et al. (2000). Current models of regional phase attenuation are created using global multiscale grids and use independently determined moments and source spectra as constraints (Fisk and Phillips, 2013a,b). Regional phases (see the Guide to Seismic Waves and Phases at the end of this document) Pg, Sn, and Lg are very well described by the 2D models, with residuals of roughly 0.1 log10 units (0.05 for coda). Pn and mantle P amplitudes are not as well described, with residuals of 0.2-0.3 log10 units. These amplitudes are likely influenced by 3D variations in upper mantle elastic properties. Sn appears not to be affected in the same manner, perhaps due to low upper mantle S velocity gradient (Park et al., 2007) and rapidly increasing attenuation with depth. One also observes increased scatter for local distance amplitude data, perhaps the result of unmodeled 3D structures, and narrow measurement windows, and more predominant azimuthal radiation effects. Accounting for 2D amplitude variations also extends from direct phases to coda (Phillips et al., 2008).

Future R&D

To improve location accuracy and monitoring capability, especially in aseismic regions, it is essential to develop higher dimensional earth models, since 1D models cannot appreciably account for traveltime variations due to crustal and upper mantle heterogeneity. Equally important is the incorporation of crustal phases to be able to model the structure at local scales. Another important topic is the joint inversion for velocity and attenuation for modeling Pn and local phase amplitudes, and will likely be important for modeling teleseismic phases as well. Use of full 3D amplitude models as well as the use of full waveform methods to constrain amplitude models are other areas that require future research.

From ray theory to full waveform (WSP3)

Waveform signal propagation R&D strives to model synthetic waveforms that perfectly match the observations at a range of different frequencies. Modeling requires the mathematical calculation of the expected ground displacement at a given remotely sited sensor from a hypothetical source, i.e., solving the wave equation. There has been impressive progress in the last decades towards properly and accurately solving the wave equation, which is a cornerstone of the monitoring mission.

Since the earth is not a homogeneous medium, approximations are used to solve the full elastic wave equation. The ray approximation allows us to predict wave propagation in smoothly varying media, and geometric ray theory forms the standard basis in most seismic tomography. To solve the two-point problem and find the correct ray geometry between source and receiver, a way must be found to determine the initial ray orientation at the source that satisfies the ray arriving at the receiver. One way to accomplish this is to use a ray-based "shooting" method in which one aims, computes, and aims again until hitting the receiver. Ray shooters (Menke, 2005) systematically perturb an initial estimate of the ray takeoff angle from a seismic source until the ray hits the seismic receiver, within some prescribed tolerance and with application of Snell's law at interfaces if necessary. In regions of significant heterogeneity, however, the shooting method may often fail to converge. Practical applications settle for an acceptable tradeoff between the percentage of two-point paths located and total computation time. For that reason, it is perhaps preferable to use a ray bending method. As the name indicates, bending methods "bend" the ray, iteratively adjusting the geometry, until its traveltime satisfies Fermat's principle of stationary time. There are also the very popular pseudo-bending methods that use the same principle of bending and adjusting the ray geometry, but avoid direct solution of the ray equations. Um and Thurber (1987) developed one of the first pseudo-bending schemes in which they describe a ray path by a set of linearly interpolated points. Zhao et al. (1992) modify the pseudo-bending scheme of Um and Thurber (1987) to allow for the presence of interfaces. These pseudo-bending methods are much more computationally efficient than conventional bending schemes and therefore they have become the method of choice when dealing with problems that require large traveltime datasets to be predicted. As such, many researchers dealing and collaborating with the monitoring mission have adopted the pseudo-bending techniques as the preferred method (e.g., Simmons et al., 2011, 2012; Syracuse et al., 2016; Ballard et al., 2016b). Simmons et al. (2015) even adapted and expanded the Zhao et al. (1992) method to numerous secondary phases, including phases such as SS or PP.

To find the right path taken by seismic energy between the source and the receiver, an alternative approach to ray tracing is to compute the global traveltime field as defined by a grid of points. There are two popular grid-based methods: a finite difference solver of the eikonal equation and the shortest path scheme. The latter is not used in the monitoring community and it is, indeed, less frequently used than eikonal solvers in general. Grid-based methods have clear advantages over conventional ray tracing approaches – efficiency and robustness in strongly heterogeneous media, stability and high probability of finding the global rather than local minimum of the traveltime – but also some serious drawbacks, mainly the fact that their accuracy is a function of grid granularity and, therefore, large 3D volumes can become computationally expensive. For these reasons, eikonal solvers are the method of choice when (i) the domain being modeled is limited in spatial extent, (ii) the domain is characterized by strong velocity gradients, and (iii) the ratio of sources to receivers (or vice versa) is high. Ballard et al. (2009) compare the performance of their implementation of the pseudo-bending scheme to the Fast-Marching Method (FMM, a finite difference eikonal solver) and concluded that their bender yields satisfactory results with substantially fewer computer resources. Nonetheless, the monitoring community has successfully employed finite difference schemes for tomographic purposes at small spatial scales (e.g., Zhang et al., 2014; Syracuse et al., 2015).

Geometric ray theory has been essential in the evolution of seismic tomography in the last four decades and even now is being used. However, the validity of ray theory is limited to cases where the seismic wavelength is much smaller than the scale length of heterogeneity that characterizes the medium through which it passes. Ray theory is an infinite-frequency approximation, but, in reality, seismic waves have a finite frequency. Unless properly accounted for, this finite frequency effect will blur the final tomographic image. The seismic imaging community has long recognized this fact, but, until recently, a workable solution was not possible due to limits in both computing power and theoretical development. Nowadays in the broader seismic tomography community, finite-frequency (FF) methods (e.g., Marquering et al., 1999; Dahlen et al., 2000; Hung et al., 2000; Tromp et al., 2005) are sometimes implemented in place of ray-theoretical (RT) methods that assume any traveltime delay observed at a station is the result of velocity anomalies along an infinitely narrow ray path between the source and receiver. Although FF provides a better forward theory to represent the wavefield (Hung et al., 2001), debate continues as to whether its application to tomography produces better models. Much of the literature concerned with the topic focuses on surface waves, and, while numerous studies report improved tomographic images (e.g., Peter et al., 2009 and references therein), others (e.g., Boschi et al., 2006 and references therein) suggest that theoretical advances of FF may be outweighed by practical considerations and that RT models are indistinguishable from FF when realistic ray coverage and noise are considered. Maceira et al. (2015) investigated the merits of the FF approach to tomography against the more traditional and approximate RT approach (Figure 34). Their study suggests that FF approaches to seismic imaging exhibit measurable improvement for pronounced low-velocity anomalies such as mantle plumes, and they postulate that the use of a single low-frequency band in the generation of their study model might have precluded larger differences between both seismic imaging methods. Another benefit of finite frequency tomography is that it is feasible to invert amplitude information (e.g., Sigloch et al., 2008) due to the phenomenon of wavefront healing. Despite all these evidences in favor of FF approaches, the monitoring community has still not fully embraced the technique.

Finally, the ultimate goal would be to predict full waveforms, but exploiting the full waveform in seismic tomography requires an efficient method for solving the elastic wave equation, which is computationally expensive, at least compared to ray methods. The use of full surface-wave waveforms was introduced early on in global seismology (e.g., Woodhouse and Dziewonski, 1984; Nolet, 1990; Li and Romanowicz, 1995), but generally only used 1D waveform inversion of long period waves, which were then combined to form a 3D model. Finite difference (FD) techniques for solving the wave equation are conceptually straightforward to implement, but large grids are required to propagate high frequency waves. A recent approach for high-accuracy modeling of the full waveform propagation is the spectral element method (SEM). The SEM solves the wave equation in its integral form on customized meshes adapted to realistic earth models made of hexahedral elements. It employs a high order finite-element method with exponential convergence for smooth solutions while maintaining the geometric flexibility of finite elements (Komatitsch and Vilotte, 1998; Komatitsch and Tromp, 1999; Komatitsch et al., 2002). SEM has been developed to the point that it can be applied at a variety of scales and can account for a range of physical phenomena including anelasticity, anisotropy, rotation of the earth, selfgravitation, presence of the oceans, etc. Full waveform simulations have been recently used for waveform prediction and validation of 3D geophysical models, either by using SEM (e.g., Maceira et al., 2015) or the FD method (e.g., Gao and Shen, 2014b; Bao and Shen, 2016). They have also been applied

Future R&D

Further research is needed for proper validation and uncertainty quantification of 3D geophysical models. Questions such as "How good is a 3D model at representing the true physics of the earth? What are some of the limiting factors to producing a particular model and how many data are needed for a model to be considered 'good enough'?", require answers which will also determine the uncertainty in source parameters computed through these models.

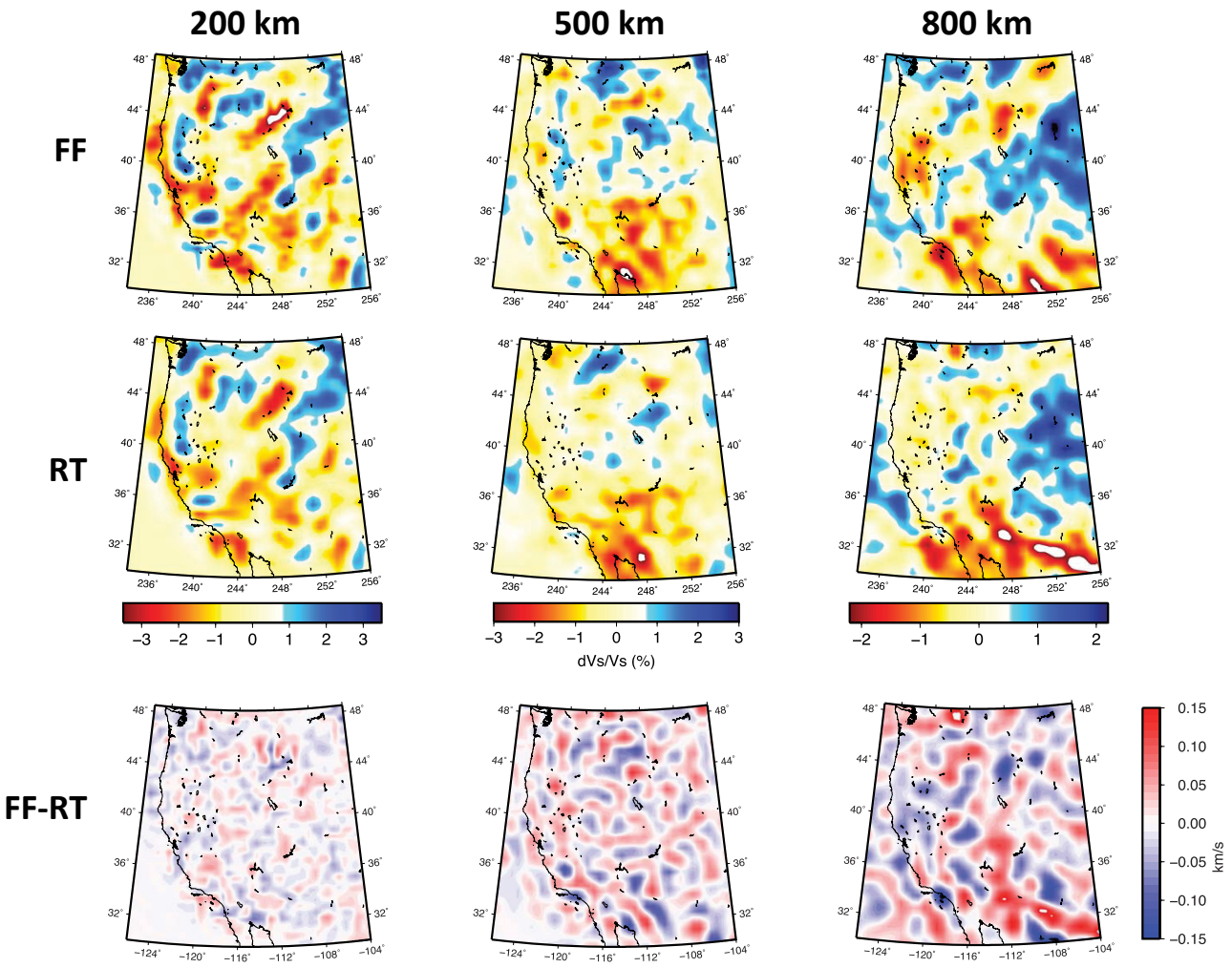

Figure 34. Dynamic North America (DNA09) model shear wave (Vs) velocity perturbations with respect to iasp91 obtained by FF (top row) and RT (middle row) imaging approaches at depths of 200 km (left column), 500 km (center column), and 800 km (right column). Bottom row shows the difference between the two models in absolute velocity. The differences in % were translated to absolute velocity using the 1D reference model iasp91 (from Maceira et al., 2015).

to constrain anisotropy (e.g., Zhu et al, 2012) and attenuation (e.g., Zhu et al., 2015) structure. However, the application of full waveform methods to the monitoring mission is not yet completely implemented. Possible reasons for the slow application of these methods to monitoring are the large data volumes that are often involved, the more complex and less well understood nature of the source mechanism (compared to active source campaigns), and the need for high performance computing environments to implement such techniques.

Currently about 10-second period and longer full waveforms for regional scale models are state-of-the-art for waveform simulation. The goal is to reduce the 10 seconds to 5 in the near future. For small local regions it is possible to calculate full waveforms up to 8 Hz, and this is being done for studies looking at effects such as topographic scattering. An important caveat to full waveform calculation is that the predicted signals are only as good as the prior model from which they are determined. Accurate prior models typically require collecting millions of measurements, culling the bad data, and combining multiple types of measurements together in ways that make statistical sense. Also such work requires large databases and high performance computing as well as a reasonable amount of time.

From regular to irregular parameterization (WSP3)

Any aspect related to solving the full elastic wave equation has a tremendous value to the monitoring mission, as the data - being seismic or infrasonic - are the physical expressions of the wave equation. One's choice of parameterization, when solving the wave equation, immediately restricts the field of permissible models and can be viewed as a form of *ad hoc* regularization. Besides limiting the range of structure that can be recovered, the choice of parameterization impacts the solution technique chosen for both the forward and inverse problems.

Since the beginning of seismic tomography in the late 1970s, researchers used regular parameterizations because they are conceptually simple, easy to formulate, and generally do not complicate the forward and inverse solvers. The most basic forms of this regular parameterization are cells or blocks with uniform seismic properties (e.g., velocity) that make initial value ray tracing simple because path segments in each block are straight lines. However, the artificial discontinuities between each block are unrealistic and can make the two-point ray tracing problem more non-linear. Using a large number of blocks with some form of smoothing regularization can mitigate these problems, but it will be at the expense of increased computing time. An alternative to block parameterizations is to define seismic properties at the vertices of a regular grid together with some interpolation function. One of the first implementations of this approach was by Thurber (1983), who used trilinear interpolation between a rectangular grid of nodes to define a continuously varying velocity field for local earthquake tomography. This scheme is now commonly used in tomography.

In regional and global tomography, regular blocks or grids in spherical coordinates are faced with the additional challenge of an artificial increase in spatial resolution towards the poles and central axis. Wang and Dahlen (1995) developed a spherical surface-spline method that parameterizes the sphere in terms of cubic B-spline basis on a triangular tessellation grid of knots with approximately equal interknot spacing. This icosahedron-based grid was first used by Van der Lee and Nolet (1997) to parameterize the Moho in a tomographic study. In global tomography, another common parameterization is spherical harmonics (e.g., Dziewonski, 1984; Trampert and Woodhouse, 2001) but with global support (Freeden and Michel, 1999). In global waveform tomography, the so-called "cubed-sphere" (Ronchi et al., 1996), which is an analytic mapping from the cube to the sphere, has become popular, particularly in conjunction with the spectral element method (e.g., Komatitsch et al., 2002).

Blocks of constant seismic properties and other types of regular parameterization have been widely used in most forms of tomography, and researchers related to the monitoring mission continue to use them at different scales and for different forms of tomography, such as traveltime tomography (e.g., Steck et al., 1998; Phillips et al., 2005a; Steck et al., 2009), surface-wave tomography (e.g., Pasyanos et al., 2001; Maceira et al., 2005; Pasyanos, 2005), amplitude/attenuation tomography (e.g., Phillips et al., 2000, 2001, 2005b, 2014; Taylor et al., 2003; Mayeda et al., 2005a; Phillips and Stead, 2008; Ford et al., 2008, 2010), and joint inversion approaches (e.g., Maceira and Ammon, 2009; Zhang et al., 2014; Syracuse et al., 2015). A slightly more sophisticated approach to avoid polar distortions associated with a regular latitude-longitude parameterization is to use triangular (2D) or tetrahedral (3D) cells with a constant velocity gradient, which, like constant velocity blocks, facilitates analytic ray tracing. This is the case for the regional seismic traveltime (aka RSTT) model (Myers et al., 2010), which is broadly used in monitoring. The RSTT model parameterization includes nodes spaced at approximately 1-degree. The nodes form a triangular tessellation that seamlessly covers the globe.

The natural distribution of earthquakes together with the irregular distribution of seismic stations makes data coverage highly uneven. This fact has fueled the idea of using irregular parameterizations, where blocks or nodes are placed only where they are required by the data. Sambridge and Rawlinson (2005) and Nolet (2008) provide excellent reviews on this topic. The approach that has become more popular inside the monitoring community to address the uneven data illumination is a multi-scale hierarchical tessellation (Ballard et al., 2009, 2016a). Under this approach, a global tessellation with a regular polyhedron is initiated and then division of the faces into smaller-size cells progresses based on some criteria prior to the inversion. This *a priori* determination (i.e., static approach) is usually based on data density (quantified by hit count) or on some measure of resolvability, but this last criteria is difficult to determine for large tomographic systems. SALSA3D and the LLNL-G3Dv3 series models were built with the idea of improving teleseismic and regional traveltime predictions for events occurring anywhere on the globe. The LLNL-G3Dv3 series (https://www-gs.llnl.gov/about/nuclear-threat-reduction/nuclear-explosion-monitoring/global-3d-seismic-tomography; Simmons et al., 2011, 2012 and 2015) and SALSA3D (http://www.sandia.gov/salsa3d) model (Ballard et al., 2016b) were constructed within a spherical tessellation based framework, allowing for explicit representation of undulating and discontinuous layers, including the crust and transition zone layers.

In an attempt to provide a common model parameterization for multi-dimensional earth models across the community, Sandia National Laboratories created GeoTess (http://www.sandia.gov/geotess/, Ballard et al., 2016a). GeoTess is a software support system that deals with the construction, population, storage and interrogation of data stored in a particular model. GeoTess is not limited to any particular type of data and, with this software, the research community can develop 3D velocity models of the earth, pre-compute station–phase–specific traveltimes and traveltime uncertainties through their model in any manner they deem appropriate and deliver that information to monitoring agencies in a format that the monitoring agencies are prepared to accept. GeoTess is now also used for multi-scale amplitude and coda tomography (Phillips et al., 2014).

Most global body wave imaging studies now use irregular meshes of one sort or another (e.g., Burdick et al., 2008). These include: (i) the use of Delaunay and Voronoi cells, which are completely unstructured meshes, and their application to whole earth tomography (e.g., Sambridge and Faletic, 2003; Sambridge and Rawlinson, 2005); (ii) the use of adaptive schemes that dynamically adjust the parameterization during the inversion (e.g., Zhang and Thurber, 2005; Ballard et al., 2016b); (iii) the use of wavelet decomposition and progressive inversion techniques to address the multi-scale nature of seismic tomography and provide a natural regularization scheme (e.g., Loris et al., 2007; Simmons et al., 2011); (iv) the use of statistical methods such as partition modeling, which uses a dynamic parameterization and does not require explicit regularization (e.g., Sambridge et al., 2006; Bodin and Sambridge, 2009b).

Even though it is not yet possible to strictly quantify the improvement in seismic tomography of going from regular to irregular parameterizations, the merit of these alternative meshes is clear, as they allow us to overcome some challenges inherent to seismic tomography, such as uneven illumination.

Future R&D

Researchers in the monitoring community should investigate the feasibility of promising and recent approaches in the broader seismic imaging community regarding irregular meshes and their practical application to monitoring. These techniques include, but are not limited to, partition modeling and Bayesian transdimensional approaches, Delaunay and Voronoi cells, and wavelet decomposition approaches.

From phase amplitudes to envelope amplitudes (WSP2)

Seismologists like to downsample their data into forms that can be modeled, such as expressing a seismogram as a series of phase picks. Instead of the timing of phase picks, one could collect amplitude information from the seismogram. The goal of amplitude work is to obtain the source spectra (versus frequency) of an event, be it an earthquake, explosion, or other disturbance. The value to nuclear explosion monitoring follows from interpretation of the event using source models (Figure 35). Source models include the omega-squared model for earthquakes (Brune, 1970) and the Mueller-Murphy model (Mueller and Murphy, 1971) for explosions. Earthquake models, for example, allow interpretation of the source via its moment and stress drop. Seismologists are especially interested in explosion models, and research is progressing on fine tuning Mueller-Murphy type models, as well as developing new models that can be fit to source spectra to constrain parameters such as yield, depth-of-burial, and other emplacement conditions. Further, recovery of compressional (P) and shear (S) wave source spectra leads to event identification, as S corner frequency is often observed to be lower than P corner frequency (the Fisk Conjecture; Fisk 2006, 2007) for nuclear explosions, while earthquake corners are similar.

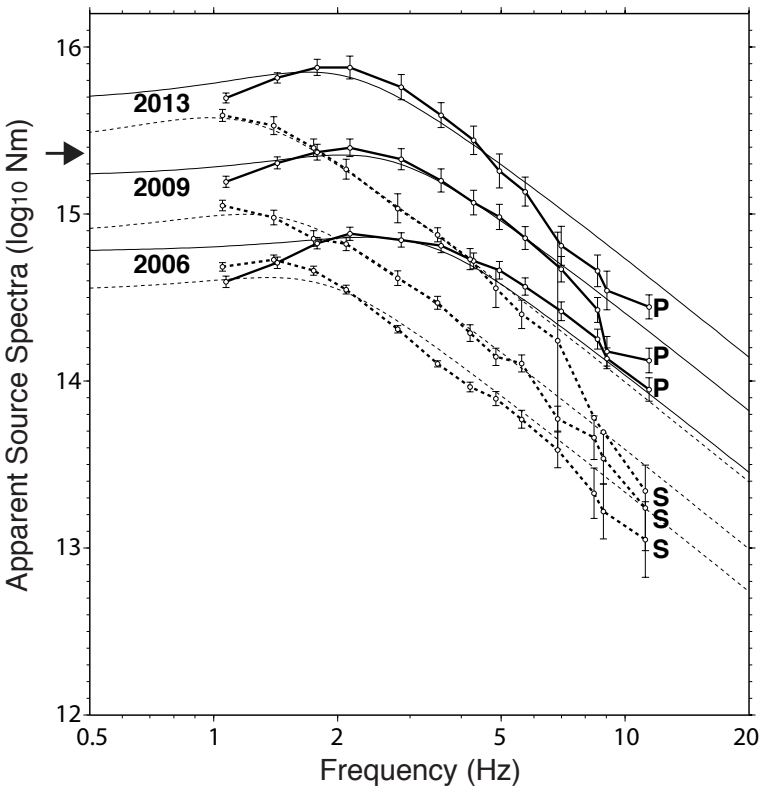

Figure 35. Compressional (P, solid) and shear (S, dashed) source spectra for the first three DPRK tests using direct wave amplitude data. Amplitudes have been corrected for path and site effects using a global model. Pn and Pg are combined for the P spectra, Sn and Lg for the S spectra. Error bars represent one standard deviation on the corrected amplitudes. An arrow marks an average of several moment estimates for the 2009 event. Spectra are fit using the Mueller-Murphy model for granite, employing the Fisk Conjecture with constant offset to include the S spectra. Model fits can be used to constrain yield, depth-of-burial and other emplacement conditions, while the offset between P and S for bands above the S corner frequency can be used to identify these DPRK events as explosions.

Amplitudes are traditionally measured by extracting a short segment of data around a phase of interest (Figure 36), taking a spectrum, and separating the spectrum into amplitude and phase components, keeping only the amplitudes for analysis and modeling. One can also bandpass filter seismograms in the time domain, measure the root-mean-square over a "boxcar shaped" signal window, and convert that measurement to the spectral domain (pseudo spectra, Taylor et al., 2002). The latter is often done in monitoring environments because it is useful to examine the time evolution of band-passed traces.

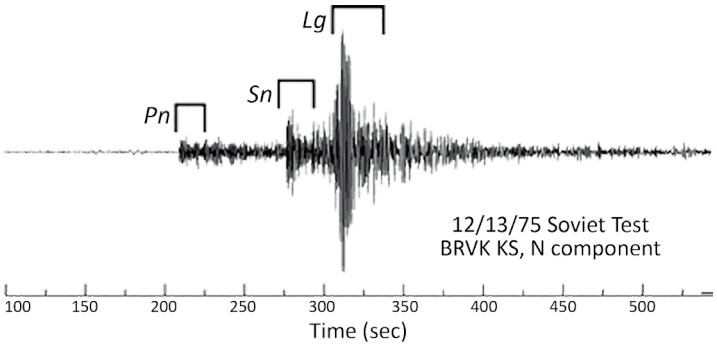

Figure 36. Signal windows (boxcars) applied to a Soviet test recorded at Borovoye. It is routine to similarly collect pre-event (before the first P) and pre-phase (before each phase window) noise measurements for quality control purposes.

Amplitudes of direct phases measured using the boxcar approach can be modeled by assuming simple earth structure, from which spreading functions are derived and removed from the data (Campillo, 1987). One assumes that the remaining distance effect is attenuation, which can be expressed as an exponential function of distance using the attenuation quality factor parameter Q (Figure 37). An inverse problem can be set up to solve for source, site, and path (Q) terms or differencing methods can be applied to solve for a subset of parameters. The inclusion of noise-censored data has been investigated (Taylor et al., 2003), and should continue to receive attention. After correction for Q, spectra (Figure 35) and discriminant ratios (Figure 38) are obtained. The Q can be a combination of intrinsic and scattering attenuation and will also reflect poor corrections for large-scale structure. Intrinsic Q is caused by

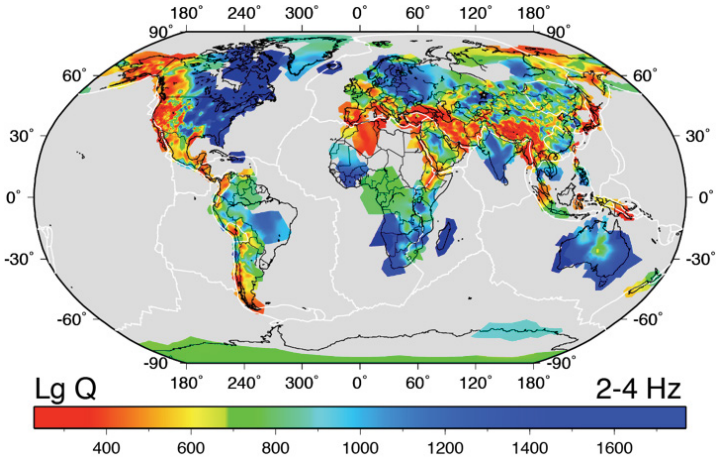

Figure 37. Global Q tomography model for 2-4 Hz Lg, based on a multiscale grid, which retains detail in well-covered regions such as Asia and the US. The Q correlates well with regional geology. Lg propagates well in shield regions and poorly in active tectonic regions. Details such as the Rio Grande Rift and the Tsaidam basin can be seen. Models for Pn, Pg, Sn and Lg are obtained simultaneously for all bands.

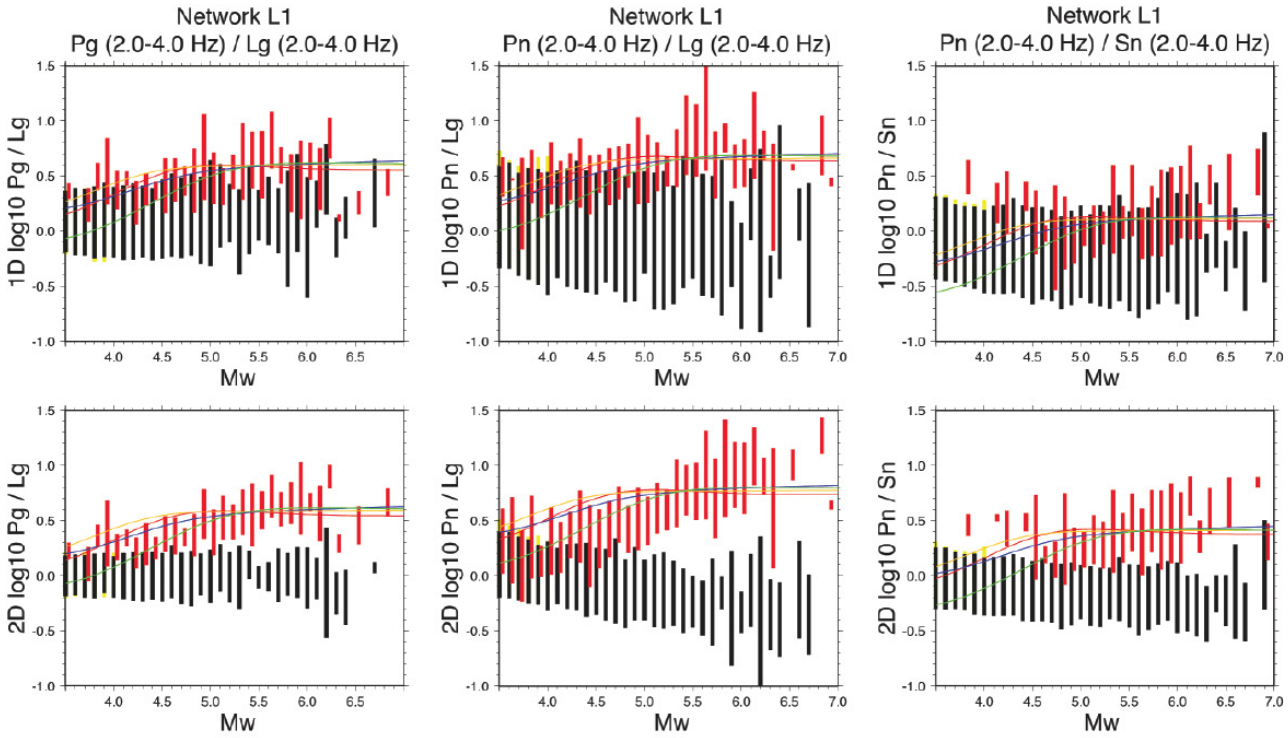

Figure 38. Global discrimination using 2-4 Hz P/S ratios. Pg/Lg, Pn/Lg and Pn/Sn results are shown from left to right. Best fit uniform (1D) models have been applied to correct results in the upper row, while 2D corrections have been applied to the lower row. Explosions (red) and earthquakes (black) are binned by Mw, bars represent one standard deviation of the ratio. One computes network medians of P and S source spectra, and employ Maximum Likelihood Estimation (MLE) methods to account for noise censored data prior to taking ratios. Curves represent predictions using the Mueller-Murphy model and Fisk Conjecture with constant offset for various emplacement media and standard burial conditions. Explosions include US, USSR, China, India, Pakistan and DPRK underground nuclear explosive tests. The 2-D results are much clearer and demonstrate convergence of the two populations towards lower Mw, which must be understood physically.

the conversion of wave energy to heat via bulk movement of water, displacement of water molecules from their electrostatic attraction to grain boundaries, or dislocation glide within crystals to name a few. Intrinsic attenuation is largely controlled by the presence of water, as Earth materials are highly attenuating compared to Lunar materials, where water is non-existent even though rock chemistry and structure are similar.

A critical facet of amplitude modeling is the use of source spectra of well-studied earthquakes as constraints. These spectra are obtained using coda spectral ratios coupled with independent moment estimates from regional or teleseismic waveform data (Mayeda et al., 2005b; Fisk and Phillips, 2013ab). The spectral constraints help resolve an inherent tradeoff between source corner frequencies and attenuation in the amplitude inversion, thus allowing multiple frequency bands to be inverted simultaneously (Phillips et al., 2014). The spectral constraints also raise the entire inversion to absolute levels, allowing recovery of absolute source spectra in Newton-meters (Figure 35), critical for inferring source parameters such as magnitude and yield. It was assumed that the efficiency by which earthquakes excite the various local and regional phases is independent of location and depth (restricting to crustal, seismogenic depths), and the constraint events will help test this. Further, the spectral constraints can be used for model validation in the same way ground-truth epicenters are used to validate traveltime models.

Regional Pg, Sn and Lg can be effectively modeled using the above approach. Data misfit can be 0.10-0.15 or so (log 10 amplitude ratio). Pn is different, however. Pn amplitudes can be highly variable, and data misfit is often a factor of 2 or more (0.3 log 10 amplitude ratio). This occurs even when advanced Pn spreading models are employed (Yang et al., 2007; Yang, 2011), although some variance reduction is observed in those cases (10-20%). The Yang models do give more realistic values for Q, however. Interestingly, Sn does not show the same behavior and is well fit by current schemes. It is believed Sn hugs the top of the Moho due to low or negative upper mantle gradients and perhaps higher attenuation with depth in the asthenosphere. Multi-phase models reduce the scatter in the phase ratios used for event identification as shown in Figure 38. Teleseismic P should be amenable to 3D inversion for attenuation, although initial efforts to determine the spreading functions using 3D velocity models need more work. Finally, it has been observed that local distance amplitudes show high scatter, which results partly from the shorter measurement time windows, but may be showing additional sensitivity to local structure and event radiation patterns.

Data quality control is the most difficult part of amplitude modeling. One can manually pick phase arrivals and apply simple signal-to-noise cuts using background and pre-phase noise estimates; however, much poor data can evade this scheme. The most effective techniques involve modeling intermediate stages using spectral ratios constructed to eliminate source, site or path effects. The relative source and site effects are very stable, and data that do not fit can be discarded. There are concerns about instrument response, which are, unfortunately, not well documented. Midnight noise measurements plotted versus time provide an effective means to locate shifts in instrument calibration, and consistent recording intervals are chosen using that method. For event-based data, residuals-to-model-fits (site, source, tomography) versus time provide a similar method, although with less time resolution.

Amplitudes can also be measured by fitting envelopes of the seismic coda to simple shape models, thus gaining a measure of redundancy in the method that leads to stability and high precision (Aki, 1969; Figure 39). The coda is also less sensitive to path effects and to radiation pattern effects because the scattered energy in the coda has left the source over a wide range of angles and traversed a wide range of paths. The redundancy of the coda measure can be thought of as having virtual stations at the scattering points of the coda waves. Amplitudes measured from coda are equivalent in terms of precision to measurements taken from an array of stations, which are not always available. The use of coda waves is, therefore, ideal for monitoring small events, for which only sparse station sets might be available.

Coda wave techniques were initially developed for use with local distance seismograms for which the coda could be measured after twice the shear wave traveltime, which allows the scattered energy to homogenize (Aki, 1969). Chouet et al. (1978) demonstrate that source spectra can be recovered from local distance coda waves, enabling seismologists to study differences in source scaling around the world in the pre-digital era. In regional distance applications, and for small events, one does not have the luxury of measuring the so-called "late" coda, and must measure the portion of the early coda that is available to us. To account for these effects, Mayeda et al. (2003) extend the local distance technique to regional distances by applying empirical distance corrections. Phillips et al. (2008) further extended the regional technique by incorporating 2D path corrections to the coda data in a manner similar to the direct wave techniques described above. Coda spreads differently from direct waves, and one uses spreading formulas that are initially flat with distance and eventually decay like direct phases, with a frequency-dependent critical distance.

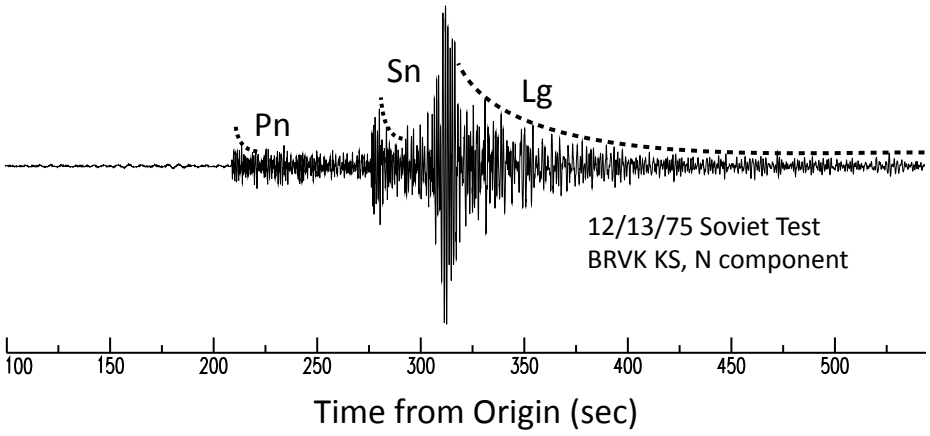

Figure 39. Coda (dashed) for the Soviet test recorded at Borovoye.

The Lg coda is the simplest to work with because it is the longest and yields the highest precision measurements. However, all local and regional phases generate coda and those are included in the method. In particular, the Pn coda is used for Mw and yield estimation in the European Arctic, and mantle phase codas are important for evaluating events in the Indian subcontinent, where Lg is quickly extinguished and cannot be relied upon.

Future R&D

Research and development on amplitude topics includes modeling entire seismic envelopes for purposes of maximizing precision and better covering the frequency domain for compressional (P) and shear (S) source spectra. The coda of an early arriving phase is difficult to measure because the coda is obscured by later arrivals. This is especially apparent in lower frequency bands, where the starting point of the coda may be obscured and what is observed is an ascending envelope. Modeling the entire envelope may be done empirically; however, a long-range goal is to produce physics-based models that describe the scattering environment that produces all envelope features. For example, ascending sections of the envelope as a secondary phase can be modeled as conversion via scattering between the primary (P) and secondary (S) phase types. This type of behavior is commonly observed and often destroys the classical envelope shape of peak and decay for a series of phases, resulting in level sections of the envelope between peaks. Forward scattering must also be modeled, which will allow the prediction of the shape of the direct wave peak, which is frequency dependent. Finally, backscattering is responsible for the undisturbed coda and that phenomena, along with attenuation, will be used to complete the model. This has long been an academic research topic with potential that is now beginning to be recognized by monitoring scientists. Radiative transfer techniques can be used to model envelopes in complex media and can be used to verify less expensive stochastic models.

Coda waves are used to construct earthquake spectra, from which Mw can be estimated by fitting to an omega-square or other source model, with stress drop constrained or unconstrained. Mw is a critical parameter for evaluating the magnitude and distance amplitude correction (MDAC) used in high frequency event identification.

Coda waves can also be used for event identification. In particular, older data with saturated direct phases can be evaluated using on-scale coda. Hartse et al. (1995) showed that a coda spectral ratio technique was effective for Nevada Test Site (NTS) events recorded at local distances.

From 1D hydroacoustic propagation to 3D models with uncertainty (WSP1, WSP3)

Hydroacoustic monitoring stations are fewer in number than any of the other three monitoring methods (radionuclide, seismic, and infrasonic), however their utility is enhanced by the unique physical efficiencies of sound propagation in the ocean. Similar to infrasound and seismic wave propagation, hydroacoustic wave propagation can be used to quickly assess event localization through back tracing the time from each receiving hydrophone.

In broad terms, coupled three-dimensional hydroacoustic wave propagation modeling has made significant progress in the last 50 years from initial efforts concentrated on simply tracing two-dimensional great circle routes on the surface of the earth from a source/receiver location to determine if there were any path blockages due to land (Dushaw, 2008; Dushaw and Menemenlis, 2014). Existing global-scale hydroacoustic models use a set of reasonable approximations to dimensionally reduce the intractable three-dimensional propagation in a fluctuating environment to a series of one- and two- dimensional problems that can account for large geological and oceanographic effects that refract paths of propagation. Today research efforts seek to extend to three dimensions the existing two-dimensional models that accurately handle acoustic propagation over range and depth, such as those using the parabolic equation finite element technique. However, computational efficiencies implemented within the existing two-dimensional models do not naturally extend to the three-dimensional case, limiting their usefulness on modest computational resources. Future computational modeling efforts are anticipated to be concentrated on two fronts: 1) modeling of probability distributions of the acoustic field that can account for arrival times and amplitudes and their fluctuations due to environmental uncertainty primarily to provide confidence limits of the acoustic amplitudes and phases, and 2) large-scale frequency domain three-dimensional propagation on high-performance computational resources. The former is an indirect attempt to solve the problem of a severely restricted set of fluctuating environmental data that can be fed to any hydroacoustic model, while the latter seeks to directly address what is an inherently unstable numerical problem (aqueous acoustic propagation overlying anisotropic thin elastic layers) through the direct application of computational power.

To a zeroth-order of approximation, sound in the ocean propagates to long ranges as if it were trapped in a cylindrical aqueous waveguide bounded by the ocean surface and the ocean bottom. There is significant spatial-temporal variation of sound speed in the ocean, and it is usually represented by an empirical relationship between ambient pressure, salinity, and temperature (Del Grosso, 1974). The predominant spatial dependence of the sound speed is in the vertical direction, with a much weaker dependence being in the transverse directions. This interplay causes a distinctive oceanographic feature called the sound fixing and ranging (SOFAR) channel to be present in much of the world's oceans for much of the calendar year. All that is required is for a warm water layer to be created through thermal heating (solar or transport of a heated surface layer) to create a thermal gradient in the upper ocean known as the thermocline. Below the thermocline, temperature and pressure interact to create a distinctive near-parabolic shape of the sound speed as a function of depth, with a minimum called the "sound-axis" located between 0 m and 2000 m of depth, depending on geographical location. This type of profile refracts acoustic energy within it toward

the minimum (i.e., central axis) and efficiently traps energy within it so that it can propagate long distances with almost no dissipative losses to the signal (Jensen et al., 2011). In fact, acoustic propagation within this channel is so efficient that even tiny explosions of a few kilograms of conventional explosives can be heard at ocean basin scale ranges.

In addition to the efficient signal propagation, the source coupling of explosive events into the water is also distinctive and efficient. An explosion, either upon or in the water, vaporizes the water, creating a vapor bubble that initially expands rapidly (Chapman, 1985, 1988; Geers and Hunter, 2002). This expansion puts a substantial amount of energy into an initial shock wave that is relatively quickly damped out and eventually converted into a high amplitude linear acoustic wave. This shock wave can be modeled to a very high degree of accuracy using a non-linear progressive technique that follows the wave front of the shock in the time domain (Ambrosiano et al., 1990). The blast front reaches a maximum radius where the pressure exerted on the water by the event is eventually balanced by the static pressure of the water, at which point the vapor bubble collapses upon itself and creates a ringing termed the "bubble pulse." Substantial amounts of low-frequency acoustic energy are transferred into the ocean and, in particular, into the SOFAR channel, wherein the energy propagates to long ranges. The resulting time/amplitude trace produced by bubble pulses can be used to achieve fairly accurate assessments of the yield.

Key insights that would prove the viability of hydroacoustic monitoring were a direct outcome of the analysis of the Acoustic Thermometry of Ocean Climate, Heard Island Experiment in the early 1990s, and a reanalysis of a 1960s event known as the Perth-to-Bermuda Experiment (Dushaw, 2008; Munk et al., 1994). Both of these events demonstrated that acoustic signals with substantial coupling of energy into the SOFAR channel could be detected at global distances in excess of 10,000 km. These insights included: 1) the horizontal/azimuthal refraction of the vertical modal structure of an acoustic signal's propagation was determined by the local effective index of refraction and the phase-speed of each vertical eigenmode (of course, interactions with the bathymetry are often not adiabatic, however their main effect is to couple the vertical eigenmodes together rather than scatter them out of plane (Shang et al., 1994)); and 2) once a proper eigenpath (i.e., the proper path from source to receiver that minimizes the cumulative phase) for each mode is determined, an approximate detection envelope could be determined by a recombination of the modes after propagation through the environment along their respective eigenpaths in a Range-Depth two-dimensional plane (McDonald et al., 1994; Collins et al., 1995). This can most easily be accomplished with a full field model such as the parabolic equation technique (Collins, 1994).

Jensen et al. (2011) provide a thorough presentation of the specifics of acoustic modeling in ocean environments and present only qualitatively the processes involved in calculating the acoustic field at global distances using a hybrid ocean acoustic model. This model uses at its heart an acoustic eigenmode model to calculate the local modal phase speed that can be used to determine the local index of refraction and hence the path that any propagating mode takes. As this is key, explanation in a little more detail follows.

It is sufficient for the present description to assume that the environment obeys the adiabatic approximation of geophysical parameters (i.e., slowly varying in space and time) with respect to latitude and longitude. Acoustic propagation to long distances between two points can be qualitatively and quantitatively described as a two-dimensional acoustic wave propagating within a waveguide with pressure release boundary conditions (air-water interface) on the upper boundary and impedance boundary conditions on the lower boundary (representing the ocean sediment interface). Implicit in the adiabatic approximation is that there is little local variation in azimuth in the environment, which results in three-dimensional propagation that can be locally regarded as Nx2D, where the N refers to independent azimuths. These approximations are wholly appropriate for those cases typically (< 10Hz) encountered within the monitoring community, where average gradients of the speed of sound in the water column as a function of depth are far larger

than those in latitude and longitude. Through the use of classic separation of variables, the problem can be reduced to a set of Sturm-Louisville differential equations that describe the dependence of the field in the vertical direction and radial directions respectively, with a common separation constant, κ_m^2 (the vertical eigenvalue), that must be determined through the solution to the vertical eigenmode equation

$$\rho \frac{\partial}{\partial z}\left(\frac{1}{\rho}\frac{\partial \psi_m(z;\mathbf{x}_\perp)}{\partial z}\right) + \left(\frac{\omega}{c(z;\mathbf{x}_\perp)}\right)^2 \psi_m(z;\mathbf{x}_\perp) = \kappa_m^2(\mathbf{x}_\perp)\,\psi_m(z;\mathbf{x}_\perp)$$

where ρ(z) is the water/sediment density, c(z) is the sound speed as a function of depth, ω is the radial frequency of the acoustic wave, and $\psi_m(z)$ is the *descrete* eigenmode associated with the vertical eigenvalue κ_m^2. Additionally, one carries the local transverse coordinate (i.e., x⊥) through to emphasize that the eigenvalue is a value local to the environmental conditions at a specific latitude and longitude. It can be shown that the pressure field within any range-independent region in the range-depth plane can be well approximated by a summation over the modal functions as

$$p(r,z) \approx \frac{ie^{-i\pi/4}}{\rho(z_0)\sqrt{8\pi r}} \sum_{m=1}^{\infty} \frac{\psi_m(z_0)\,\psi_m(z)}{\sqrt{\kappa_m}} e^{i\kappa_m r}$$

where the source is assumed to be at r=0 and $z = z_0$.

This modal expression, while appropriate for short distances, cannot capture all of the physics of horizontal refraction or range dependence. The adiabatic approximation and the discrete nature of the eigenmode solution implies that each eigenmode can be considered to travel independently of all the other eigenmodes in the range-depth plane. It can be shown that the $\psi_m(z)$ are discrete but mathematically complete and create an ability to model any propagating signal using a summation of modes. Secondly, weak horizontal coupling implies that each eigenmode also travels independently in latitude and longitude. Thirdly, each eigenmode attenuates in range with an attenuating amplitude that monotomically increases with increasing index m, thus at long distances only eigenmodes with low index survive. This allows us to further reduce the problem to one of tracking the lowest order eigenmodes (typically only the first). Clearly coupling exists between eigenmodes, however this energy redistribution mechanism is only efficient when there are strong interactions with the boundaries or abrupt changes in sound speed where energy can be scattered either out of plane or into other modes. Finally, each eigenmode has a unique phase speed and, because the mode is local, this phase speed determines the local modal index of refraction and, hence, the rate at which the mode refracts in the transverse directions (i.e., latitude and longitude):

$$v_{\text{phase}}^{(m)}(\mathbf{x}_\perp) = \frac{\omega}{\kappa_m(\mathbf{x}_\perp)},$$

or

$$\kappa_m(\mathbf{x}_\perp) = k_0 n_m(\mathbf{x}_\perp).$$

It can be shown that each mode refracts individually as a ray in a solution to an eikonal equation with shallow water squeezing the modes into higher phase speeds until each mode is cut off in turn and is either extinguished or propagates through via another energy conversion mechanism such as a T-phase. To achieve accurate results, the modal ray equation must be solved on the surface of the earth, an oblate spheroid with finite eccentricity (Heaney et al., 1991). Thus, one must not only take into consideration the local index of refraction due to changes in the local modal spectrum which in turn are due to changes in the local bathymetry and oceanography, but also the local curvature of the earth. If using the coordinates (ϕ; λ; α), where ϕ is the longitude, λ the latitude, and α the local heading of the ray, then the modal ray equations can

be shown to be:

$$\frac{d\phi}{ds} = \frac{\cos(\alpha)}{\mu(\phi)},$$
$$\frac{d\lambda}{ds} = \frac{\sin(\alpha)}{\nu(\phi)\cos(\phi)},$$
$$\frac{d\alpha}{ds} = \frac{\sin(\alpha)}{\nu(\phi)}\tan(\phi) - \left(\frac{\sin(\alpha)}{\mu(\phi)}\frac{\partial \log \kappa_n}{\partial \phi} - \frac{\cos(\alpha)}{\nu(\phi)\cos(\phi)}\frac{\partial \log \kappa_n}{\partial \lambda}\right),$$

where

$$\mu(\phi) = \frac{R\left(1-\epsilon_{\oplus}^2\right)}{\left(1-\epsilon_{\oplus}^2 \sin\phi^2\right)^{\frac{3}{2}}},$$
$$\nu(\phi) = \frac{R}{\left(1-\epsilon_{\oplus}^2 \sin\phi^2\right)^{\frac{1}{2}}},$$

where $\epsilon_{\oplus}$= 0.0818 is the eccentricity of the earth, and κ_n is the local modal eigenvalue. The solutions to these equations also naturally result in a travel time between any two points on a ray path and give timing solutions that can be used to accurately estimate a source position. Formally, these paths are called "eigenpaths". It should also be kept in mind that ray approximations are theoretically *only* valid in the limit of infinite signal frequency. While very good agreement between ocean acoustic ray models and measurements can be obtained at frequencies as low as a few hundred Hertz, this is clearly very far from the hydro/seismo-acoustic regime of nuclear explosion monitoring (typically <10Hz) (Forbes and Munk, 1994; Harrison, 1977; Weinberg and Burridge, 1974; Yan and Yen, 1995).

These solutions led to research pursuing more accurate predictions of the latitude-longitude path of each vertical acoustic eigenmode. Modal ray paths can be determined when a detailed knowledge of the local modal decomposition is known along that path. This requires a continuous and detailed understanding of the local (i.e., half-wavelength scale) environmental conditions, including the oceanography, bathymetry, and geology (e.g., Smith and Sandwell, 1997). Using this, a modal database can be created. Typically, one starts from some seasonally averaged values. The entire procedure must be repeated for *each* frequency, as both vertical and horizontal propagation effects are strong functions of frequency. However, once computed, these eigenvalues can be stored and used at will for any future calculation, making the initial computational cost high, but successive computations are very low cost based on the work of Kuperman et al. (1991).

These methods are well equipped to investigate water borne explosions, but are not directed at the problem of land-based events, as the eigenmodes are determined by a waveguide and require some vertical stratification in the propagation medium. Furthermore, geological events can emit energies that are nearly equal or larger in magnitude than explosive events. While this can be thought of as a source problem, its manifestation on the hydrophones can in fact be purely a wave propagation and scattering issue. Energy that couples in this manner, whether from an explosive event of interest to the monitoring community or a geological one, is known as a T-phase and is extremely difficult to model and predict correctly (de Groot-Hedlin and Orcutt, 1999, 2001; D'Spain et al., 2001; Talandier and Okal, 1998). This difficulty has to do with a distinct lack of knowledge of much of the ocean bathymetry and sedimentology, as a specific type of geometry must exist for the coupling to take place. These are areas where seismic-only waves can interact with facets and faults in the ocean sediment that are nearly perpendicular to the wave motion and in contact with the water (Piserchia et al., 1998). Events that couple well into the SOFAR channel can be used as secondary or tertiary methods of event localization and yield estimates. On the other hand, the bathymetry and sedimentology near islands with seismic stations is generally well characterized

so that the acoustic propagation is understood. Inverse T-phases, i.e., seismically recorded hydroacoustic arrivals, can be used as a detection mechanism (Hanson and Bowman 2006). Thus, a set of "virtual" hydroacoustic stations can be used to ameliorate the paucity of hydroacoustic triads.

In the deep ocean, the main physical variables that affect SOFAR propagation are temperature, salinity, and pressure (or depth)(Figure 40). Thus, it would seem natural to expect that better characterization of these parameters throughout the ocean volume would lead to more accurate predictions of both yield and localization using hydroacoustic monitoring. Current research into long-range acoustic propagation continues as an outgrowth of efforts to monitor the mean temperature of the oceans over global scales from well-known fixed sites between which paths and azimuthal effects are well understood. These newer efforts seek to probe the SOFAR channel for perturbations by understanding the vertical arrival structure that can be used to gain detailed knowledge of the eigenmode distribution/dispersion characteristics, due to path, and sound speed fluctuations (Colosi et al., 1994, 1999). Stochastic models of the acoustic field due to the uncertainty and fluctuations can be used to determine detailed oceanographic structures that can be fed into oceanographic models via data assimilation techniques (Colosi, 2016; Dushaw, 2014; de Groot-Hedlin et al., 2009). These efforts have investigated numerically efficient algorithms to propagate the uncertainty and also the adjoint field that can give information about the gradients of the relevant environmental parameters (Gerdes and Finette, 2012; Hursky et al., 2004).

Long-range ocean acoustic propagation is substantially more complicated than these zeroth-order descriptions would seem to imply for four main reasons (Figure 41). Firstly, there can be substantial acoustic coupling between the ocean and submarine geological structures due to the closer impedance match between the two wave-supporting media (relative, for example, to atmospheric coupling back into seismic propagation). Modern accurate hydroacoustic

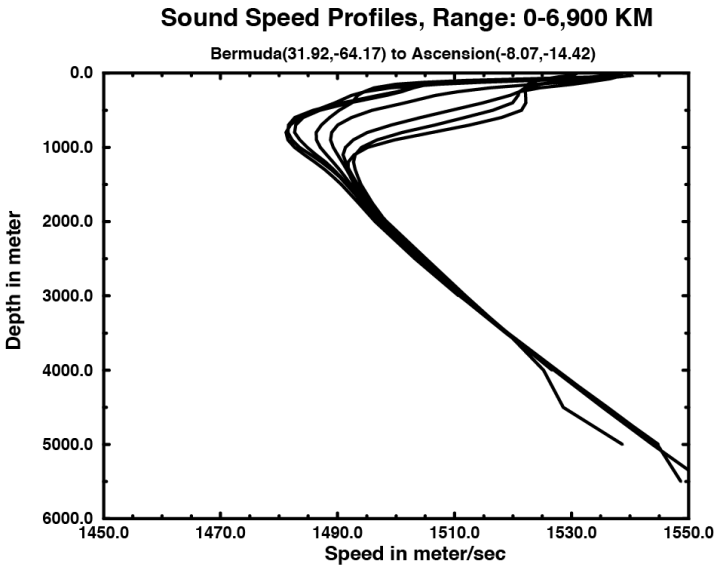

Figure 40. Seasonally averaged sound speed data retrieved from a set of ray paths from Bermuda Island to Ascension Island through the mid- and equatorial -Atlantic. Note the pronounced SOFAR channel present in typically warm waters. Fluctuations in sound speed due to internal waves and other oceanographic phenomena can be treated as perturbations on these data.

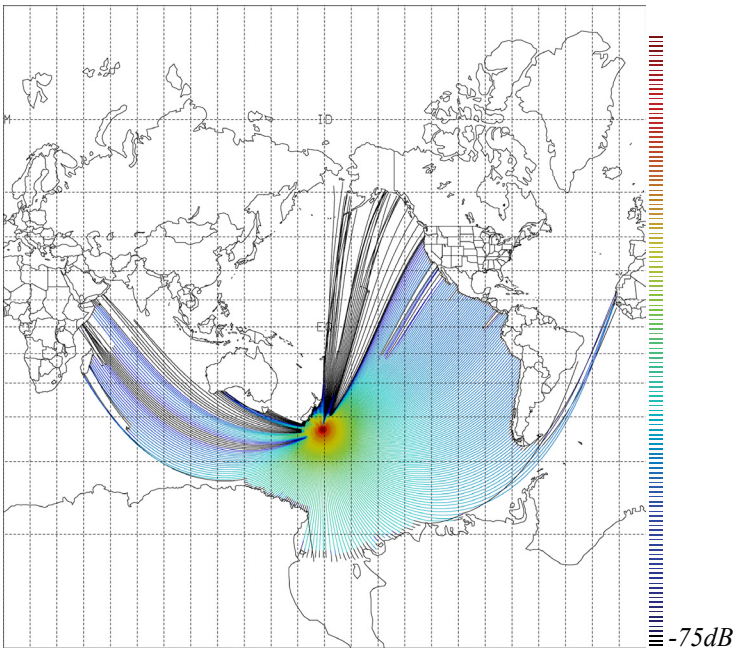

Figure 41. The results of the solution to the ray equations for the first mode (m=1) assuming a source location near the southeastern edge of New Zealand. This example clearly shows the effects of land masses and bathymetry as either complete extinction of the ray path or diffraction around islands, shallow waters, and the general refraction of the modes into warmer waters. Color scale represents loss in decibels with dynamic range of 60dB relative to source level at 1m.

propagation models will need to be able to accurately handle the non-trivial hydro/seismo-acoustic problem, i.e., interactions between the solid earth and the fluid ocean. Secondly, at regional ranges (i.e., < 10-100 km) water-borne acoustic energy, to a very good approximation, propagates roughly radially within the water in a cylindrical geometry, interacting locally with the bathymetry and water without much azimuthal coupling (i.e., range-depth). Dispersion and scattering, in addition to the refractive effects discussed above, while ever present, become increasingly complicated and can play substantial roles in altering the propagation path as the range increases and the signal wavelengths increase so as to create more coupling with the ocean sediment (McDonald, 1996).

It should be noted that the ocean is a dynamic environment with three-dimensional variability (e.g., Figure 42) that is opaque to remote sensing techniques. In the distant past, the ocean acoustic parameters were assumed to be some functional form with minor perturbations over entire basins. This gave way generally throughout the 1960s and 1970s to seasonal averages collected and interpolated over a global scale that could be used as a starting point for the temperature and salinity measurements that result in the vertical sound speed dependence. Recent advances in earth monitoring systems have been primarily associated with global climatology to better characterize the oceanic volume using both sea surface measurements using satellites and direct physical sampling via gliders as well as drifting buoys. While these data provide points of reference and help bound oceanographic processes, point measurements do not generally provide sufficient coverage to accurately capture the state of the ocean as a wave propagation medium.

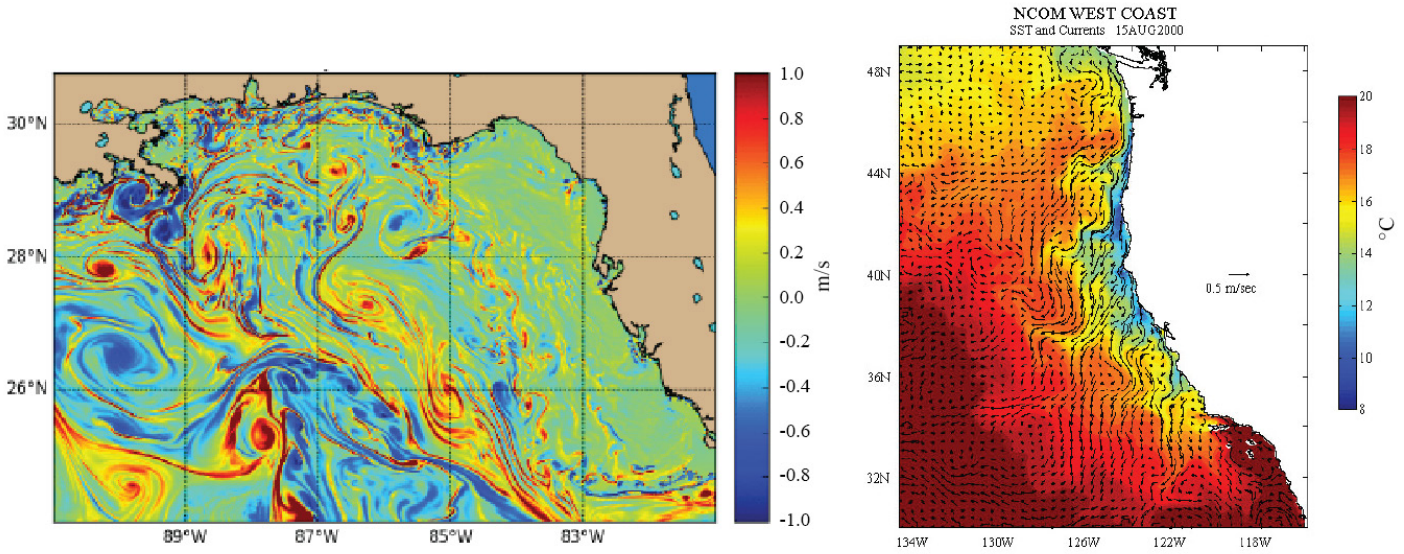

Figure 42. High resolution hydrodynamic ocean models can be used to capture eddies and fluctuations in density, temperature, and salinity, as well as currents. These can result in exceptionally complicated pictures of the ocean as an acoustic wave propagation medium. These examples can be used in conjunction with point measurements and acoustic thermometry measurements to give bounds on the space and time dependence of the physical parameters that determine the sound speed. The left image is a model output of the surface currents effects on the sound speed in the Gulf of Mexico, including large scale eddies. The right image shows both sea surface temperature (color) and currents off the California coast (arrows). These types of models can be used to determine the fluctuations in sound speed encountered by a passing acoustic signal.

A subject of current research is the methods to use these measurements of the oceanographic features within global circulation models to provide bounds on the fluctuations of the sound speed profile as a function of both space and time. By using statistical arguments, these in turn can provide confidence limits on the acoustic propagation. Additional current research is aimed at using direct long-distance acoustic propagation to infer the ocean state at length scales smaller than what is typically calculated, so as to increase the accuracy of the ocean model and predict the acoustic environment given a current state of the ocean (Figure 43). However, for the foreseeable future, the accuracy of any hydroacoustic model will be what

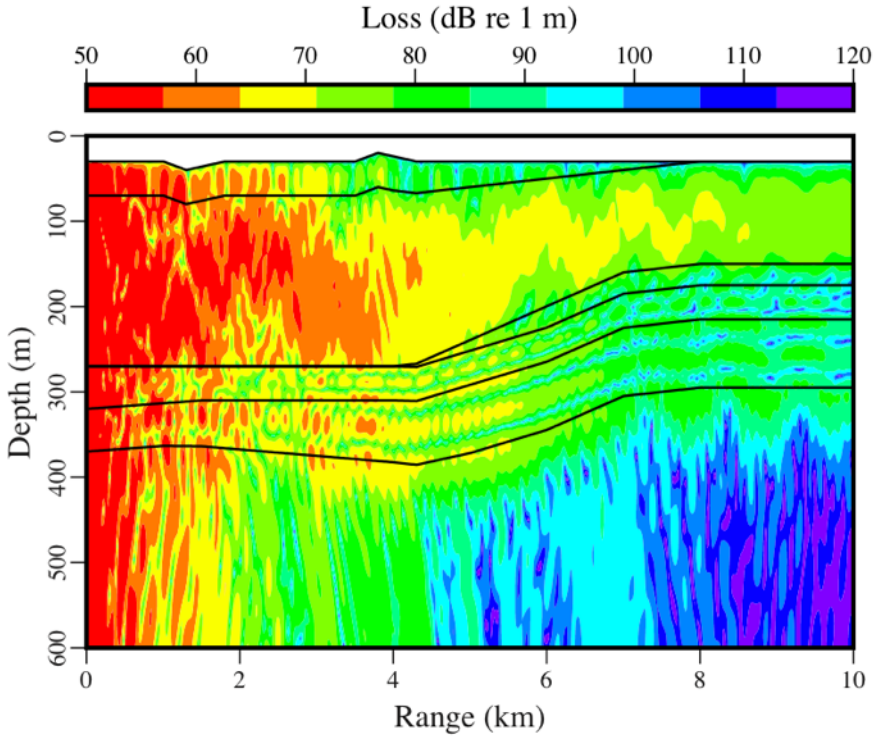

Figure 43. Current research has emphasized the Arctic region where thinning ice sheets overlaying ocean and anisotropic layered sedimentary rock presents a series of very difficult modeling problems. The output from the seismo-acoustic parabolic equation shows that this solution method can now handle ice cover, elastic sediment layers, porous sediment layers, variable layer thickness, sloping interfaces, and variable topography.

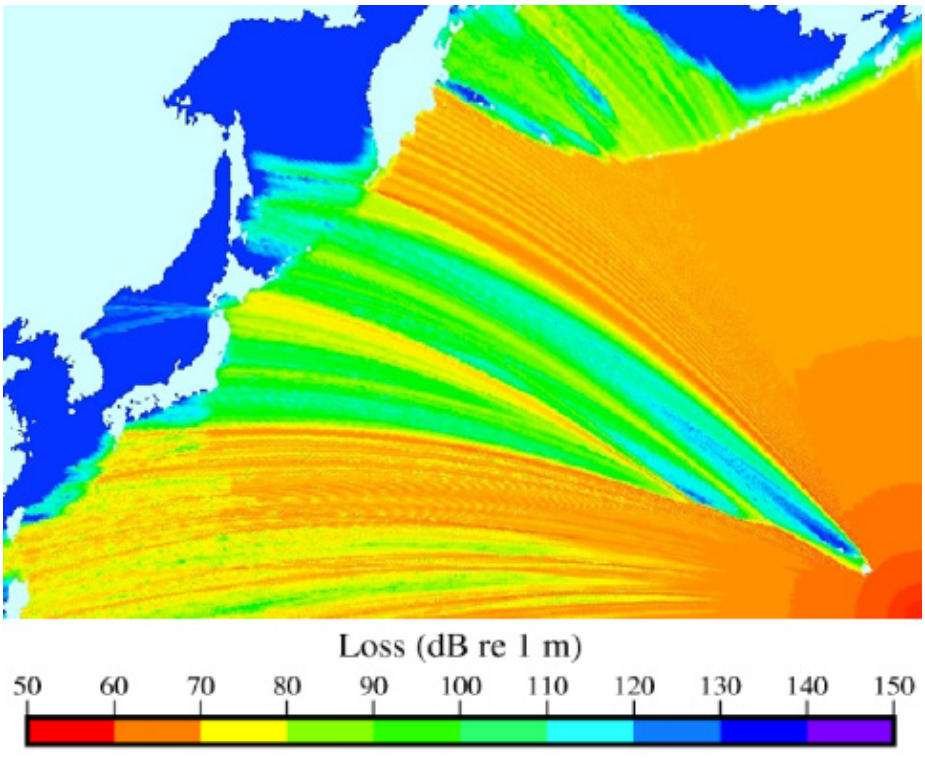

Figure 44. Diffraction and refraction can be qualitatively studied in this single mode solution, wherein the first eigenmode is assumed to be adiabatically decoupled from the other eigenmodes, and is propagated with horizontal coupling from a source location placed southeast of the Hawaiian Islands. Quantitative results from this approximation are only approximate, as vertical mode coupling is neglected.

is termed "input-data limited" and no deterministic forward propagation model will be able to capture all of the instantaneous effects the environment will impress upon the propagating wave (Figure 44). The best that can be hoped for is to propagate the effects of the uncertainty in the environment within the acoustic field predictions. Perturbations to the sound speed shape caused by the physical effects of local phenomena, e.g., temperature, salinity, and depth variations, as well as larger-scale oceanographic effects such as currents, circulation, and internal waves can essentially randomize the phase (Dushaw, 2014). The path from past to present to future research in ocean acoustics is a function mainly of more accurate high resolution environmental data.

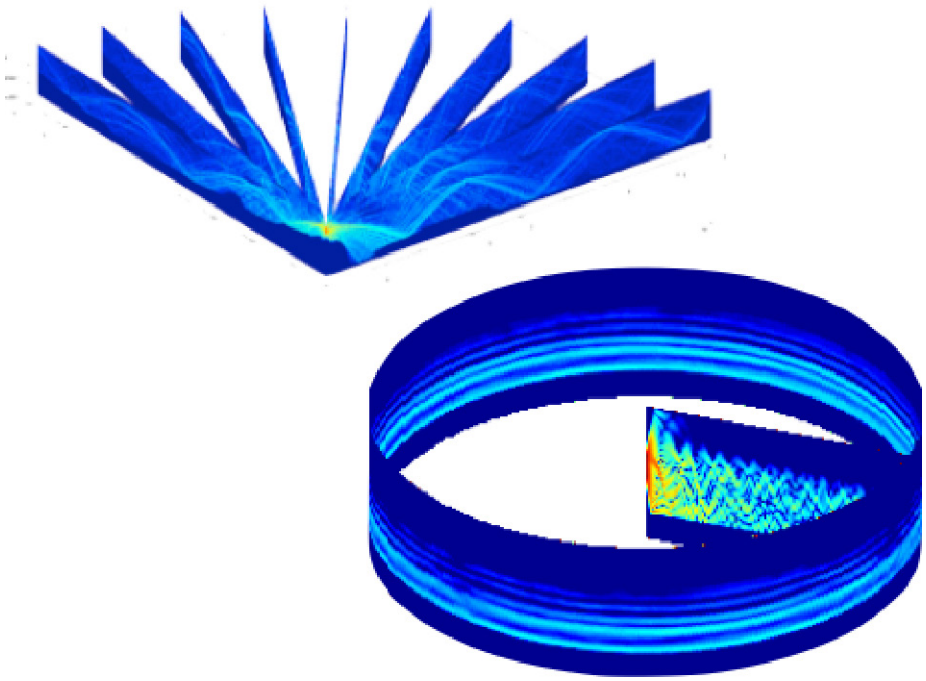

Figure 45. Propagation in three dimensions can be well approximated as in the Nx2D method that ignores coupling between azimuths (upper left). In such cases the crux of the problem is determining the exact path over long distances over which to model the range-depth propagation. Tremendous efficiencies in numerics allow for both qualitative and quantitative assessments of the acoustic field to be determined at global distances. Truly three-dimensional propagation simulations, such as that shown on the lower right, include coupling between azimuths, but suffer from their inefficient and unstable numerical implementations. As yet, three dimensional hydroacoustic can only be implemented on large computational resources or over only regional ranges.

There is also a substantial effort to create an efficient three-dimensional hydroacoustic propagation model (e.g., Figure 45). There are significant hurdles to achieving that goal, not the least of which is numerical stability. The physics of wave propagation in a liquid overlying an elastic substrate is in fact an underdetermined numerical problem. Most often, stability of the solution can be achieved through the addition of an additional, but ill-defined, constraint equation, often the conservation of energy flux. Continuing efforts at including more complex two-dimensional geometries and geophysics have been included within the parabolic equation method. These have included anisotropic sediment layering, rough interfaces, and the inclusion of ice (Collins and Siegmann, 2015). In the frequency region below 2 Hz, it has been possible for some time to use the hybrid method briefly described above and a reformulation of the parabolic equation technique in the horizontal plane to account for basin scale refraction and bathymetric effects that are nearly adiabatic (Collins, 1993).

Future R&D

Truly three-dimensional seismo-acoustic propagation and systems performance models for nuclear explosion monitoring purposes are under continuous development, but for the foreseeable future, hydroacoustic modeling approximates the physics by using high performance computing to process large amounts of environmental data.

From dilution estimates to source probability distribution functions (RSP1)

Detection of radionuclides can serve as the confirmation of a nuclear explosion, but it must be known where the radionuclides originated to obtain the full potential of the radionuclide signatures. Once radionuclides are released from a nuclear explosion, they are carried by atmospheric transport to International Monitoring System stations. With a proper understanding of how atmospheric transport affects the signature, it is possible to infer information about the source of the radionuclides, which in turn has implications about location.

When the CTBT was first opened for signature in 1996, atmospheric transport was relatively crude compared to today's standards. The standard for that period in time was to use air parcel trajectories for a cloud of an assumed size to predict the activity concentration and the path of the cloud across detectors (Bjurman et al., 1990). While these simulations could project a path for a large radionuclide cloud, they were not able to provide the information desired for monitoring small underground nuclear explosions.

As detector systems around the world began to be capable of increased sensitivity, it was required that the atmospheric transport modeling (ATM) employed by the CTBTO Preparatory Commission follow suit. In 2003, ATM began to be explored for use within the verification regime of the CTBT (Wotawa et al., 2003). Using a source-receptor matrix mixology, the International Data Centre was able to estimate the dilution factors that were orders of magnitude larger than with the air parcel calculations.

Once dilution factors could be estimated, an emphasis was directed both towards better estimates of the dilution factors and trajectories of the radionuclide signals. It was important to not only know what the dilution factor was at a given IMS station, but also what IMS stations would see a signal. With advances in this field, ATM became successful in estimating dilution factors and the probable trajectories of radionuclide releases.

A *de facto* test scenario for the ATM programs was the Fukushima reactor accident. With the release of such large amounts of radionuclides, it allowed for the testing and verification of ATM at much larger distances and dilution factors (Eslinger et al., 2014) (Figure 46). The forward modeling projections of signals can also be useful in combination with stack monitoring data from a medical isotope production facility. Knowing the source released from the facility, potential events within the IMS can be predicted prior to a positive detection (McIntyre et al., 2016b).

Another important factor for ATM related to the IMS is to be able to estimate the source strength via backtracking of detected results. With more advanced atmospheric models and data from around the world, it is now possible to perform signal backtracking following an IMS station event. The source backtracking allows for the identification of a possible source region, while forward modeling is often used for the ATM analytical analysis of the source estimate. Source backtracking is another technique that was demonstrated during the Fukushima reactor accident.

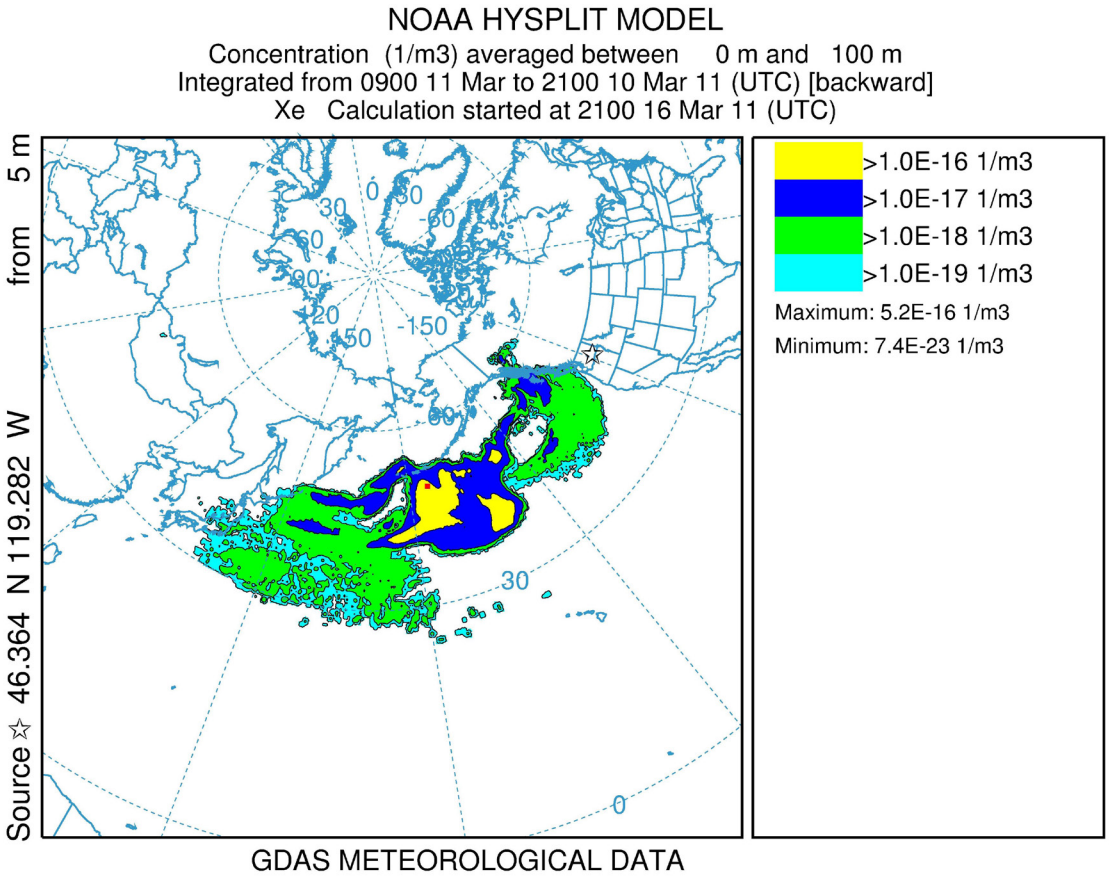

Figure 46. ATM model of the Fukushima reactor accident using HYSPLIT.

Unfortunately, due to the wide range of possible parameters and input conditions, the uncertainty on the source localization estimates can be quite large. Recent research has looked into the use of Bayesian techniques with probability density functions to utilize the results from multiple stations (either positive or null hits) to better estimate the source location (Eslinger and Schrom, 2016). The additional information from multiple stations provides further constraints on the models, resulting in a more accurate estimate of the initial release location.

As research into signal propagation progresses, it will be more important to utilize additional detection information to better estimate the source of origin and reduce uncertainty. In addition, shorter collection periods will help to better pinpoint the location of the source.

Future R&D

Research into the utilization of advanced atmospheric transport modeling techniques and measurements from multiple stations will be required to better estimate the source of radionuclide releases.

Sensors - Recording the Signals

In an operational monitoring system, sensors come into play after source physics and signal propagation. Sensors collect the continuous data (waveform and radionuclide) that will be processed to detect, locate, and categorize events of monitoring interest. Waveform sensor systems record seismic, hydroacoustic, and infrasonic signals and archive those data along with their metadata. Radionuclide sensors are complete sampler/analyzers rather than simply transducers. The radionuclide systems encompass automatic collection of particulate material or gases, chemical processing if required, then measurement of temperatures, pressures, and radioactive decay.

From limited dynamic range sensor stations to high-resolution broad-band seismic arrays (WSE1)

Increasing the detectability of seismic signals from nuclear detonations at teleseismic distances required significant improvements in instrumentation, for both seismic sensors and recorders. Improvements came from enhancing the response of individual sensors, moving from only-vertical short period to tri-axial broadband sensor arrays. Although beneficial, increasing frequency band and dynamic range for individual sensors is not enough, as the seismic background noise imposes a significant constraint on the limit of detectability. As described by Douglas (2002), a 1 kt detonation would result in a signal of 1 nanometer at 1 Hz recorded at long distances, which is below the seismic background noise. Thus, seismic arrays, a type of seismic station with sensors spaced closely enough that signals are coherently recorded by the sensors, were identified as a necessity for nuclear detonation detection at these distances (Barth, 2003). Arrays for nuclear monitoring evolved from very large (teleseismic array) designs in the early 1970s with apertures of 100s of km and 100s of elements, such as the LASA array in the U.S. and the NORSAR array in Norway (Husebye et al., 1989), to regional ones (with apertures of several kms) such as ARCESS and NORESS in Norway in the 1980s, to improve detection by optimizing signal and noise characteristics (Ingate et al, 1985). The IMS network features a sparse global distribution with a combination of seismic stations composed of short period sensor arrays and individual three-component broadband sensors. Future seismic instrumentation may provide an improved global distribution of very dense, large aperture, high-fidelity, three-component broadband seismic sensor arrays (Koper and Ammon, 2013) complemented with dense, ubiquitous networks of low-cost vibrational sensors (seismometers and accelerometers).

Measurement of the vibration of the earth produced by earthquakes has evolved from one-component electro-mechanical short-period sensors with low frequency response around 1 Hz, to tri-axial broadband sensors with low and high frequency limits around 0.001 Hz and higher than 10 Hz, respectively. Seismic instrumentation has also decreased in self-noise with modern seismic sensor noise below the background noise of the earth (Ringler and Hutt, 2010). For example, the seismic noise for modern broadband sensors is tens of dBs below the low noise models for seismic background (Brown et al., 2014). Sensor arrays enable signal processing techniques where the non-coherent components of the acquired time series are suppressed while the coherent components are enhanced. The larger the number of elements in the array, the greater the noise reduction. Temporary array deployments featuring a large number of sensors, e.g., USArray, NodalSeismic (Nakata et al., 2015), or the Mount St. Helens nodal array (Hansen and Schmandt, 2015) have shown their value for significantly improving characterization of seismic phases and imaging. Future seismic instrumentation for scientific purposes, i.e., imaging the interior of the solid earth and its interactions with the surface, may include the deployment of dense sensor arrays with high fidelity three-component broad-band sensors (Koper and Ammon, 2013), as recommended by the "Seismological grand challenges in understanding Earth's dynamic systems" (Lay, 2009).

Along with high-fidelity instrumentation, a significant change in seismic sensors technology, driven by consumer products, is the development of low-cost vibrational sensors based on Micro Electro Mechanical System (MEMS) technology. These sensors do not have low noise compared to research-rated seismic sensors but can be mass-produced, leading to a significant increase in the number of sensors that can be deployed at a fraction of the cost. For example, the Community Seismic Network (Clayton et al., 2015) features several hundreds of MEMS sensors deployed in an urban environment (Pasadena, California). These inexpensive vibration sensors are being deployed densely in buildings for structural health monitoring (Sabato et al., 2017), and embedded in commercial products (e.g., computers and cell phones) and are creating the potential for ubiquitous urban networks. Such sensor networks differ from traditional networks in that the sensors and the analog-to-digital conversion systems are not high-fidelity, some elements of the network are not fixed in space, and the urban environment imposes highly variable noise (variable in intensity and frequency characteristics). Several projects are underway to test the utility of such dynamic seismic networks such as the Quake Catcher Network (Cochran et al., 2009), MyShake (Kong et al., 2016) and the Earthquake Network (Finazzi, 2016) for earthquake early warning systems. Assessing the data quality as well as archiving and analyzing the very large amounts of data produced by such networks are some aspects that need to be addressed for this emerging technology. Also, fusing the information from ubiquitous networks with well-established high-fidelity seismic instrumentation is another important aspect that needs to be addressed to assess the actual utility of such networks for scientific and monitoring purposes.

Future R&D

Emerging seismic instrumentation may provide an improved global distribution of large-aperture, very dense, high-fidelity, three-component broadband seismic sensor arrays. Also, networks of low-cost vibrational sensors are being deployed ubiquitously in urban environments and generating large amounts of data. Such networks can be deployed inexpensively and feature large numbers of elements. Their utility for complementing high-fidelity instrumentation for scientific and monitoring efforts remains to be demonstrated and will require, in addition to fundamental physics validation, adapting our current data analysis techniques and developing new ones to use large volumes of data from very dense networks deployed in potentially noisy environments.

From sparse monitoring stations to a dense network (WSE2)

Sensor networks for the purpose of monitoring nuclear explosions have evolved over time.

A fundamental challenge that any nuclear monitoring system faces is being able to observe and make accurate measurements of the signal energy propagating from the nuclear explosion. For all of the monitoring technologies, whether it is seismic, hydroacoustic, infrasound, or radionuclide, the instruments deployed must be able to measure the signals of interest at levels that are above the background noise at the station. The most straightforward way to make significant improvements to the monitoring thresholds is to improve station coverage and reduce the anticipated distance between the station and explosive source locations.

Prior to the CTBT being open for signature in 1996, the International Monitoring System (IMS) did not yet exist. There were, however, other national monitoring networks. These monitoring networks were largely established for the purpose of monitoring for large explosions at teleseismic distances (> 2000 km) or earthquake monitoring. Initially, many of these earlier stations were incorporated into the IMS and certified to be functional to IMS requirements. This adoption of existing stations facilitated rapid growth in the early years of the establishment of the IMS. The status of IMS station installation is maintained by the CTBTO Preparatory Commission at http://www.ctbto.org/map. New stations take significant time and resources to

construct, and with the IMS substantially complete and operational, the establishment of the remaining IMS stations is occurring at a slower rate. Many of these planned stations present unique challenges, such as difficult physical access, harsh weather, lack of infrastructure, and political instability.

Examples of current research into dense monitoring networks include the California Community Seismic Network (Clayton et al., 2011), the Quake-Catcher Network (Cochran et al., 2009), and the USGS "Did You Feel It" web portal (Wald et al., 2011). Networks such as the Community Seismic Network or Quake-Catcher rely upon wide involvement of the community to host low cost monitoring equipment. In the case of the USGS "Did You Feel It" system, the monitoring system relies upon individuals self-reporting their qualitative observations of observed ground motion. It is worth mentioning also the project Raspberry Shake (http://www.raspberryshake.org) that utilizes inexpensive analog geophones and a small computer (https://www.raspberrypi.org) to collect and process seismic data and report seismic events that are shared over the network to the public. It remains to be seen what contribution such networks could have to enhance nuclear explosion monitoring. Although the performance of non-traditional sensors is much lower than that of a traditional monitoring station, the large number of monitoring stations that could be deployed would result in an increase in station density and a commensurate increase in the probability of detecting a nuclear explosion.

The Transportable Array (http://onlinelibrary.wiley.com/doi/10.1002/2015JB011870/abstract) and Big-N networks (https://www.iris.edu/hq/initiatives/recording-the-full-seismic-wavefield) are examples of coordinated efforts to deploy a very dense network of stations across some regions. For the time being, such networks are only temporarily deployed, which can limit their usefulness for longer-term monitoring applications. They do, however, provide useful geophysical source and path parameters that are needed for monitoring.

Future R&D

Finding ways to leverage dense networks deployed for other purposes should be explored for their potential to improve nuclear explosion monitoring.

The impact of increasing the number of stations in the monitoring network and decreasing the corresponding distance from any given location on the earth to the nearest station is a general improvement in the detection threshold of the monitoring system.

From simple to complex sensor deployment planning (WSE3)

The establishment of a global monitoring network requires the commitment of significant resources to build the stations, construct a reliable communications infrastructure, and institute a data analysis center. System planners evaluate station location options based on projections of the performance of the overall network. In addition, deployment planning capability is useful in assisting decision makers in understanding the impact of station outages as well as maintaining and upgrading existing networks.

The performance metrics of a monitoring network that are typically identified as essential include the likelihood that the network will detect an event, the ability for the event to be accurately located, the ability to extract the information to categorize the event as a man-made explosion versus a natural occurrence such as an earthquake, and the reliability of the network over a range of operating conditions. Of these metrics, detection is of primary concern. To successfully simulate the performance of a monitoring network, detailed information is required in the form of models for the characteristics of the source (energy vs. frequency, energy partitioning, etc.), models for how the signals propagate through the geophysical media (earth, water, or air), and details on the monitoring network (station locations, instrument pass-bands, background site-noise, etc.). Prior to building any stations, it is necessary to plan what types of monitoring stations will be used and where they will be located to meet the specifications of the monitoring network.

For all of the waveform monitoring technologies (whether it is seismic, hydroacoustic, and infrasound) the instruments deployed must be able to measure the signals of interest. This means that the amplitude of the signals of interest must be larger than that of the noise at the station making the measurement. The observed signal amplitude at a station depends upon the yield of the source explosion, how well it couples to the ground material, and the amount of path attenuation.

The noise present at a station is due to both the local site noise and the self-noise of the equipment being used. Local site noise is typically established in a site survey prior to installing a station. Once sited, there is not much that can be done to improve local site noise. For this reason, monitoring stations are deployed in quiet, isolated regions of the earth when possible. To address the self-noise of the equipment, monitoring system requirements are already in place to limit the sensor and data recorder noise levels to be less than the local site noise.

Estimates of the signal and noise amplitudes and their associated uncertainties at each station allow for calculation of a signal-to-noise-ratio (SNR). This SNR estimate is then used to calculate the likelihood that the individual station and, by combinatorics extension, the entire network will have detected the event.

To establish confidence in the results of such a planning capability, there must be a significant amount of validation of the methodology and models that are being used. Typically, this validation is performed against existing stations and ground-truth sources. Once confidence in the methods and models is established, the simulations may be performed with greater confidence for situations in which there is less available empirical data, such as when establishing new stations or simulating events in locations where there has not previously been activity.

Early implementation of network performance modeling dealt largely with global teleseismic networks. Simple models were used that assumed that the event's source was fairly homogeneous across the earth and that the stations were at distances such that the teleseismic path attenuation models were sufficient and used an approximate averaged model of local site-noise (Sereno et al, 1990; Ringdal et al, 1992).

Over time, a number of improvements were made to the models to improve the fidelity of the simulations. For seismic, these include the incorporation of regional path attenuation models, site-specific empirical corrections (Walter and Taylor, 2001), and the incorporation of real-time site-noise models (Brown et al., 2014). Hydroacoustic modeling became possible through the development of blockage models that predict how shallow water and land masses attenuate or block signals propagating through the ocean (Farrell, 1997). Infrasound modeling presents a unique challenge due to the diversity of assumptions in the source characteristics (Kinney and Graham, 1985) and the unpredictability of the propagation through the atmosphere. However, recent improvements in atmospheric and wind models (Le Pichon et al., 2012) have allowed for improvements in infrasound modeling capability.

The result of improvements to the simulation methodologies and methods has been better fidelity of the simulations that may be performed. This improved fidelity has allowed for planning tools to have increased usefulness at increasingly closer distances. It is expected that improvements to local (< 200 km) source and propagation models will allow for further performance prediction and planning of local networks.

Future R&D

Improvements to source amplitude and propagation models will improve the fidelity of network planning tools at increasingly closer distances.

From dedicated calibration facilities to on-sensor calibrations (WSE4)(RSE2)

Evaluating instrumentation and providing "factory quality" calibration for nuclear explosion monitoring equipment has historically been performed in highly capable facilities with dedicated resources. This is primarily due to the specialized equipment, costs, and experience necessary to perform this work. Examples of such facilities include the Facility for Acceptance, Calibration and Testing (FACT) site at Sandia National Laboratories, which has capabilities in testing digitizers, infrasound sensors, and short-period seismometers, and the USGS Albuquerque Seismological Laboratory (Hutt et al., 2011) (http://earthquake.usgs.gov/contactus/albuquerque/history.php), which has extensive capabilities in testing seismometers.

Such large facilities continue to be necessary to provide the underlying verification and validation of instrument calibrations. However, it is becoming increasingly common for smaller facilities with fewer capabilities to be used to perform limited evaluations. Such facilities serve a role providing less expensive and more rapid turn-around time, such as in the case of production evaluation of an existing design or in low-consequence monitoring system deployments, when more complete evaluations may not be needed. For example, the IRIS/PASSCAL Instrument Center operates an equipment depot for instrumentation in support of geophysics experiments (http:www.passcal.nmt.edu). They have a capability for performing fast turn-around calibration of large numbers of instruments as is prudent both before and after fielding.

In addition, many components exist which can perform in-field self-calibrations. These self-calibrations do not provide traceability or accuracy in their measurements. However, they do provide a consistency check to build confidence that the equipment may not have changed since being deployed. Digitizers and seismometers have had self-calibration capabilities for decades. In the past few years, there has been an infrasound sensor introduced which also has a built-in self-calibration capability (Merchant and McDowell, 2014). Such capabilities will allow for more confirmatory calibrations to be performed in the field in addition to the typical facility calibrations performed before a deployment. It is expected that the implementation and use of instrument calibration will only increase as the users of monitoring systems expect ever increasing levels of accuracy and traceability in the data that they are analyzing.

When verification of the CTBT through radioxenon detection first began in 1996, the radioxenon detection community was just learning how to calibrate a nuclear detector for the variety of signals measured from the four relevant radioxenon isotopes (Bowyer et al., 2002; Ringbom et al., 2003). Initial detector calibrations were relative to a known activity of a given xenon isotope. Unfortunately, while this method is perhaps the most straightforward and requires minimal scientific knowledge to perform, the initial activity, initial xenon volume, and transfer efficiency can impact the accuracy of the calibration and future measurements.

Isotopically pure samples would be most useful for calibration, but were not available during the development of first generation of radioxenon detection systems. The primary source of radioxenon for calibration (prior to 2009) was emissions from fission-based medical isotope production, which consisted of only ^{133}Xe and ^{131m}Xe.

In 2008, work was performed to simulate the beta-gamma coincidence signals from isotopically pure radioxenon samples (Haas et al., 2008). The simulation of isotopically pure samples paved the way for the development of isotopically pure experimental calibration spikes. In 2009, the University of Texas developed a means of producing isotopically pure radioxenon isotopes (^{135}Xe, ^{133}Xe, and ^{131m}Xe) through neutron irradiation of isotopically enriched stable xenon isotopes (^{134}Xe, ^{132}Xe, and ^{130}Xe) (Haas et al., 2009). The fraction of ^{133m}Xe to ^{133}Xe is enhanced through the optimization of the neutron spectrum used for irradiation.

With the availability of pure radioxenon isotopes, the use of the absolute calibration method became a possibility for beta-gamma detectors (Cooper et al., 2013). Through the comparison of the relative beta and gamma signals seen in a detector, the effective beta and gamma detector efficiencies can be calculated for the coincidence signals. This method works for beta-gamma detectors, but systems relying on gamma spectroscopy through the use of a HPGe detector still have to use the relative calibration method.

IMS stations are calibrated with ^{133}Xe and ^{131m}Xe in conjunction with detector simulations. There has been recent work on the preparation of highly accurate calibration samples using unequal length proportional counters to determine the activity concentration with a high degree of accuracy. Sample preparation and deployment solutions have been developed for the laboratory environment, but more specifically, for the IMS stations in the field (Foxe et al., 2015b). With a detector going through an in-depth factory calibration, it may be possible to perform more relative field calibrations (Figure 47) to ensure that the factory calibration is still valid.

Figure 47. The calibration suitcase was developed to repeatedly and consistently deliver calibration gas to IMS stations.

Future R&D

It is likely that research will be done to find a useful combination of in-depth calibration of detectors at the factory and a simple confirmatory calibration technique in the field.

It should be noted that the calibration of proportional counters used in the detection of ^{37}Ar are calibrated in a much different manner. The fill gas for the proportional counter must be calibrated on a sample-by-sample basis through the use of a quality control source. Generally, a ^{241}Am source is used to produce 8-keV X-rays within the copper proportional counter. The X-rays from the inner wall then produce an 8-keV event within the proportional counter, serving as a calibration peak.

From uncertainty to traceability in measurements (WSE4, RSA1)

An important development in sensor and instrumentation evaluation has been an increased level of traceability in the measurements that are made. Traceability in this context refers to there being a comparison of an instrument's measurement to a known calibrated standard, such as those defined by the U.S. National Institute of Standards and Technology (NIST). Traceability provides confidence in the accuracy and reproducibility of the measurements that are being made when evaluating monitoring systems.

Traceability has long been in place for the evaluation of data recorders through the calibration of reference instruments at an accepted standards laboratory. Data recorders are typically evaluated by generating signals with known characteristics and then feeding the signals into the channels of the data recorder. The performance of the data recorder is then determined by analyzing the characteristics of the recorded signals. The calibrated instruments are able to verify the characteristics of the reference voltage signals that are input to the data recorder.

For seismometers, there are a couple of options for traceable calibrations. Comparison calibrations using a reference instrument and coherent measurements of natural seismicity or background noise have typically been performed. For passive spring-coil designs, a lift test has historically been performed to determine sensitivity. More recently, improvements to shaketables have resulted in products that, with reasonable effort and augmentation, could provide a standards traceable input signal to the sensor (Larsonnier et al., 2014a). Previous calibration shake/step tables could not address the precision, frequency passband, or load weight required for the seismic domain. For infrasound sensors, calibration has been more of a challenge (Larsonnier et al., 2014b). Infrasound sensors include a wind noise reduction system for which calibration must be performed on site in an uncontrolled environment (Gabrielson, 2011). Current standards available for traceability of pressure measurements exist for static pressures and for acoustic frequencies above 20 Hz, however not for frequencies within the passband of infrasound between 0.02 and 20 Hz. As improvements in capabilities are made, traceability can increase from a single or few frequencies to cover the entire frequency passband of the instrument.

When radioxenon and particulate detectors were first implemented for verification of the CTBT, there were limited measurement indicators available for the nuclear analysts. These measurement indicators consisted of the collection and acquisition cycle durations and the sample volume. The state-of-health data was limited and was stored in databases (if at all) with manual query systems.

In 2000, research began to focus on the utilization of other measurement indicators that were available from a radionuclide monitoring station. These included detector and gas background comparisons and temporal measurement comparisons (activity trends). Along with the additional measurement indicators, state-of-health reports began to be generated for stations. In approximately 2015, research began generating sophisticated state-of-health monitoring systems. The goal is to predict when maintenance is required for the system or when the uncertainty on the data will be too large to draw a reasonable conclusion.

In the case of radionuclide signatures, one's ability to confidently determine if a nuclear explosive test indeed took place depends on the uncertainties associated with the radionuclide measurements.

There have always been uncertainties associated with the radionuclide measurements (both activity measurement uncertainties and gas quantification uncertainties). More recently (Axelsson and Ringbom, 2014) there has been in-depth analysis of the uncertainty associated with specific radioxenon measurements and radioxenon ratios. This uncertainty analysis provides a detailed understanding of one piece of the puzzle, but there are many other aspects that are unknown (e.g., atmospheric transport dilution factors). Once the uncertainties from each of these pieces are incorporated, it will allow for the production of a radionuclide event categorization matrix (ECM) as a framework for dealing with associated uncertainties.

Future R&D

Monitoring capabilities will be improved if and when measurement traceability for a given technology is improved. By improving the traceability of the calibration standards, more confidence can be had in the sensor measurements. In addition, increased state-of-health monitoring within the monitoring system will help to improve the reliability of the system.

From noble gas experiment to network demonstration (RSE1)

Since the detection of radioxenon is the primary method of determining the nuclear nature of an explosion, the development of radioxenon monitoring systems has been a vital part of the verification regime for the Comprehensive Nuclear-Test-Ban Treaty (CTBT).

The first radioxenon detection systems developed were in support of the CTBT in approximately 1996 – 2000. A variety of radioxenon monitoring systems emerged: the Automated Radioxenon Sampler-Analyzer (ARSA) (Bowyer et al., 1999) (Figure 48), the Swedish Automatic Unit for Noble-gas Acquisition (SAUNA) (Ringbom et al., 2003) (Figure 49), the Système de Prélèvement Automatique en Ligne avec l'Analyse du Xénon (SPALAX) (Fontaine et al., 2004) (Figure 50), and the Analyzer of Radio-Isotopes of Xenon (ARIX) (Dubasov et al., 2005; Popov, 2005) (Figure 51). Initial testing of these systems took place with the International Noble Gas Experiment (INGE) (Auer et al., 2004) wherein the radioxenon systems were brought to a central location for comparison and validation. As of March 2017, 31 of the 40 allowed noble gas stations in the IMS were populated with 15 SAUNA, 12 SPALAX, and 4 ARIX systems. The ARSA system was not implemented within the IMS.

Figure 48. The U.S. ARSA system.

Figure 49. The SAUNA system developed in Sweden.

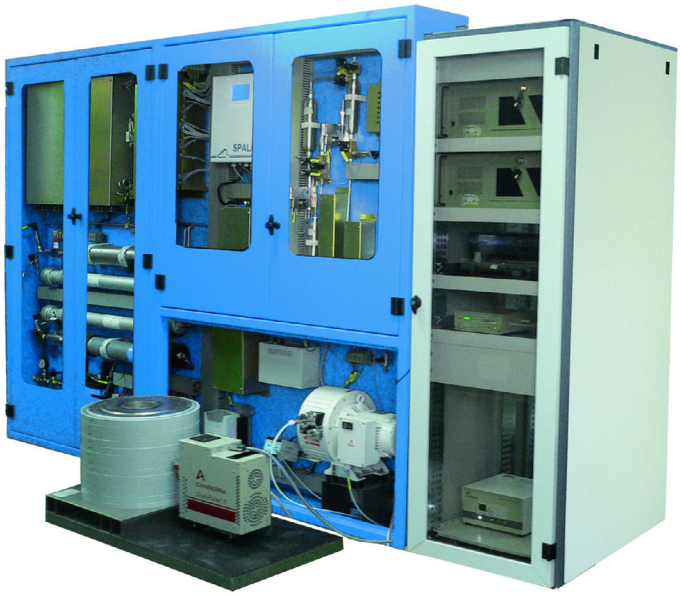

Figure 50. The French SPALAX system.

Figure 51. The Russian-developed ARIX system.

Following the initial implementation of the first generation of radioxenon detectors within the IMS, there was research that resulted in improved detection limits of the systems. This research focused on collecting more xenon in a shorter period of time, better detection of the radioxenon once it was inserted into the nuclear detector, and better operational performance of the system (reliability and maintainability).

To collect more xenon in a shorter period of time, more air needs to be processed and a higher collection efficiency needs to be achieved. Research into more efficient collection techniques (i.e., pressure swing adsorption) has been a key in the reduction of both the complexity and duration of the collection process (Williams et al., 2010).

The operational reliability of radioxenon systems has been enhanced by the elimination of consumables. Through the transition from helium to nitrogen as a carrier gas (Hayes et al., 2015), an expensive consumable gas has been replaced with an inexpensive/renewable alternative that can be generated on-site. Liquid nitrogen, on the other hand, which is used for cooling during the xenon collection process, is expensive to generate on-site, or transport to remote sites. The elimination of liquid nitrogen for cooling was possible through the use of improved adsorbents and highly efficient small micro-channel heat exchangers to reduce the power required for the collections process. With the reduced cooling power, the liquid nitrogen was replaced with Stirling-cycle mechanical coolers.

The improvements to the various components of the radioxenon detectors allows for a continuous decrease in the minimum detectable concentration. With the advances in xenon collection, system robustness, elimination of consumables, and the nuclear detector improvements, a new generation of detectors are being prepared, specifically, Xenon International (Hayes et al., 2015), SAUNA-3, SPALAX-NG (Le Petit et al., 2015), and ARIX-2. This suggests that testing will be needed for these second generation systems.

Future R&D

Research will need continued focus on the removal of consumables and improved detection limits of the nuclear detectors and chemistry processes.

From a single spectrum to coincidence detection (RSE1)

Two important factors in achieving greater sensitivity for aerosols and radioxenon systems are collecting more sample (i.e., processing more air) and improving the detector sensitivity. Detection mechanism and detector type improvements have gone a long way in improving the detector sensitivity, but there still exist areas for continued development.

Some of the early nuclear explosion monitoring measurements of ^{133}Xe as a result of a nuclear explosive test occurred in May of 1965 following the Chinese bomb test CHIC-2 (Schölch et al., 1966). The first measurements of ^{133}Xe were made using a gas chromatograph to separate out the xenon from other gases, then measuring the beta spectrum with a proportional counter used for ^{14}C age dating at the C-14 laboratory in Heidelberg. With ^{133}Xe being the only isotope measured at the time, it was relatively easy to measure the ^{133}Xe activity after xenon purification took place.

In the mid to late 1990s, when radioxenon systems were being developed for verification of the CTBT, the quest to measure lower concentrations of radioxenon and multiple radioxenon isotopes led to the utilization of two detector types, HPGe and NaI. The excellent isotope identification properties of HPGe led to the detection and identification of the radioxenon isotopes through gamma spectroscopy. The SPALAX system operates with a HPGe detector (Fontaine et al., 2004). On the other hand, NaI became practical with the advent of the beta-gamma coincidence (Figure 52) detection method which was widely adopted and developed by the United States (ARSA) (Bowyer et al., 1997) and Sweden (SAUNA) (Ringbom et al., 2003). The beta-gamma coincidence counting method with a plastic scintillator beta detector and a NaI

gamma detector has been widely adopted at IMS radionuclide stations, notably in the form of the SAUNA (Ringbom et al., 2003). Several countries are currently exploring systems with improved energy resolution and multiple coincidence detection for reducing ambient background species (e.g., ^{133}Xe), thereby increasing sensitivity to other relevant xenon isotopes.

Research is continuously performed to try to enhance the capabilities of the beta detector. On a parallel research path, in 2012, work began on the process of enhancing a HPGe gamma spectrometer with beta-gamma coincidence methods (Le Petit et al., 2015). With the utilization of a HPGe detector for the gamma detector, there is potential for enhanced isotope discrimination between the radioxenon isotopes, which could make the system ideally suited for a laboratory environment (Foxe et al., 2015a).

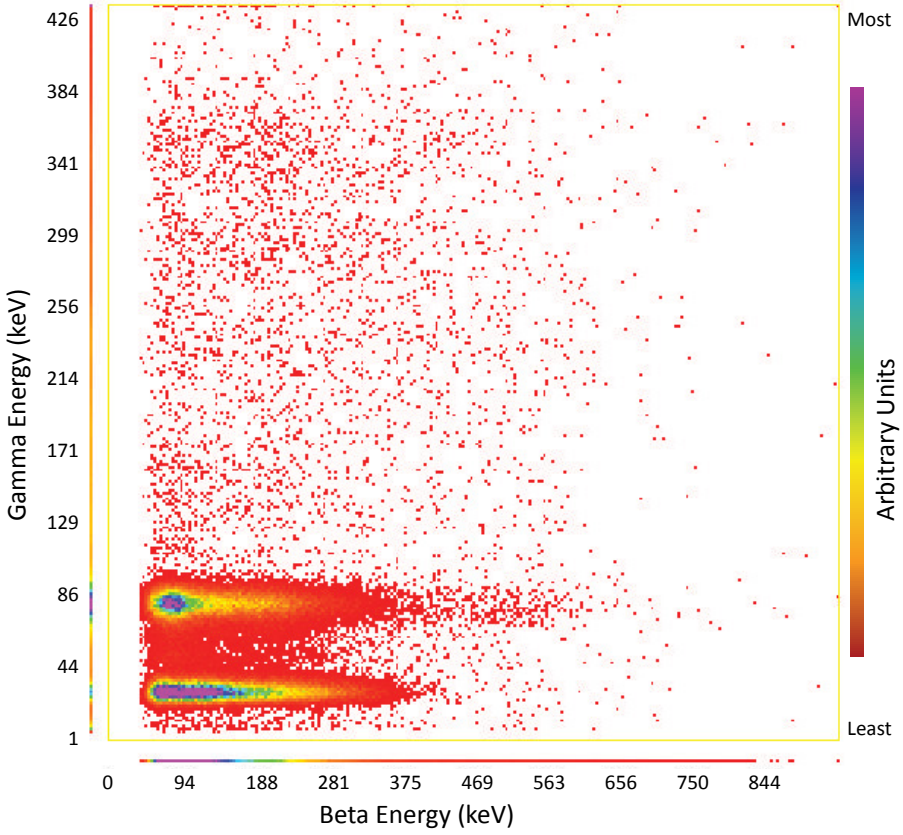

Figure 52. A two-dimensional beta-gamma coincidence histogram of an intense ^{133}Xe sample taken at IAR (Heimbigner et al., 2000). If an event consists of both a beta event (X-axis) and a gamma event (Y-axis), then the beta energy is plotted against the gamma energy. The color bar on the right provides a scaling for the number of events in each bin, with red being the least and purple being the most (white means zero events). Each of the 4 radioxenon isotopes have a distinct coincidence signature, allowing for regions-of-interest to be defined.

It seems clear that beta-gamma coincidence will continue to be utilized heavily for the detection of radioxenon.

Similar to the improvements obtained with radioxenon through the use of beta-gamma detection, coincidence measurements can be used in the particulate monitoring regime as well (beta-gamma, alpha-gamma, and gamma-gamma (Keillor et al., 2011)). The goal of all of these detection methods is to provide better sensitivity and reduce the backgrounds associated with the measurement.

Future R&D

Leveraging decay physics, such as gamma-gamma coincidence or detectors with improved radioxenon ratios to better characterize and discriminate the isotopes of interest, remains a productive focus of research.

From longer to shorter integration periods for in-field analysis (RSE1)

The primary purpose of a radionuclide monitoring system is to detect the radionuclides in the air mass that passes over the monitoring station. As a radionuclide plume from a nuclear explosion traverses a radionuclide monitoring station, it is important that the radionuclide detector systems adequately collect the radionuclide particulate and gases. In cases where the sample integration time is too long, there is potential to dilute the radioxenon with stable xenon that is collected before or after the radioxenon air mass passes over the monitoring station. Additionally, longer integration periods increase the uncertainty of source localization using ATM.

When radionuclide detection systems were first developed for the verification of the CTBT (Bowyer et al., 1997; Miley et al., 1998a,b), both the particulate detectors and the radioxenon detectors utilized what is now understood to be a long sample integration time of 12-24 hours. Unfortunately, the radioactive plumes have the potential to pass by stations in much less than 24 hours. Due to the long sample integration times, the analysis of the acquired data in some original systems took place more than a day after the sample was collected.

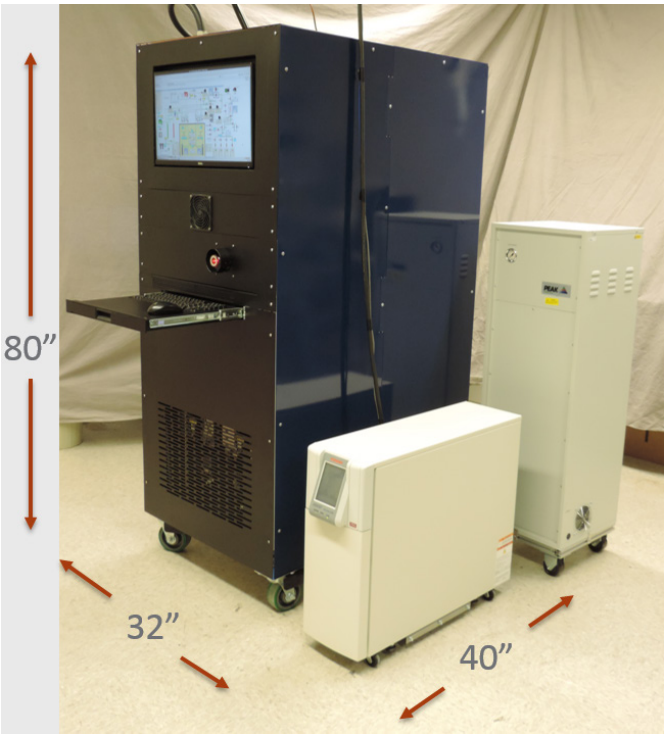

Figure 53. Xenon International (http://tbe.com/energyenvironment/xenon-international) prototype system (center) with an external UPS (front right) and nitrogen generator (back right).

With second generation radionuclide systems, air can be collected and processed more quickly. Using higher flow rates, the detection systems require less collection time to reach the desired detection limits. In 2015, new prototype radioxenon systems began to be capable of sample integration times of 6 hours and 8 hours (Figure 53). Even with shorter sample integration times, there is still the possibility that a plume may span multiple collection periods, resulting in collections being below the minimum detectable activity of the detectors.

Future R&D

If the radionuclide stations had an early warning alert (e.g., from a seismic event consistent with an explosion), they could potentially alter their collection cycle to better detect radioactivity present in the atmosphere.

Studies for the new generation of systems has shown that the shorter integration periods greatly benefit the monitoring system, even in cases where the minimum detectable concentration increases due to less sample as compared to a longer sampling time for the same system. This is possible for the new generation of systems because of the higher air-flow rates, resulting in increased sample volumes.

From plastic scintillator to solid-state detectors (RSE1)

Solid-state detectors have the potential to greatly improve the energy resolution and remove the memory effect associated with plastic scintillator beta cells. The correct utilization of these solid-state materials could be an important advancement in the detection of radioxenon, a key radionuclide signature of nuclear explosions. Beta-gamma coincidence detectors have long utilized a plastic scintillator (Figure 54) as the detection mechanism for electrons emitted during the decay of radioxenon. Two areas of improvement with

plastic scintillator beta cells are: improving the energy resolution, and removing the adsorption of xenon into the plastic, referred to as the memory effect. The removal of memory effect and improvement of the energy resolution have been focuses of nuclear detector research to improve the detection limits, and guided the research towards the use of solid-state detectors. The combination of these two detector requirements has been a primary driver for radioxenon beta cell development over the years. The initial beta-gamma coincidence detectors were developed for verification of the CTBT in 1996 (ARSA, SAUNA) and consisted of BC-404 plastic scintillator for the beta cell, along with a NaI gamma detector. A high-resolution beta cell was not previously required when only ^{133}Xe was of interest; due to the continuous nature of the beta spectrum, it is more important to see the same spectrum each time than to see a specific spectrum. As more radioxenon measurements were made, it was realized that improved energy resolution was desirable.

Figure 54. Example of a 4 cm^3 (~1 cm x 4 cm) plastic scintillator beta cell used in current ß-γ detectors, designed to fit inside of a NaI detector well.

As the radioxenon monitoring community started to measure the four traditional radioxenon isotopes (^{135}Xe, ^{133}Xe, ^{133m}Xe, ^{131m}Xe), it became evident that beta cells must be able to adequately discriminate between the ^{131m}Xe conversion electron and that of ^{133m}Xe. Improved energy resolution of the beta cell allows for less interference between the conversion electron peaks (129 keV for ^{131m}Xe, and 198 keV for ^{133m}Xe), resulting in improved discrimination between the metastable xenon isotopes.

A standard practice to reduce the memory effect is to perform a series of pump-and-flushes, in which the beta cell is evacuated, filled with a carrier gas, and subsequently evacuated again. The mixing of the carrier gas and the xenon within the cell promotes more complete extraction of the xenon. While this is a key aspect of reducing the memory effect, it does not eliminate the impact. The memory effect can sometimes be accounted for through the measurement of a gas background (measuring the percent memory effect) between samples. There are instances when this is not enough for the system though; one such extreme example is the Fukushima reactor accident (Bowyer et al., 2011; Stohl et al., 2012). During the accident, there was so much radioxenon released into the environment that the memory effect resulted in a large radioxenon signal. In this instance, if there were a small concentration of radioxenon observed by the detector (~1 mBq/m^3) from a nuclear explosion, it could have been masked by the memory effect (this would likely not be the case for Xe-135 as the memory effect would decay with a short half-life).

A variety of materials were tested to see if they would improve the energy resolution, reduce the memory effect, or both. These materials included Stilbene (Warburton et al., 2013), scintillating glass, and yttrium aluminum perovskite (YAP) (Seifert et al., 2005), and it was found that they possessed the potential to reduce the memory effect, but often times lost energy resolution as a result. A more widely adopted method of reducing the memory effect is through the use of Al_2O_3 coatings on the surface of the plastic scintillator (Blackberg et al., 2011). The Al_2O_3 coating impedes the diffusion of the xenon into the plastic scintillator, but the coating process often results in a loss of energy resolution by a few percent.

An alternative path to the memory effect coatings has been the development of beta cells using silicon detectors instead of plastic scintillators (Le Petit et al., 2013; Cagniant et al., 2014; Foxe and McIntyre, 2015; Foxe et al., 2015a, 2016). The use of silicon (or other solid state detectors) greatly improves the energy resolution as compared to plastic scintillators: 10 keV compared to 30 keV, respectively.

Additionally, the silicon detector does not absorb xenon, and potentially it could be a zero-memory-effect detector. Initial detector tests in 2015 have shown that while promising, the silicon detector systems can exhibit memory effect at the ~0.5% level if plastic housings are used to hold the detectors (Foxe and McIntyre, 2015), however electronic noise and fragility of the detectors are two obstacles that must be overcome.

While silicon has not yet surpassed plastic scintillator as the primary beta cell material for field systems, it is gaining traction for operation in a laboratory type environment (Figure 55). It appears that the benefits offered by silicon detectors have them poised to take over as beta detectors in beta-gamma systems, assuming the detector robustness and desired costs are achieved.

Figure 55. PIPSBox, a silicon-based beta cell (~10 cm^3) developed by CEA for use with the SPALAX for beta-gamma radioxenon detection.

It should be noted, however, that silicon results in a larger electron backscatter signal. This effect has the potential to decrease detection efficiency of the conversion electrons and complicate the analysis. The analysis will need to be adjusted accordingly.

Future R&D

Future research is needed to improve the energy resolution and eliminate the memory effect, while also improving the detection limits to allow for improved likelihood of detection of a nuclear explosion, even with a small fractional release.

From simple to intelligent radioxenon processing (RSE2)

A key to the performance and sensitivity of a radioxenon system is efficient collection and purification of xenon from whole-air. With systems more efficiently collecting the xenon from whole-air, the detection of smaller radionuclide signals becomes possible, which is vital for effective nuclear explosion monitoring.

For radioxenon, the chemistry processing is relatively complex and intensive as compared to the processing required for particulate detection. While the end goal has remained the same (extract xenon from whole-air), the chemistry steps taken to achieve that goal and the degree to which that goal is achieved have changed over time.

When the first generations of systems were being developed in 1995-2000, the chemistry processes were performed with cryotraps and separations columns that were over-sized for the system. The systems were oversized to collect all of the xenon, which meant that large amounts of cooling power were required for the systems to operate effectively.

Then process modeling became more available through tools such as COMSOL (Humble et al., 2009). With detailed models, more sophisticated and intelligent chemistry processes could be implemented. These intelligent chemistry processes included smaller traps and separation columns as well as highly efficient heat exchangers (Williams et al., 2010).

The combination of these chemistry process improvements has allowed for engineered designs with higher capacity and better selectivity through process science (as distinct from the use of specific materials).

Future R&D

Improvement in the chemisty process will continue to be important, but the search for optimal sorbent materials will always be of interest.

From passive to active particulate collection (RSE3)

Nuclear explosions produce both airborne particulate debris, much of it radioactive, as well as noble gases. This is why the IMS radionuclide stations call for both particulate and noble gas monitoring systems.

As with radioxenon systems, the more particulate sample collected, the easier it is for a radionuclide particulate detector to observe a given activity concentration within the sample. When particulate detection was first brought on-line for verification of the CTBT in 1998, the collection of the particulate samples was done using a large blower to push air through a filter, which would collect the particulates (Miley et al., 1998a). The air filter is then compressed into a small puck and counted with a HPGe detector.

Some research has dealt with optimization of the filters used in the RASA system (Forrester et al., 2013). In addition, there is potential to further improve sensitivity limits and size through the use of electrostatic deposition instead of, or in conjunction with, air filters. There has been research into the use of electrostatic deposition to extract particulates from the air as it flows through the two plates of the collector (Sharma et al., 2007). By using electrostatic deposition collection techniques, there is potential that the airflow rate could be increased, without the larger pressure drop associated with the air filter. With the larger flow rate, more sample could be collected in a shorter period of time allowing for both shorter cycle times (better temporal resolution of the plume) and increased sensitivity limits for detection of the radionuclides. Electrostatic deposition could also allow for much smaller pumps and flow rates to either allow for smaller sampling systems or acquire more sample for less power.

Future R&D

Further research is needed to quantify the improvement promised by electrostatic deposition or other methods of improved particulate collection. How much better sensitivity is possible while using less power and less air flow?

From manual to robust automated systems (RSE4)

To have reliable results from radionuclide sampling systems, the systems must operate in a robust and repeatable manner. This applies to both the radioxenon detection systems and automated aerosol detection systems.

Figure 56. The Snow White air sampler as developed by Finland. Credit: CTBTO Preparatory Commission.

Figure 57. The RASA system as developed by the U.S., with a system footprint of 1m x 2m.

Since the implementation of radionuclide detection for CTBT nuclear explosion monitoring in 1995-2000, there has been some form of automation available. Examples of a manual air sampler (Snow White) and an automated sampler/analyzer (RASA) are shown in Figure 56 and Figure 57, respectively. Robustness in operation has been achieved through mechanical advances, for example, the RASA rollers were machined to prevent the filters from jamming during the transport and measurement process (Figure 58). The process of the RASA (and other systems) was automated through the use of computer programs to perform actions such as rolling filter paper through the system. The automation included sample collection, preparation (valve control for gas systems), and measurement.

While there are often operators present for the systems, the ability of a given operator has the potential to vary dramatically in the field. Because of this, the automation of the operation is needed to keep the system operating in a robust manner.

As improvements to robustness are made, it will be important to include automation for the new collection techniques that are being explored. It will also be important to have a form of automated system diagnostics. The ability to predict when mechanical failures are imminent will allow for the reduction of station downtime.

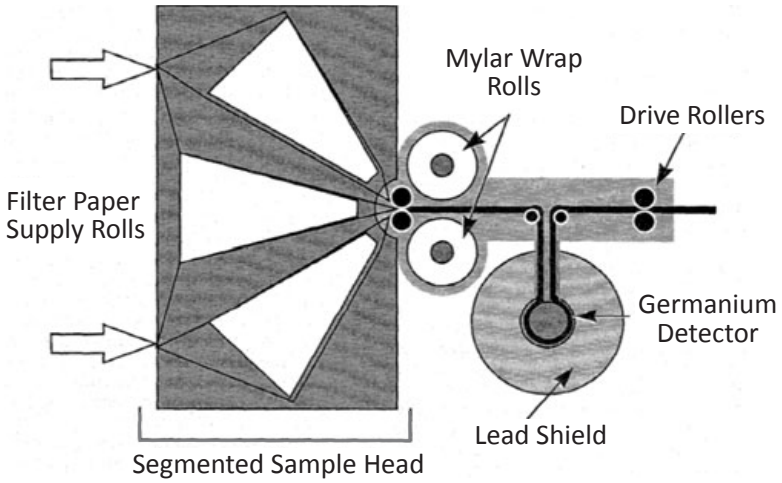

Figure 58. Schematic of the filter handling system on the RASA, which operates automatically collecting and measuring particulate samples (Forrester et al., 2013).

Future R&D

Focus on automation of collection techniques and system diagnostics can improve reliability of results.

From fission to combined fission/activation signatures for on-site inspections (RSE5)

Radionuclide signatures from a nuclear explosion can be usefully separated into prompt and delayed. Prompt radionuclides are those formed in the initial explosion. Of these the most useful radionuclides for nuclear explosion monitoring purposes are the short lived ones like the xenon isotopes because they do not build up in the environment and therefore can be viewed as the indicator of an underground nuclear explosion. Radioxenon is produced directly as a result of the fission process, and has long been known to be a signature of a nuclear explosion and its role is described in other research trends in this document. Some radionuclides have potential as delayed signatures that are formed by neutron activation and may not escape to the atmosphere for an extended period of time and typically have longer half-lives.

The potential for ^{37}Ar to be produced by neutron activation and be a potential delayed signature of a nuclear explosion was first suggested in 1996 (Carrigan et al., 1996). It was suggested that the large flux of neutrons generated during a nuclear explosion had the potential to interact with the calcium within the rock surrounding an underground nuclear explosive test. Through the use of gaseous tracers (^{3}He and SF_6), it was determined that gaseous signatures (e.g., ^{37}Ar) from a nuclear explosion had the potential to migrate to the surface and be detected.

There was no equipment designed for field measurement of ^{37}Ar in 1996, so such equipment was not part of the INGE. One of the primary reasons for the initial inability to detect ^{37}Ar is the extremely low energy of the particles emitted during the decay of ^{37}Ar. The decay of ^{37}Ar results in the emission of 2.8 keV Auger electrons or X-rays. For particles of such low energy, the argon must be placed internal to the detector.

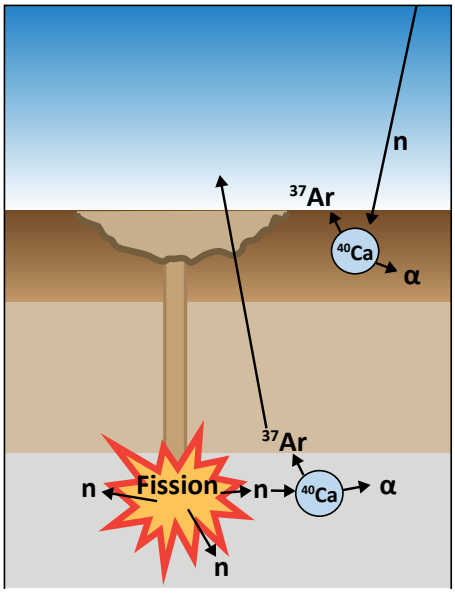

Tutorial:

Argon-37 (^{37}Ar) can be produced from neutron bombardment of calcium in the ground (Figure 59). This typically occurs from cosmic neutrons, depicted in the upper right of the figure, but it also occurs during an underground nuclear explosion, as shown lower in the figure. Nuclear explosions release vast quantities of both fission products and fission (fast) neutrons. These fast neutrons, in turn, interact with the materials in the ground, including calcium. The predominant naturally-occurring calcium isotope is ^{40}Ca. A fast neutron striking a ^{40}Ca nucleus can knock out an alpha particle, transmuting the ^{40}Ca nucleus into ^{37}Ar. Unlike calcium atoms, the ^{37}Ar atoms, as a noble gas, will vent or slowly seep through the ground to the surface where they can be detected.

Figure 59. Ar-37 formation as a result of neutron bombardment of calcium present in the ground surrounding an underground nuclear explosion (image not to scale).

In approximately 2010, proportional counters began to be looked at for their use in the detection of ^{37}Ar. Proportional counters had previously been used for environmental monitoring of isotopes such as ^{39}Ar, but only became capable and began to measure low activities of ^{37}Ar around 2010 (Riedmann and Purtschert, 2011; Aalseth et al., 2011). With the first measurements of the sub-surface soil gas backgrounds measured, the nuclear explosion monitoring community was now able to compare the expected ^{37}Ar signals with naturally produced backgrounds, and provide the science basis for measuring ^{37}Ar for nuclear explosion monitoring (Haas et al., 2010).

The first ^{37}Ar measurements (Figure 60) were primarily performed in shallow underground laboratories (such as those at the University of Bern and Pacific Northwest National Laboratory (http://tour.pnnl.gov/shallow-lab.html)). While shallow underground laboratories reduce backgrounds and allow for the sensitivity required for background ^{37}Ar measurements (~10-100 mBq/m^3), such sensitivity requires that the collected argon be conveyed to an off-site location for measurement, an action that is generally not possible within an OSI.

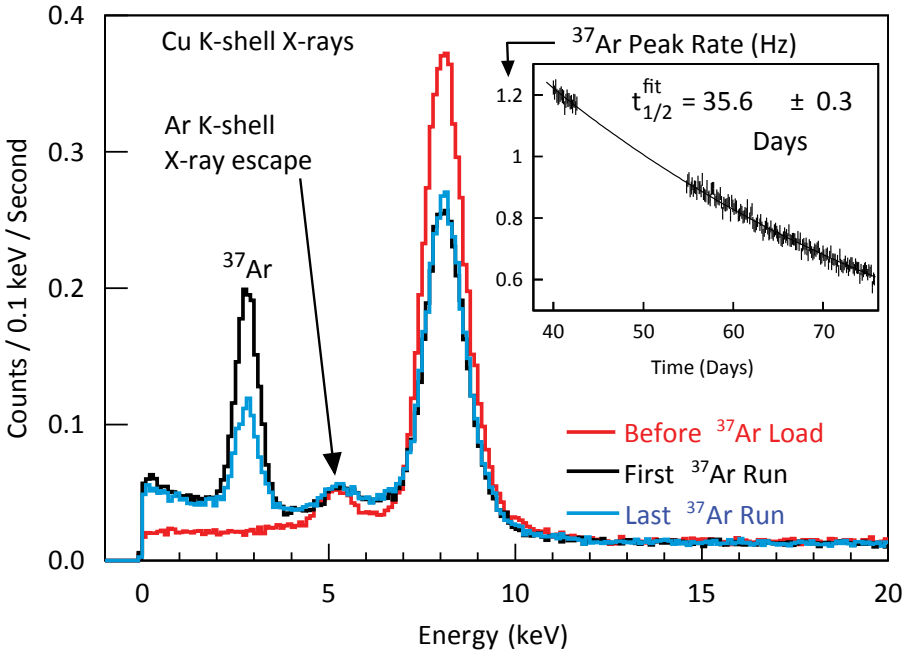

Figure 60. Spectrum of ^{37}Ar, along with the 8-keV Cu X-ray calibration peak. The first and last ^{37}Ar runs are shown for reference, and the inset shows the half-life decay of the ^{37}Ar peak intensity (Aalseth et al., 2011). This demonstrates the detection sensitivity required for ^{37}Ar measurements in an OSI.

The Chinese developed the first field system, called Movable Argon-37 Rapid Detection System (MARDS), for purification of argon from whole air in 2006 (Xiang et al., 2008), but the sensitivity limits were much higher than would be desired for field applications such as an OSI (100-800 mBq/m^3) (Figure 61). MARDS was further improved, and it operated during the Integrated Field Exercise 2014, in which it demonstrated a detection limit of 25 mBq/m^3. In 2015, PNNL introduced a prototype laboratory and field ^{37}Ar measurement system capable of processing 6 samples per day with a detection limit of 10 mBq/m^3. These systems continue to improve the detection limits, with capabilities of measuring activities below 1 mBq/m^3 for extended counting durations and 2 L of purified argon measured. The chemistry process for extracting argon from air must be sure to remove all of the nitrogen and oxygen from the sample to maintain repeatable measurements with the proportional counters. At levels below 1 mBq/m^3, the ^{37}Ar detection systems become capable of measuring atmospheric argon backgrounds, which opens the door to explore mechanisms for reducing the amount of required argon or investigate isotopic ratios.

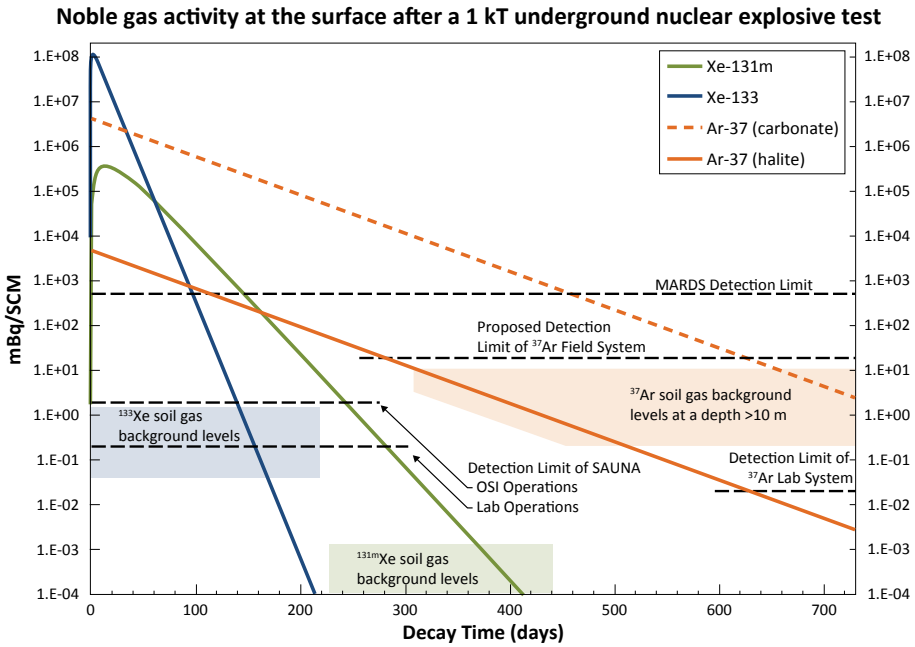

Figure 61. Radioargon and radioxenon levels expected at the surface after a 1 kT subsurface nuclear explosion and probable background levels (Haas et al., 2010).

With proportional counters beginning to be able to measure the low quantities of ^{37}Ar throughout the world, one can expect that the research trends might shift to explore different concepts of operations for field systems and extracting additional information out of the gas collected such as isotopic ratios (either ^{37}Ar to ^{131m}Xe or ^{37}Ar to ^{133}Xe).

While proportional counters have dominated the detection of ^{37}Ar, there have also been other detection mechanisms investigated for nuclear explosion monitoring. In 2013, ^{37}Ar was used as a calibration source in a small liquid argon detector (Sangiorgio et al., 2013). More recently, a liquid argon scintillation detector has been under development. The liquid argon detectors have the potential to reach very low detection limits, but they require a large quantity of argon (approximately 100 m^3 whole-air equivalent). The liquid argon detectors may be a means of measuring the argon backgrounds over a large volume of air, but they will likely not meet the detection sensitivities of the proportional counters for smaller gas volumes as would be expected during field operations including during an OSI.

Future R&D

It will be important to lower detection sensitivities so that atmospheric concentrations of ^{37}Ar can be measured long after a nuclear explosion. Research into lowering the detection limits by a factor of approximately 10x and determining isotopic ratios is needed.

From gamma spectroscopy to measurement restrictions (RSE5)

If a nuclear explosion takes place, it is expected that there may be particulate around the blast site. In an on-site inspection, one of the goals is to detect any radionuclide particulate. Traditionally, this would need to be done by taking samples in the field and counting them on HPGe detectors in the Base of Operations laboratory. As HPGe detectors became more portable, it became possible to do surveys in the field without needing to return the sample to the Base of Operations lab. Since a HPGe detector has the potential to easily pick out isotopes which are not relevant to nuclear explosion monitoring, it is desirable to only show the inspector what the activities of relevant radionuclides are. One way of doing this, called On-Site Inspection RadioIsotopic Spectroscopy (OSIRIS) (http://www.ortec-online.com/products/nuclear-security-and-safeguards/nuclear-safeguards/osiris), is through the use of software controls to analyze the HPGe spectra and display the results in an easy to use format for the inspector (Caffrey et al., 2015) (Figures 62 and 63).

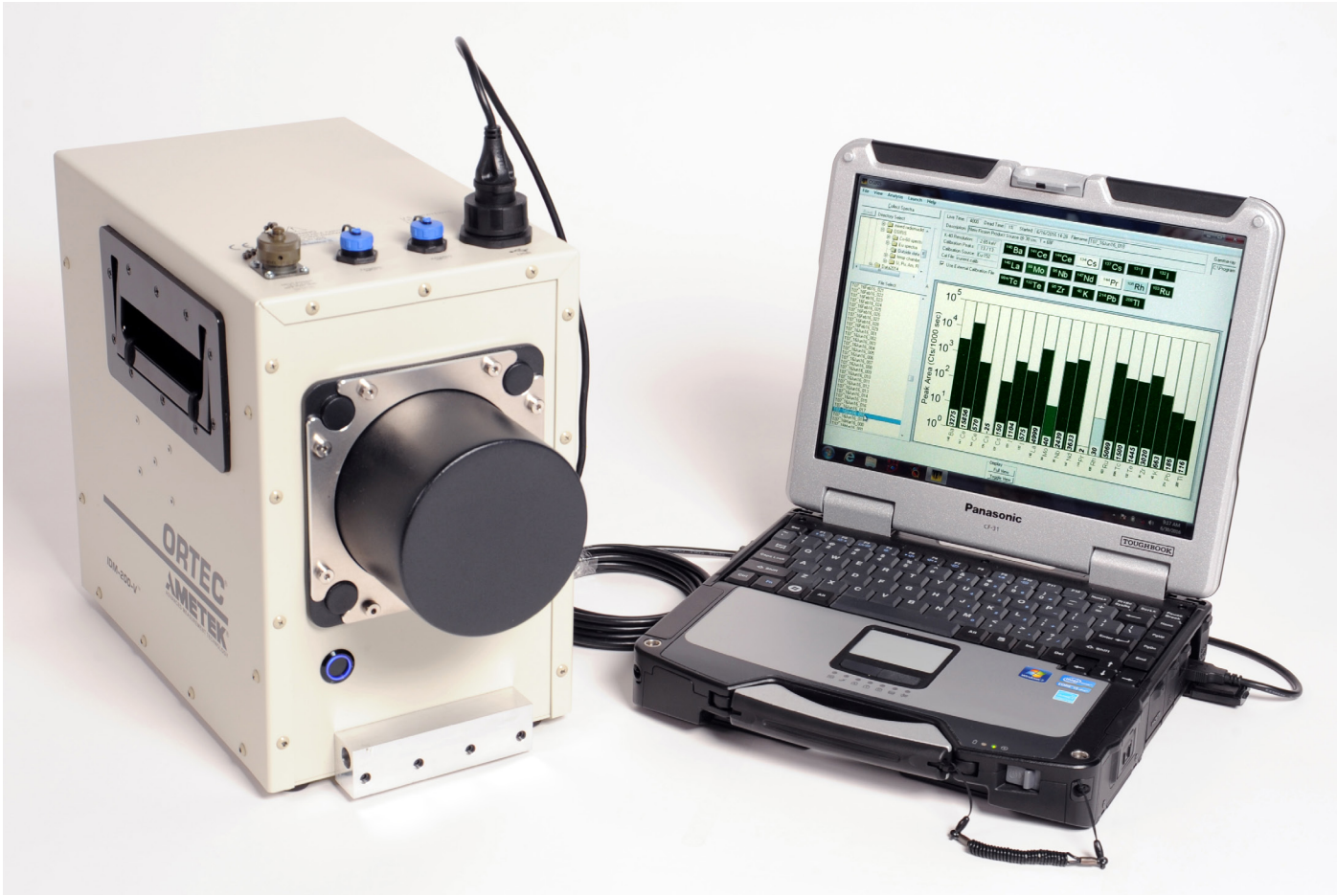

Figure 62. The OSIRIS gamma-ray spectrometer and its control computer. The spectrometer includes a mechanically-cooled HPGe detector and requires no liquid nitrogen.

Figure 63. Field test of an OSIRIS spectrometer at the Nevada National Security Site. The small cylinder directly below the spectrometer contains a microcurie-strength fission-product source.

Another potential alternative is to use sodium iodide gamma-gamma coincidence. Since the energy resolution of the NaI detectors is much worse than the HPGe detectors, it is non-trivial to pick out the various signals from a 1D spectrum. Additional research may make it possible to use gamma-gamma coincidence techniques to measure a portion of the relevant radionuclides with detection limits as low as those of an HPGe spectrometer.

Future R&D

Refining the means (both hardware and software) of focusing inspectors on the OSI -relevant radionuclides while restricting information of other isotopes is important to OSI planning.

Signal Analysis - Processing the Signals

Signals generated by the sources, propagated through the solid earth, oceans, or atmosphere, and recorded by the sensors must be processed to pull indications out of the data of possible nuclear explosions. This final processing step is referred to as Signal Analysis, and it employs algorithms used to detect arrivals at stations and integrate the detections into event hypotheses consisting of location, time, and source type. The number of signal detections increases significantly as detection thresholds decrease, and signal analysis methods must keep pace to dismiss events that are not relevant to the monitoring mission and cull events of relevance through advanced discrimination methods. Relevant events are those with clear explosion characteristics, as well as indeterminate events that cannot be dismissed without potentially missing an explosion. Analyst review of these culled events can still represent a large operational burden, that, if not addressed with transformational signal processing methods, will result in unacceptable costs to the nuclear explosion monitoring mission and undermine a goal of "miss no explosions."

In general, the operational processing flow begins with detections from sensor data. Data from each sensor are processed separately and grouped through association analysis as coming from the same source (event formation). The signals from an event are rigorously analyzed to estimate an event location (latitude, longitude, depth and event origin time), complete with associated error estimates. Event magnitude is also calculated and provides an estimate of event size. Event discrimination then culls monitoring-mission-relevant events and dismisses non-relevant events. In the past, researchers developed algorithms to enable time-critical source identification, estimation of magnitude, and origin time and location for an event. More recently, computational capability has advanced to enable new approaches, and make data-intensive processing tractable. In addition, radionuclide signal analysis R&D is focused on developing methods and techniques to increase the sensitivity and selectivity of radionuclide detection, improving discrimination of detected signals from background with automated algorithms, and evaluating intra-station dependencies to maximize network capabilities. Future signal analysis research strives to improve our ability to detect, locate, and discriminate small events, without adding to the workload at monitoring agencies.

From single- to multi-phenomenology integrated analysis (WSA4)

An underground explosion will generate several important physical signatures. The shock front from the explosion couples energy into the earth, which propagates as a seismic wave. An acoustic/infrasonic wave is generated at the interface of earth and air from the motion of the surface of the earth; this, in turn, couples into the earth generating more seismic waves. Driven by pressure, heat, diffusion and atmospheric pumping, radioactive gas injected into rock from an explosion can propagate (seep) to the surface through both the explosion fracturing and natural fracturing. Figure 64 illustrates the dynamic interplay between physical processes generated by an underground nuclear explosion. For all the signatures, a near source process couples to far field

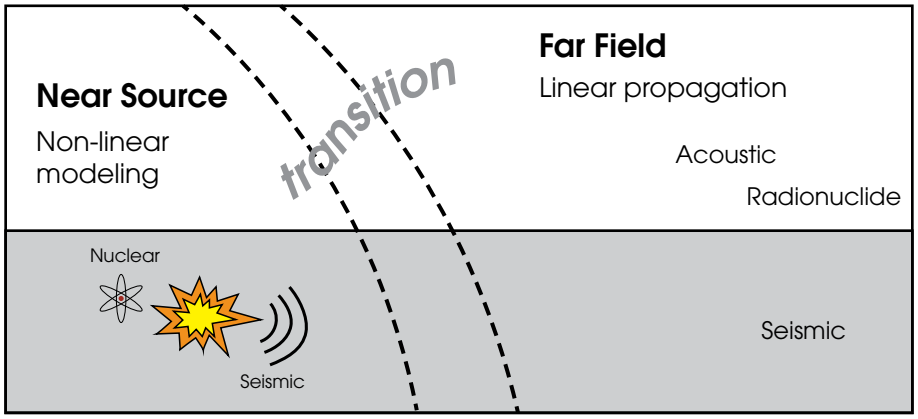

Figure 64. Modeling multi-phenomenology explosion processes requires near-source hydrodynamic modeling to account for nonlinear effects, coupled to far field propagation modeling that captures the dynamic interplay between physical processes.

propagation to sensors. If high-fidelity physical models of measurements from these and other processes can be developed and embedded into a new, transformational, error model, then, through comparison of model predictions with signatures, significant advances are possible when assessing three mission-critical questions: What was the source? How large was the source? What is the confidence level of assessments?

A physics-based error model is essential to unified multi-phenomenology sensor analysis because these measurements must be correctly weighted, and the error in physical models must be correctly propagated along with measurement error (Anderson et al., 2010b). An innovative error model for sensor data should quantify physical model error with statistical variances so that improvements in accuracy and precision from new physical models can be quantified, and error propagation and analysis can be developed with well-established mathematical theory. Explosion yield and unique nuclear identification are often the most important pieces of decision information in explosion monitoring and provide critical constraints in understanding the nature of an event. There are documented examples in explosion monitoring missions where inconsistent assessments from single-phenomenology data resulted in protracted confusion and indecision. New multi-phenomenology methods could eliminate, or at least minimize, ambiguity in assessments.

A general mathematical framework for the rigorous integration of physics and statistics is fundamental and differs from contemporary "data fusion" methods that usually rely on mathematical representations of a large number of physical measurements. An explosion is likely to be observed by disparate sensors, providing signatures to identify the source and estimate yield. Contemporary error models for physical sensor measurements often incorrectly represent all sources of error as a single propagating error term. To address error better, a *univariate* formulation of sensor measurement errors (Anderson et al., 2009, 2014; Arrowsmith et al., 2012) has been developed and validated by extending the statistical random effects models to the physical sensor measurements. Research to develop a multivariate error model that partitions total error into components of model and measurement error, and correctly manages error propagation is needed. This advanced error model will fully extend the univariate model to a multivariate random effects model for disparate sensor measurements. The research is challenging because a multivariate random effects model is intractable due to the number of parameters in the model. A notable exception is a one-way multivariate random effects model developed by Schott and Saw (1984).

Future R&D

Future research will extend an advanced single phenomenology analysis framework to a multiphenomenology (multivariate) framework, minimizing false alarms and maximizing the probability of detecting a source of interest.

Tutorial: Waveform Error Modeling

A useful representation of a waveform measurement is

$$X_{ijk} = \mu + \log_{10} S_i(\theta) + \log_{10} P_{ij} + \epsilon_{ijk} \qquad (1)$$

where $X_{ijk} = \log_{10}(A_{ijk})$ is the logarithm of the k-th measurement (amplitude) taken on the j-th path from the i-th source. The source term $\log_{10} S_i(\theta)$ is a function of physical parameters θ, with source yield W an element of θ. The term $\log_{10} P_{ij}$ represents the effect of the j-th path on the recorded measurement from the i-th source and μ represents a constant bias adjustment. The source terms $\mu + \log_{10} S_i(\theta)$ represent the source signal, which is attenuated with the path effect term $\log_{10} P_{ij}$, and randomly corrupted with the measurement error term ϵ_{ijk}, giving measurement X_{ijk}. An analogous equation to represent nuclear emissions can be written, and a multivariate formulation of Equation (1) will fully accommodate the integration of seismoacoustic, electromagnetic, and nuclear measurements.

In the univariate model Equation (1), all sources of error are combined into a single zero-mean term ϵ, and this is non-physical because it mathematically implies that the ensemble of physical terms in the model is always unbiased. Also, Equation (1) gives mathematically derived standard error equations that can be made arbitrarily small with data – also non-physical (bias in either the model or the acquisition of data cannot be overcome with an increased number of measurements). Research has extended the single-phenomenology Equation (1) to the general random effects form shown in Equation (2) as

$$X_{ijk} = \mu + \log_{10} S_i(\theta) + E_{S,i} + \log_{10} P_{ij} + E_{P,ij} + \epsilon_{ijk} \qquad (2)$$

with model error terms $E_{S,i}$ for source, $E_{P,ij}$ for path effects, and measurement error ϵ_{ijk}. A multivariate (p-phenomenology) random effects model of sensor measurements can be written in vector notation by collecting all terms by source and by path within each source for each phenomenology as

$$\begin{pmatrix} X_1 \\ \vdots \\ X_p \end{pmatrix} = \begin{pmatrix} \mu_1 1_{n_1} + \log_{10} S_1(\theta_1) + E_{S_1} + \log_{10} P_1 + E_{P_1} \\ \mu_p 1_{n_p} + \log_{10} S_p(\theta_p) + E_{S_p} + \log_{10} P_p + E_{P_p} \end{pmatrix} + \begin{pmatrix} \epsilon_1 \\ \vdots \\ \epsilon_p \end{pmatrix} \qquad (3)$$

where n_h is the number of measurements taken by phenomenology h and 1_m is a vector of ones of dimension m. The notation subscript h (q_h) indicates that source model parameters may vary by phenomenology, which does not preclude a subset of them (including source yield W) from being common across phenomenologies. Also note that a physical bias that may influence two or more different source functions is mathematically captured in the off-diagonal elements of the model error covariance matrices. This new multivariate approach to multiple phenomenology analysis partitions total error into vector model error components, and vector measurement error, and provides the foundation for maximum likelihood estimation for all model parameters. Equation (3) is a system of equations (likelihood) that may be used to estimate unknown source and error terms for each phenomenology. Importantly, model Equation (3) provides for physically meaningful model error correlations between phenomenologies.

Source and error parameters may also be estimated using a generic Bayesian probability model, which in this case the posterior can be written as

$$P(S(\theta), P_1, P_2 \ldots P_N, \mu_1, \mu_2 \ldots \mu_N, \varepsilon_1, \varepsilon_2, \ldots \varepsilon_N \mid X_1, X_2, \ldots X_N) \qquad (4)$$

Expression (4) states that the joint probability of source parameters $S(\theta)$, signal propagation for each phenomenology $P_{(1,2,\ldots,N)}$, bias for each phenomenology $\mu_{(1,2,\ldots,N)}$, and error in the measurement of each phenomenology $\varepsilon_{(1,2,\ldots,N)}$ is determined conditionally based on data vectors for each phenomenology $X_{(1,2,\ldots,N)}$.

Waveform Error Modeling Tutorial (continued)

The specific formulation of Expression (4) can vary depending on how the researcher chooses to parameterize the physical model. In this case Expression (4) differs subtly from Equation (3) in that it requires independent source models for each phenomenology to be consolidated into a single, multi-phenomenological source. Similar to the approach outlined by Myers et al. (2007, 2009) for the multiple-event location problem, Expression (4) can be rewritten using Bayes formula as a collection of independent (uncorrelated) forward calculations

$$P(S(\theta), P_1, P_2 \ldots P_N, \mu_1, \mu_2 \ldots \mu_N, \varepsilon_1, \varepsilon_2, \ldots \varepsilon_N \mid X_1, X_2, \ldots X_N) =$$
$$P(X_1 \mid S(\theta), P_1, \varepsilon_1) P(X_2 \mid S(\theta), P_2, \varepsilon_2) P(X_2 \mid S(\theta), P_2, \varepsilon_2) / (P(X_1)(P(X_1)(P(X_1)) \quad (5)$$

Equation (5) can be used in conjunction with Markov-Chain Monte Carlo (MCMC) methods to sample the joint probability on the left-hand-side of Equation (5) (Expression 4). MCMC conditionally accepts random proposals for source, propagation, and error terms based on the probability computed for the right-hand-side of Equation (5). The Bayesian/MCMC approach to determining parameters can be more accurate and uncertainty estimates using this approach can be more representative than linear inversion if the physical forward problem is non-linear. MCMC *may be* more computationally tractable for multi-dimensional models and large observational data sets if the forward calculations are inexpensive.

From idealized to adaptive infrasonic signal detection algorithms (WSA1)

The challenge of detecting infrasound signals from underground explosions is complex because signal amplitudes from recent underground nuclear explosive tests have been relatively low compared to background noise levels, and to signals from other background events. The challenge of detecting signals typically requires signal and noise models. In the past, simple idealized models were used based on assumptions that were often oversimplified or invalid. For example, noise was modeled as being uncorrelated across array channels and signals were modeled as the same waveform time-shifted between array elements. In addition to the fact that these assumptions are often incorrect, they also provide limited constraints to differentiate signals of interest from coherent waves from other sources.

Recent studies working towards improving infrasound detection algorithms by reducing the false alarm rate have explored two strategies for solving the problem. The first strategy is to implement detection categorization algorithms as a post-processing step to identify detections of interest based on signal features from the large number of background detections from local and continuous-wave sources (Brachet et al., 2010). The second strategy is to redefine the noise model to handle correlated noise by adaptively adjusting the noise model to ambient data (Arrowsmith et al., 2009). Both strategies have been shown to improve the false alarm problem, but still rely on the arrival of a coherent signal across the infrasound array.

In contrast with seismology, most infrasound signal detection work has focused on arrays (e.g., Le Pichon et al., 2008). At long ranges, combining multiple features such as the coherence and duration of infrasound signals is showing promise for improving the detection of weakly-correlated signals. At regional and local ranges, the use of multiple features of signals of interest aligns the detection problem with the categorization problem, allowing one to significantly reduce the false alarm rate by targeting detectors towards more specific types of signal.

Future R&D

There remains significant work to be done on developing detectors that result in fewer false alarms and on maximizing the probability of detection for signals of interest. Continued research and investigations of multifeature analysis as well as new multi-phenomenology sensor systems should increase the detection probability for events of concern and significantly reduce nuisance detections.

From time-or-frequency analyses to time-and-frequency analyses (WSA2)

Time-domain and frequency-domain methods in signal analysis have and will continue to play an important role in waveform monitoring research.

Frequency-time analysis (FTAN) has long been used to make surface-wave dispersion measurements (Dziewonski et al., 1969; Levshin et al., 1972; Herrmann, 1973). The time series recorded by seismic and infrasound sensors provide the fundamental time and frequency features, such as phase arrivals and spectral amplitude ratios, which have been successful in countless discrimination studies and monitoring applications. Examples include regional spectral amplitude ratios for discrimination (Hartse et al., 1997, Figure 65) as well as cepstrum and spectral scalloping studies for ripple-fire mine blasts (Allmann et al., 2008). Recent work highlights the increasing time-frequency features that employ signal processing techniques that extend the traditional Fourier Transform. Meza-Fajardo et al. (2015) employ the Stockwell transform (Stockwell et al., 1996) on three component seismic data to isolate several types of surfaces waves (Figure 66). Some of the most novel uses of time-frequency features, however, comes from leveraging machine learning methods in monitoring applications. Yoon et al. (2015) develop a computationally efficient waveform similarity search method that transforms

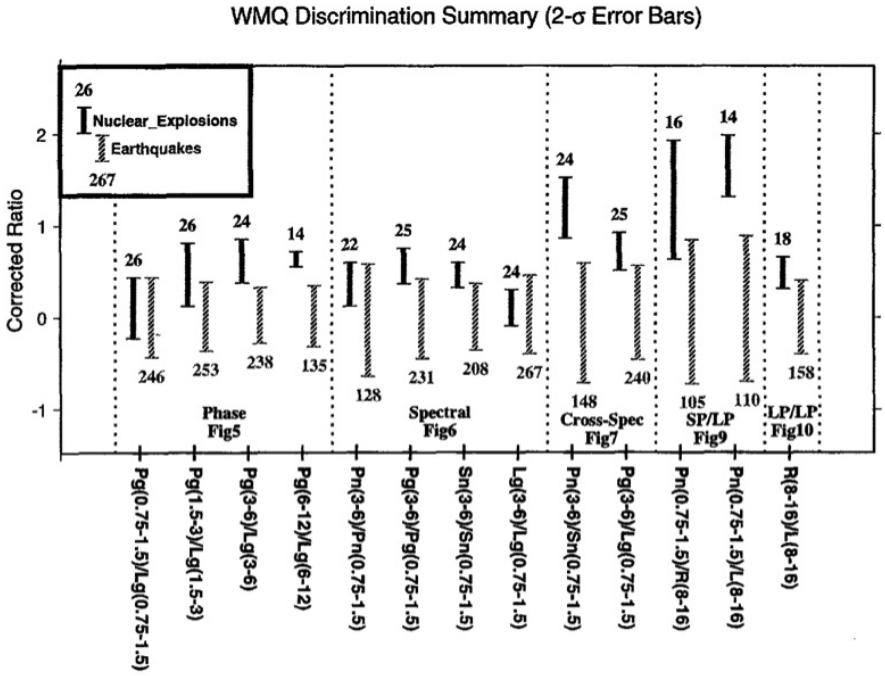

Figure 65. Summary of regional discriminants tested for station WMQ, from Hartse et al. (1997). For each discriminant, 2-sigma error bars are shown about the mean of the earthquakes and explosions. A simple regression was used to approximately remove the corner-frequency (or magnitude) effect present in the spectral and cross-spectral ratio results.

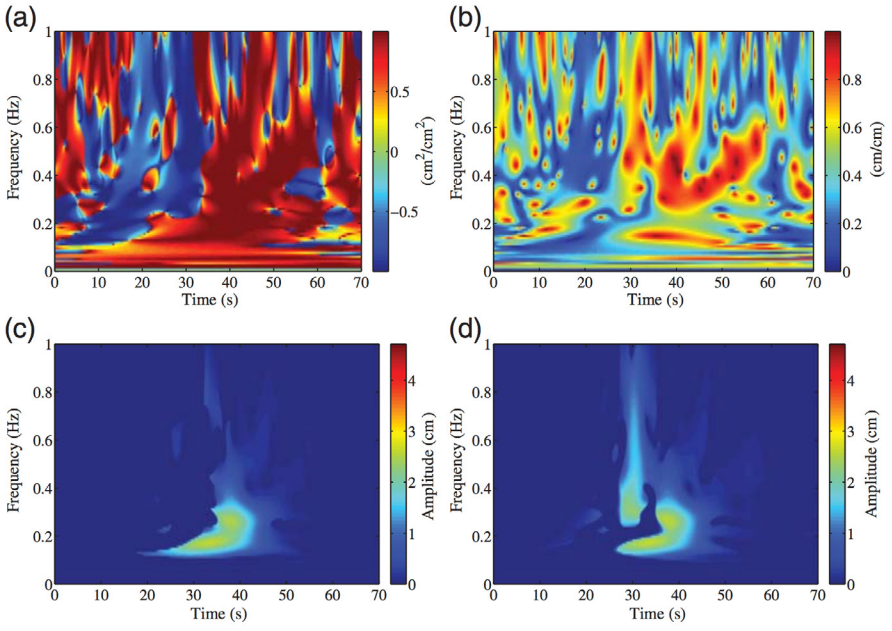

Figure 66. Surface wave extraction using time-frequency transforms, from Meza-Fajardo et al. (2015). (a) The Normalized Inner Product (NIP) of the radial and vertical component time-frequency (Stockwell) transforms for retrograde Rayleigh waves. (b) The corresponding instantaneous reciprocal ellipticity (IRE), for comparison. (c) The radial component Stockwell transform, filtered using the NIP. (d) The radial component Stockwell, transform filtered using the IRE, for comparison.

spectrogram image data into wavelet transform "fingerprints," which is then used with clustering methods to quickly associate similar waveforms (Figure 67).

New algorithms and advances in computational efficiency and power, however, have opened the door to novel multidimensional analyses that provide additional windows into the data used in monitoring and the underlying physical phenomena. These new views, and combinations thereof, are the basis for future detection and discrimination methods and signal similarity studies.

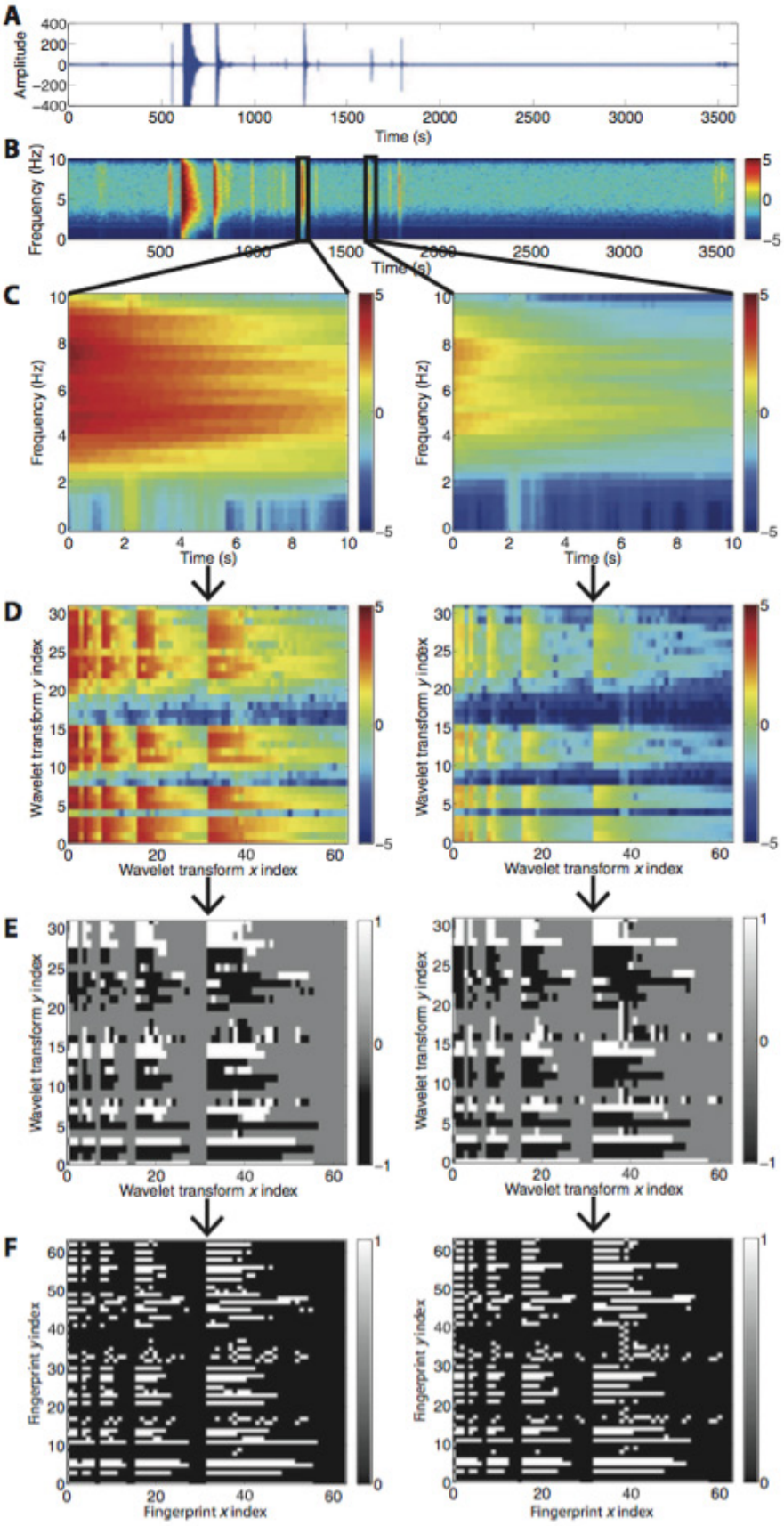

Figure 67. Waveform time-frequency feature extraction, from Yoon et al., 2015. (A) Continuous time series data. (B) Spectrogram: amplitude on log scale. (C) Spectral images from two similar earthquakes at 1267 and 1629 s. (D) Haar wavelet coefficients: amplitude on log scale. (E) Sign of top standardized Haar coefficients after data compression. (F) Binary fingerprint: output of feature extraction. Notice that similar spectral images result in similar fingerprints.

Future R&D

Natural extensions of multidimensional analyses include expanded application of machine learning techniques to the problem of signal categorization and discrimination, as well as advanced similarity methods, such as hashing and other clustering techniques.

From simple, statistical location algorithms to physics-informed algorithms for infrasonic analysis (WSA3)

Source localization is a key component of network-level analysis in nuclear explosion monitoring because further analysis (estimation of source energy, height-of-burst/depth-of-burial, etc.) is dependent on the relative locations of the source and receivers. Correctly quantifying the uncertainty in the localization estimate is required to quantify uncertainties in the results of this continued analysis.

All network-level analysis requires a combination of physical models to represent the propagation of energy between network nodes and a statistical framework to quantify the uncertainty in the computed results. For localization estimates specifically, possible source locations and times are considered and the probability of each hypothesized source generating the observed signals is computed and analyzed, typically using a least squares or similar methodology. In the case of infrasound studies, the physical models for propagation have rapidly increasing uncertainties with propagation range; therefore, a portion of the research in infrasonic source identification has focused on locating sources from observations at short distances (Olson et al., 2005; Szuberla et al., 2006). At larger propagation distances, quantification of the uncertainty in localization estimates has been a long-term area of research (Norris and Gibson, 2002). The development of models for infrasonic propagation in the vicinity of a network of arrays has led to multiple studies aimed at quantifying the detection and localization performance of such networks (Brown et al., 2002ab; Ceranna et al., 2008).

Recently, a Bayesian framework has been applied to the problem of infrasonic source localization with promising results. Initially, a simple likelihood definition was developed for identifying possible source locations for an infrasonic detection (Modrak et al., 2010). Continued research regarding Bayesian infrasonic source localization methods has focused on refining propagation models, quantifying observation and model uncertainties, and modifying the likelihood definitions to include additional physical realism (Arrowsmith et al., 2014; Marcillo et al., 2014; Blom et al., 2015). Much of this initial work has focused on analysis using signals at regional propagation distances (within ~1,000 kilometers), but continued work is aimed at extending this propagation distance so that the method can be applied to monitoring a larger area utilizing a sparse infrasound network such as the IMS.

Continued improvements in infrasonic source localization studies are likely to be along two distinct research paths. Firstly, joint seismo-acoustic methods will be crucial for applications at lower yields as the quantity and quality of detections in such cases decrease and analysis using a single phenomenology will be limited. Because such scenarios will likely include shorter propagation distances, the uncertainties introduced by long distance infrasound propagation will be limited; however, the appropriate method of combining multiple phenomenologies into a single localization estimate will require significant research efforts. A second research path of interest for localization and similar analysis would leverage acoustic tomography methods to improve the atmosphere specification and reduce uncertainty in propagation effects. This type of detailed analysis would be more computationally intensive and primarily of interest in analysis of specific events of interest. Infrasonic signals have been found to be useful in estimating corrections to the atmospheric state obtained from more traditional sounding methods; however, such methods typically have sources with known ground-truth locations and times (Arrowsmith et al., 2013; Assink, et al., 2013).

Future R&D

The propagation model predictions utilized by localization methods will continue to improve as atmospheric specifications improve and computational efficiency becomes less of a hindrance for infrasonic propagation simulation efforts.

Tutorial: Infrasound localization methods - an overview

The estimation of infrasonic sources from distant observations relies on using the observed back azimuth (often termed the direction of arrival, or DOA) at each observing station. In more recent research, models have been developed to utilize the arrival times of the signals and physically realistic propagation models for possible infrasonic velocities to better constrain such estimates. In the left panel of Figure 68, three infrasound arrays in the western U.S. are shown that detected infrasound produced by an above-ground explosion at the Utah Test and Training Range (UTTR). The blue lines show the observed DOAs for the signals detected at these arrays.

The region around the DOA intersection has been analyzed using the methods in the Bayesian Infrasonic Source Localization (BISL) algorithm using simple propagation models as well as the propagation-based, stochastic models. The results of this analysis are shown in the right panel. The computed spatial distribution for the source using the stochastic celerity model is shown in the blue color scale distribution. The orange ellipses denote the 95% and 99% confidence bounds approximating this distribution. The green ellipses show the relatively larger area corresponding to the 95% and 99% confidence bounds using more general propagation models. The magenta point is the maximum posteriori point, and the red star is the ground-truth source location at the UTTR. In this case, the infrasonic source can be accurately identified; though, the precision of the estimate could be improved if additional observations were available or the propagation models were more refined.

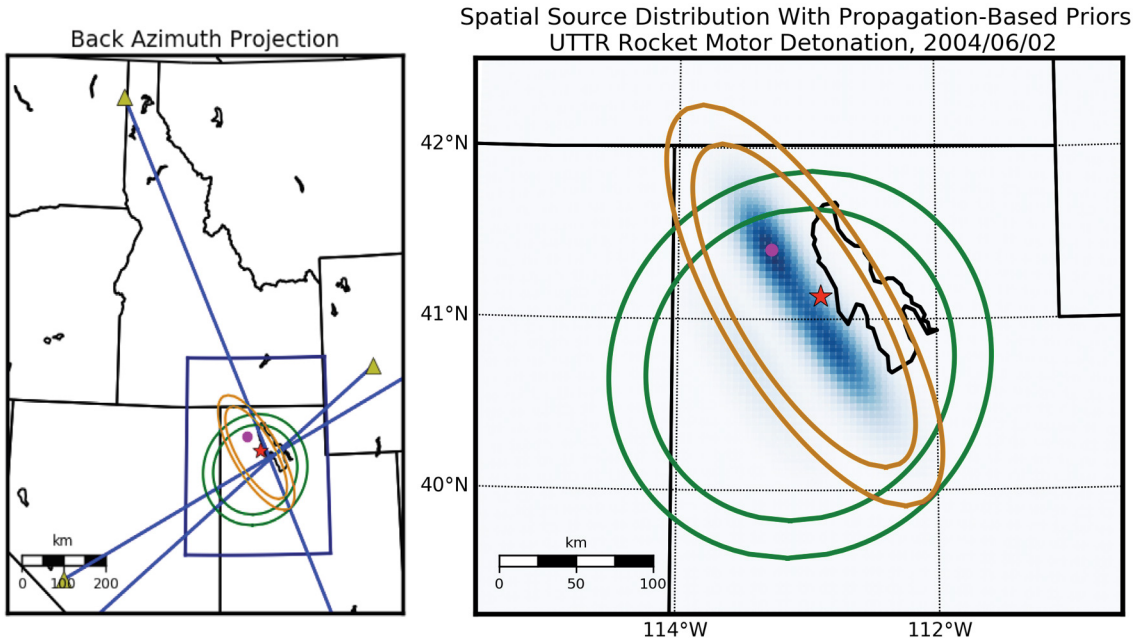

Figure 68. Localization estimate for a rocket motor detonation at the Utah Test and Training Range (UTTR) during the summer of 2004. The larger (green) set of ellipses denote the 95% confidence region using a generic propagation model, while the narrower (orange) set of ellipses shows the improvement when using a propagation-based, stochastic model.

From pick-based seismic event processing to full-waveform processing (WSA4)

Moving from pick-based methods to full-waveform methods has significant benefit for the monitoring community. Full waveform methods leverage advances in computational infrastructure to allow improvements to both monitoring accuracy and efficiency. Repeated events, whether from nuclear explosions, mining, or aftershocks, can be located and given estimated magnitudes, origin times, and source types immediately upon detection. For a monitoring agency, this translates into analysts spending less time processing nuisance events, and having more time to process events of interest.

Seismic event detection algorithms currently in use at the International Data Centre and National Data Centers use so-called pick-based methods. Incoming seismic phases (e.g., P-waves) are detected using energy detectors; their arrival times are picked (either via algorithm or using a human analyst), then sent to an associator which combines the information from at least 3 stations to locate and build an event. Detection, association, location and discrimination are each done as separate steps, performed one at a time in linear fashion. Since this method requires that only pick times are sent to the associator, it was well suited to days when it was necessary to minimize the amount of data to be transmitted before an event could be built. But what if one could use all the information in the waveform, not just its arrival time?

As the wave travels, it reflects and refracts according to the properties of the material through which it is traveling, and the waveform recorded at a station is a complex signal that is a function both of the source-time function of the earthquake or explosion, and of the travel path. This means that if an earthquake occurs in San Francisco, the waveform plotted at a seismic station in Berkeley will be different than the waveform plotted at a seismic station the same distance away in San Jose. Moreover, if the earthquake location moved just a few kilometers, to a different part of San Francisco, the recordings seen at each station would also change. In essence, the waveform recorded at a station acts as a unique fingerprint, and, if that waveform is ever seen again, it indicates to a high degree of certainty that there was another event in the same location, with the same source type. Pattern matching approaches are all fundamentally about scanning the incoming data at a station to see if the waveform coming across the station looks similar to something seen before. If so, a detection is declared, complete with an immediate location estimate. Moreover, quick comparison of the detected and historical waveforms generates an estimated magnitude, and the detection's origin time can be easily derived. In addition, the source-time function can be assumed to be similar to the historical event's source-time function, so the detection comes with an initial suggestion of whether it was an earthquake or an explosion. Thus, as soon as waveforms arrive at the nearest station, quite a lot is known about an event. All in all, pattern matching approaches offer tremendous advantages. There is, of course, one significant caveat – pattern matching techniques only work to detect events that are similar to historical events in an archive. Fortunately, seismic events tend to congregate along fault lines, mining locations, and test sites, so it is likely that pattern matching approaches (See tutorial on Template Matching) will be able to detect a large percentage of seismic events. Although this caveat means pattern matching detection methods will never fully replace the traditional, pick-based, methods, the two approaches can work in tandem to detect and characterize events with maximal efficiency.

The original and simplest template detector is a correlation detector. Here the waveform of a known historical event, as seen at a particular station, is compared to waveform data at the station by performing the mathematical operation of correlation (See tutorial on Waveform Correlation Detection). This is the optimal detector for detecting an identical signal in the presence of noise (e.g., background station noise, or the coincident arrival of energy from another event). The idea to implement this approach for seismic monitoring has been around since the 1960s (Capon et al., 1967), however for many years it was seen as computationally unfeasible. Later, researchers began exploring the concept anew, running small-scale studies to explore its effectiveness, quantify its benefits, and think through how it might be used to build a

Tutorial: Waveform Correlation Detection

Waveform Correlation Detection gives us a method to detect events arriving at a station that are similar to something seen before. It relies on the mathematical operation of correlation, which is a measure of similarity between two vectors. Correlation gives us a score between -1 and 1 to indicate how similar two things are: 1 means they are identical, 0 means they are essentially random, and -1 means one waveform is the flipped version of the other. Mathematically, the normalized correlation score is the sum of the element-by-element multiplication of the two vectors, normalized by the energy in the vectors. The normalized correlation score is written as

$$\text{corrscore} = \frac{\sum_{n=1}^{W} m[n]d[n]}{\sqrt{\sum_{n=1}^{W} m^2[n] \sum_{n=1}^{W} d^2[n]}}$$

for data streams m[n] and d[n], and W points.

The concept of how to use this as a detector is demonstrated in Figure 69. At the top of the figure, highlighted in blue, is a template event waveform; this is the waveform seen at a particular station generated by a known event. All the significant things about the template event – where it was, when it was, how big it was, and whether it was an earthquake or mining event. In the middle of the figure the incoming data stream is drawn; this is the data flowing into a station. One can take W points of this data and calculate the correlation between this window of data and the template event waveform. Then the incoming data stream is advanced one sample, and the calculation repeated. Although this concept is explained here in the time domain, it is worth noting that in practice correlation routines are implemented in the frequency domain, for speed. Most of the time, the correlation score is a small value close to 0. Occasionally, however, as is shown in Figure 69, the incoming data stream window captures a waveform very similar to the template event waveform. Then the correlation score may be close to 1. In order to determine if a similar event has been detected, or not, a detection threshold must be chosen. The detection threshold is the cutoff value above which the two waveforms are deemed similar enough to call the incoming data a detection. In Figure 69, the correlation score is above the detection threshold, so a waveform correlation detection can be declared.

Figure 69. Waveform Correlation Detection.

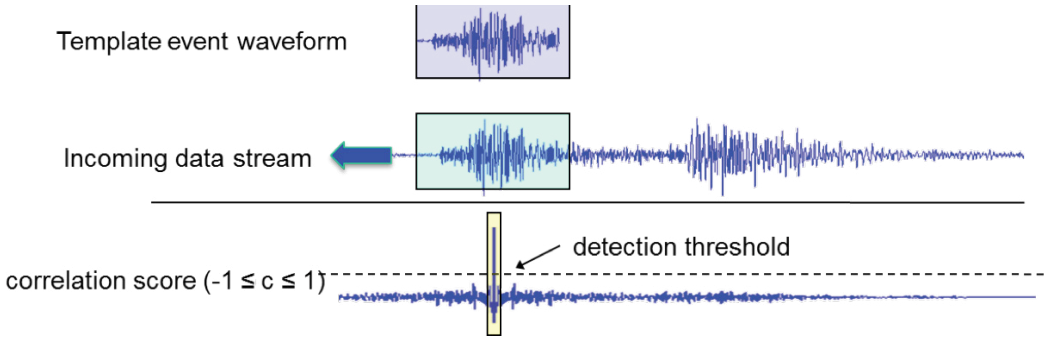

detector. These efforts were well described in a paper by Gibbons and Ringdal from NORSAR, where they used correlation to detect low magnitude events on a Norwegian array (Gibbons and Ringdal, 2006). This paper gives a good layout of the fundamental math and method, and explores questions of how to make this useful in routine processing. It also lays out a widely-used method for calculating magnitude based on the relative amplitudes of the detected and template events. Schaff (2004) used correlation to identify repeating events in China, showing that correlation could give insight into the nature of seismicity and help in location studies. He also showed waveform correlation detects events up to about one magnitude unit smaller than traditional detection (Schaff, 2009; Schaff and Waldhauser, 2010).

Tutorial: Template Matching

Waveform correlation detections are often plotted as families of similar events. Figure 70 shows an example of this type of plot, recorded at the station LPAZ during a Chilean aftershock sequence. At the top, in red, is the template event waveform. Below are many waveforms that were detected using waveform correlation; as to be expected, they all look very similar to the template waveform. In this example, the correlation was done on the *Lg* arrival, the segment between the red lines. Although only the *Lg* window was used to do the correlation, the P arrivals also align, confirming the validity of the detections. Using a plot like this, an analyst could easily process the family as a whole, adding *P* and *Lg* arrivals quickly and easily.

Figure 70. Family of waveform correlation detections during Chilean aftershock sequence. LEB picks are shown above the waveforms; correlation scores and calculated event times printed on the right.

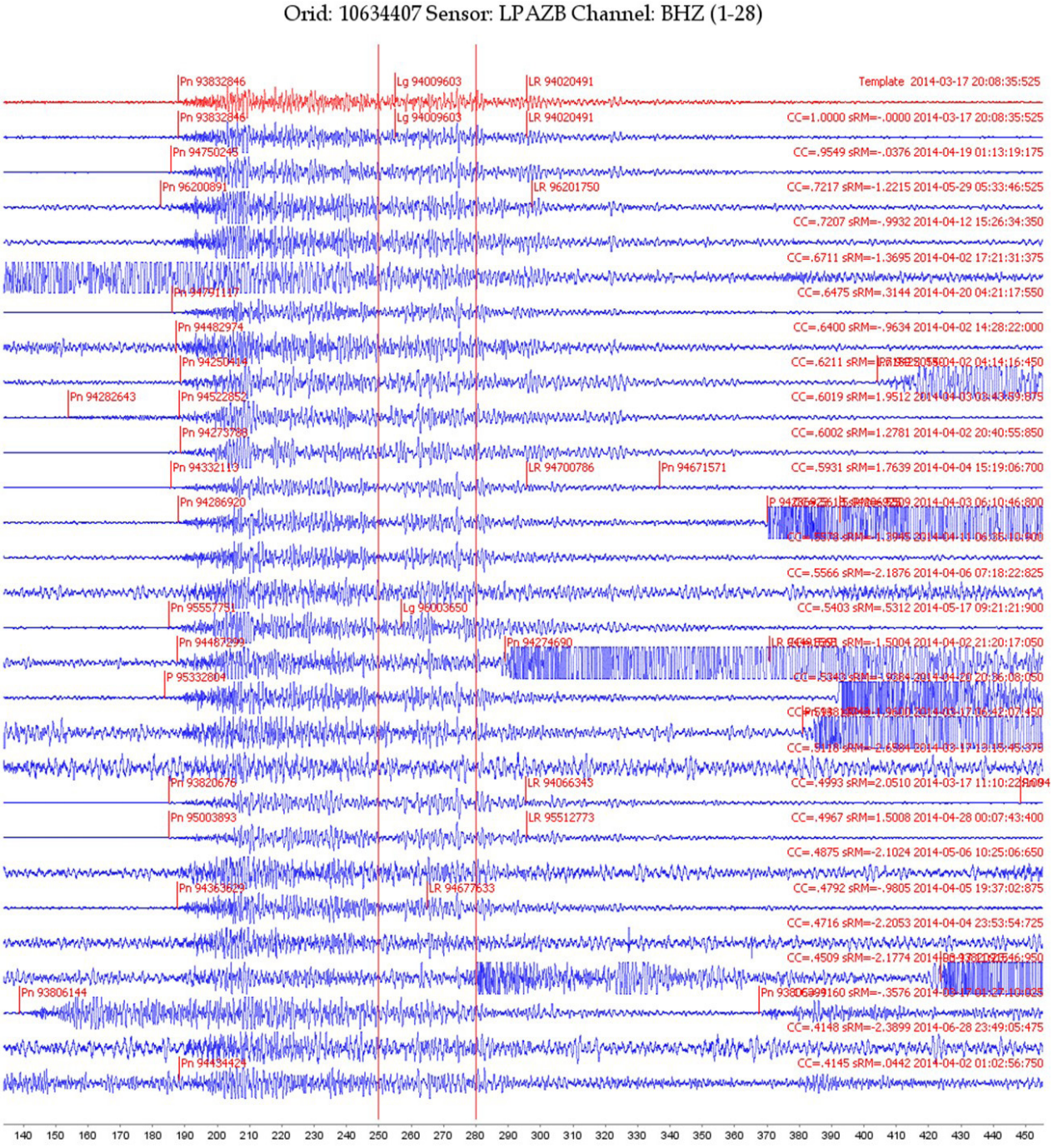

David Harris, then at LLNL, was an early pioneer of exploring how to implement template methods, and introduced an approach known as subspace to the seismology community. Subspace detectors are built from a suite of events, rather than from just one. For example, a suite might include the waveforms of several blasts from a mine. By applying singular value decomposition to the collection of waveforms, one can determine the building blocks (basis functions) that can be linearly combined (weighted and summed) to create any of the original waveforms. The idea is that the variation anticipated in mining events is captured by the basis functions, and thus one could replicate (or almost replicate) any future mining event's waveform by weighting and summing the basis functions. Rather than using a single template to look for a specific signal, one builds a subspace detector to detect a range of waveforms. Harris explored how subspace techniques could benefit the seismic monitoring community through two papers in 2006: first his report on subspace theory (Harris, 2006), then his report on practical implementations of subspace (Harris and Paik, 2006). He later collaborated with NORSAR in the development of another detection method, empirical matched field processing (EMFP) (Harris and Kværna, 2010). EMFP compares narrowband phase shifts measured between different array sensors for an incoming wavefield with the same measurements made from a master event, rather than comparing the waveforms themselves. The method is able to find events from the same source region while being insensitive to the events' source time histories.

More recently, researchers started executing global, multi-year studies. The mechanics of doing continuous monitoring on a broad region were explored by studying years of continuous waveform data at IMS stations in central Asia (Slinkard et al., 2014) using thousands of template waveforms. Automated processing found about 20% of the International Data Centre LEB events in that region during the 3 year period. To gain insight into the inherent number of events that can expect to be detected via waveform correlation, Dodge and others used a global bulletin and dataset containing almost 4 million events and cross-correlated waveform segments from events to find how many waveforms were highly correlated with other waveforms. Their results suggest that somewhere in the neighborhood of 18% of seismic events could be detected using waveform correlation using a global network; this might be a low estimate that increases as station density improves (Dodge and Walter, 2015). The emphasis on global detection capabilities continues with a study using 25 array stations to monitor continuous waveform data for nearly 16 years (Dodge and Harris, 2016). Their results conclude that more that 47% of global events can be detected using correlation detection.

Even as many researchers are focused on large scale implementations, old algorithms and approaches are constantly being revisited and improved. Recently, an innovative way of making intuitive sense of, and building, subspace detectors was proposed (Barrett and Beroza, 2014). Also, a new method to select template thresholds was proposed (Slinkard et al., 2014) that does not assume noise is Gaussian and sets thresholds based on a desired false alarm rate. It was noticed (Schaff and Richards, 2014) that it is best to use a different formula to calculate relative magnitude when the underlying waveforms are not quite the same, such as for a mining explosion a kilometer away from the original (the original formula is still best if the underlying signals are identical but have superimposed noise). A new subspace magnitude estimation approach was introduced for dense networks (Chambers et al., 2015) and autonomous event detection in aftershocks using subspace detectors was refined (Junek et al., 2015). Carmichael (2016) introduced a new detection method, the cone detector, which is optimized to detect events similar, but not identical to, a template.

Template matching can also be accomplished in the frequency domain, and with the fast Fourier transform algorithm, frequency domain methods are also amenable to automated processing of large numbers of seismic waveforms. Real seismic data is periodic and the approximate independence of adjacent frequencies enables statistical properties and techniques that are not available in the time domain. Shumway and Stoffer (2017) develop the theory and methods of time series analysis, including signal detection, waveform source classification, and source assessments, with examples using seismic waveforms. Fundamental frequency-domain statistical theory is rigorous and well-established, and further development of these theories for the analysis of large numbers of seismic waveforms offers promise for the future needs of underground nuclear test monitoring. Additional frequency-domain template matching approaches with statistical formality as explored in Shumway and Stoffer (2017) also offers promise for future needs of underground nuclear test monitoring.

There are several ideas and visions for how to incorporate template matching methods into processing. One is that similar events can be presented to an analyst together, enabling rapid and consistent phase picking (See tutorial on Template Matching). Another is to remove nuisance events from the processing stream; an iterative pipeline to remove aftershocks from raw data (Gibbons et al., 2016) shows promise. Yet another vision is using metadata from template detections (e.g., the origin time, location, and magnitude estimates) to improve the accuracy and speed of the association process (Slinkard et al., 2015). Recent research into using approximate nearest neighbor methods to search large archives (Yoon et al., 2015; Young et al., 2015) promises the ability to search for similar events orders of magnitude faster than current methods allow. Future research is required to continue the exploration of these paths, the forging of new ones, and the synthesizing of these various ideas until an optimal method for integrating template matching into automated processing and analyst workflow is converged upon. Template matching methods may one day be fully integrated into the processes used at monitoring agencies, and improve speed, ease, and accuracy in the detection and identification of seismic events.

Future R&D

Full-waveform processing improves detection accuracy and efficiency for earthquake, mining, and nuclear test events. Research into how to incorporate template matching approaches into the monitoring pipelines has the potential to revolutionize monitoring.

From simple to sophisticated radionuclide spectral analysis (RSA1)

When gamma spectroscopy was first utilized in the analysis of particulate and radioxenon data for verification of the CTBT, it relied heavily on simple HPGe spectral analysis and 2D region-of-interest software. The basis of the spectral fitting within software has largely been unchanged over the years, but the analysis has evolved to better help with the goal of monitoring for nuclear explosions.

When the first radioxenon detectors were developed for nuclear explosion monitoring, a means of analyzing the beta-gamma data was developed. In 2003, the radioxenon detection community met in Stockholm and developed a suite of equations for radioxenon activity analysis. These equations focus on the calculation of both the activity concentration for each of the xenon isotopes, and the minimum detectable concentration (MDC) to provide the significance of the radioxenon concentration measured and calculated. The MDC provides a metric for the sensitivity of the system and the ability to prevent false negative and false positive results. The equations utilized spectral regions-of-interest (McIntyre et al., 2006) for each of the radioxenon isotopes, and included a subset of interference terms to determine the impact of the presence of one isotope on the measurement of another (i.e., ^{133}Xe interfering with ^{133m}Xe) (See tutorial on Calculation of the MDC).

As the understanding of the radionuclide signals increased, work was performed on the development of simulations to better test analysis software. The simulations included both radioxenon signals (Haas et al., 2008) and particulate gamma ray simulations. In recent years, the beta-gamma simulation tool (BGSim) was developed to easily simulate radioxenon signals (McIntyre et al., 2016a). The combination of these simulation tools with atmospheric transport modeling allows for the benchmarking of the analysis routines.

With the transition from the ARSA-style beta-gamma detectors to single module beta-gamma detectors, similar to the SAUNA detectors, the absolute calibration method became possible. Using the absolute calibration method (Cooper et al., 2013) in conjunction with isotopically pure radioxenon samples (Haas et al., 2009), it becomes possible to measure the impact of the signal from one isotope on the measurement of another isotope. By knowing the impact of each isotope on a radioxenon measurement, a more accurate measurement of the isotopic activities can be performed.

Recent measurements have been made with a wide range of isotopic ratios. Some of these ratios have begun to push the limits of the current calibration and analysis techniques for the interference ratios. One specific example is a sample of high ^{131m}Xe activity with a small activity of ^{133}Xe. In this instance the compton scatter events from ^{131m}Xe impact the calculated activity within the 80-keV spectral region-of-interest for ^{133}Xe. The inclusion of additional interference ratios may allow for improved activity analysis in cases where the activity of one isotope is much smaller than other isotopes in the sample.

Future R&D

Source discrimination can be facilitated with more use of sophisticated spectral analysis, such as interferences between radioxenon isotopes and radioxenon/particulate ratios.

Tutorial: Calculation of the minimum detectable concentration

Activity analysis calculations make heavy use of the minimum detectable concentration (MDC). The MDC focuses on the counts present from background sources, while the activity analysis included counts present from the isotope of interest in the sample. The detection limit (Currie, 1968) for the detector is defined as:

$$L_D = 2.71 + 3.29\sigma_0$$

Where

$$\sigma_0 = \sqrt{BckCnt + \sigma^2_{BckCnt} + InterferenceCnt + \sigma^2_{InterferenceCnt} + MemoryCnt + \sigma^2_{MemoryCnt}}$$

The detection limit can then be combined with the physical parameters associated with the radioxenon isotope, sample processing, and sample measurement. The parameters in the MDC equation are broken up into three terms 1) counts detected and efficiencies, 2) half-life decay corrections, and 3) xenon collected.

$$MDC(\frac{mBq}{m^3 air}) = \frac{2.71 + 4.65\sigma_0}{\epsilon_\gamma \epsilon_\beta \gamma_{BR} \beta_{BR}} \cdot \frac{\lambda^2}{(1 - \exp(-\lambda T_C))(\exp(-\lambda T_P)(1 - \exp(-\lambda T_A))} \cdot \frac{T_C \cdot 1000}{V_{Air}}$$

where:

$\sigma_0 = \sqrt{BckCnts + (\sigma_{Interfences})^2}$

ε_γ = γ Efficiency

ε_β = β Efficiency

γ_{BR} = γ Branching Ratio

β_{BR} = β Branching Ratio

$\lambda = Ln(2)/\ t_{1/2}$

T_C = Xenon Collection Time

T_P = Processing Time of Gas

T_A = Acquisition Time of Counts

V_{Air} = cc of Xenon / 0.087 cc of Xenon per m^3 air

This equation can be modified depending on the interferences present from the other radioxenon isotopes (i.e., ^{133}Xe interference with ^{131m}Xe). A more detailed description of how the MDC is calculated for each of the xenon isotopes can be found in McIntyre et al., (2006).

From radionuclide detection to source discrimination (RSA1)

Radionuclide backgrounds have become increasingly convoluted over time. As the complexity of the backgrounds increases, so too must the sophistication of the analysis used for nuclear explosion monitoring.

During the period of nuclear explosive testing from the 1960s to the 1980s, the nuclear explosion verification analysis performed relied heavily on determining the gross amount of radionuclides released during the nuclear explosion. This often consisted of the identification of a few isotopes, but mainly focused on determining the total activity released (Schölch et al., 1966).

The radionuclide analysis software consisted of simple customized software or commercial software that was not specifically designed for nuclear explosion monitoring. With these types of generic analyses, it was possible to determine if the relevant radionuclides were observed (Bowyer et al., 2002).

Stand-alone analysis routines were developed that were focused on the complete analysis of radionuclide data and being able to provide accurate activity concentrations (Haas et al., 2008; Biegalski et al., 2006). It was determined that the detection of radionuclide particulate and radioxenon alone was not enough to indicate a nuclear explosion. Finding a method to discriminate a nuclear explosion from those produced from anthropogenic sources became a vital task. In 2006, a method was developed to discriminate between radionuclide sources using isotopic ratios (Kalinowski and Pistner, 2006) using accurate measurement of the radioxenon concentrations. Using the isotopic ratios to determine the nature of the source of the radioxenon (e.g., nuclear explosion, nuclear reactor, and medical isotope facility), additional information can be extracted from the measurements. Radioxenon signals are used in conjunction with the particulate signatures to provide information regarding the time and nature of the radionuclide release.

The use of isotopic ratios paved the way for more rigorous analyses of the source term to determine a wide range of source parameters such as the production mechanism and time since release (Bowyer et al., 2011). In conjunction with the improved ATM, the analysis routines were also able to add another layer of verification on the radionuclide source. Correlation of both the source location and the type of source allows for enhanced discrimination between a nuclear explosion and anthropogenic sources (Eslinger et al., 2014). For example, if shorter-lived isotopes are observed, it provides additional constraints on the duration of atmospheric backtracking.

Analysis tools began to be developed that focused on providing an integrated analysis and interpretation of the data for radioxenon and particulate. These tools utilize both isotopic ratios, as well as atmospheric transport, to obtain a better understanding of the radionuclide scenario. By folding in the analysis from multiple samples and stations, it is possible to provide insight into the source (Eslinger and Schrom, 2016).

The characterization of radionuclide signals relies on the incorporation of multiple aspects of analysis. This requires correlation between the radionuclide signals measured, the signal transport, and the waveform signals as a means of flagging or verifying the presence of an explosion. Similar to the waveform technologies, an event categorization matrix (ECM) can be made to include in the analysis the effects of various sources of the radionuclides including nuclear explosions, medical isotope production facilities, and nuclear reactors.

Future R&D

It will be important to develop analysis routines that incorporate both signals from radionuclides and seismic/hydroacoustic/infrasound into a single framework.

These efforts to combine multiple areas of analysis into a single framework seek to generate a more complete picture of the radioxenon signals. Examples of these research efforts are "Sentry" being developed by the United States and "Xecon" being developed by Sweden. These tools aim to provide the analyst with the most complete picture as possible of the xenon source by bringing the relevant information (i.e., ratios, ATM, possible sources) into an integrated framework. Through the inclusion of additional non-radioxenon-related information, such as seismic/hydroacoustic/infrasound signals, it will be possible to further refine the analysis of potential events. This refined analysis technique will allow for increased detection and discrimination of seismic, hydroacoustic, infrasound, and radionuclide signals. It will not be the enhancement of just one technology, but the use of these technologies in parallel that will help to further improve nuclear explosion monitoring capabilities.

Research Potential for Further Performance Improvements

There is an enduring need to monitor the earth for signatures of nuclear explosions. Since October 16, 1980, the date of the last atmospheric explosion, all declared nuclear explosions have occurred underground. Subsurface testing appears to be the most likely scenario for future testing, given that it allows for the control of radioactive explosive products (historically termed "fallout") which was a strong incentive for the speedy passage of the Limited Test Ban Treaty.

The first underground nuclear explosive tests in the late 1950s and early 1960s surprised scientists with their complex seismic signatures, including the generation of strong S-waves and Love surface waves and sometimes reversed Rayleigh surface waves. It had been expected that the seismic signals from underground explosions would be simple, consisting of mainly seismic P-waves and Rayleigh surface waves, which would allow them to be easily discriminated from the earth's natural background of earthquake signals. As a result of these surprises, significant research efforts were undertaken to improve nuclear monitoring. This effort was mainly empirical, focused on utilizing the collection and analysis of data from the active test sites during 1960-1990. This work resulted in significant improvement in overall monitoring capabilities.

Looking forward, it is important to have confidence that current empirical and limited test-site-based methods will work in all regions of the world and under untested emplacement conditions and media. This is driving physics-based simulation and modeling supported by chemical explosion data, such as the Source Physics Experiments. While there has been a tremendous amount of research conducted over the past several decades, a number of fundamental questions remain about how explosions generate seismic waves, particularly shear and surface waves. In addition, basic questions remain about the differences between chemical and nuclear explosions in terms of the signals they produce. This is extremely important as current and future monitoring R&D without nuclear explosive testing will make use of only historical nuclear explosive test data and future field experiments which will involve only chemical explosives.

Subsurface monitoring requires a series of steps: detection of signals in background noise, association of these signals with a physical event, accurate location of that event, and discrimination of the event as nuclear from other possible explanations. Each of these steps requires solving a number of scientific challenges related to 1) source physics, 2) signal propagation, 3) sensors, and 4) signal analysis.

Source physics represents our understanding of how different source types produce signals that might be observable. For example, understanding and discriminating between subsurface explosions and other "nuisance signals" (e.g., earthquake, mine blasts, cavity collapses, medical isotope production) is predicated on understanding differences in the source function between nuclear explosions and such signals. These differences in the seismic wave and radionuclide release characteristics are what can be observed at standoff distances and used by operational monitoring agencies. Similarly, determining the size of an explosion requires knowledge of source physics to relate the explosion energy (or radionuclide) release to the amplitude and frequency characteristics of the seismic waves (or radionuclide activities and isotopic ratios) generated. For example, the seismoacoustic wave amplitude-yield relationship depends upon many source factors such as the depth-of-burial, the media properties and the emplacement conditions. Significant improvements in monitoring can be achieved with further research in:

- Coupling the observed event spectra for the whole frequency band to earthquake and explosion models [seismic]
- Explosion and earthquake source models including uncertainty calculations [seismic]
- Improved explosion source models to make them applicable to a wide variety of geologic media and a wide range of yields and depths [seismic]

- Quantifying the effect of tectonic stress and evaluating the effect of the free-surface and near-surface scattering on underground explosion seismic signals with experiments [seismic]
- Incorporating new discriminants into the Event Categorization Matrix framework [seismic-infrasound-radionuclide-hydroacoustic]
- Methods to increase accuracy and realism of blastwave propagation simulations in the near-field of an explosion using advanced high performance computing and computational fluid dynamics [infrasound]
- Models of wave-coupling between the solid earth and atmosphere [infrasound]
- Additional discrimination techniques for anthropogenic radiological backgrounds to understand signals for monitoring purposes [radionuclide]
- Improved ratio measurements of the xenon isotopes and measurement of non-traditional xenon isotopes [radionuclide]
- Measurement of real transport parameters, or the correlation between xenon or argon isotopes and their surrogates [radionuclide]

Signal propagation represents our understanding of how the source signals are altered by the solid earth, air, and water as they travel from the source to the sensor. Accurate knowledge of the velocity, density, and attenuation structure of the propagation media leads directly to the ability to more accurately locate the source of a signal and determine its size. Background sources are being exploited to build more accurate models. Significant improvements in monitoring can be achieved with further research in:

- Better imaging of crustal heterogeneities via full waveform inversion at higher frequencies and advanced multivariate crustal models that simultaneously fit different geophysical observations [seismic]
- Development of surface wave attenuation models to account for focusing and defocusing and multipathing caused by elastic heterogeneities [seismic]
- Development of high-resolution data-driven crustal models with embedded ultra-high-resolution regions [seismic]
- Exploring the suitability of ambient noise for retrieval of amplitude information [seismic]
- Incorporation of crustal phases into regional models, to be able to model the structure at local scales, and development of full 3D velocity and amplitude models [seismic]
- Accurate uncertainty quantification of 3D geophysical models [seismic]
- New approaches for multi-scale and irregular meshes as applied to whole earth tomography [seismic]
- Forward and inverse modeling of the stochastic properties of the earth to match seismic envelope data and better recover source spectra [seismic]
- Infrasonic simulation capabilities to account for the unique challenges of the middle- and upper atmosphere [infrasound]
- Statistical propagation models and acoustic tomography methods using large data sets and events of interest [infrasound]
- Improving/validating 3D physics representation of hydroacoustic propagation models [hydroacoustic]
- Propagation of signals from multiple locations to define the possible source region [radionuclide]

Research Potential for Further Performance Improvements

Sensors record the signal of interest. In contrast to some other fields, commercially available seismic sensors have long been sensitive enough to record the nanometer-scale displacements that represent the earth's background noise at the quietest sites. The focus of R&D is on reducing power requirements, size, and costs. As these are achieved, sensors become more ubiquitous, allowing processing at closer standoff distances and entirely new types of processing. Alternatively for radionuclides, the focus of R&D is on the nuclear detection mechanisms, reducing power and size requirements, integrating analysis tools into the sensor, as well as increasing the sample processed. Significant improvements in monitoring can be achieved with further research in:

- Exploring the usefulness and limitations of low cost vibration sensors to complement high-fidelity sensor measurements [seismic]
- Finding cost effective ways to expand the density of the monitoring network so as to improve performance [seismic]
- Improved fidelity of local network performance assessment tools for network planning [seismic-hydroacoustic-infrasound-radionuclide]
- Usage of laboratory calibrations and in-field state of health determination to improve accuracy and reliability [seismic-infrasound-hydroacoustic-radionuclide]
- Improved traceability in calibration measurements to ensure confidence in sensor performance [seismic-infrasound-hydroacoustic-radionuclide]
- Improved chemistry processes and removal of consumables [radionuclide]
- Complex decay physics to better identify the isotopes of interest [radionuclide]
- Remotely or automatically adjusting sampling times to optimize collection of potential radionuclide plumes [radionuclide]
- Refining radionuclide detection limits while improving energy resolution and reducing memory effect [radionuclide]
- Optimizing radionuclide system processing chemistry including sorbent research [radionuclide]
- Use of electrostatic precipitation on particulate collectors/analyzers to use less air flow and power [radionuclide]
- Use of automated systems to minimize station down-time [radionuclide]
- Improved ^{37}Ar detection limits and correctly separating out delayed-activation signatures from background for on-site inspection [radionuclide]
- Focusing on-site inspectors on OSI-relevant radionuclides and restricting non-relevant information [radionuclide]

Signal analysis can be thought of as the algorithms that turn signals into knowledge. From filtering signals as a means to enhance the signal relative to the background noise to very sophisticated automated sensor network processing, these algorithms are the heart of both operational monitoring and R&D efforts. Signal analysis capabilities have dramatically advanced over several decades following the Moore's Law trajectory of computational processing. These are changing monitoring from a human-intensive endeavor toward a much more automated one supported by computer-aided analysis by experts for the signal of most interest. Significant improvements in monitoring can be achieved with further research in:

- Integration of advanced signal processing techniques (including template matching techniques) into data processing pipelines [seismic]
- Mathematically combining physical sensor data from all monitoring technologies for all assessments [seismic-infrasound-hydroacoutic-radionuclide]
- Combining signals and analysis from all monitoring technologies within an event categorization matrix [seismic-infrasound-hydroacoustic-radionuclide]
- Utilizing new multidimensional analyses and computational techniques to develop new discriminants [seismic-infrasound]
- Improving detection capabilities by leveraging multiple signal features and combining phenomenologies when data is limited [infrasound]
- Infrasound localization algorithms by leveraging more physically realistic propagation models [infrasound]
- Improving source discrimination by fully exploiting multiple radioxenon and particulate spectral analyses [radionuclide]

The role of simulation in R&D is increasingly useful in improving monitoring capability. Physics-based simulation codes have advanced significantly in recent years, greatly aided by progress in high performance computing and a more definitive understanding of underlying geological structures. The science behind these simulation codes needs to be supported by a vigorous R&D program in the key monitoring science areas of source physics, signal propagation, sensors, and signal analysis. Then the codes need to undergo rigorous evaluation and testing against the full historical nuclear data set, including data from local distances that has never been fully studied from a monitoring perspective, as well as against new field and lab experimental data that expand the range of testing conditions. The resulting tested and validated numerical simulation codes will be physics-based and allow prediction of nuclear explosion signatures anywhere in the world providing high confidence assurance that the monitoring data on any given day shows whether or not nuclear explosions are occurring. While this computationally intensive physics-based research has great potential for significantly further improving the performance of the monitoring systems, such an effort will require guidance from evolving policy perspectives.

R&D Themes from the GNDD Technology Roadmap

The trends are keyed to the R&D themes from the NNSA GNDD Technology Roadmap (Casey, 2014). The intent of keying the trends to the themes is to quickly orient the reader to the "why," and therefore the importance, of the research. The R&D themes are summarized below and associated with a metric that is useful for measuring R&D progress.

Source Physics R&D Themes & Metrics
Waveform Source Physics (WSO)1. Identify new and more effective methods to identify sources of waveform signals *Metric: Improved identification of sources*
WSO2. Predict nuclear explosion seismic S-wave amplitudes near the source for all emplacements *Metric: Explosion models that better match observables*
WSO3. Tune earthquake waveform amplitude models to their tectonic setting *Metric: Improved earthquake models that better match observables*
WSO4. Predict industrial explosion local and regional waveform amplitudes *Metric: New mine blast models that better match observables*
WSO5. Predict local and regional waveform signals from the collapse of underground cavities *Metric: New collapse models that better match observables*
WSO6. Calculate energy partitioning for sources near earth-water-air interfaces *Metric: Improved models that better match observables*
Radionuclide Source Physics (RSO)1. Determine the risk of innocuous background false alarms *Metric: Calculate risk*
RSO2. Improve knowledge of subsurface gas transport *Metric: Reduce the number of samples by an order of magnitude*
RSO3. Determine the amount of radionuclides produced in various nuclear testing conditions *Metric: Improve input to geologic and atmospheric transport models*
Signal Propagation R&D Themes & Metrics
Waveform Signal Propagation (WSP)1. Improve traveltime predictions *Metric: Improved traveltime and dispersion predictions that better match observables*
WSP2. Improve amplitude modeling *Metric: Improved amplitude predictions that better match observables*
WSP3. Predict travel-time, amplitude and full waveform signals from these models *Metric: Improved synthetic waveforms that better match observables*
Radionuclide Signal Propagation (RSP)1. Fine tune atmospheric modeling by bettering local sources *Metric: Reduce uncertainty in the deduced release point for radionuclides*

Sensors R&D Themes & Metrics
Waveform Sensors (WSE)1. Build new short-period (SP) micro seismometers and micro acoustic sensors *Metric: Design and build low power (<100 mW) micro-seismometers with internal noise levels below the reference low noise models*
WSE2. Prototype local monitoring sensor system *Metric: Demonstrate local monitoring system performance*
WSE3. Develop sensor network deployment software *Metric: Demonstrate capability to accurately model local network performance prior to deployment*
WSE4. Maintain a sensor testing and evaluation facility *Metric: Provide testing and evaluation for data acquisition systems for waveform technologies*
Radionuclide Sensors (RSE)1. More sensitivity *Metric: Increase sensitivity to aerosols and short-lived xenons by an order of magnitude*
RSE2. More xenon for less energy, less liquid nitrogen, in less size, or with less adsorbent material *Metric: Increase xenon yield while reducing complexity*
RSE3. Improve transfer of collected radionuclides into the radiation detector *Metric: Improve radionuclide detection sensitivity by a factor of 2X*
RSE4. Higher uptime and less maintenance *Metric: Meet or exceed an operation uptime of 95%*
RSE5. Solving near-field radionuclide measurement and operations problems, including on-site inspection *Metric: Demonstrate technologies*
Signal Analysis R&D Themes & Metrics
Waveform Signal Analysis (WSA)1. Improve the robustness and accuracy of parameter estimation *Metric: Demonstrate improved parameter and uncertainty estimates*
WSA2. Develop new waveform parameters *Metric: Demonstrate improved monitoring capability due to new waveform parameters*
WSA3. Improve parameter-based methods for monitoring *Metric: Improved detection, location, and/or identification*
WSA4. Improve waveform-based methods for monitoring *Metric: Improved detection, location, and/or identification*
Radionuclide Signal Analysis (RSA)1. Develop methods and techniques to increase the sensitivity and selectivity of radionuclide detection *Metric: Improve radionuclide detection sensitivity and selectivity by an order of magnitude or more*
RSA2. Improve discrimination of detected signals from background with algorithms *Metric: Demonstrate refined algorithms*
RSA3. Evaluation of intra-station dependencies to maximum network capabilities *Metric: Improved understanding of global coverage*

Guide to Seismic Waves and Phases

This Guide to Seismic Waves and Phases reviews the fundamentals of seismic waves, highlights the most important phases seen at both teleseismic and regional distances, connects these phases to what is seen on a seismograph, and shows an example of seismometer recordings generated by a large earthquake for seismometers located around the globe.

Underground seismic events generate seismic waves that travel through the body and along the surface of the earth. In the verification context, wave propagation in earth is divided into teleseismic paths (event to station distances greater than 2000 kilometers) and regional paths (distances less than 2000 kilometers). The phases we expect to see recorded by a seismometer vary depending on whether an event is at teleseismic or regional distance. The presence, timing, and amplitudes of these phases reveals information about the seismic source.

The material in this guide draws heavily from, or reproduces, selected material relevant to nuclear monitoring applications from monitoring applications from the following sources:

- http://www.ldeo.columbia.edu/res/pi/Monitoring/Doc/Srr_2006/GUIDE.PDF
- http://www.isc.ac.uk/standards/phases
- http://www.iris.edu
- http://web.ics.purdue.edu/~braile/edumod/waves/WaveDemo.htm

Seismic wave types

Explosions and earthquakes generate seismic waves which travel both in the interior and on the surface of the earth. Underground events directly generate compressional waves (P waves, also known as "pressure" or "primary") and shear waves (S waves, also known as "secondary"). These waves travel through the interior of the earth, and are referred to as body waves. As body waves interact with the surface of the earth, energy is transferred into surface waves; these Rayleigh (R) and Love (L) waves are high amplitude, low velocity waves which travel in the crust.

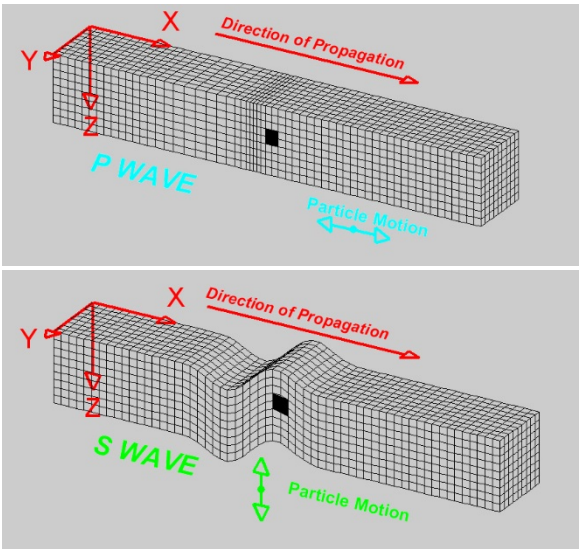

Body Waves (P and S)

- Travel through *planet interior*, e.g. crust, mantle, inner and outer core.
- P-waves (primary or pressure) usually arrive at seismic stations first (higher velocity).
- S-waves (secondary or shear) have lower velocities, arriving after P-waves.
- Transmission, reflection, and refraction through each region/boundary create multiple phases of each wave.

Surface Waves (L and R)

- Only propagate through the *crust*, with amplitude decreasing greatly with depth and distance.
- Generated by P- and S- wave interaction with the surface of the earth.
- Slower than either P- or S- waves.
- Most destructive of seismic waves.
  - Longer periods and greater comparable amplitudes.

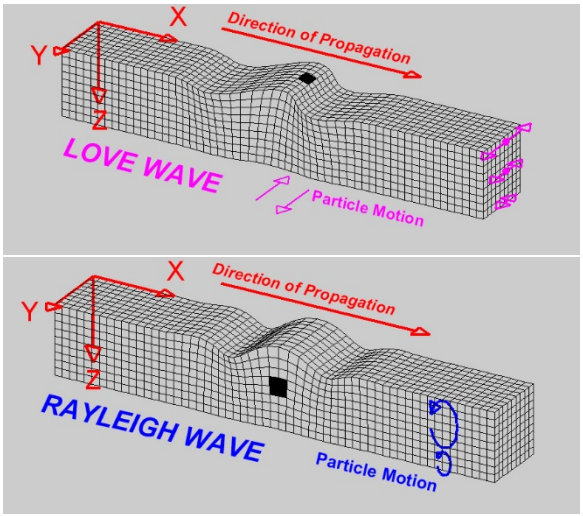

https://www.iris.edu/hq/inclass/animation/seismic_wave_motions

Seismic Phases

Seismic energy takes a plethora of travel paths through the earth, reflecting and refracting as it encounters velocity gradients. Each path produces a separate seismic phase on a seismogram. Hundreds of phases have been identified, however, only on the order of 10 are commonly used in nuclear explosion monitoring.

Phases recorded at teleseismic distances (>~2000 km)

- Teleseismic phases have travelled long distances through the mantle before being recorded at a seismic station.
- The change of seismic velocities within Earth, as well as the possibility of conversions between wave types, results in many possible wave paths.
- Seismic phases are described with one or more letters, each of which describes a part of the wave path. Upper case letters denote the type of wave, and lower case letters denote reflections from boundaries.
- Each path produces a separate seismic phase on a seismogram. The exact phases recorded at a seismometer depend on the distance from event to seismometer.

COMMON TELESEISMIC PHASES	
P	A compressional wave that follows a simple path from event source to the station
PcP	A P wave that goes downward through the mantle (the first "P"), is reflected from the top of the outer core ("c"), and goes upward through the mantle to the station (second "P")
Pdiff	A P wave that has been bent (diffracted) around the outer core boundary and arrives at a station in the ray "shadow" of the outer core
PKP	A P wave that has traveled through the mantle ("P"), been transmitted across the mantle-outer core boundary and traveled through the outer core ("K"), transmitted back across the outer core-mantle boundary and traveled as a P wave to the station ("P"). Because of the large difference between the P wave velocity in the mantle and the outer core, this wave is bent (refracted) strongly at the boundary
S	A shear wave that follows a simple path from event source to the station (Additional S phases follow the naming convention described for P phases)

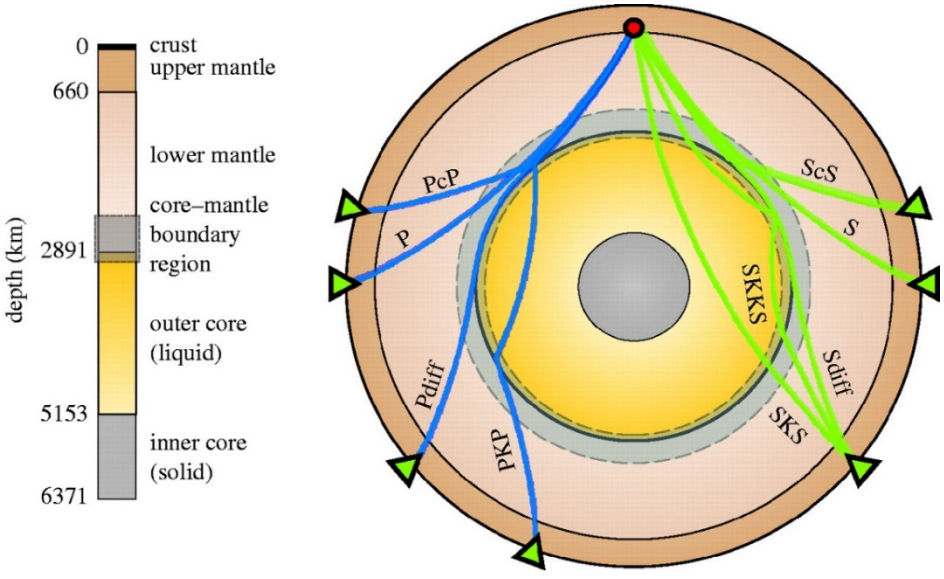

http://rsta.royalsocietypublishing.org/content/366/1885/4543

- At regional and local distances, waves travel through the crust as well as the mantle. Body waves (P, S) and surface waves (L, R) are both observed.
- The phases recorded at a seismometer depend both on the depth of the event and on the distance from seismometer to the event.

Expected local and regional phases for 3 event depths

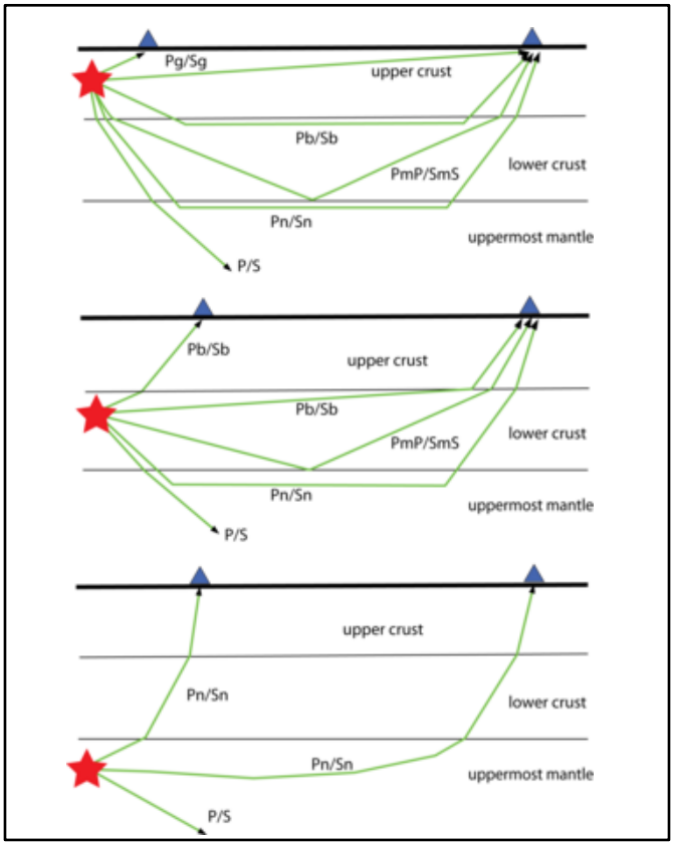

http://www.isc.ac.uk/standards/phases/

COMMON CRUSTAL and MANTLE PHASES	
Pg	At short distances, either an upgoing P wave from a source in the *upper crust* or a P wave bottoming in the upper crust. At larger distances, also arrivals caused by multiple P-wave reverberations inside the whole crust with a group velocity around 5.8 km/s
Pb	Either an upgoing P wave from a source in the *lower crust* or a P wave bottoming in the lower crust
Pn	Any P wave bottoming in the *uppermost mantle* or an upgoing P wave from a source in the uppermost mantle
P	*A longitudinal wave, bottoming below the uppermost mantle*; also an upgoing longitudinal wave from a source below the uppermost mantle
Sg	At short distances, either an upgoing S wave from a source in the *upper crust* or an S wave bottoming in the upper crust. At larger distances, also arrivals caused by superposition of multiple S-wave reverberations and SV to P and/or P to SV conversions inside the whole crust
Sb	Either an upgoing S wave from a source in the *lower crust* or an S wave bottoming in the lower crust
Sn	Any S wave bottoming in the *uppermost mantle* or an upgoing S wave from a source in the uppermost mantle
S	*Shear wave, bottoming below the uppermost mantle*; also an upgoing shear wave from a source below the uppermost mantle
Lg	A wave group *observed at larger regional distances* and caused by superposition of multiple S-wave reverberations and SV to P and/or P to SV conversions inside the whole crust. The maximum energy travels with a group velocity around 3.5 km/s
Rg	Short period *crustal* Rayleigh wave

Seismic waves as recorded by a seismometer

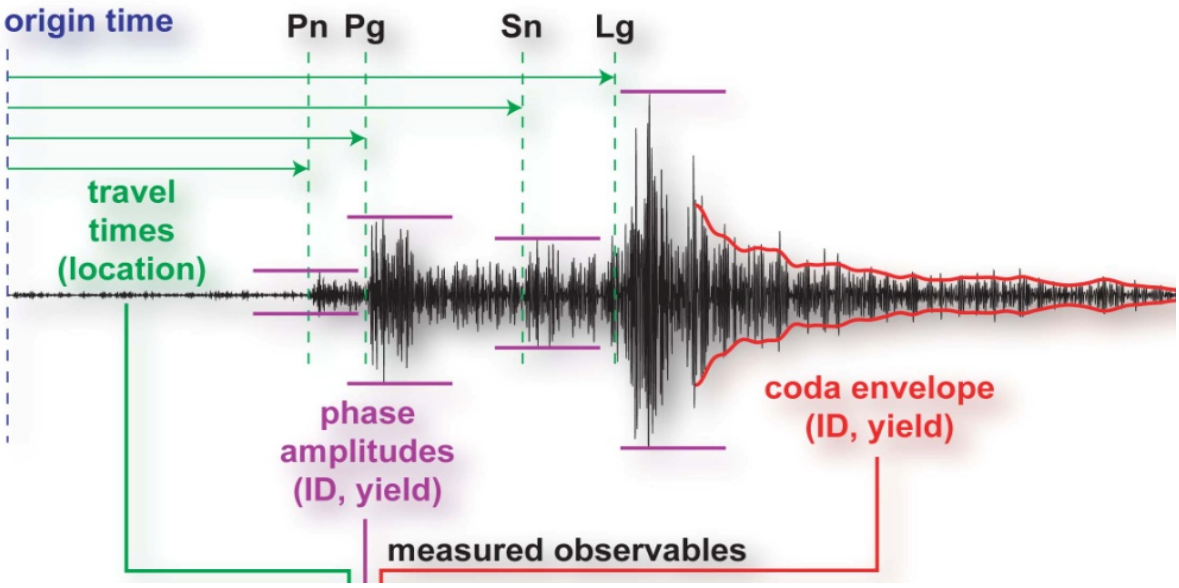

- Shown here is the signal at a seismometer from the time that a seismic event occurs until the signal decays away.
- P waves arrive first; in this example two P phases (Pn and Pg) are present. S waves arrive next; here just phase Sn. Last arrive the surface waves, here the Lg phase.
- The timing of phase arrivals imparts information about the location and depth of the event.
- The amplitude of phase arrivals imparts information about yield and identification.
- "Coda" refers to later arriving waves - waves delayed by scattering caused by the earth's heterogeneities. Coda also imparts information related to yield and identification.

Signals recorded around the world from the same event

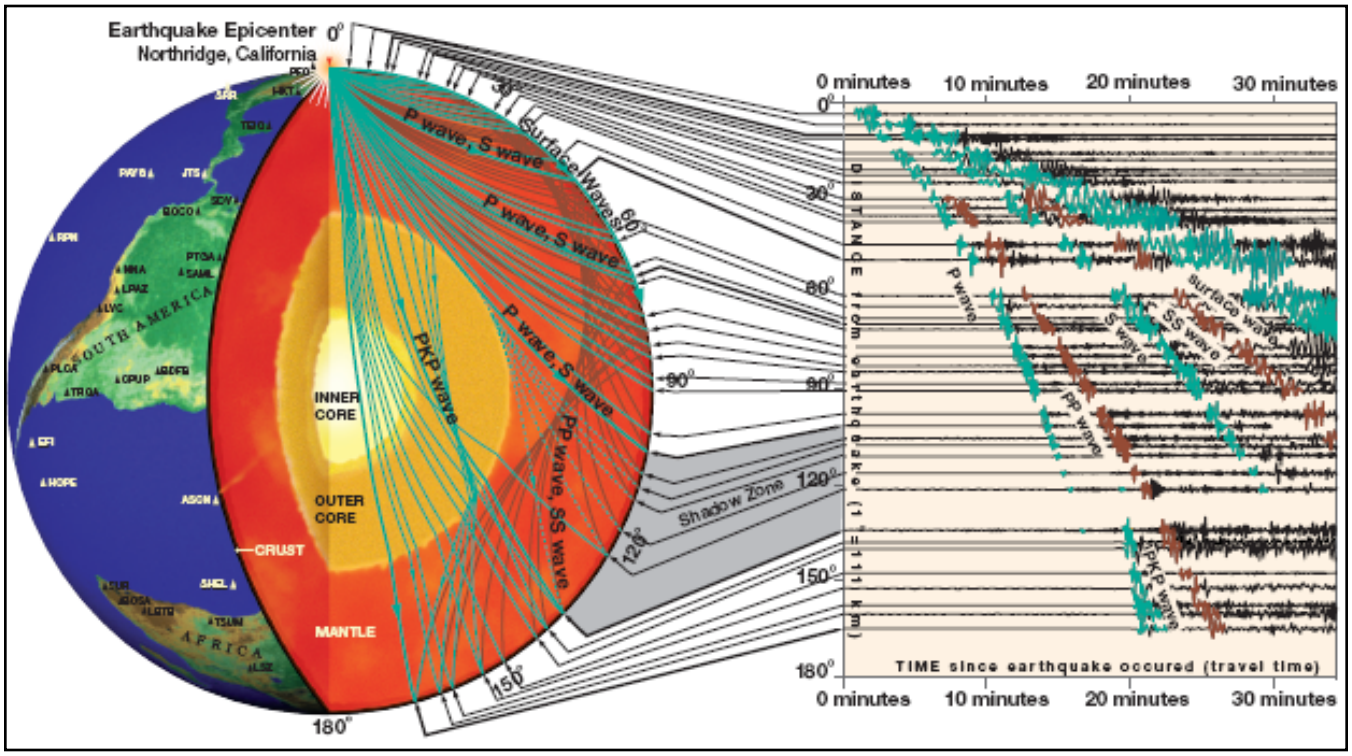

https://www.iris.edu/gallery3/general/posters/exploring_earth/WavePropagation

- Signals generated by the Northridge earthquake are shown at seismographs around the world.
- The phases recorded, and the timing of the phases, depends on the distance between the event and the station.
- P and S waves generally travel the same path, but at different speeds.
- The liquid core halts transmission of S waves and refracts incoming P waves, creating the phase known as PKP.

References

Aalseth, C.E., A.R. Day, D.A. Haas, E.W. Hoppe, B.J. Hyronimus, M.E. Keillor, E. K. Mace, J.L. Orrell, A. Seifert, V.T. Woods, 2011, **Measurement of Ar37 to support technology for On-Site Inspection under the Comprehensive Nuclear-Test-Ban Treaty**, *Nuclear Instruments & Methods in Physics Research*, *652*, *no. 1*, *58-61*, doi:10.1016/j.nima.2010.09.135.

Addair, T. G., D.A. Dodge, W.R. Walter, and S.D. Ruppert, 2014, **Large-scale seismic signal analysis with Hadoop**, *Computers & Geosciences*, *66*, *145-154*, doi:10.1016/j.cageo.2014.01.014.

Adushkin, V., and W. Leith, 2001, **The containment of Soviet underground nuclear explosions**, *United States Geological Survey*, *Open-File Report 2001-312*, https://pubs.usgs.gov/of/2001/0312/report.pdf.

Afanasiev M., D. Peter, K. Sager, S. Simute. L. Ermert, L. Krischer, and A. Fichtner, 2016, **Foundations for a multiscale collaborative Earth model**, *Geophysical Journal International*, *204*, *no. 1*, *39-58*, doi:10.1093/gji/ggv439.

Aki, K., 1966, **4. Generation and propagation of G waves from the Niigata earthquake of June 14, 1964. Part 2. Estimation of earthquake moment, released energy and stress-strain drop from G wave spectrum**, *Bulletin of the Earthquake Research Insitute*, *44*, *no. 1*, *73-88*, http://repository.dl.itc.u-tokyo.ac.jp/dspace/handle/2261/12238.

Aki, K., 1969, **Analysis of the seismic coda of local earthquakes as scattered waves**, *Journal of Geophysical Research: Solid Earth*, *74*, *no. 2*, *615-631*, doi:10.1029/JB074i002p00615.

Aki, K., A. Christoffersson, and E. S. Husebye, 1977, **Determination of the three-dimensional seismic structure of the lithosphere**, *Journal of Geophysical Research: Solid Earth*, *82*, *277-296,* doi:10.1029/JB082i002p00277.

Aki, K., and P. G. Richards, 2002, **Quantitative Seismology**, *University Science Books*, *ISBN 978-1-891389-63-4*, http://www.uscibooks.com/.

Allmann, B. P., P. M. Shearer, and E. Hauksson, 2008, **Spectral discrimination between quarry blasts and earthquakes in Southern California**, *Bulletin of the Seismological Society of America*, *98*, *no. 4*, *2073-2079*, doi:10.1785/0120070215.

Ambrosiano, J. J., D. R. Plante, B. E. McDonald and W. A. Kuperman, 1990, **Nonlinear propagation in an ocean acoustic waveguide**, *Journal of the Acoustical Society of America*, *87*, *1473-1481*, doi:10.1121/1.399444.

American National Standards Institute, 1983, **American National Standard Estimating Air Blast Characteristics for Single Point Explosions in Air, with a Guide to Evaluation of Atmospheric Propagation and Effects**, *Acoustical Society of America*, *ANSI S2.20-1983*, *26 pp*.

Anderson, D.N., T. Redgate, K.K. Anderson, and A.C. Rohay, 1997, **Quadratic Negative Evidence Discrimination**, *Pacific Northwest National Laboratory*, *PNNL-11579*, doi:10.2171/549314.

Anderson, D. N., S. R. Taylor, and K. K. Anderson, 1999, **Discrimination information in phase amplitude thresholds with application to Western China regional data**, *Bulletin of the Seismological Society of America*, *89*, *no. 3*, *648-656*, http://www.bssaonline.org/content/89/3/648.short.

Anderson, D. N., and S. R. Taylor, 2002, **Application of regularized discrimination analysis to regional seismic event identification**, *Bulletin of the Seismological Society of America*, *92*, *no. 6*, *2391-2399*, doi:10.1785/0120010218.

Anderson, D. N., R. Willemann, H. Miley, C. L. Edwards, P. B. Herrington, J. M. Harris, J. C. Wehlburg, D. B. Harris, J. J. Zucca, and L. A. Casey, 2004, **Trends in nuclear explosion monitoring**, *Los Alamos National Laboratory*, *LA-UR-04-5801, Proceedings of the 26th Seismic Research Review, Vol. 1, 3-15*, http://www.osti.gov/bridge/servlets/purl/1027446/.

Anderson, D. N., D. K. Fagan, M. A. Tinker, G. D. Kraft, and K. D. Hutchenson, 2007, **A mathematical statistics formulation of the teleseismic explosion identification problem with multiple discriminants**, *Bulletin of the Seismological Society of America*, *97*, *no. 5*, *1730-1741*, doi:10.1785/0120060052.

Anderson, D. N., W. R. Walter, D. K. Fagan, T. M. Mercier, and S. R. Taylor, 2009, **Regional multistation discriminants: magnitude, distance, and amplitude corrections, and sources of error**, *Bulletin of the Seismological Society of America*, *99*, *no. 2A*, *794-808*, doi:10.1785/0120080014.

Anderson, D. N., G. E. Randall, R. W. Whitaker, S. J. Arrowsmith, M. D. Arrowsmith, D. K. Fagan, S. R. Taylor, N. D. Selby, F. R. Schult, G. D. Kraft, and W. R. Walter, 2010a, **Seismic event identification**, in *Wiley Interdisciplinary Reviews: Computation Statistics*, *2*, *no. 4*, *July/August 2010, edited by E. Wegman, Y. H. Said and D. W. Scott, John Wiley & Sons, New York, NY*, *414-432*, doi:10.1002/wics.105.

Anderson, D. N., R. H. Shumway, R. R. Blandford, and S. T. Taylor, 2010b, **Statistical methods in seismology**, in *Wiley Interdisciplinary Reviews: Computation Statistics*, *2*, *no. 3*, *May/June 2010, edited by E. Wegman, Y. H. Said and D. W. Scott, John Wiley & Sons, New York, NY*, *303-316*, doi:10.1002/wics.74.

Anderson, D. N., H. J. Patton, S. R. Taylor, J. L. Bonner, and N. D. Selby, 2014, **Sources of error and the statistical formulation of Ms:mb seismic event screening analysis**, *Pure and Applied Geophysics*, *171*, *no. 3-5*, *537-547*, doi:10.1007/s00024-012-0627-9.

Archambeau, C. B., 1972, **The Theory of Stress Wave Radiation from Explosions in Prestressed Media**, *Geophysical Journal International*, *29*, *no. 3*, *329-366*, doi:10.1111/j.1365-246X.1972.tb06163.x.

Arrowsmith, S. J., R. Whitaker, C. Katz, and C. Hayward, 2009, **The F-detector revisited: An improved strategy for signal detection at seismic and infrasound arrays**, *Bulletin of the Seismological Society of America*, *99*, *no. 1*, *494-453*, doi:10.1785/0120080180.

Arrowsmith, S. J., R. Burlacu, K. Pankow, B. Stump, R. Stead, R. Whitaker, and C. Hayward, 2012, **A seismoacoustic study of the 2011 January 3 Circleville earthquake**, *Geophysical Journal International*, *189, no. 2, 1148-1158*, doi:10.1111/j.1365-246X.2012.05420.x.

Arrowsmith, S. J., O. Marcillo, and D. P. Drob, 2013, **A framework for estimating stratospheric wind speeds from unknown sources and application to the 2010 December 25 bolide**, *Geophysical Journal International*, *195, no. 1, 491-503*, doi:10.1093/gji/ggt228.

Arrowsmith, S., D. Norris, R. Whitaker, and D. Anderson, 2014, **Sources of error model and progress metrics for acoustic/infrasonic analysis: Location estimation**, *Pure and Applied Geophysics*, *171*, *no. 3-5*, *587-597*, doi:10.1007/s00024-012-0576-3.

Assink, J. D., R. Waxler, W. G. Frazier, and J. Lonzaga, 2013, **The estimation of upper atmospheric wind model updates from infrasound data**, *Journal of Geophysical Research: Atmospheres*, *118*, *no. 19*, *10,707–10,724*, doi:10.1002/jgrd.50833.

Auer, M., A. Axelsson, X. Blanchard, T.W. Bowyer, G. Brachet, I. Bulowski, Y. Dubasov, K. Elmgren, J.P. Fontaine, W. Harms, J.C. Hayes, T.R. Heimbigner, J.I. McIntyre, M.E. Panisko, Y. Popov, A. Ringbom, H. Sartorius, S. Schmid, J. Schulze, et al., 2004, **Intercomparison experiments of systems for the measurement of xenon radionuclides in the atmosphere**, *Applied Radiation and Isotopes*, *60, 863-877*, doi:10.1016/j.apradiso.2004.01.011.

Axelsson, A., and A. Ringbom, 2014, **On the calculation of activity concentrations and nuclide ratios from measurements of atmospheric radioactivity**, *Applied Radiation and Isotopes*, *92*, *12-17*, doi:10.1016/j.apradiso.2014.05.020.

Baker, W. E., 1973, **Explosions in Air**, *University of Texas Press*, *ISBN 0292720033*, *268 pp*, https://www.amazon.com/Explosions-Air-Wilfred-Edmund-Baker/dp/0292720033.

Baker, G. E., J. L. Stevens, and H. Xu, 2012a, **Explosion shear-wave generation in high-velocity source media**, *Bull. Seism. Soc. Am., 102, no. 4, 1301-1319*, doi:10.1785/0120110119.

Baker, G. E., J. L. Stevens, and H. Xu, 2012b, **Explosion shear-wave generation in low-velocity source media**, *Bull. Seism. Soc. Am., 102, no. 4, 1320-1334*, doi:10.1785/0120110165.

Ballard, S., J. R. Hipp, and C. J. Young, 2009, **Efficient and accurate calculation of ray theory seismic travel time through variable resolution 3D earth models**, *Seismological Research Letters*, *80, no. 6, 989-1000*, doi:10.1785/gssrl.80.6.989.

Ballard, S., J. R. Hipp, B. J. Kraus, A. V. Encarnacao, and C. J. Young, 2016a, **GeoTess: A generalized Earth model software utility**, *Seismological Research Letters*, *87*, *no. 3*, doi:10.1785/0220150222.

Ballard, S., J. R. Hipp, M. L. Begnaud, C. J. Young, A. V. Encarnacao, E.P. Chael, W. S. Phillips, 2016b, **SALSA3D - A tomographic model of compressional wave slowness in the earth's mantle for improved travel time prediction and travel time prediction uncertainty**, *Bulletin of the Seismological Society of America*, *106*, *no. 6*, *17 pp*, doi:10.1785/0120150271.

Bao, X., X. Song, and J. Li, 2015, **High-resolution lithospheric structure beneath Mainland China from ambient noise and earthquake surface-wave tomography**, *Earth and Planetary Science Letters*, *417*, *132-141*, doi:10.1016/j.epsl.2015.02.024.

Bao, X., and Y. Shen, 2016, **Assessing waveform predictions of recent three-dimensional velocity models of the Tibetan plateau**, *Journal of Geophysical Research: Solid Earth*, *121*, doi:10.1002/2015JB012619.

Barrett, S. A., and G. C. Beroza, 2014, **An empirical approach to subspace detection**, *Seismological Research Letters*, *85*, *no. 3*, *594-600*, doi:10.1785/0220130152.

Barth, K. H., 2003, **The politics of seismology: Nuclear testing, arms control, and the transformation of a discipline**, *Social Studies of Science*, *33*, *no. 5*, *743-781*, doi:10.1177/0306312703335005.

Bassin, C., G. Laske, and G. Masters, 2000, **The current limits of resolution for surface wave tomography in North America**, *Eos, Transactions of the American Geophysical Union*, *81*, *F897*, http://igppweb.ucsd.edu/~gabi/crust2.html.

Baumgardt, D. R., and G. B. Young, 1990, **Regional Seismic Waveform Discriminants and Case-based Event Identification using Regional Arrays**, *Bulletin of the Seismological Society of America*, *80*, *no. 6*, *1874-1892*.

Becquerel, H., 1896, **Sur les radiations émises par phosphorescence**, *Comptes Rendus*, *122*, *420-421*, http://gallica.bnf.fr/ark:/12148/bpt6k30780/f422.chemfindefer.

Becquerel, H., 1900, **Contribution à l'étude du rayonnement du radium**, *Séances de la Société française de physique*, *28-38*, doi:10.1051/jphystap:019000090019000.

Benoit, M. H., A. A. Nyblade, and M. E. Pasyanos, 2006, **Crustal thinning between the Ethiopian and East African Plateaus from modeling Rayleigh wave dispersion**, *Geophysical Research Letters*, *33*, *no. 13*, *L13301*, doi:10.1029/2006GL025687.

Bensen, G. D., M. H. Ritzwoller, M. P. Barmin, and A. Levshin, 2007, **Processing seismic ambient noise data to obtain reliable broad-band surface wave dispersion measurements**, *Geophysical Journal International*, *169*, *no. 3*, *1239-1260*, doi:10.1111/j.1365-246X.2007.03374.x.

Berger, J., P. Davis, and G. Ekström, 2004, **Ambient Earth noise: A survey of the Global Seismographic Network**, *Journal of Geophysical Research: Solid Earth*, *109*, *no. B11*, *B11307*, doi:10.1029/2004JB003408.

Biegalski, K. M. F., S. R. Biegalski, and D. A. Haas, 2006, **Further development of the spectral deconvolution analysis tool (SDAT) to improve counting statistics and detection limits for nuclear explosion radionuclide measurements**, *Los Alamos National Laboratory*, *LA-UR-06-5471, Proceedings of the 28th Seismic Research Review: Ground-Based Nuclear Explosion Monitoring Technologies*, *774-783*, http://www.osti.gov/scitech/biblio/1027448.

Bjurman, B., L. R. De Geer, I. Vintersved, A. L. Rudjord, F. Ugletveit, H. Aaltonen, L. Sinkko, A. Rantavaara, S. P. Nielsen, A. Aarkrog, and W. Kolb, 1990, **The detection of radioactive material from a venting underground nuclear explosion**, *Journal of Environmental Radioactivity*, *11*, *no. 1*, *1-14*, doi:10.1016/0265-931X(90)90040-3.

Blackberg, L., A. Fay, I. Jogi, S. Biegalski, M. Boman, K. Elmgren, T. Fritioff, A. Johansson, L. Martensson, F. Nielsen, A. Ringbom, M. Rooth, H. Sjostrand, and M. Klintenberg, 2011, **Investigations of surface coatings to reduce memory effect in plastic scintillator detectors used for radioxenon detection**, *Nuclear Instruments & Methods in Physics Research*, *656*, *no. 1*, *84-91*, doi:10.1016/j.nima.2011.07.038.

Blandford, R., 1977, **Discrimination between earthquakes and underground explosions**, *Annual Review of Earth and Planetary Sciences*, *5*, *111-122*, doi:10.1146/annurev.ea.05.050177.000551.

Blom, P. S., O. Marcillo, and S. J. Arrowsmith, 2015, **Improved Bayesian infrasonic source localization for regional infrasound**, *Geophysical Journal International*, *203*, *no. 3*, *1682-1693*, doi:10.1093/gji/ggv387.

Bodin, T., and M. Sambridge, 2009a, **Seismic tomography with the reversible jump algorithm**, *Geophysical Journal International*, *178*, *1411-1436*, doi:10.1111/j.1365-246X.2009.04226.x.

Bodin, T., and M. Sambridge, 2009b, **A self-parametrizing partition model approach to tomographic inverse problems**, *Inverse Problems*, *25*, *22*, doi:10.1088/0266-5611/25/5/055009.

Bolmsjo, M. S., and B. R. R. Persson, 1982, **A new instrument for survey monitoring of airborne xenon-133**, *Physics in Medicine and Biology*, *27*, *no. 6*, *861-866*, doi:10.1088/0031-9155/27/6/007.

Bondár, I., S. C. Myers, E. R. Engdahl, and E. Bergman, 2004, **Epicentre accuracy based on seismic network criteria**, *Geophysical Journal International*, *156*, *no. 3*, *483-496*, doi:10.1111/j.1365-246X.2004.02070.x.

Bondár, I., and K. McLaughlin, 2009, **Seismic Location Bias and Uncertainty in the Presence of Correlated and Non-Gaussian Travel Time Errors**, *Bulletin of the Seismological Society of America*, *99*, *no. 1*, *172-199*, doi:10.1785/0120080922.

Bondár, I., S. C. Myers, and E. R. Engdahl, 2014, **Earthquake location**, in *Springer*, *Encyclopedia of Earthquake Engineering, ed. M. Beer, E. Patelli, I. Kougioumtzoglou, and I Siu-Kui,* doi:10.1007/978-3-642-36197-5_184-1.

Bonner, J., R. Waxler, Y. Gitterman, and R. Hofstetter, 2013, **Seismo-Acoustic Energy Partitioning at Near-Source and Local Distances from the 2011 Sayarim Explosions in the Negev Desert, Israel**, *Bulletin of the Seismological Society of America*, *103*, *no. 2A*, *741-758*, doi:10.1785/0120120181.

Bonner, J. L., D. C. Pearson, and W. S. Blomberg, 2003, **Azimuthal variation of short-period Rayleigh waves from cast blasts in northern Arizona**, *Bulletin of the Seismological Society of America*, *93*, *no. 2*, *724-736*, doi:10.1785/0120020115.

Bonner, J. L., D. Russell, D. Harkrider, D. Reiter, and R. Herrmann, 2006, **Development of a time-domain, variable-period surface wave magnitude measurement procedure for application at regional and teleseismic distances, Part II: application and Ms —mb performance**, *Bulletin of the Seismological Society of America*, *96*, *no. 2*, *678-696*, doi:10.1785/0120050056.

Bonner, J. L., M. R. Leidig, C. Sammis, and R. J. Martin, 2009, **Explosion coupling in frozen and unfrozen rock: experimental data collection and analysis**, *Bulletin of the Seismological Society of America*, *99*, *no. 2A*, *830-851*, doi:10.1785/0120080259.

Bonner, J. L., D. R. Russell, and R. E. Reinke, 2013, **Modeling surface waves from aboveground and underground explosions in alluvium and limestone**, *Bulletin of the Seismological Society of America*, *103*, *no. 6*, *2953-2970*, doi:10.1785/0120130069.

Boschi, L., T. W. Becker, G. Soldati, and A. M. Dziewonski, 2006, **On the relevance of Born theory in global seismic tomography**, *Geophysical Research Letters*, *33*, *no. L06302*, doi:10.1029/2005GL025063.

Bowyer, T. W., K. H. Abel, W. K. Hensley, M. E. Panisko, and R. W. Perkins, 1997, **Ambient 133Xe levels in the northeast US**, *Journal of Environmental Radioactivity*, *37*, *no. 2*, *143-153*, doi:10.1016/S0265-931X(97)00005-2.

Bowyer, S. M., H. S. Miley, R. C. Thompson, and C. W. Hubbard, 1997, **Automated particulate sampler for Comprehensive Test Ban Treaty verification (The DOE Radionuclide Aerosol Sampler/ Analyzer)**, *IEEE Transactions on Nuclear Science*, *44, no. 3*, doi:10.1109/23.603709.

Bowyer, T.W., K.H. Abel, C.W. Hubbard, M.E. Pankiso, P.L. Reeder, R.C. Thompson, and R.A. Warner, 1999, **Field testing of collection and measurement of radioxenon for the Comprehensive Test Ban Treaty**, *Journal of Radioanalytical and Nuclear Chemistry*, *240*, *no. 1*, *109-122*, doi:10.1007/BF02349143.

Bowyer, T. W., C. Schlosser, K. H. Abel, M. Auer, J. C. Hayes, T. R. Heimbigner, J.I. McIntyre, M. E. Panisko, P. L. Reeder, H. Satorius, J. Schulze, and W. Weiss, 2002, **Detection and analysis of xenon isotopes for the comprehensive nuclear-test-ban treaty international monitoring system**, *Journal of Radioanalytical and Nuclear Chemistry*, *59*, *139-151*, doi:10.1016/S0265-931X(01)00042-X.

Bowyer, T.W., S.R. Biegalski, M. Cooper, P.W. Eslinger, D. Haas, J.C. Hayes, H.S. Miley, D.J. Strom, V. Woods, 2011, **Elevated radioxenon detected remotely following the Fukushima nuclear accident**, *Journal of Environmental Radioactivity*, *102, no. 7, 681-687*, doi:10.1016/j.jenvrad.2011.04.009.

Bowyer, T. W., R. Kephart, P. W. Eslinger, J. I. Friese, H. S. Miley, and P. R. J. Saey, 2013, **Maximum reasonable radioxenon releases from medical isotope production facilities and their effect on monitoring nuclear explosions**, *Journal of Environmental Radioactivity*, *115, 192-200*, doi:10.1016/j.jenvrad.2012.07.018.

Bozdag E., D. Peter, M. Lefebvre, D. Komatisch, J. Tromp, J. Hill, N. Podhorszki, and D. Pugmire, 2016, **Global adjoint tomography: first-generation model**, *Geophysical Journal International*, *207*, *no. 3*, *1739-1766*, doi:10.1093/gji/ggw356.

Brachet, N., D. Brown, R. LeBras, Y. Cansi, P. Mialle, and J. Coyne, 2010, **Monitoring the Earth's Atmosphere with the Global IMS Infrasound Network**, in *Springer*, *Infrasound Monitoring for Atmospheric Studies*, *ISBN 978-1-4020-9508-5*, *77-118*, doi:10.1007/978-1-4020-9508-5.

Brown, D. J., C. N. Katz, R. Le Bras, M. P. Flanagan, J. Wang, and A. K. Gault, 2002a, **Infrasonic signal detection and source location at the Prototype International Data Centre**, *Pure and Applied Geophysics*, *159*, *no. 5*, doi:10.1007/s00024-002-8674-2.

Brown, P. G., R. W. Whitaker, D. O. ReVelle, and E. Tagliaferri, 2002b, **Multi-station infrasonic observations of two large bolides: signal interpretation and implications for monitoring of atmospheric explosions**, *Geophysical Research Letters*, *29(13), 1636, 10.1029/2001GL013778*, doi:10.1029/2001GL013778.

Brown, D., L. Ceranna, M. Prior, P. Mialle, and R. J. Le Bras, 2014, **The IDC Seismic, Hydroacoustic and Infrasound Global Low and High Noise Models**, *Pure and Applied Geophysics*, *171*, *no. 2*, *361-375*, doi:10.1007/s00024-012-0573-6.

Brune, J. N., 1970, **Tectonic stress and the spectra of seismic shear waves from earthquakes**, *Journal of Geophysical Research*, *75*, *no. 26*, *4997–5009,* doi:10.1029/JB075i026p04997.

Burdick, S., C. Li, V. Martynov, T. Cox, J. Eakins, L. Astiz, F. L. Vernon, G. L Pavlis, and R. D. Van der Hilst, 2008, **Upper mantle heterogeneity beneath North America from travel time tomography with global and USArray transportable array data**, *Seismological Research Letters*, *79*, *384-392*, doi:10.1785/gssrl.79.3.384.

Burgmann, R., P. Rosen, and E. Fielding, 2000, **Synthetic aperture radar interferometry to measure Earth's surface topography and its deformation**, *Annual Review of Earth and Planetary Sciences*, *28*, *no. 1*, *169-209*, doi:10.1146/annurev.earth.28.1.169.

Caffrey, A. J., T. W. Bowyer, A. E. Egger, J. C. Hall, S. M. Kelly, K. M. Krebs, S. A. Kreek, D. V. Jordan, B. D. Milbrath, S. W. Padgett, C. J. Wharton, and N. G. Wimer, 2015, **OSIRIS—Gamma-ray spectroscopy software for on-site inspections under the Comprehensive Nuclear-Test-Ban Treaty**, *Nuclear Instruments & Methods in Physics Research*, *784*, *405–411*, doi:10.1016/j.nima.2014.10.066.

Cagniant, A., G. Le Petit, P. Gross, G. Douysset, H. Richard-Bressand, and J.-P. Fontaine, 2014, **Improvements of low-level radioxenon detection sensitivity by a state-of-the art coincidence setup**, *Applied Radiation and Isotopes*, *87*, *48-52*, doi:10.1016/j.apradiso.2013.11.078.

Campillo, M., 1987, **Lg wave propagation in a laterally varying crust and the distribution of the apparent quality factor in central France**, *Journal of Geophysical Research: Solid Earth*, *92*, *12604-12614*, doi:10.1029/JB092iB12p12604.

Capon, J., R. J. Greenfield, and R. J. Kolker, 1967, **Multidimensional maximum-likelihood processing of a large aperture seismic array**, *Proceedings of the IEEE*, *55*, *no. 2*, *192-211*, doi:10.1109/proc.1967.5439.

Carluccio R., A. Giuntini, V. Materni, S. Chiappini, C. Bignami, D. Caracciolo, A. Pignatelli, S. Stramondo, R. Console, and M. Chiappini, 2014, **A multidisciplinary study of the DPRK nuclear tests**, *Pure and Applied Geophysics*, *171*, *no. 3-5*, *341-359*, doi:10.1007/s00024-012-0628-8.

Carmichael, J. D., 2016, **A waveform detector that targets template-decorrelated signals and achieves its predicted performance: Part I: Demonstration with IMS data**, *Bulletin of the Seismological Society of America*, *106*, *no. 5*, *15 pp*, doi:10.1785/0120160047.

Carrigan, C. R., R.A. Heinle, G. B. Hudson, J. J. Nitao, and J. J. Zucca, 1996, **Trace gas emissions on geological faults as indicators of underground nuclear testing**, *Nature*, *382*, *528*, doi:10.1038/382528a0.

Carrigan, C. R., R. A. Heinle, G. M. Hudson, J. J. Nitao, and J. J. Zucca, 1997, **Barometric Gas Transport Along Faults and its Application to Nuclear Test-Ban Monitoring**, *Lawrence Livermore National Laboratory*, *UCRL-JC-127585*, *34 pp*, http://www.iaea.org/inis/collection/NCLCollectionStore/_Public/37/073/37073988.pdf.

Carrigan, C. R., Y. Sun, S. L. Hunter, D. G. Ruddle, J. L. Wagoner, K. B. L. Myers, D. F. Emer, S. L. Drellack, and V. D. Chipman, 2016, **Delayed signatures of underground nuclear explosions**, *Scientific Reports*, *6*, *no. 23032*, doi:10.1038/srep23032.

Casey, L. A., 2014, **Ground-based Nuclear Detonation Detection (GNDD) Technology Roadmap**, *National Nuclear Security Administration*, *DOE/NNSA/NA-22/GNDD-Roadmap-2014*, doi:10.2172/1130087.

Cauchy, A. L., 1828, **Exercices De Mathematiques**, *Kessinger Publishing, LLC*, *ISBN-13: 978-1168129918*, *160-187, and 328-355*, https://www.amazon.com/Exercices-Mathematiques-French-Augustin-Cauchy/dp/1168129915/ref=sr_1_2?s=books&ie=UTF8&qid=1470005452&sr=1-2&keywords=Cauchy.

Ceranna, L., A. Le Pichon, J. Vergoz and L. Evers, 2008, **Detection and localization capability of the European infrasound network**, *Journal of the Acoustical Society of America*, *123*, *3827*, doi:10.1121/1.2935598.

Chambers, D.J., K.D. Koper, K.L. Pankow, and M.K. McCarter,, 2015, **Detecting and characterizing coal mine related seismicity in the Western US using subspace methods**, *Geophysical Journal International*, *203*, *no. 2*, *1388-1399*, doi:10.1093/gji/ggv383.

Chang, S. J., S. van der Lee, M. P. Flanagan, H. Bedle, F. Marone, E. M. Matzel, M. E. Pasyanos, A. J. Rodgers, B. Romanowicz, and C. Schmid, 2010, **Joint inversion for three-dimensional S velocity mantle structure along the Tethyan margin**, *Journal of Geophysical Research: Solid Earth*, *115, no. B8*, doi:10.1029/2009JB007204.

Chapman, N. R., 1985, **Measurement of the waveform parameters of shallow explosive charges**, *Journal of the Acoustical Society of America*, *78*, *no. 2*, *672-681*, doi:10.1121/1.392436.

Chapman, N. R., 1988, **Source levels of shallow explosive charges**, *Journal of the Acoustical Society of America*, *84*, *no. 2*, *697-702*, doi:10.1121/1.396849.

Chen, P., L. Zhao, and T. H. Jordan, 2007a, **Full 3D tomography for crustal structure of the Los Angeles Region**, *Bulletin of the Seismological Society of America*, *97*, *no. 4*, *1094-1120*, doi:10.1785/0120060222.

Chen, P., T. H. Jordan, and L. Zhao, 2007b, **Full three-dimensional tomography: a comparison between the scattering-integral and adjoint-wavefield methods**, *Geophysical Journal International*, *170*, *175-181*, doi:10.1111/j.1365-246X.2007.03429.x.

Chiang, A., D. S. Dreger, S. R. Ford, W. R. Walter, 2014, **Source Characterization of Underground Explosions from Combined Regional Moment Tensor and First Motion Analysis**, *Bulletin of the Seismological Society of America*, *104*, *1587- 1600*, doi:10.1785/0120130228.

Chouet, B., K. Aki, and M. Tsujiura, 1978, **Regional variation of the scaling law of earthquake source spectra**, *Bulletin of the Seismological Society of America*, *68*, *no. 1*, *49-79*, http://www.bssaonline.org/content/68/1/49.

Chunchuzov, I. P. et al., 2011, **Infrasound scattering from atmosopheric anisotropic inhomogeneities**, *Izvestiya Atmospheric and Oceanic Physics*, *47*, *540*, doi:10.1134/S0001433811050045.

Clayton, R. W., T. Heaton, M. Chandy, A. Krause, M. Kohler, J. Bunn, R. Guy, M. Olson, M. Faulkner, M. Cheng, L. Strand, R. Chandy, D. Obenshain, A. Liue, and M. Aivazis, 2011, **Community Seismic Network**, *Annals of Geophysics*, *54*, *no. 6*, *738-747*, doi:10.4401/ag-5269.

Clayton, R. W., T. Heaton, M. Kohler, M. Chandy, R. Guy, and J. Bunn, 2015, **Community Seismic Network: A Dense Array to Sense Earthquake Strong Motion**, *Seismological Research Letters*, *86*, *no. 5*, *1354-1363*, doi:10.1785/0220150094.

Cochran, E., J. Lawrence, C. Christensen, and A. Chung, 2009, **A novel strong-motion seismic network for community participation in earthquake monitoring**, *IEEE Instrumentation & Measurement Magazine*, *12*, *no. 6*, *8-15*, doi:10.1109/MIM.2009.5338255.

Collins, M. D., 1993, **The adiabatic mode parabolic equation**, *Journal of the Acoustical Society of America*, *94*, *no. 4*, *2269-2278*, doi:10.1121/1.407498.

Collins, M. D., 1994, **Generalization of the split-step Padé solution**, *Journal of the Acoustical Society of America*, *96*, *382-385*, doi:10.1121/1.410488.

Collins, M. D., B. E. McDonald, K. D. Heaney, and W. A. Kuperman, 1995, **3-dimensional effects in global acoustics**, *Journal of the Acoustical Society of America*, *97*, *1567–1575*, doi:10.1121/1.413050.

Collins, M. D., and W. L. Siegmann, 2015, **Treatment of a sloping fluid- solid interface and sediment layering with the seismo-acoustic parabolic equation**, *Journal of the Acoustical Society of America*, *137*, *no. 1*, *492-497*, doi:10.1121/1.4904526.

Colosi, J. A., S. M. Flatte, and C. Bracher, 1994, **Internal-wave effects on 1000-km oceanic acoustic pulse propagation: Simulation and comparison with experiment**, *Journal of the Acoustical Society of America*, *96*, *no. 1*, *452-468*, doi:10.1121/1.411331.

Colosi, J. A., A. B. Baggeroer, T. G. Birdsall, C. Clark, B. D. Cornuelle, D. Costa, B. D. Dushaw, et al., 1999, **A review of recent results on ocean acoustic wave propagation in random media: basin scales**, *IEEE Journal of Oceanic Engineering*, *24*, *no. 2*, *138-155*, doi:10.1109/48.757267.

Colosi, J. A., 2016, **Sound Propagation through the Stochastic Ocean**, *Cambridge University Press*, *ISBN: 9781107072343*, *424 pp*.

Cooper, M. W., J. H. Ely, D. H. Haas, J. C. Hayes, J. I. McIntyre, L. S. Lidey, and B. T. Schrom, 2013, **Absolute efficiency calibration of a beta-gamma detector**, *IEEE Transactions on Nuclear Science*, *60, no. 2*, doi:10.1109/TNS.2013.2243165.

Covellone, B., B. Savage, and Y. Shen, 2015, **Seismic wave speed structure of the Ontong Java plateau**, *Earth and Planetary Science Letters*, *420*, *140-150*, doi:10.1016/j.epsl.2015.03.033.

CTBT, 1996, **Comprehensive Nuclear-Test-Ban Treaty**, *Comprehensive Nuclear-Test-Ban Treaty Organization*, https://www.ctbto.org/the-treaty/.

Curie, M., 1904, **Radium and Radioactivity**, *Century Magazine*, *461-466*, http://cwp.library.ucla.edu/articles/curie.htm.

Currie, L. A., 1968, **Limits for qualitative detection and quantitative determination.** *Application to radiochemistry, Analytical Chemistry, 40, no. 3, 586–593*, doi:10.1021/ac60259a007.

Curtis, A., H. Nicolson, D. Halliday, J. Trampert, and B. Baptie, 2009, **Virtual seismometers in the subsurface of the earth from seismic interferometry**, *Nature Geoscience*, *2*, *no. 10*, *700-704*, doi:10.1038/ngeo615.

D'Spain, G. L., L. P. Berger, W. A. Kuperman, J. L. Kuperman, and G. E. Baker, 2001, **Normal mode composition of earthquake T phases**, *Pure and Applied Geophysics*, *158*, *no. 3*, *475-512*, doi:10.1007/PL00001192.

Dahlen, F. A., S.-H. Hung, and G. Nolet, 2000, **Frechet kernels for finite-frequency traveltimes – I. Theory**, *Geophysical Journal International*, *141*, *157-174*, doi:10.1046/j.1365-246X.2000.00070.x.

Dahlman, O., and H. Israelson, 1977, **Monitoring Underground Nuclear Explosions**, *Elsevier*, *450 pp*, Electronic chapters available.

Day, S. M., N. Rimer, and J. T. Cherry, 1983, **Surface waves from underground explosions with spall: Analysis of elastic and nonlinear source models**, *Bulletin of the Seismological Society of America*, *73*, *no. 1*, *247-264*, http://www.bssaonline.org/content/73/1/247.

Day, S. M., J. T. Cherry, N. Rimer, and J. L. Stevens, 1987, **Nonlinear model of tectonic release from underground explosions**, *Bulletin of the Seismological Society of America*, *77*, *no. 3*, *996-1016*, http://www.bssaonline.org/content/77/3/996.

de Groot-Hedlin, C. D., and J. A. Orcutt, 1999, **Synthesis of earthquake-generated T-waves**, *Geophysical Research Letters*, *26*, *no. 9*, *1227–1230*, doi:10.1029/1999GL900205.

de Groot-Hedlin, C., and J. A. Orcutt, 2001, **Excitation of T-phases by seafloor scattering**, *Journal of the Acoustical Society of America*, *109*, *1944-1954*, doi:10.1121/1.1361057.

de Groot-Hedlin, C., D. K. Blackman, and C. S. Jenkins, 2009, **Effects of variability associated with the antarctic circumpolar current on sound propagation in the ocean**, *Geophysical Journal International*, *176*, *no. 2*, *478-490*, doi:10.1111/j.1365-246X.2008.04007.x.

de Groot-Hedlin, C., 2016, **Long-range propagation of nonlinear infrasound waves through an absorbing atmosphere**, *Journal of the Acoustical Society of America*, *139*, *no. 4*, *1565-1577*, doi:10.1121/1.4944759.

Del Grosso, V. A., 1974, **New equation for the speed of sound in natural waters (with comparisons to other equations)**, *Journal of the Acoustical Society of America*, *56*, *no. 4*, *1084-1091*, doi:10.1121/1.1903388.

Denny, M. D., and L. R. Johnson, 1991, **The explosion seismic source function: Models and scaling laws reviewed**, in *Explosion Source Phenomenology, American Geophysical Union, Geophysical Monograph 65*, *(eds S. R. Taylor, H. J. Patton and P. G. Richards)*, doi:10.1029/GM065p0001.

Denny, M.D., 1994, **Symposium on the Non-Proliferation Experiment: Results and Implications for Test Ban Treaties**, *Lawrence Livermore National Laboratory*, *CONF-9404100*, http://www.osti.gov/scitech/biblio/1095232.

Denny, M. D., and J. J. Zucca, 1994, **The Non-Proliferation Experiment**, *Department of Energy*, *Arms Control and Nonproliferation Technologies*, *DOE/AN/ACNT-94A*, *76*, doi:10.2172/10145196.

Dewey, J., and P. Byerly, 1969, **The early history of seismometry (to 1900)**, *Bulletin of the Seismological Society of America*, *59*, *no. 1*, *183-227*, http://bssa.geoscienceworld.org/content/59/1/183.

Di Luccio, F., and M. Pasyanos, 2007, **Crustal and upper-mantle structure in the Eastern Mediterranean from the analysis of surface wave dispersion curves**, *Geophysical Journal International*, *169*, *no. 3*, *1139-1152*, doi:10.1111/j.1365-246X.2007.03332.x.

Dodge, D. A. and W. R. Walter, 2015, **Initial global seismic cross-correlation results: Implications for empirical signal detectors**, *Bulletin of the Seismological Society of America*, *105*, *240-256*, doi:10.1785/0120140166.

Dodge, D. A., and D. B. Harris, 2016, **Large-scale test of dynamic correlation processors: Implications for correlation-based seismic pipelines**, *Bulletin of the Seismological Society of America*, *106*, *no. 2*, *435-452*, doi:10.1785/0120150254.

DOE, 1994, **Technology Options and Associated Measures for Monitoring a Comprehensive Test Ban**, *Department of Energy*, *Arms Control and Nonproliferation Technologies*, *DOE/AN/ANCT-94B*, doi:10.2172/10176867.

DOE National Nuclear Security Administration Nevada Field Office, 2015, **United States Nuclear Tests - July 1945 through September 1992**, *Department of Energy*, *DOE/NV--209-REV 16*, *186 pp*, https://www.nnss.gov/docs/docs_LibraryPublications/DOE_NV-209_Rev16.pdf.

Donn, W. L., and D. Rind, 1971, **Natural infrasound as an atmospheric probe**, *Geophysical Journal International*, *26*, *no. 1-4*, *111-133*, doi:10.1111/j.1365-246X.1971.tb03386.x.

Douglas, A., and P. D. Marshall, 1996, **Seismic source size and yield for nuclear explosions**, in *NATO Advanced Study Institutes Series*, *303*, *Monitoring a Comprehensive Test Ban Treaty, E.S. Husebye and A. M Dainty, eds.*, *309-353*, doi:10.1007/978-94-011-0419-7_19.

Douglas, A., 2002, **Seismometer arrays—Their use in earthquake and test ban seismology**, in *International Geophysics*, *81*, *no. A*, *International Handbook of Earthquake and Engineering Seismology*, *357–367*, doi:10.1016/S0074-6142(02)80226-1.

Douglas, A., 2013, **Forensic Seismology and Nuclear Test Bans**, *Cambridge University Press*, *Edition: 1st, ISBN: 9781107033948*, *555 pp*, http://www.cambridge.org/us/academic/subjects/earth-and-environmental-science/solid-earth-geophysics/forensic-seismology-and-nuclear-test-bans.

Douglas, D. A., 1987, **Blast Operational Overpressure Model (BOOM): An Airblast Prediction Method**, *Air Force Weapons Laboratory*, *Final Report AFWL-TR-85-150, 51 pp*, http://www.dtic.mil/docs/citations/ADA182025.

Dreger, D. S., and D. V. Helmberger, 1993, **Determination of source parameters at regional distances with single station or sparse network data**, *Journal of Geophysical Research: Solid Earth*, *98*, *no. B5*, *8107-8125*, doi:10.1029/93JB00023.

Dreger, D., and B. Woods, 2002, **Regional distance seismic moment tensors of nuclear explosions**, *Tectonophysics*, *356*, *no. 1-3*, *139-156*, doi:10.1016/S0040-1951(02)00381-5.

Drob, D. P., J. M. Picone, and M. Garcés, 2003, **Global morphology of infrasound propagation**, *Journal of Geophysical Research: Atmospheres*, *108*, *no. D21*, doi:10.1029/2002jd003307.

Drob, D. P., M. Garcés, M. Hedlin, and N. Brachet, 2010, **The temporal morphology of infrasound propagation**, *Pure and Applied Geophysics*, *167*, *437-453*, doi:10.1007/s00024-010-0080-6.

Dubasov, Y. V., Y. S. Popov, V. V. Prelovskii, A. Y. Donets, N. M. Kazarinov, V. V. Mishurinskii, V. Y. Popov, Y. M. Rykov, and N. V. Skirda, 2005, **The АРИКС-01 (ARIX-01) automatic facility for measuring concentrations of radioactive xenon isotopes in the atmosphere**, *Instruments and Experimental Techniques*, *48*, *no. 3*, *373-379*, doi:10.1007/s10786-005-0065-3.

Dumbgen, L., B. Igl and A. Munk, 2008, **P-values for classification**, *Electronic Journal of Statistics*, *2*, *468-493*, doi:10.1214/08-EJS245.

Dushaw, B. D., 2008, **Another look at the 1960 Perth to Bermuda long-range acoustic propagation experiment**, *Geophysical Research Letters*, *35*, *no. 8*, *L08601*, doi:10.1029/2008GL033415.

Dushaw, B. D., 2014, **Assessing the horizontal refraction of ocean acoustic tomography signals using high-resolution ocean state estimates**, *Journal of the Acoustical Society of America*, *136*, *122-129*, doi:10.1121/1.4881928.

Dushaw, B. D., and D. Menemenlis, 2014, **Antipodal acoustic thermometry: 1960, 2004**, *Deep Sea Research Part I: Oceanographic Research Papers*, *86*, *1-20*, doi:10.1016/j.dsr.2013.12.008.

Dziewonski, A., S. Bloch, and M. Landisman, 1969, **A technique for the analysis of transient seismic signals**, *Bulletin of the Seismological Society of America*, *59*, *no. 1*, *427-444*, http://www.bssaonline.org/content/59/1/427.short.

Dziewonski, A. M., B. H. Hager, and R. J. O'Connell, 1977, **Large-scale heterogeneities in the lower mantle**, *Journal of Geophysical Research: Solid Earth*, *82*, *no. 2*, *239-255*, doi:10.1029/JB082i002p00239.

Dziewonski, A. M., and D. L. Anderson, 1981, **Preliminary reference Earth model**, *Physics of the Earth and Planetary Interiors*, *25*, *no. 4*, *297-356*, doi:10.1016/0031-9201(81)90046-7.

Dziewonski, A. M., T.-A. Chou, and J. H. Woodhouse, 1981, **Determination of earthquake source parameters from waveform data for studies of global and regional seismicity**, *Journal of Geophysical Research: Solid Earth*, *86*, *no. B4*, *2825-2852*, doi:10.1029/JB086iB04p02825.

Dziewonski, A. M., 1984, **Mapping the lower mantle: Determination of lateral heterogeneity in P velocity up to degree and order 6**, *Journal of Geophysical Research*, *89*, *no. B7*, *5929–5952*, doi:10.1029/JB089iB07p05929.

Ekström, G., M. Nettles, and A. M. Dziewonski, 2012, **The global CMT project 2004-2010: Centroid-moment tensors for 13,017 earthquakes**, *Physics of the Earth and Planetary Interiors*, *200-201*, *1-9*, doi:10.1016/j.pepi.2012.04.002.

Elvers, E., 1974, **Seismic event identification by negative evidence**, *Bulletin of the Seismological Society of America*, *64*, *no. 6*, *1671-1683*, http://bssa.geoscienceworld.org/content/64/6/1671.

Embleton, T. F. W., 1996, **Tutorial on sound propagation outdoors**, *Journal of the Acoustical Society of America*, *100*, *31-48*, doi:10.1121/1.415879.

Eslinger, P. W., S. R. Biegalski, T. W. Bowyer, M. W. Cooper, D. A. Haas, J. C. Hayes, I. Hoffman, E. Korpach, J. Yi, H. S. Miley, J. P. Rishel, K. Ungar, B. White, and V. T. Woods, 2014, **Source term estimation of radioxenon released from Fukushima Dai-ichi nuclear reactors using measured air concentrations and atmospheric transport modeling**, *Journal of Environmental Radioactivity*, *127*, *127-132*, doi:10.1016/j.jenvrad.2013.10.013.

Eslinger, P. W., and B. T. Schrom, 2016, **Multi-detection events, probability density functions, and reduced location area**, *Journal of Radioanalytical and Nuclear Chemistry*, *307*, *no. 3*, *1599-1605*, doi:10.1007/s10967-015-4339-3.

Evernden, J.F., 1967, **Magnitude determination at regional and near-regional distances in the United States**, *Bulletin of the Seismological Society of America*, *57*, *no. 4*, *591-639*.

Evernden, J. F., 1969, **Identification of earthquakes and explosions by use of teleseismic data**, *Journal of Geophysical Research: Solid Earth*, *74*, *no. 15*, *3828-3856*, doi:10.1029/JB074i015p03828.

Evernden, J. F., 1976, **Study of seismological evasion Part II. Evaluation of evasion possibilities using normal microseismic noise**, *Bulletin of the Seismological Society of America*, *66*, *no. 1*, *281-324*.

Evernden, J.F., 1976, **Study of seismological evasion Part I. General discussion of various evasion schemes**, *Bulletin of the Seismological Society of America*, *66*, *no. 1*, *245-280*.

Farrell, T., 1997, **Users guide for the hydroacoustic coverage assessment model (HydroCAM)**, *Lawrence Livermore National Laboratory*, *BBN Technical Memorandum W1309, UCRL-CR-130729*, *163 pp*, doi:10.2172/325370.

Fee, D., R. Waxler, J. Assink, Y. Gitterman, J. Given, J. Coyne, P. Mialle, M. Garces, D. Drob, D. Kleinart, R. Hofstetter, and P. Grenard, 2013, **Overview of the 2009 and 2011 Sayarim Infrasound Calibration Experiments**, *Journal of Geophysical Research: Atmospheres*, *118*, *6122-6143*, doi:10.1002/jgrd.50398.

Fermi, E., 1946, **The Development of the First Chain Reaction Pile**, *Proceedings of the American Philosophical Society*, *90*, *no. 1*, *20-24*, http://www.jstor.org/stable/3301034.

Fichtner, A., B. L. N. Kennett, H. Igel, and H-P Bunge, 2009, **Full seismic waveform tomography for upper-mantle structure in the Australasian region using adjoint methods**, *Geophysical Journal International*, *179*, *1703-1725*, doi:10.1111/j.1365-246X.2009.04368.x.

Fichtner, A., and J. Trampert, 2011, **Resolution analysis in full waveform inversion**, *Geophysical Journal International*, *187*, *1604-1624*, doi:10.1111/j.1365-246X.2011.05218.x.

Finazzi, F., 2016, **The earthquake network project: Toward a crowdsourced smartphone-based earthquake early warning system**, *Bulletin of the Seismological Society of America*, *106*, *no. 3*, *1088-1099*, doi:10.1785/0120150354.

Fisk, M. D., 2006, **Source spectral modeling of regional P/S discriminants at nuclear test sites in China and the Former Soviet Union**, *Bulletin of the Seismological Society of America*, *96*, *no. 6*, *2348-2367*, doi:10.1785/0120060023.

Fisk, M. D, 2007, **Corner frequency scaling of regional seismic phases for underground nuclear explosions at the Nevada Test Site**, *Bulletin of the Seismological Society of America*, *97*, *no. 3*, *977-988*, doi:10.1785/0120060186.

Fisk, M. D, and W. S. Phillips, 2013a, **Constraining regional phase amplitude models for Eurasia, Part 1: Accurate source parameters and geometric spreading**, *Bulletin of the Seismological Society of America*, *103*, *no. 6*, *3248-3264*, doi:10.1785/0120130018.

Fisk, M. D, and W. S. Phillips, 2013b, **Constraining regional phase amplitude models for Eurasia, Part 2: Frequency-dependent attenuation and site results**, *Bulletin of the Seismological Society of America*, *103*, *no. 6*, *3265-3288*, doi:10.1785/0120130022.

Flatté, S. M., 1981, **Sound transmission as a probe of ocean internal waves and microstructure**, *Journal of the Acoustical Society of America*, *70*, *S37*, doi:10.1121/1.2018846.

Fontaine, J.-P., F. Pointurier, X. Blanchard, and T. Taffary, 2004, **Atmospheric xenon radioactive isotope monitoring**, *Journal of Environmental Radioactivity*, *72*, *no. 1-2*, *129-135*, doi:10.1016/S0265-931X(03)00194-2.

Forbes, A., and W. Munk, 1994, **Doppler-inferred launch angles of global acoustic ray paths**, *Journal of the Acoustical Society of America*, *96*, *2425-2427*, doi:10.1121/1.410114.

Ford, S., and W. R. Walter, 2013, **An explosion model comparison with insights from the source physics experiments**, *Bulletin of the Seismological Society of America*, *103, no. 5*, doi:10.1785/0120130035.

Ford, S. R., D. S. Dreger, K. Mayeda, W. R. Walter, L. Malagnini, and W. S. Phillips, 2008, **Regional attenuation in northern California: A comparison of five 1-D Q methods**, *Bulletin of the Seismological Society of America*, *98*, *no. 4*, *2033-2046*, doi:10.1785/0120070218e.

Ford, S. R., D. S. Dreger, and W. R. Walter, 2009, **Identifying isotropic events using a regional moment tensor inversion**, *Journal of Geophysical Research: Solid Earth*, *114*, *no. B1*, doi:10.1029/2008JB005743.

Ford, S. R., D. S. Dreger, and W. R. Walter, 2010, **Network sensitivity solutions for regional moment-tensor inversions**, *Bulletin of the Seismological Society of America*, *100*, *no. 5A*, *1962-1970*, doi:10.1785/0120090140.

Ford, S. R., W. S. Phillips, W. R. Walter, M. E. Pasyanos, K. Mayeda, and D. S. Dreger, 2010, **Attenuation tomography of the Yellow Sea / Korean Peninsula from coda-source normalized and direct Lg amplitudes**, *Pure and Applied Geophysics*, *167, no. 10, 1163-1170*, doi:10.1007/s00024-009-0023-2.

Ford, S. R., A. J. Rodgers, H. Xu, D. C. Templeton, P. Harben, W. Foxall, and R. E. Reinke, 2014, **Partitioning of seismo-acoustic energy and estimation of yield and height-of-burst/depth-of-burial for near-surface explosions**, *Bulletin of the Seismological Society of America*, *104*, *no. 2*, *608-623*, doi:10.1785/0120130130.

Forrester, J. B., F. F. Carty, L. Comes, J. C. Hayes, H. S. Miley, S. J. Morris, M. Ripplinger, R. W. Slaugh, and P. VanDevelaar, 2013, **Engineering upgrades to the radionuclide aerosol sampler/analyzer for the CTBT international monitoring system**, *Journal of Radioanalytical and Nuclear Chemistry*, *296, 1055-1060*, doi:10.1007/s10967-012-2199-7.

Foxe, M. P., and J. I. McIntyre, 2015, **Testing of the KRI-developed Silicon PIN Radioxenon Detector**, *Pacific Northwest National Laboratory*, *PNNL-23995*, doi:10.2172/1258733.

Foxe, M. P., B. W. Miller, R. Suarez, and J. C. Hayes, 2015a, **A Figure-of-Merit for Beta Cell Detector Characterization**, *Pacific Northwest National Laboratory*, *PNNL-24760*, doi:10.2172/1258732.

Foxe, M. P., I. M. Cameron, M. W. Cooper, D. A. Haas, J. C. Hayes, A. A. Kriss, L. S. Lidey, J. M. Mendez, A. M. Prinke, and R. A. Riedmann, 2015b, **Radioxenon detector calibration spike production and delivery systems**, *Journal of Radioanalytical and Nuclear Chemistry*, *307*, *no. 3*, *2021-2027*, doi:10.1007/s10967-015-4668-2.

Foxe, M. P., J. C. Hayes, M. F. Mayer, J. I. McIntyre, C. B. Sivels, and R. Suarez, 2016, **Characterization of a Commercial Silicon Beta Cell**, *Pacific Northwest National Laboratory*, *PNNL-25297*, doi:10.2172/1258729.

Freeden, W., and V. Michel, 1999, **Constructive approximation and numerical methods in geodetic research today – an attempt at a categorization based on an uncertainty principle**, *Journal of Geodesy*, *73*, *no. 9*, *452-465*, doi:10.1007/PL00004001.

Gabrielson, T. B., 2011, **In-situ calibration of infrasound array elements**, *Journal of the Acoustical Society of America*, *129*, *2443*, doi:10.1121/1.3588002.

Gao, H., and Y. Shen, 2014a, **Upper mantle structure of the Cascades from full-wave ambient noise tomography: Evidence for 3D mantle upwelling in the back-arc**, *Earth and Planetary Science Letters*, *390*, *222-233*, doi:10.1016/j.epsl.2014.01.012.

Gao, H., and Y. Shen, 2014b, **Validation of recent shear-wave velocity models in the United States with full-wave simulation**, *Journal of Geophysical Research: Solid Earth*, *120*, doi:10.1002/2014JB011369.

Garcés, M. A., R. A. Hansen, and K. G. Lindquist, 1998, **Traveltimes fro infrasonic waves propagating in a stratified atmosphere**, *Geophysical Journal International*, *135 (1), 255-263*, doi:10.1046/j.1365-246X.1998.00618.x.

Garnero, E. J., 2000, **Heterogeneity of the lowermost mantle**, *Annual Review of Earth and Planetary Sciences*, *28*, *509-537*, doi:10.1146/annurev.earth.28.1.509.

Geers, T. L., and K. S. Hunter, 2002, **An integrated wave-effects model for an underwater explosion bubble**, *Journal of the Acoustical Society of America*, *111*, *no. 4*, *1584-1601*, doi:10.1121/1.1458590.

Gerdes, F., and S. Finette, 2012, **A stochastic response surface formulation for the description of acoustic propagation through an uncertain internal wave field**, *Journal of the Acoustical Society of America*, *132*, *no. 4*, *2251-2264*, doi:10.1121/1.4746032.

Gibbons, S. J., and F. Ringdal, 2006, **The detection of low magnitude seismic events using array-based waveform correlation**, *Geophysical Journal International*, *165*, *no. 1*, *149-166*, doi:10.1111/j.1365-246X.2006.02865.x.

Gibbons, S. J., and F. Ringdal, 2012, **Seismic monitoring of the North Korea nuclear test site using a multichannel correlation detector**, *IEEE Transactions on Geoscience and Remote Sensing*, *50*, *no. 5*, doi:10.1109/TGRS.2011.2170429.

Gibbons, S. J., T. Kværna, D. B. Harris, and D. A. Dodge, 2016, **Iterative Strategies for Aftershock Classification in Automatic Seismic Processing Pipelines**, *Seismological Research Letters*, doi:10.1785/0220160047.

Gilbert, F., 1971, **Excitation of the normal modes of the earth by earthquake sources**, *Geophysical Journal of the Royal Astronomical Society*, *22*, *no. 2*, *223-226*, doi:10.1111/j.1365-246X.1971.tb03593.x.

Gitterman, Y., and R. Hofstetter, 2014, **GT0 Explosion Sources for IMS Infrasound Calibration: Charge Design and Yield Estimation from Near-source Observations**, *Pure and Applied Geophysics*, *171*, *no. 3-5*, *599-619*, doi:10.1007/s00024-012-0575-4.

Gok, R., M. E. Pasyanos, and E. Zor, 2007, **Lithospheric structure of the continent-continent collision zone: Eastern Turkey**, *Geophysical Journal International*, *169*, *no. 3*, *1079-1088*, doi:10.1111/j.1365-246X.2006.03288.x.

Gok, R., R. J. Mellors, E. Sandvol, M. Pasyanos, T. Hauk, R. Takedatsu, G. Yetirmishli, U. Teoman, N. Turkelli, T. Godoladze, and Z. Javakishvirli, 2011, **Lithospheric velocity structure of the Anatolian plateau-Caucasus-Caspian Region**, *Journal of Geophysical Research: Solid Earth*, *116, no. B5*, doi:10.1029/2009JB000837.

Goldstein, P., 1995, **Slopes of P- to S-wave spectral ratios-A broadband regional seismic discriminant and a physical model**, *Geophysical Research Letters*, *22*, *no. 23*, *3147–3150*, doi:10.1029/95GL03315.

Green, D. N., and D. Bowers, 2010, **Estimating the detection capability of the International Monitoring System infrasound network**, *Journal of Geophysical Research: Atmospheres*, *115*, *D18116*, doi:10.1029/2010JD014017.

Gutenberg, B., 1945, **Magnitude determination for deep focus earthquakes**, *Bulletin of the Seismological Society of America*, *35*, *no. 3*, *117-130,* http://www.bssaonline.org/content/35/3/117.

Gutenberg, B., 1946, **Interpretation of records obtained from the New Mexico atomic bomb test**, *Bulletin of the Seismological Society of America*, *36*, *327-330*.

Gutenberg, B., 1951, **PKKP, P'P', and the Earth's core**, *Eos, Transactions of the American Geophysical Union*, *32*, *no. 3*, *373-390*, doi:10.1029/TR032i003p00373.

Gutenberg, B., and C. F. Richter, 1956, **Magnitude and energy of earthquakes**, *Annals of Geophysics*, *9*, *no. 1*, *1-15*, doi:10.4401/ag-5590.

Gutenberg, B., 1959, **Physics of the Earth's Interior (Vol. 1)**, *Academic Press - An Imprint of Elsevier*, *ISBN 9781483282121*, http://store.elsevier.com/product.jsp?isbn=9781483282121&pagename=search.

Haas, D. A., S. R. Biegalski, and K. M. F. Biegalski, 2008, **Modeling ß-γ coincidence spectra of 131mXe, 133Xe, 133mXe, and 135Xe**, *Journal of Radioanalytical and Nuclear Chemistry*, *277, no. 3, 561-565*, doi:10.1007/s10967-007-7178-z.

Haas, D. A., S. R. Biegalski, and K. M. F. Biegalski, 2009, **Radioxenon production through neutron irradiation of stable xenon gas**, *Journal of Radioanalytical and Nuclear Chemistry*, *282, no. 3, 677-680*, doi:10.1007/s10967-009-0291-4.

Haas, D.A., J.L. Orrell, T.W. Bowyer, J.I. McIntyre, H.S. Miley, C.E. Aalseth, and J.C. Hayes, 2010, **The Science Case for 37Ar as a Monitor for Underground Nuclear Explosions**, *Pacific Northwest National Laboratory*, *PNNL-19458*, doi:10.2172/992009.

Hahn, O., and F. Strassmann, 1939, **Über den Nachweis und das Verhalten der bei der Bestrahlung des Urans mittels Neutronen entstehenden Erdalkalimetalle**, *Die Naturwissenschaften*, *27*, *no. 11*, doi:10.1007/BF01488241.

Hand, D. J., 2006, **Classifier technology and the illusion of progress**, *Statistical Science*, *21*, *no. 1*, *1-14*, doi:10.1214/088342306000000060.

Hanks, T. C., and H. Kanamori, 1979, **A moment magnitude scale**, *Journal of Geophysical Research: Solid Earth*, *84*, *no. B5*, *2348-2350*, doi:10.1029/JB084iB05p02348.

Hansen, S. M., and B. Schmandt, 2015, **Automated detection and location of microseismicity at Mount St. Helens with a large-N geophone array**, *Geophysical Research Letters*, *42*, *no. 18*, *7390-7397*, doi:10.1002/2015GL064848.

Hanson, J. A., and J. R. Bowman, 2006, **Methods for monitoring hydroacoustic events using direct and reflected T waves in the Indian Ocean**, *Journal of Geophysical Research: Solid Earth*, *Vol. 111*, *no. B2*, doi:10.1029/2004JB003609.

Harkrider, D. G., 1964, **Surface waves in multilayered elastic material 1. Rayleigh and Love waves from buried sources in a multilayered elastic half-space**, *Bulletin of the Seismological Society of America*, *54*, *no. 2*, *627-679*.

Harkrider, D. G., 1970, **Surface waves in multilayered elastic material. Part II. Higher mode spectra and spectral ratios from point sources in plane layered Earth models**, *Bulletin of the Seismological Society of America*, *60*, *no. 6*, *1937-1987*.

Harris, D. B., 2006, **Subspace Detectors: Theory**, *Lawrence Livermore National Laboratory*, *UCRL-TR-222758*, *46*, doi:10.2172/900081.

Harris, D. B., and T. Paik, 2006, **Subspace Detectors: Efficient Implementation**, *Lawrence Livermore National Laboratory*, *UCRL-TR-223177*, *36*, doi:10.2172/898451.

Harris, D. B., and T. Kvaerna, 2010, **Superresolution with seismic arrays using empirical matched field processing**, *Geophysical Journal International*, *182*, *no. 3*, *1455-1477*, doi:10.1111/j.1365-246X.2010.04684.x.

Harris, D. B., and D. A. Dodge, 2011, **An autonomous system for grouping events in a developing aftershock sequence**, *Bulletin of the Seismological Society of America*, *101*, *no. 2*, *763-774*, doi:10.1785/0120100103.

Harris, D. B., S. J. Gibbons, A. J. Rodgers, and M. E. Pasyanos, 2012, **Nuclear test ban treaty verification**, *IEEE Signal Processing Magazine*, *29, no. 3*, doi:10.1109/MSP.2012.2184869.

Harrison, C. H., 1977, **Three-dimensional ray paths in basins, troughs, and near seamounts by use of ray invariants**, *Journal of the Acoustical Society of America*, *62*, *no. 6*, *1382-1388*, doi:10.1121/1.381670.

Hartmann, G., N. Gestermann, and L. Cerrana, 2016, **Seismological analysis of the fourth North Korean nuclear test**, *European Geophysics Union*, *18*, *EGU2016-15713*, EGU site.

Hartse, H. E., W. S. Phillips, M. C. Fehler, and L. S. House, 1995, **Single-station spectral discrimination using coda waves**, *Bulletin of the Seismological Society of America*, *85*, *no. 5*, *1464-1474*, http://www.bssaonline.org/content/85/5/1464.

Hartse, H. E., S. R. Taylor, W. S. Phillips, and G. E. Randall, 1997, **A preliminary study of regional seismic discrimination in central Asia with emphasis on western China**, *Bulletin of the Seismological Society of America*, *87*, *no. 3*, *551-568*, http://www.bssaonline.org/content/87/3/551.

Hartse, H. E., G. E. Randall, D. N. Anderson, W. S. Phillips, and S. J. Arrowsmith, 2012, **Regional event identification research in central Asia**, *Department of Energy*, *Proceedings of the 2012 Monitoring Research Review: Ground-based Nuclear Explosion Monitoring Technologies*, *397-406*, http://www.osti.gov/scitech/biblio/1050499.

Haskell, N. A., 1967, **Analytic approximation for the elastic radiation from a contained underground explosion**, *JGR: Solid Earth, 72, no. 10, 2583-2587*, doi:10.1029/JZ072i010p02583.

Hauser, J., K. M. Dyer, M. E. Pasyanos, H. Bungum, J. I. Faleide, S. A. Clark, and J. Schweitzer, 2011, **A probabilistic seismic model for the European Arctic**, *Journal of Geophysical Research: Solid Earth*, *116, no. B01303*, doi:10.1029/2010JB007889.

Hayes, J. C., M.W. Cooper, M.A. Covert, J.H. Ely, M.P. Foxe, D.A. Haas, W.W. Harper, T.R. Heimbigner, C. W. Hubbard, D.T. Keller, P.H. Humble, J.C. Madison, S.J. Morris, M. E. Panisko, A.M. Prinke, M.D. Ripplinger, and T.L. Stewart, 2015, **Requirements for Xenon International: Revision 1**, *Pacific Northwest National Laboratory*, *PNNL-22227 (Rev 1)*, doi:10.2172/1122330.

Heaney, K. D., W. A. Kuperman, and B. E. McDonald, 1991, **Perth-Bermuda sound propagation (1960): Adiabatic mode interpretation**, *Journal of the Acoustical Society of America, 90, 2586*, doi:10.1121/1.402062.

Helmberger, D. V., and D. G. Harkrider , 1972, **Seismic source descriptions of underground explosions and a depth discriminate**, *Geophys. J. Int., 31, no. 1-3, 45-66*, doi:10.1111/j.1365-246X.1972.tb02358.x.

Heimbigner, T.R., T.W. Bowyer, J.I. McIntyre, K.H. Abel, J.C. Hayes, M.E. Panisko, and W.K. Pitts, 2000, **The DOE Automated Radioxenon Sampler-Analyzer (ARSA) Beta-Gamma Coincidence Spectrometer Data Analyzer**, *Pacific Northwest National Laboratory*, *PNNL-33456*.

Herrmann, R. B., 1973, **Some aspects of band-pass filtering of surface waves**, *Bulletin of the Seismological Society of America*, *63*, *no. 2*, *663-671*, http://www.bssaonline.org/content/63/2/663.short.

Hong, T. K., and W. Menke, 2006, **Tomographic investigation of the wear along the San Jacinto fault, southern California**, *Physics of the Earth and Planetary Interiors*, *155*, *no. 3*, *236-248*, doi:10.1016/j.pepi.2005.12.005.

Hong, T.-K., 2013, **Seismic discrimination of the 2009 North Korean nuclear explosion based on regional source spectra**, *Journal of Seismology*, *17*, *753-769*, doi:10.1007/s10950-012-9352-1.

Hooper, H., J. Bonner, and M. Leidig, 2006, **Effects of confinement on short-period surface waves: observations from a new dataset**, *Bulletin of the Seismological Society of America*, *96*, *no. 2*, *697-712*, doi:10.1785/0120050075.

Hudson, J. A., R. G. Pearce, and R. M. Rogers, 1989, **Source type plot for inversion of the moment tensor**, *Journal of Geophysical Research: Solid Earth*, *94*, *no. B1*, *765-774*, doi:10.1029/JB094iB01p00765.

Humble, P. H., R. M. Williams, and J. C. Hayes, 2009, **Finite Element Modeling of Adsorption Processes for Gas Separation and Purification**, *Los Alamos National Laboratory*, *Vol. II*, *LA-UR-09-05276*, *659-666*, http://www.osti.gov/scitech/biblio/992203.

Hung, S.-H., F. A. Dahlen, and G. Nolet, 2000, **Frechet kernels for finite-frequency traveltimes – II. Examples**, *Geophysical Journal International*, *141*, *175-203*, doi:10.1046/j.1365-246X.2000.00072.x.

Hung, S.-H., F. A. Dahlen, and G. Nolet, 2001, **Wavefront healing: a banana-doughnut perspective**, *Geophysical Journal International*, *146*, *289-312*.

Hursky, P., M. B. Porter, B. D. Cornuelle, W. S. Hodgkiss, and W. A. Kuperman, 2004, **Adjoint modeling for acoustic inversion**, *Journal of the Acoustical Society of America*, *115*, *no. 2*, *607-619*, doi:10.1121/1.1636760.

Husebye, E. S., and B. O. Ruud, 1989, **Array Seismology - Past, Present and Future Developments**, in *University of California Press*, *Observational Seismology, Litehiser (ed.)*, *123-153*, http://ark.cdlib.org/ark:/13030/ft7m3nb4pj/.

Hutt, C. R., J. Peterson, L. Gee, J. Derr, A. Ringler, and D. Wilson, 2011, **Albuquerque Seismological Laboratory – 50 years of global seismology**, *United States Geological Survey*, *U.S. Geological Survey Fact Sheet, FS 2011-3065*, http://pubs.usgs.gov/fs/2011/3065/.

Ingate, S. F., E. S. Husebye, and A. Christoffersson, 1985, **Regional Arrays and Optimum Data-Processing Schemes**, *Bulletin of the Seismological Society of America*, *75*, *no. 4*, *1155-1177*, http://www.bssaonline.org/content/75/4/1155.short.

Jeffreys, H., and K. E. Bullen, 1940, **Seismological Tables**, *British Association for the Advancement of Science*.

Jensen, F. B., W. A. Kuperman, M. B. Porter, and H. Schmidt, 2011, **Computational Ocean Acoustics**, *Springer*, *ISBN 978-1-4419-8677-1*, *794 pp*, doi:10.1007/978-1-4419-8678-8.

Jones, K.R., R.W. Whitaker, and S. J. Arrowsmith, 2015, **Modeling infrasound signal generation from two underground explosions at the Source Physics Experiment using the Rayleigh integral**, *Geophysical Journal International*, *200*, *no. 2*, *777-788*, http://gji.oxfordjournals.org/content/200/2/777.abstract.

Julià, J., C. J. Ammon, R. B. Herrmann, and A. M. Correig, 2000, **Joint inversion of receiver function and surface wave dispersion observations**, *Geophysical Journal International*, *143*, *99-112*, doi:10.1046/j.1365-246x.2000.00217.x.

Junek, W. N., T. Kværna, M. Pirli, J. Schweitzer, D. B. Harris, D. A. Dodge, and M. T. Woods, 2015, **Inferring aftershock sequence properties and tectonic structure using empirical signal detectors**, *Pure and Applied Geophysics*, *172*, *no. 2*, *359-373*, doi:10.1007/s00024-014-0938-0.

Kalinowski, M. B., and C. Pistner, 2006, **Isotopic signature of atmospheric xenon released from light water reactors**, *Journal of Environmental Radioactivity*, *88*, *no. 3*, *215-235*, doi:10.1016/j.jenvrad.2006.02.003.

Kalinowski, M. B., 2011, **Characterisation of prompt and delayed atmospheric radioactivity releases from underground nuclear tests at Nevada as a function of release time**, *Journal of Environmental Radioactivity*, *102*, *no. 9*, *824–836*, doi:10.1016/j.jenvrad.2011.05.006.

Kalinowski, M. B., and A. Becker, eds., 2014, **Recent Advances in Nuclear Explosion Monitoring, Volume II**, *Pure and Applied Geophysics Topical Volumes*, *171*, *no. 3-5*, *442 pp.*, http://www.springer.com/birkhauser/geo+science/book/978-3-0348-0818-7.

Kanamori, H., 1977, **The energy release in great earthquakes**, *Journal of Geophysical Research: Solid Earth*, *82*, *2981–2987*, doi:10.1029/JB082i020p02981.

Kawasumi, H., and R. Yosiyama, 1935, **On an elastic wave animated by the potential energy of initial strain**, *Bulletin of the Earthquake Research Insitute*, *13*, *496-503*.

Keillor, M. E., C. E. Aalseth, A. R. Day, L. E. Erikson, J. E. Fast, B. D. Glasgow, E. W. Hoppe, T. W. Hossbach, B. J. Hyronimus, H. S. Miley, A. W. Myers, A. Seifert, and T. J. Stavenger, 2011, **CASCADES: An ultra-low-background germanium crystal array at Pacific Northwest National Laboratory**, *AIP Conference Proceedings*, *1412*, *208-215*, doi:10.1063/1.3665316.

Kennett, B. L. N., and E. R. Engdahl, 1991, **Traveltimes for global earthquake location and phase identification**, *Geophysical Journal International*, *105*, *429-465*, doi:10.1111/j.1365-246X.1991.tb06724.x.

Kennett, B. L. N., E. R. Engdahl, and R. Buland, 1995, **Constraints on seismic velocities in the Earth from traveltimes**, *Geophysical Journal International*, *122*, *no. 1*, *108-124*, doi:10.1111/j.1365-246X.1995.tb03540.x.

Kgaswane, E. M., A. A. Nyblade, J. Julia, P. H. Dirks, R. J. Durrheim, and M. E. Pasyanos, 2009, **Shear wave velocity structure of southern African crust: Evidence for compositional heterogeneity within Archaean and Proterozoic terrains**, *Journal of Geophysical Research: Solid Earth*, *114*, *no. B12*, *B12304*, doi:10.1029/2008JB006217.

Kim, K., D. Fee, J. M. Lees, A. Yokoo, and M.C. Ruiz, 2015, **Acoustic multipole source inversions of volcano infrasound**, *Acoustical Society of America*, *137*, *no. 2371*, doi:10.1121/1.4920615.

Kim, W. Y., D. W. Simpson, and P. G. Richards, 1993, **Discrimination of earthquakes and explosions in the eastern United States using regional high-frequency data**, *Geophysical Research Letters*, *20*, *no. 14*, *1507-1510*, doi:10.1029/93GL01267.

Kim, W. Y., and P. G. Richards, 2007, **North Korean nuclear test: seismic discrimination at low yield**, *Eos, Transactions of the American Geophysical Union*, *88*, *no. 14*, *158-161*, doi:10.1029/2007EO140002.

Kinney, G., and K. Graham, 1985, **Explosive Shocks in Air**, *Springer*, *2nd ed., ISBN 3642866840*, *269 pp*, http://www.alibris.com/Explosive-shocks-in-air-Gilbert-Ford-Kinney/book/2210672.

Klingberg, F. J., S. R. Biegalski, D.A. Haas, and A. Prinke, 2015, **^{127}Xe coincidence decay analysis in support of CTBT verification**, *Journal of Radioanalytical and Nuclear Chemistry*, *305*, *no. 1*, *225-232*, doi:10.1007/s10967-014-3871-x.

Komatitsch, D., and J-P. Vilotte, 1998, **The spectral element method: an effective tool to simulate the seismic response of 2D and 3D geological structures**, *Bulletin of the Seismological Society of America*, *88*, *no. 2*, *368-392*, http://bssa.geoscienceworld.org/content/88/2/368.

Komatitsch, D., and J. Tromp, 1999, **Introduction to the spectral element method for three-dimensional seismic wave propagation**, *Geophysical Journal International*, *139*, *806-822*, doi:10.1046/j.1365-246x.1999.00967.x.

Komatitsch, D., J. Ritsema, and J. Tromp, 2002, **The spectral-element method, beowulf computing, and global seismology**, *Science*, *298*, *1737-1742*, doi:10.1126/science.1076024.

Kong, Q., R. M. Allen, and L. Schreier, 2016, **MyShake: Initial observations from a global smartphone seismic network**, *Geophysical Research Letters*, *43*, *no. 18*, *9588-9594*, doi:10.1002/2016GL070955.

Koper, K. D., T. C. Wallace, R. E. Reinke, and J. A. Leverette, 2002, **Empirical scaling laws for truck bomb explosions based on seismic and acoustic data**, *Bulletin of the Seismological Society of America*, *92*, *no. 2*, *527 – 542*, doi:10.1785/0120000242.

Koper, K. D., R.B. Herrmann, and H.M. Benz, 2008, **Overview of Open Seismic Data from the North Korean Event of 9 October 2006**, *Seismological Research Letters*, *79*, *no. 2*, *178-185*, doi:10.1785/gssrl.79.2.178.

Koper, K. D., and C. J. Ammon, 2013, **Planning a global array of bradband seismic arrays**, *Eos, Transactions of the American Geophysical Union*, *94*, *no. 34*, *300*, doi:10.1002/2013EO34.

Korobeinikov, V. P., 1971, **Gas dynamics of explosions**, *Annual Review of Fluid Mechanics*, *3*, *317-346*, doi:10.1146/annurev.fl.03.010171.001533.

Kuperman, W. A., M. B. Porter, J. S. Perkins and R. B. Evans, 1991, **Rapid computation of acoustic fields in three-dimensional ocean environments**, *Journal of the Acoustical Society of America*, *89*, *no. 1*, *125-133*, doi:10.1121/1.400518.

Kuroda, P.K., 1956, **On the nuclear physical stability of the uranium minerals**, *Journal of Chemical Physics*, *25*, *781-782*, doi:10.1063/1.1743058.

Larsonnier, F., G. Nief, P. Dupon, and P. Millier, 2014a, **Seismometers calibration: comparison between a relative electrical method and a vibration exciter based absolute method**, *International Measurement Confederation*, *TC22 Conference 2014, Cape Town, SOUTH AFRICA, 2014*, https://www.imeko.org/publications/tc22-2014/IMEKO-TC22-2014-013.pdf.

Larsonnier, F., H. Uszakiewicz, and M. Mende, 2014b, **Infrasound sensors and their calibration at low frequency**, *Institute of Noise Control Engineering - InterNoise Conference Proceedings*, *43rd International Congress on Noise Control Engineering November 16-19, 2014*, *153-162*, https://www.acoustics.asn.au/conference_proceedings/INTERNOISE2014/papers/p153.pdf.

Laske., G., and G. Masters, 1997, **A global digital map of sediment thickness**, *Eos, Transactions of the American Geophysical Union*, *78*, *F483*, http://igppweb.ucsd.edu/~gabi/sediment.html.

Laske, G., G. Masters, Z. Ma, and M. Pasyanos, 2013, **Update on CRUST1.0 - A 1-degree global model of Earth's crust**, *Geophysical Research Abstracts*, *15*, *Abstract EGU2013-2658*, http://igppweb.ucsd.edu/~gabi/crust1.html.

Lay, T., ed., 2009, **Seismological grand challenges in understanding Earth's dynamic systems**, *IRIS Consortium*, *Report to the National Science Foundation*, http://www.iris.edu/hq/lrsps/.

Le Petit, G., A. Cagniant, M. Morelle, P. Gross, P. Achim, G. Douysset, T. Taffary, and C. Moulin, 2013, **Innovative concept for a major breakthrough in atmospheric radioactive xenon detection for nuclear explosion monitoring**, *Journal of Radioanalytical and Nuclear Chemistry*, *298*, *no. 2*, *1159-1169*, doi:10.1007/s10967-013-2525-8.

Le Petit, G. G. Douysset, G. Ducros, P. Gross, P. Achim, M. Monfort, P. Raymond, Y. Pontillon, C. Jutier, X. Blanchard, T. Taffary, and C. Moulin, 2014, **Analysis of Radionuclide Releases from the Fukushima Dai-Ichi Nuclear Power Plant Accident Part I**, *Pure and Applied Geophysics*, *171*, *no. 3*, *629-644*, doi:10.1007/s00024-012-0581-6.

Le Petit, G., A. Cagniant, P. Gross, G. Douysset, S. Topin, J.P. Fontaine, T. Taffary, and C. Moulin, 2015, **Spalax™ new generation: A sensitive and selective noble gas system for nuclear explosion monitoring**, *Applied Radiation and Isotopes*, *103*, *102–114*, doi:10.1016/j.apradiso.2015.05.019.

Le Pichon, A., L. Ceranna, M. Garcés, D. Drob, and C. Millet, 2006, **On using infrasound from interacting ocean swells for global continuous measurements of winds and temperature in the stratosphere**, *Journal of Geophysical Research: Atmospheres*, *111*, *no. D11*, doi:10.1029/2005jd006690.

Le Pichon, A., N. Brachet and L. Ceranna, 2008, **Continuous infrasound monitoring for atmospheric studies**, *Journal of the Acoustical Society of America*, *123*, *3827*, doi:10.1121/1.2935599.

Le Pichon, A., L. Ceranna, and J. Vergoz, 2012, **Incorporating numerical modeling into estimates of the detection capability of the IMS infrasound network**, *Journal of Geophysical Research: Atmospheres*, *117*, *no. D5*, *D05121*, doi:10.1029/2011JD016670.

Lee, E-J., P. Chen, T. H. Jordan, P. B. Maechling, M. A. M. Denolle, and G. C. Beroza, 2014, **Full-3-D tomography for crustal structure in Southern California based on the scattering-integral and the adjoint-wavefield methods**, *Journal of Geophysical Research: Solid Earth*, *119*, *6421-6451*, doi:10.1002/2014JB011346.

Leet, L. D., 1962, **The detection of underground explosions**, *Scientific American*, *206*, *no. 6*, *55-59*, doi:10.1038/scientificamerican0662-55.

Lehmann, I., 1936, **Inner Earth**, *Bureau Central International de Séismologie*, *14*, *3-31*.

Leidig, M., J. L. Bonner, T. Rath, and D. Murray, 2010, **Quantification of ground vibration differences from well-confined single-hole explosions with variable velocity of detonation**, *International Journal of Rock Mechanics and Mining Sciences*, *47*, *42-49*, doi:10.1016/j.ijrmms.2009.07.006.

Leith, W., 2000, **Geologic and engineering constraints on the feasibility of clandestine nuclear testing by decoupling in large underground cavities**, *United States Geological Survey*, *Open-File Report 2001-28*, https://pubs.usgs.gov/of/2001/0028/report.pdf.

Lekic, V., and B. Romanowicz, 2011, **Inferring mantle structure by full waveform tomography using the spectral element method**, *Geophysical Journal International*, *185*, *799-831*, doi:10.1111/j.1365-246X.2011.04969.x.

Levshin, A. L., V. F. Pisarenk, and G. A. Pogrebin, 1972, **On a frequency-time analysis of oscillations**, *Annales de Geophysique*, *28*, *no. 2*, *(The paper was presented at the 8th International Symposium on geophysical theory and computers, held in Moscow during 30-31 July 1971)*, *pp 211-218*.

Levshin, A. L., X. Yang, M.P. Barmin, and M.H. Ritzwoller, 2010, **Midperiod Rayleigh wave attenuation model for Asia**, *Geochemistry Geophysics Geosystems*, *Volume 11, Number 8Q08017*, doi:10.1029/2010GC003164 ISSN: 1525-2027.

Li, C., R. D. van der Hilst, E. R. Engdahl, and S. Burdick, 2008, **A new global model for P wave speed variations in Earth's mantle**, *Geochemistry Geophysics Geosystems*, *9*, *no. Q05018*, doi:10.1029/2007GC001806.

Li, X-D., and B. Romanowicz, 1995, **Comparison of global waveform inversions with and without considering cross-branch modal coupling**, *Geophysical Journal International*, *121*, *no. 3*, *695-709*, doi:10.1111/j.1365-246X.1995.tb06432.x.

Liberman, R. C., and P. W. Pomeroy, 1969, **Relative excitation of surface waves by earthquakes and underground explosions**, *Journal of Geophysical Research*, *74*, *1574-1590*.

Lin, F.-C., and M.H. Ritzwoller, 2011, **Helmholtz surface wave tomography for isotropically and azimuthally anisotropic structure**, *Geophysical Journal International*, *186*, *1104-1120*, doi:10.111/j.1365-246X.2011.05070.x.

Lin, F. -C., V. C. Tsai, and M. H. Ritzwoller, 2012, **The local amplification of surface waves: A new observable to constrain elastic velocities, density, and anelastic attenuation**, *Journal of Geophysical Research: Solid Earth*, *117*, *no. B6*, *B06302*, doi:10.1029/2012JB009208.

Lingevitch, J. F., M. D. Collins, and W. L. Siegmann, 1999, **Parabolic equations for gravity and acousto-gravity waves**, *Journal of the Acoustical Society of America*, *105*, *no. 6*, *3049-3056*, doi:10.1121/1.424634.

Lonzaga, J. B., R. M. Waxler, J. D. Assink, and C. L. Talmadge, 2015, **Modelling waveforms of infrasound arrivals from impulsive sources using weakly non-linear ray theory**, *Geophysical Journal International*, *200*, *no. 3*, *1347-1361*, doi:10.1093/gji/ggu479.

Loris, I., G. Nolet, I. Daubechies, and F. Dahlen, 2007, **Tomographic inversion using L1-norm regularization of wavelet coefficients**, *Geophysical Journal International*, *170*, *359-370*, doi:10.1111/j.1365-246X.2007.03409.x.

Love, A. E. H., 1888, **The free and forced vibrations of an elastic spherical shell containing a given mass of liquid**, *Proceedings of the London Mathematical Society*, *s1-19*, *no. 1*, *170-207*, http://plms.oxfordjournals.org/content/s1-19/1/170.full.pdf+html.

Love, A. E. H., 1892, **A Treatise on the Mathematical Theory of Elasticity**, *Cambridge University Press*, *I*, https://hal.archives-ouvertes.fr/hal-01307751/document.

Lowrey, J., D. Haas, M. Paul, S. Biegalski, T. Bowyer, and J. Hayes, 2015, **Exploring the Effect of Ground Water on the Detection of Radioactive Noble Gases from Underground Nuclear Explosions: How Smokin' is the Smoking Gun?**, *Pacific Northwest National Laboratory*, *PNNL-24806*.

LTBT, 1963, **Limited Test Ban Treaty: Treaty Banning Nuclear Weapon Tests in the Atmosphere, in Outer Space, and Under Water**, *Department of State*, http://www.state.gov/t/avc/trty/199116.htm.

Ma, Z., and G. Masters, 2014, **A new global Rayleigh- and Love-Wave group velocity dataset for constraining lithosphere properties**, *Bulletin of the Seismological Society of America*, *104*, *no. 4*, *2007-2026*, doi:10.1785/0120130320.

Ma, Z., G. Masters, G. Laske, and M. E. Pasyanos, 2014, **A comprehensive dispersion model of surface wave phase and group velocity for the globe**, *Geophysical Journal International*, *119*, *no. 1*, *113-135*, doi:10.1093/gji/ggu246.

Ma, Z., G. Masters, and N. Mancinelli, 2016, **Two-dimensional global Rayleigh wave attenuation model by accounting for finite-frequency focusing and defocusing effect**, *Geophysical Journal International*, *204*, *no. 1*, *631-649*, doi:10.1093/gji/ggv480.

Maceira, M., S. R. Taylor, C. J. Ammon, X. N. Yang, and A. A. Velasco, 2005, **High-resolution Rayleigh wave slowness tomography of central Asia**, *Journal of Geophysical Research: Solid Earth*, *110*, *no. B6*, doi:10.1029/2004JB003429.

Maceira, M., and C. J. Ammon, 2009, **Joint inversion of surface wave velocity and gravity observations and its application to central Asian basins shear velocity structure**, *Journal of Geophysical Research: Solid Earth*, *114*, *no. B2*, doi:10.1029/2007JB005157.

Maceira, M., C. Larmat, R. W. Porritt, D. M. Higdon, C. A. Rowe, and R. M. Allen, 2015, **On the validation of seismic imaging methods: Finite frequency or ray theory?**, *Geophysical Research Letters*, *42*, *no. 2*, *323–330*, doi:10.1002/2014GL062571.

Maceira, M., E. M. Syracuse, E. Bergman, W. S. Phillips, M. Begnaud, S. Nippress, and H. Zhang, 2016, **Improvements in earthquake location from joint inversion of seismic and gravity observations – Application to the Iran region**, *Seismological Research Letters*, *87*, *no. 2B*, *461*, doi:10.1785/0220160046.

Mallet, R., 1859, **Report to the Royal Society of the expedition into the Kingdom of Naples to investigate the circumstances of the earthquake of the 16th December 1857**, *Proceedings of the Royal Society of London*, *10*, *486-494*, doi:10.1098/rspl.1859.0092.

Mallin, M. A., 2017, **The Comprehensive Nuclear-Test-Ban Treaty Negotiations: A Case Study**, *National Defense University*, *Case Study Series 7*, *1-24*, http://wmdcenter.ndu.edu/Media/News/Article/1093696/the-comprehensive-nuclear-test-ban-treaty-negotiations-a-case-study/.

Marcillo, O., S. J. Arrowsmith, R. Whitaker, D. Anderson, A. Nippress, D. Green, and D. Drob, 2014, **Using physics-based priors in a Bayesian algorithm to enhance infrasound source location**, *Geophysical Journal International*, *196*, *no. 1*, *375-385*, doi:10.1093/gji/ggt353.

Marquering H., F. A. Dahlen, and G. Nolet, 1999, **Three-dimensional sensitivity kernels for finite-frequency traveltime: the banana-doughnut paradox**, *Geophysical Journal International*, *137*, *805-815*.

Marshall, P. E., and P. W. Basham, 1972, **Discrimination between earthquakes and underground explosions employing an improved Ms scale**, *Geophysical Journal of the Royal Astronomical Society*, *28*, *431-438*.

Massonet, D., M. Rossi, C. Carmona, F. Adragna, G. Peltzer, K. Feigl, and T. Rabaute, 1993, **The displacement field of the Landers earthquake mapped by radar interferometry**, *Nature*, *364*, *no. 6433*, *138-142*, doi:10.1038/364138a0.

Matthews, K. M., T. W. Bowyer, P. R. J. Saey, and R. F. Payne, 2012, **The Workshop on Signatures of Medical and Industrial Isotope Production – WOSMIP; Strassoldo, Italy, 1–3 July 2009**, *Journal of Environmental Radioactivity*, *110*, *1-6*, doi:10.1016/j.jenvrad.2012.01.012.

Mayeda, K., and W. R. Walter, 1996, **Moment, energy, stress drop, and source spectra of western United States earthquakes from regional coda envelopes**, *Journal of Geophysical Research: Solid Earth*, *101*, *no. B5*, *11195-11208*, doi:10.1029/96JB00112.

Mayeda, K., A. Hofstetter, J. O'Boyle, and W. R. Walter, 2003, **Stable and transportable regional magnitudes based on coda derived moment-rate spectra**, *Bulletin of the Seismological Society of America*, *93*, *no. 1*, *224-239*, doi:10.1785/0120020020.

Mayeda, K., L. Malagnini, W. S. Phillips, W. R. Walter, and D. S. Dreger, 2005a, **2-D or not 2-D, that is the question: A northern California test**, *Geophysical Research Letters*, *32, June 2005*, doi:10.1029/2005GL022882.

Mayeda, K., R. Gok, W. R. Walter, and A. Hofstetter, 2005b, **Evidence for non-constant energy/moment scaling from coda-derived source spectra**, *Geophysical Research Letters*, *32*, doi:10.1029/2005GL022405.

McDonald, B. E., M. D. Collins, W. A. Kuperman, and K. D. Heaney, 1994, **Comparison of data and model predictions for Heard Island acoustic transmissions**, *Journal of the Acoustical Society of America*, *96*, *2357-2370*, doi:10.1121/1.410108.

McDonald, B. E., 1996, **Bathymetric and volumetric contributions to ocean acoustic mode coupling**, *Journal of the Acoustical Society of America*, *100*, *219-224*, doi:10.1121/1.415951.

McEvilly, T. V., and W. A. Peppin, 1972, **Source Characteristics of Earthquakes, Explosions and Afterevents**, *Geophysical Journal International*, *31*, *no. 1-3*, *67-82*, doi:10.1111/j.1365-246X.1972.tb02359.x.

McIntyre, J. I., T.W. Bowyer, and P.L. Reeder, 2006, **Calculation of Minimum Detectable Concentration Levels of Radioxenon Isotopes Using the PNNL ARSA System**, Pacific Northwest National Laboratory, PNNL-13102, doi:10.2172/888707.

McIntyre, J. I., B. T. Schrom, M. W. Cooper, A. M. Prinke, T. J. Suckow, A. Ringbom, and G. A. Warren, 2016a, **A program to generate simulated radioxenon beta–gamma data for concentration verification and validation and training exercises**, *Journal of Radioanalytical and Nuclear Chemistry*, *307*, *no. 3*, *2381-2387*, doi:10.1007/s10967-015-4620-5.

McIntyre, J. I., A. Agusbudiman, I.M. Cameron, J.R. Dumais, P.W. Eslinger, A. Gheddou, K. Khrustalev, P. Marsoem, H.S. Miley, M. Nikkinen, A.M. Prinke, M.D. Ripplinger, B.T. Schrom, W.A. Sliger, U. Stoehlker, G. Suhariyono, G.A. Warren, S. Widodo, T. Woods, 2016b, **Real-time stack monitoring at the BaTek medical isotope production facility**, *Journal of Radioanalytical and Nuclear Chemistry*, *308*, *no. 1*, *311-316*, doi:10.1007/s10967-015-4348-2.

McKenna, M. H., R. G. Gibson, B. E. Walker, J. McKenna, N. W. Winslow and A. S. Kofford, 2012, **Topographic effects on infrasound propagation**, *Journal of the Acoustical Society of America*, *131*, *35*, doi:10.1121/1.3664099.

McLachlan, G., 2004, **Discriminant Analysis and Statistical Pattern Recognition**, *Wiley Series in Probability and Statistics, New York*, *ISBN: 978-0-471-69115-0*.

McMorrow, D., 2014, **Open and Crowd-Sourced Data for Treaty Verification**, *The MITRE Corporation*, *Technical Report: JSR-14_Task-015*, http://oai.dtic.mil/oai/oai?verb=getRecord&metadataPrefix=html&identifier=ADA614684.

Meitner, L., and O. R. Frisch, 1939, **Disintegration of uranium by neutrons: A new type of nuclear reaction**, *Nature*, *143*, *no. 3615*, *239-240*, doi:10.1038/143239a0.

Menke, W., 2005, **Case studies of seismic tomography and earthquake location in a regional context**, in *Geophysical Monograph Series*, *157*, *no. Seismic Earth: Array Analysis of Bradband Seismograms, ed. A. Levander and G. Nolet*, *7-36*, doi:10.1029/157GM02.

Merchant, B. J., and K. D. McDowell, 2014, **MB3a Infrasound Sensor Evaluation**, *Sandia National Laboratories, Albuquerque*, *SAND2014-20108*, *59 pp*, doi:10.2172/1165050.

Meza-Fajardo, K. C., Papageorgiou, A. S., and J.-F. Semblat, 2015, **Identification and Extraction of Surface Waves from Three-Component Seismograms Based on the Normalized Inner Product**, *Bulletin of the Seismological Society of America*, *105*, *no. 1*, *210-229*, doi:10.1785/0120140012.

Miley, H. S., S. M. Bowyer, C. W. Hubbard, A. D. McKinnon, R. W. Perkins, R. C. Thompson, and R. A. Warner, 1998a, **Automated aerosol sampling and analysis for the Comprehensive Test Ban Treaty**, *IEEE Transactions on Nuclear Science*, *0-7803-4258-5/98*, *779-785*, doi:10.1109/23.682702.

Miley, H. S., S. M. Bowyer, C. W. Hubbard, A. D. McKinnon, R. W. Perkins, R. C. Thompson, and R. A. Warner, 1998b, **A description of the DOE Radionuclide Aerosol Sampler/Analyzer for the Comprehensive Test Ban Treaty**, *Journal of Radioanalytical and Nuclear Chemistry*, *235*, *no. 1-3*, *83-87*, doi:10.1007/BF02385942.

Modrak, R. T., S. J. Arrowsmith, and D. N. Anderson, 2010, **A Bayesian framework for infrasound location**, *Geophysical Journal International*, *181*, *no. 1*, *399-405*, doi:10.1111/j.1365-246X.2010.04499.x.

Mohorovicic, A., 1909, **Das Beben**, *Jb. Met. Obs. Zagreb (Agram)*, *9*, *1-63*.

Mooney, W. D., G. Laske, and T. G. Masters, 1998, **CRUST 5.1: A global crustal model at 5°×5°**, *Journal of Geophysical Research: Solid Earth*, *103*, *no. B1*, *727–747*, doi:10.1029/97JB02122.

Moore, G.E., 1965, **Cramming more components onto integrated circuits**, *Electronics*, *38*, *no. 8*, http://www.monolithic3d.com/uploads/6/0/5/5/6055488/gordon_moore_1965_article.pdf.

Morton, E. A. and S. J. Arrowsmith, 2014, **The development of global probabilistic propagation look-up tables for infrasound celerity and back-azimuth deviation**, *Seismological Research Letters*, *85*, *no. 6*, *1223-1233*, doi:10.1785/0220140124.

Mueller, R. A., and J. R. Murphy, 1971, **Seismic characteristics of underground nuclear detonations Part I. Seismic spectrum scaling**, *Bulletin of the Seismological Society of America*, *61*, *no. 6*, *1675-1692*, http://www.bssaonline.org/content/61/6/1675.

Munk, W. H., R. C. Spindel, A. Baggeroer, and T. G. Birdsall, 1994, **The Heard Island feasibility test**, *Journal of the Acoustical Society of America*, *96*, *no. 4*, *2330-2342*, doi:10.1121/1.410105.

Murphy, J. R., 1981a, **P wave coupling of underground explosions in various geologic media**, in *NATO Advanced Study Institutes Series*, *74*, *Identification of Seismic Sources — Earthquake or Underground Explosion*, *201-205*, doi:10.1007/978-94-009-8531-5_6.

Murphy, J. R., 1981b, **Near-field Rayleigh waves from surface explosions**, *Bulletin of the Seismological Society of America*, *71*, *no. 1*, *223-248*, http://www.bssaonline.org/content/71/1/223.full.pdf+html.

Murphy, J. R., 1996, **Types of seismic events and their source descriptions**, in *NATO Advanced Study Institutes Series*, *303*, *Monitoring a Comprehensive Test Ban Treaty*, *225-245*, doi:10.1007/978-94-011-0419-7_16.

Murphy, J. R., and B. W. Barker, 2009, **An analysis of the seismic source characteristics of explosions in low-coupling dry porous media**, *Los Alamos National Laboratory*, *Proceedings of the 2009 Monitoring Research Review, LA-UR-09-05276*, *pp 506-515*, http://www.osti.gov/scitech/biblio/992203.

Murphy, K. R., K. Mayeda, and W. R. Walter, 2009, **Lg-coda methods applied to Nevada Test Site events: Spectral peaking and yield estimation**, *Bulletin of the Seismological Society of America*, *99*, *no. 1*, *441-448*, doi:10.1785/0120080046.

Myers, S. C., and C. A. Schultz, 2000, **Improving sparse network seismic location with bayesian kriging and teleseismically constrained calibration events**, *Bulletin of the Seismological Society of America*, *90*, *no. 1*, *199-211*, doi:10.1785/0119980171.

Myers, S. C., G. Johannesson, and W. Hanley, 2007, **A Bayesian hierarchical method for multiple-event seismic location**, *Geophysical Journal International*, *171*, *no. 3*, *1049-1063*, doi:10.1111/j.1365-246X.2007.03555.x.

Myers, S. C., G. Johannesson, and W. Hanley, 2009, **Incorporation of probabilistic seismic phase labels into a Bayesian multiple-event seismic locator**, *Geophysical Journal International*, *177*, *no. 1*, *193-204*, doi:10.1111/j.1365-246X.2008.04070.x.

Myers, S. C., M. L. Begnaud, S. Ballard, M. E. Pasyanos, W. S. Phillips, A. L. Ramirez, M. S. Antolik, K. D. Hutchenson, J. J. Dwyer, C. A. Rowe, and G. S. Wagner, 2010, **A crust and upper mantle model of Eurasia and North Africa for Pn travel time calculation**, *Bulletin of the Seismological Society of America*, *100*, *no. 2*, *640-656*, doi:10.1785/0120090198.

Myers, S. C., N. A. Simmons, G. Johannesson, and E. Matzel, 2015, **Improved regional and teleseismic P-wave travel time prediction and event location using a global, 3-dimensional velocity model**, *Bulletin of the Seismological Society of America*, *105*, *no. 3*, *1642-1660*, doi:10.1785/0120140272.

Nakata, N., J. P. Chang, J. F. Lawrence, and P. Boué, 2015, **Body wave extraction and tomography at Long Beach, California, with ambient-noise interferometry**, *Journal of Geophysical Research: Solid Earth*, *120*, *no. 2*, *1159-1173*, doi:10.1002/2015JB011870.

NAS-National Academy of Sciences, Committee on Technical Issues Related to Ratification of the Comprehensive Nuclear Test Ban Treaty, 2002, **Technical Issues Related to the Comprehensive Nuclear Test Ban Treaty**, *National Academies Press*, doi:10.17226/10471.

NAS-National Academy of Sciences, Committee on Reviewing and Updating Technical Issues Related to the Comprehensive Nuclear Test Ban Treaty, 2012, **The Comprehensive Nuclear Test Ban Treaty: Technical Issues for the United States**, *National Academies Press*, *ISBN 978-0-309-14998-3*, doi:10.17226/12849.

Nolet, G., 1990, **Partitioned waveform inversion and two-dimensional structure under the network of autonomously recording seismographs**, *Journal of Geophysical Research: Solid Earth*, *95*, *8499-8512*, doi:10.1029/JB095iB06p08499.

Nolet, G., 2008, **A breviary of seismic tomography: imaging the interior of the earth and sun**, *Cambridge University Press*.

Norris, D. E. and R. G. Gibson, 2002, **Propagation variability and localization accuracy of infrasonic networks**, *Journal of the Acoustical Society of America*, *112*, *2380*, http://dx.doi.org/10.1121/1.4808604.

Norris, D., K. Bongiovanni and J. Masi, 2008, **Nonlinear propagation modeling of infrasound**, *Journal of the Acoustical Society of America*, *123*, *3829*, doi:10.1121/1.2935605.

Nuttli, O.W., 1973, **Seismic wave attenuation and magnitude relations for eastern North America**, *Journal of Geophysical Research*, *78*, *no. 5*, *876-885*, doi:10.1029/JB078i005p00876.

Oldham, R. D., 1914, **The constitution of the interior of the earth as revealed by earthquakes**, *Nature*, *92*, *no. 2312*, *684-685*, doi:10.1038/092684c0.

Oliver, J., 1962, **A summary of observed seismic surface wave dispersion**, *Bulletin of the Seismological Society of America*, *52*, *no. 1*, *81-86*, http://www.bssaonline.org/content/52/1/81.

Olsen, K. B., R. R. Kirkham, V. T. Woods, D. H. Haas, J. C. Hayes, T. W. Bowyer, D. P. Mendoza, J. D. Lowrey, C. D. Lukins, et al., 2016, **Noble gas migration experiment to support the detection of underground nuclear explosions**, *Journal of Radioanalytical and Nuclear Chemistry*, *307*, *no. 3*, *2603-2610*, doi:10.1007/s10967-015-4639-7.

Olsen, K. H., and A. L. Peratt, 1994, **Freefield ground motions from the NPE: Preliminary comparisons with nearby nuclear events**, *Department of Energy*, *Proc. of the Symposium on the Non-Proliferation Experiment (NPE): Results and implications for the Test Ban Treaties, 19-21 April 1994, Rockville, Maryland*.

Olson, J. V., K. Arnoult and C. A. S. Szuberla, 2005, **A method for locating nearby sources**, *Journal of the Acoustical Society of America*, *117*, *2610*, doi:10.1121/1.1854651.

O'Rourke, C. T., G. E. Baker, and A. F. Sheehan, 2016, **Using P/S Amplitude Ratios for Seismic Discrimination at Local Distances**, *Bulletin of the Seismological Society of America*, *106*, *no. 5*, *2320-2331*, doi:10.1785/0120160035.

Ostashev, V. E., I. P. Chunchuzov, and D. K. Wilson, 2005, **Sound propagation through and scattering by internal gravity waves in a stably stratified atmosphere**, *Journal of the Acoustical Society of America*, *118*, *no. 6*, doi:10.1121/1.2126938.

Park, Y., A. A. Nyblade, A. Rodgers, and A. Al-Amri, 2007, **Upper mantle structure beneath the Arabian Peninsula from regional body-wave tomography: Implications for the origin of Cenozoic uplift and volcanism in the Arabian Shield**, *Geochemistry Geophysics Geosystems*, *8*, *no. 6*, *Q06021*, doi:10.1029/2006GC001566.

Pasyanos, M. E., D. S. Dreger, and B. Romanowicz, 1996, **Toward real-time estimation of regional moment tensors**, *Bulletin of the Seismological Society of America*, *86*, *no. 5*, *1255-1269*, http://www.bssaonline.org/content/86/5/1255.

Pasyanos, M. E., W. R. Walter, S. E. Hazler, 2001, **A surface wave dispersion study of the Middle East and North Africa for monitoring the Comprehensive Nuclear-Test Ban Treaty**, *Pure and Applied Geophysics*, *158*, *no. 8*, *1445-1474*, doi:10.1007/PL00001229.

Pasyanos, M. E., and W. R. Walter, 2002, **Crust and upper-mantle structure of North Africa, Europe and the Middle East from the inversion of surface waves**, *Geophysical Journal International*, *149*, *no. 2*, *463-481*, doi:10.1046/j.1365-246X.2002.01663.x.

Pasyanos, M. E., W. R. Walter, M. P. Flanagan, P. Goldstein, and J. Bhattacharyya, 2004, **Building and testing an a priori geophysical model for Western Eurasia and North Africa**, *Pure and Applied Geophysics*, *161, 235-281*, doi:10.1007/s00024-003-2438-5.

Pasyanos, M. E., 2005, **A variable resolution surface wave dispersion study of Eurasia, North Africa, and surrounding regions**, *Journal of Geophysical Research: Solid Earth*, *110*, *no. B12*, doi:10.1029/2005JB003749.

Pasyanos, M. E., G. A. Franz, and A. L. Ramirez, 2006, **Reconciling a geophysical model to data using Markov Chain Monte Carlo: An application to the Yellow Sea - Korean Peninsula region**, *Journal of Geophysical Research: Solid Earth*, *111, no. B3*, doi:10.1029/2005JB003851.

Pasyanos, M. E., and A. A. Nyblade, 2007, **A top to bottom lithospheric study of Africa and Arabia**, *Tectonophysics*, *444, no. 1-4, 27-44*, doi:10.1016/j.tecto.2007.07.008.

Pasyanos, M. E., H. Tkalcic, R. Gok, A. Al-Enezi, and A. J. Rodgers, 2007, **Seismic structure of Kuwait**, *Geophysical Journal International*, *170*, *no. 1*, *299-312*, doi:10.1111/j.1365-246X.2007.03398.x.

Pasyanos, M. E., and W. R. Walter, 2009, **Improvements to regional explosion identification using attenuation models of the lithosphere**, *Geophysical Research Letters*, *36, L14304*, doi:10.1029/2009GL038505.

Pasyanos, M. E., 2010, **Lithospheric thickness modeled from long-period surface wave dispersion**, *Tectonophysics*, *481, 38-50*, doi:10.1016/j.tecto.2009.02.023.

Pasyanos, M. E., 2011, **A case for the use of 3D attenuation models in ground-motion and seismic-hazard assessment**, *Bulletin of the Seismological Society of America*, *101*, *no. 4*, *1965-1970*, doi:10.1785/0120110004.

Pasyanos, M. E., W. R. Walter, and K. M. Mayeda, 2012, **Exploiting regional amplitude envelopes: a case study for earthquakes and explosions in the Korean Peninsula**, *Bulletin of the Seismological Society of America*, *102*, *no. 5*, *1938-1948*, doi:10.1785/0120120012.

Pasyanos, M. E., 2013, **Lithospheric attenuation model of North America**, *Bulletin of the Seismological Society of America*, *103*, *no. 6*, *3321-3333*, doi:10.1785/0120130122.

Pasyanos, M. E., T.G. Masters, G. Laske, and Z. Ma, 2014, **LITHO1.0: An updated crust and lithospheric model of the earth**, *Journal of Geophysical Research: Solid Earth*, *119*, *2153-2173*, doi:10.1002/2013JB010626.

Pasyanos, M. E., and S. R. Ford, 2015, **Determining the source characteristics of explosions near the Earth's surface**, *Geophysical Research Letters*, *42*, *no. 10*, *3786-3792*, doi:10.1002/2015GL063624.

Pasyanos, M. E., R. Gok, and W. R. Walter, 2016, **2-D variations in coda amplitudes in the Middle East**, *Bulletin of the Seismological Society of America*, *106*, *no. 4*, doi:10.1785/0120150336.

Patton, H. J., J. L. Bonner, and I. N. Gupta, 2005, **Rg excitation by underground explosions: insights from source modelling the 1997 Kazakhstan depth-of-burial experiment**, *Geophysical Journal International*, *163*, *no. 3*, *1006-1024*, doi:10.1111/j.1365-246X.2005.02752.x.

Patton, H. J., and S. R. Taylor, 2011, **The apparent explosion moment: Inferences of volumetric moment due to source medium damage by underground nuclear explosions**, *Journal of Geophysical Research: Solid Earth*, *116*, *no. B3*, *B03310*, doi:10.1029/2010JB007937.

Peräjärvi, K., T. Eronen, V.-V. Elomaa, J. Hakala, A. Jokinen, H. Kettunen, V. S. Kolhinen, M. Laitinen, I. D. Moore, H. Penttilä, J. Rissanen, A. Saastamoinen, H. Toivonen, J. Turunen, and J. Äystö, 2010, **Ultra-high resolution mass separator—Application to detection of nuclear weapons tests**, *Applied Radiation and Isotopes*, *68*, *no. 3*, *450-453*, doi:10.1016/j.apradiso.2009.12.020.

Peter, D., L. Boschi, and J. H. Woodhouse, 2009, **Tomographic resolution of ray and finite-frequency methods: a membrane-wave investigation**, *Geophysical Journal International*, *177*, *624-638*, doi:10.1111/j.1365-246X.2009.04098.x.

Phillips, W. S., G. E. Randall, and S. R. Taylor, 1998, **Path correction using interpolated amplitude residuals: An example from central China**, *Geophysical Research Letters*, *25*, *no. 14*, *2729-2732*, doi:10.1029/98GL51940.

Phillips, W. S., 1999, **Empirical path corrections for regional-phase amplitudes**, *Bulletin of the Seismological Society of America*, *89*, *no. 2*, *384-393*, http://www.bssaonline.org/content/89/2/384.short.

Phillips, W. S., H. E. Hartse, S. R. Taylor, and G. E. Randall, 2000, **1 Hz Lg Q tomography in Central Asia**, *Geophysical Research Letters*, *27*, *no. 20*, *3425-3428*, doi:10.1029/2000GL011482.

Phillips, W. S., H. E. Hartse, and L. K. Steck, 2001, **Precise relative location of 25-ton chemical explosions at Balapan using IMS stations**, *Pure and Applied Geophysics*, *158*, *no. 1-2*, *173-192*, doi:10.1007/PL00001154.

Phillips, W. S., H. E. Hartse, S. R. Taylor, A. A. Velasco, and G. E. Randall, 2001, **Application of regional phase amplitude tomography to seismic verification**, *Pure and Applied Geophysics*, *158*, *no. 7*, *1189-1206*, doi:10.1007/PL00001220.

Phillips, W. S., C. A. Rowe, and L. K. Steck, 2005a, **The use of interstation P wave arrival time differences to account for regional path variability**, *Geophysical Research Letters*, *32, L11301*, doi:10.1029/2005GL022558.

Phillips, W. S., H. E. Hartse, and J. T. Rutledge, 2005b, **Amplitude ratio tomography for regional phase Q**, *Geophysical Research Letters*, *32, L21301*, doi:10.1029/2005GL023870.

Phillips, W. S., M. L. Begnaud, C. A. Rowe, L. K. Steck, S. C. Myers, M. E. Pasyanos, and S. Ballard, 2007, **Accounting for lateral variations of the upper mantle gradient in Pn tomography studies**, *Geophysical Research Letters*, *34*, *no. 14*, doi:10.1029/2007GL029338.

Phillips, W. S., and R. J. Stead, 2008, **Attenuation of Lg in the western US using the USArray**, *Geophysical Research Letters*, *35*, *no. 7*, *L07307*, doi:10.1029/2007GL032926.

Phillips, W. S., R. J. Stead, G. E. Randall, H. E. Hartse, and K. M. Mayeda, 2008, **Source effects from broad area network calibration of regional distance coda waves**, in *Advances in Geophysics*, *50*, *Elsevier Academic Press*, *319-351*, doi:10.1016/S0065-2687(08)00012-5.

Phillips, W. S., K. M. Mayeda, and L. Malagnini, 2014, **How to invert multi-band, regional phase amplitudes for 2-D attenuation and source parameters: Tests using the USArray**, *Pure and Applied Geophysics*, *171*, *no. 3-5*, *469-484*, doi:10.1007/s00024-013-0646-1.

Pierce, A. D., 1967, **Guided infrasonic modes in a temperature- and wind-stratified atmosphere**, *Journal of the Acoustical Society of America*, *41*, *no. 3*, *597-611*, doi:10.1121/1.1910386.

Pierce, A. D., J. W. Posey, and E. F. Iliff, 1971, **Variation of nuclear explosion generated acoustic-gravity wave forms with burst height and with entery yield**, *Journal of Geophysical Research*, *76*, *no. 21*, *5025-5042*, doi:10.1029/JC076i021p05025.

Piserchia, P. F., J. Virieux, D. Rodrigues, S. Gaffet, and J. Talandier, 1998, **Hybrid numerical modelling of T-wave propagation:application to the Midplate experiment**, *Geophysical Journal International*, *133*, *no. 3*, *789-800*, doi:10.1046/j.1365-246X.1998.00546.x.

Pitarka, A., R. J. Mellors, W. R. Walter, S. Ezzedine, O. Vorobiev, T. Antoun, J. L. Wagoner, E. M. Matzel, S. R. Ford, A. J. Rodgers, L. Glenn, and M. Pasyanos, 2015, **Analysis of ground motion from an underground chemical explosion**, *Bulletin of the Seismological Society of America*, *105*, *no. 5*, *2390-2410*, doi:10.1785/0120150066.

Poisson, S. D., 1828, **Mémoire sur l'équilibre et mouvement des corps élastiques**, *L'Académie des sciences*, http://www.worldcat.org/title/memoire-sur-lequilibre-et-mouvement-des-corps-elastiques/oclc/22885091.

Pomeroy, P. W., W. J. Best, and T. V. McEvilly, 1982, **Test Ban Treaty Verification with Regioanl Data - A Review**, *Bulletin of the Seismological Society of America*, *72*, *no. 6*, *S89-S129*.

Popov, V., 2005, **The ARIX automatic facility for measuring concentrations of radioactive xenon isotopes in the atmosphere**, *Instruments and Experimental Techniques*, *48*, *390-386*, doi:10.1007/s10786-005-0066-2.

Price, E., and D. Sandwell, 1998, **Small-scale deformations associated with the 1992 Landers, California, earthquake mapped by synthetic aperture radar interferometry phase gradients**, *Journal of Geophysical Research: Solid Earth*, *103*, *no. B11*, *27001-27016*, doi:10.1029/98jb01821.

Proceedings, 1985, **Proceedings of the 7th Annual DARPA/AFGL Seismic Research Symposium**, *Air Force Geophysics Laboratory*, *GL-TR-90-0306, Environmental Research Papers, No. 1071, 458 pp*, http://www.dtic.mil/docs/citations/ADA229915.

Proceedings, 1986, **Proceedings of the 8th Annual DARPA/AFGL Seismic Research Symposium**, *Air Force Geophysics Laboratory*, *GL-TR-90-0333, Environmental Research Papers, No. 1074, 233 pp*, http://www.dtic.mil/docs/citations/ADA230519.

Proceedings, 1987, **Proceedings of the 9th Annual DARPA/AFGL Seismic Research Symposium**, *Air Force Geophysics Laboratory*, *GL-TR-90-0300, Environmental Research Papers, No. 1069, 259 pp*, http://www.dtic.mil/docs/citations/ADA229025.

Proceedings, 1988, **Proceedings of the 10th Annual DARPA/AFGL Seismic Research Symposium**, *Air Force Geophysics Laboratory*, *GL-TR-90-0332(A), Environmental Research Papers, No. 1073, 257pp*, http://www.dtic.mil/docs/citations/ADA230066.

Proceedings, 1989, **Proceedings of the 11th Annual DARPA/AFGL Seismic Research Symposium**, *Air Force Geophysics Laboratory*, *GL-TR-90-0301, Environmental Research Papers, No. 1070, 521 pp*, http://www.dtic.mil/docs/citations/ADA229228.

Proceedings, 1991, **Proceedings of the 13th Annual PL/DARPA Seismic Research Symposium**, *Air Force Phillips Laboratory*, *PL-TR-91-2208, 555 pp*, http://www.dtic.mil/docs/citations/ADA241325.

Proceedings, 1992, **Proceedings of the 14th Annual PL/DARPA Seismic Research Symposium**, *Air Force Phillips Laboratory*, *PL-TR-92-2210, Environmental Research Papers, No. 1106, 487 pp*, http://www.dtic.mil/docs/citations/ADA256711.

Proceedings, 1993, **Proceedings of the 15th Annual Seismic Research Symposium**, *Air Force Phillips Laboratory*, *PL-TR-93-2160, Environmental Research Papers, No. 1125, 449 pp*, http://www.dtic.mil/docs/citations/ADA271458.

Proceedings, 1994, **Proceedings of the 16th Annual Seismic Research Symposium**, *Air Force Phillips Laboratory*, *PL-TR-94-2217, Environmental Research Papers, No. 1157, 424 pp*, http://www.dtic.mil/docs/citations/ADA284667.

Proceedings, 1995, **Proceedings of the 17th Annual Seismic Research Symposium on Monitoring a Comprehensive Test Ban Treaty**, *Air Force Phillips Laboratory*, *PL-TR-95-2108, Environmental Research Papers, No. 1173, 1071 pp*, http://www.dtic.mil/docs/citations/ADA310037.

Proceedings, 1996, **Proceedings of the 18th Annual Seismic Research Symposium on Monitoring a Comprehensive Test Ban Treaty**, *Air Force Phillips Laboratory*, *PL-TR-96-2153, Environmental Research Papers, No. 1195, 1070 pp*, http://www.dtic.mil/docs/citations/ADA313692.

Proceedings, 1997, **Proceedings of the 19th Annual Seismic Research Symposium on Monitoring a Comprehensive Test Ban Treaty, 23-25 September 1997**, *Defense Special Weapons Agency - Special Programs*, *978 pp.*, http://www.dtic.mil/docs/citations/ADA584228.

Proceedings, 1999, **Proceedings of the 21st Seismic Research Symposium: Technologies for Monitoring the Comprehensive Nuclear-Test-Ban Treaty**, *Los Alamos National Laboratory*, *LA-UR-99-4700, 796 pp*, http://www.osti.gov/scitech/biblio/1027323.

Proceedings, 2000, **Proceedings of the 22nd Annual DoD/DOE Seismic Research Symposium: Planning for Verification of and Compliance with the Comprehensive Nuclear-Test-Ban Treaty**, *Defense Threat Reduction Agency*, *1255 pp*, http://www.osti.gov/scitech/biblio/1027442.

Proceedings, 2001, **Proceedings of the 23rd Seismic Research Review: Worldwide Monitoring of Nuclear Explosions**, *Los Alamos National Laboratory*, *LA-UR-01-4454, 596 pp*, http://www.osti.gov/scitech/biblio/1027443.

Proceedings, 2002, **Proceedings of the 24th Seismic Research Review: Nuclear Explosion Monitoring: Innovation and Integration**, *Los Alamos National Laboratory*, *LA-UR-02-5048, 625 pp*, http://www.osti.gov/scitech/biblio/1027444.

Proceedings, 2003, **Proceedings of the 25th Seismic Research Review: Nuclear Explosion Monitoring: Building the Knowledge Base**, *Los Alamos National Laboratory*, *LA-UR-03-0629, 520 pp*, http://www.osti.gov/scitech/biblio/1027445.

Proceedings, 2004, **Proceedings of the 26th Seismic Research Review: Trends in Nuclear Explosion Monitoring**, *Los Alamos National Laboratory*, *LA-UR-04-5801, 556 pp*, http://www.osti.gov/scitech/biblio/1027446.

Proceedings, 2005, **Proceedings of the 27th Seismic Research Review: Ground-Based Nuclear Explosion Monitoring Technologies**, *Los Alamos National Laboratory*, *LA-UR-05-6407, 722 pp*, http://www.osti.gov/scitech/biblio/1027447.

Proceedings, 2006, **Proceedings of the 28th Seismic Research Review: Ground-Based Nuclear Explosion Monitoring Technologies**, *Los Alamos National Laboratory*, *LA-UR-06-5471, 720 pp*, http://www.osti.gov/scitech/biblio/1027448.

Proceedings, 2007, **Proceedings of the 29th Monitoring Research Review: Ground-Based Nuclear Explosion Monitoring Technologies**, *Los Alamos National Laboratory*, *LA-UR-07-5613, 700 pp*, http://www.osti.gov/scitech/biblio/1027449.

Proceedings, 2008, **Proceedings of the 30th Monitoring Research Review: Ground-Based Nuclear Explosion Monitoring Technologies**, *Los Alamos National Laboratory*, *LA-UR-08-05261, 720 pp*, http://www.osti.gov/scitech/biblio/992203.

Proceedings, 2009, **Proceedings of the 2009 Monitoring Research Review: Ground-Based Nuclear Explosion Monitoring Technologies**, *Los Alamos National Laboratory*, *LA-UR-09-05276*, http://www.osti.gov/scitech/biblio/992203.

Proceedings, 2010, **Proceedings of the 2010 Monitoring Research Review: Ground-Based Nuclear Explosion Monitoring Technologies**, *Los Alamos National Laboratory*, *LA-UR-10-05578*, *824 pp*, http://www.osti.gov/scitech/biblio/1027452.

Proceedings, 2011, **Proceedings of the 2011 Monitoring Research Review: Ground-based Nuclear Explosion Monitoring Technologies**, *Los Alamos National Laboratory*, *LA-UR-11-04823*, *888 pp*, http://www.osti.gov/scitech/biblio/1027453.

Proceedings, 2012, **Proceedings of the 2012 Monitoring Research Review, Ground-based Nuclear Explosion Monitoring Technologies**, *Los Alamos National Laboratory*, *LA-UR-12-24325, 835 pp*, http://www.osti.gov/scitech/biblio/1050499.

Randall, M. J., 1971, **Elastic multipole theory and seismic moment**, *Bulletin of the Seismological Society of America*, *61*, *no. 5*, *1321-1326*, http://www.bssaonline.org/content/61/5/1321.

Rayleigh, L., 1877, **On progressive waves**, *Proceedings of the London Mathematical Society*, *9*, *21-26*, http://tinyurl.com/jldmp43.

Rayleigh, L., 1885, **On waves propagated along the plane surface of an elastic solid**, *Proceedings of the London Mathematical Society*, *17*, *4-11*, http://preview.tinyurl.com/hl3r4jg.

Richards, P. G., F. Waldhauser, D. Schaff, and W. Y. Kim, 2006, **The applicability of modern methods of earthquake location**, *Pure and Applied Geophysics*, doi:10.1007/s00024-005-0019-5.

Richards, P. G., and W.-Y. Kim, 2009, **Monitoring for nuclear weapon testing**, *Scientific American*, *300*, *no. 3*, *70-77*, http://www.scientificamerican.com/article/advances-in-monitoring-nuclear.

Richter, C. F., 1935, **An instrumental earthquake magnitude scale**, *Bulletin of the Seismological Society of America*, *25*, *no. 1*, *1-32*, http://www.bssaonline.org/content/25/1.toc.

Riedmann, R. A., and R. Purtschert, 2011, **Natural 37Ar concentrations in soil air: implications for monitoring underground nuclear explosions**, *Environmental Science & Technology*, *45*, *no. 20*, *8656-8664*, doi:10.1021/es201192u.

Ringbom, A., T. Larson, A. Axelsson, K. Elmgren, and C. Johansson, 2003, **SAUNA—a system for automatic sampling, processing, and analysis of radioactive xenon**, *Nuclear Instruments & Methods in Physics Research*, *508*, *no. 3*, *542-553*, doi:10.1016/S0168-9002(03)01657-7.

Ringbom, A., A. Axelsson, M. Aldener, M. Auer, T. W. Bowyer, T. Fritioff, I. Hoffman, K. Khrustalev, M. Nikkinen, V. Popov, Y. Popov, K. Ungar, and G. Wotawa, 2014, **Radioxenon detections in the CTBT international monitoring system likely related to the announced nuclear test in North Korea on February 12, 2013**, *Journal of Environmental Radioactivity*, *128*, *47-63*, doi:10.1016/j.jenvrad.2013.10.027.

Ringdal, F., P. D. Marshall, and R. W. Alewine, 1992, **Seismic yield determination of Soviet underground nuclear explosions at the Shagan River test site**, *Geophysical Journal International*, *109*, *no. 1*, *65–77*, doi:10.1111/j.1365-246X.1992.tb00079.x.

Ringler, A. T., and C. R. Hutt, 2010, **Self-Noise models of seismic instruments**, *Seismological Research Letters*, *81, no. 6*, *972-983*, doi:10.1785/gssrl.81.6.972.

Ritsema, J., and T. Lay, 1995, **Long-period regional wave moment tensor inversion for earthquakes in the western United States**, *Journal of Geophysical Research: Solid Earth*, *100*, *no. B6*, *9853–9864*, doi:10.1029/95JB00238.

Ritzwoller, M. H., and A. L. Levshin, 1998, **Eurasian surface wave tomography: Group velocities**, *Journal of Geophysical Research: Solid Earth*, *103*, *no. B3*, *4839-4878*, doi:10.1029/97JB02622.

Ritzwoller, M. H., N. M. Shapiro, E. A. Levshin, E. A. Bergman, and E. R. Engdahl, 2003, **Ability of a global three-dimensional model to locate regional events**, *Journal of Geophysical Research: Solid Earth*, *108*, *no. B7*, *2353*, doi:10.1029/2002JB002167.

Rodgers, A. J., W. R. Walter, C. A. Schultz, S. C. Myers, and T. Lay, 1999, **A comparison of methodologies for representing path effects on regional P/S discriminants**, *Bulletin of the Seismological Society of America*, *89*, *394-408*, http://www.bssaonline.org/content/89/2/394.

Romanowicz, B., D. Dreger, M. Pasyanos, and R. Uhrhammer, 1993, **Monitoring of strain release in Central and Northern California using broadband data**, *Geophysical Research Letters*, *20*, *no. 15*, *1643–1646*, doi:10.1029/93GL01540.

Romanowicz, B., 2008, **Using seismic waves to image Earth's internal structure**, *Nature*, *451*, *266-268*, doi:10.1038/nature06583.

Romney, C., 2009, **Detecting the Bomb: The Role of Seismology in the Cold War**, *New Academia Publishing*, *ISBN 978-0-9818654-3-0*, http://www.newacademia.com/academic-books/history-political-science/detecting-the-bomb-the-role-of-seismology-in-the-cold-war/.

Ronchi, C., R. Iacono, and P. S. Paolucci, 1996, **The "Cubed Sphere": a new method for the solution of partial differential equations in spherical geometry**, *Journal of Computational Physics*, *124*, *93-114*, doi:10.1006/jcph.1996.0047.

Rougier, E., H. J. Patton, E. E. Knight, and C. R. Bradley, 2011, **Constraints on burial depth and yield of the 25 May 2009 North Korean test from hydrodynamic simulations in a granite medium**, *Geophysical Research Letters*, *38*, *no. 16*, *L16316*, doi:10.1029/2011GL048269.

Rougier, E., and H. J. Patton, 2015, **Seismic source functions from free-field ground motions recorded on SPE: Implications for source models of small, shallow explosions**, *Journal of Geophysical Research: Solid Earth*, *120*, doi:10.1002/2014JB011773.

Russell, D. R., 2006, **Development of a time-domain, variable-period surface wave magnitude measurement procedure for application at regional and teleseismic distances, Part I: Theory**, *Geophysical Research Letters*, *96*, *no. 2*, *665-677*, doi:10.1785/0120050055.

Rutherford, E., and T. Royds, 1908, **XXIV. Spectrum of the radium emanation**, *Philosophical Magazine*, *16*, *no. 92*, *313-317*, doi:10.1080/14786440808636511.

Rutherford, E., 1911, **The scattering of alpha and beta particles by matter and the structure of the atom**, *Taylor & Francis*, *688*, http://www.math.ubc.ca/~cass/rutherford/rutherford688.html.

Sabato, A., C. Niezrecki, and G. Fortino, 2017, **Wireless MEMS-based accelerometer sensor boards for structural vibration monitoring: A review**, *IEEE Sensors Journal*, *17*, *no. 2*, *226-235*, doi:10.1109/JSEN.2016.2630008.

Saey, P. R. J., M. Auer, A. Becker, E. Hoffmann, M. Nikkinen, A. Ringbom, R. Tinker, C. Schlosser, and M. Sonck, 2010a, **The influence on the radioxenon background during the temporary suspension of operations of three major medical isotope production facilities in the Northern Hemisphere and during the start-up of another facility in the Southern Hemisphere**, *Journal of Environmental Radioactivity*, *101*, *no. 9*, *730-738*, doi:10.1016/j.jenvrad.2010.04.016.

Saey, P. R. J., T. W. Bowyer, and A. Ringbom, 2010b, **Isotopic noble gas signatures released from medical isotope production facilities - simulations and measurements**, *Applied Radiation and Isotopes*, *68, no. 9, 1846-1854*, doi:10.1016/j.apradiso.2010.04.014.

Saikia, C. K., 2017, **Time-Domain Source Function (TDSF) for Nuclear and Chemical Explosions - Analysis around Nevada National Security Site (NNSS)**, *Geophysical Journal International, 209, 1048-1063*, doi:10.1093/gji/ggx072.

Salomons, E. M., 2001, **Computational Atmospheric Acoustics**, *Springer*, *ISBN 978-1-4020-0390-5*, *335 pp*, doi:10.1007/978-94-010-0660-6.

Sambridge, M., and R. Faletic, 2003, **Adaptive whole Earth tomography**, *Geochemistry Geophysics Geosystems*, *4*, *no. 3*, *1022-1042*, doi:10.1029/2001GC000213.

Sambridge, M., and N. Rawlinson, 2005, **Seismic tomography with irregular meshes**, in *American Geophysical Union*, *Seismic Earth: Array Analysis of Broadband Seismograms (eds. A. Levander and G. Nolet)*, *252 pp*, doi:10.1029/GM157.

Sambridge, M., K. Gallagher, A. Jackson, and P. Rickwood, 2006, **Trans-dimensional inverse problems, model comparison and the evidence**, *Geophysical Journal International*, *167*, *528-542*, doi:10.1111/j.1365-246X.2006.03155.x.

Sammis, C. G., and A. J. Rosakis, 2015, **Generation of High-Frequency P and S Wave Energy by Rock Fracture During a Buried Explosion**, *Air Force Geophysics Laboratory*, *AFRL-RV-PS-TR-2015-0145*, *34*, http://www.dtic.mil/dtic/tr/fulltext/u2/a627074.pdf.

Sangiorgio, S., T. H. Joshi, A. Bernstein, J. Coleman, M. Foxe, C. Hagmann, I. Jovanovic, K. Kazkaz, K. Mavrokoridis, V. Mozin, S. Pereverzev, and P. Sorensen, 2013, **First demonstration of a sub-keV electron recoil energy threshold in a liquid argon ionization chamber**, *Nuclear Instruments & Methods in Physics Research*, *728*, *no. 11*, *69-72*, doi:10.1016/j.nima.2013.06.061.

Schaff, D. P., and P. G. Richards, 2004, **Repeating seismic events in China**, *Science, 303, no. 5661, 1176-1178*, doi:10.1126/science.1093422.

Schaff, D. P., 2009, **Broad-scale applicability of correlation detectors to China seismicity**, *Geophysical Research Letters*, *36*, *no. 11*, *L11301*, doi:10.1029/2009GL038179.

Schaff, D. P., and F. Waldhauser, 2010, **One magnitude unit reduction in detection threshold by cross correlation applied to Parkfield (California) and China seismicity**, *Bulletin of the Seismological Society of America*, *100*, *no. 6*, *3224-3238*, doi:10.1785/0120100042.

Schaff, D. P., and P. G. Richards, 2014, **Improvements in magnitude precision, using the statistics of relative amplitudes measured by cross correlation**, *Geophysical Journal International*, *197*, *no. 1*, *335-350*, doi:10.1093/gji/ggt433.

Schölch, J., W. Stich, and K. O. Münnich, 1966, **Measurement of radioactive xenon in the atmosphere**, *Tellus*, *18*, *no. 2-3*, *298-300*, doi:10.1111/j.2153-3490.1966.tb00241.x.

Schott, J R. and J. G. Saw, 1984, **A multivariate one-way classification model with random effects**, *Journal of Multivariate Analysis*, *15*, *no. 1*, *1-12*, doi:10.1016/0047-259X(84)90063-0.

Schultz, G. A., S. C. Myers, J. Hipp, and C. J. Young, 1998, **Nonstationary bayesian kriging: A predictive technique to generate spatial corrections for seismic detection, location, and identification**, *Bulletin of the Seismological Society of America*, *88*, *no. 5*, *1275-1288*, http://www.bssaonline.org/content/88/5/1275.short.

Seifert, C. E., J. I. McIntyre, K. C. Antolick, A. J. Carman, M.W. Cooper, J. C. Hayes, T. R. Heimbigner, C.W. Hubbard, K. E. Litke, M. D. Ripplinger, and R. Suarez, 2005, **Mitigation of memory effects in beta scintillation cells for radioactive gas detection**, *Los Alamos National Laboratory*, *LA-UR-05-6407*, *804-814*, http://www.osti.gov/scitech/biblio/1027447.

Selby, N. D., P. D. Marshall, and D. Bowers, 2012, **mb:Ms event screening revisited**, *Bulletin of the Seismological Society of America*, *102*, *no. 1*, *88-97*, doi:10.1785/0120100349.

Sereno, Jr., T. J., S. R. Bratt, and G. Yee, 1990, **NETSIM: A Computer Program for Simulating Detection and Location Capability of Regional Seismic Networks**, *Science Applications International Corporation*, *Annual technical report, SAIC 90/1163*, *108 pp*, http://www.dtic.mil/docs/citations/ADA224811.

Shang, E. C., Y. Y. Wang, and T. M. Georges, 1994, **Dispersion and repopulation of Heard–Ascension modes**, *Journal of the Acoustical Society of America*, *96*, *2371-2379*, doi:10.1121/1.410109.

Shapiro, N. M., and M. Campillo, 2004, **Emergence of broadband Rayleigh waves from correlations of the ambient seismic noise**, *Geophysical Research Letters*, *31*, *no. 7*, *L07614*, doi:10.1029/2004GL019491.

Shapiro, N. M., M. Campillo, L. Stehly, and M. H. Ritzwoller, 2005, **High-resolution surface-wave tomography from ambient seismic noise**, *Science*, *307*, *no. 5715*, *1615-1618*, doi:10.1126/science.1108339.

Sharma, A. K., H. Wallin, and K. A. Jensen, 2007, **High volume electrostatic field-sampler for collection of fine particle bulk samples**, *Atmospheric Environment*, *41*, *no. 2*, *369–381*, doi:10.1016/j.atmosenv.2006.07.034.

Sharpe, J. A., 1942, **The production of elastic waves by explosion pressures. I. Theory and empirical field observations**, *Geophysics*, *7*, *no. 2*, *144-154*, doi:10.1190/1.1445002.

Shumway, R. H., 2003, **Time-frequency clustering and discriminant analysis**, *Statistics & Probability Letters*, *63*, *no. 3*, *307-314*, doi:10.1016/S0167-7152(03)00095-6.

Shumway, R. H., and D. S. Stoffer, 2017, **Time series analysis and its applications with R-examples**, *Springer, 4th edition*, doi:10.1007/978-3-319-52452-8.

Sigloch, K., N. McQuarrie, and G. Nolet, 2008, **Two-stage subduction history under North America inferred from multiple-frequency tomography**, *Nature Geoscience*, *1*, *458-462*, doi:10.1038/ngeo231.

Simmons, N. A., A. M. Forte, L. Boschi, and S. P. Grand, 2010, **GyPSuM: A joint tomographic model of mantle density and seismic wave speeds**, *Journal of Geophysical Research: Solid Earth*, *115*, *no. B12*, doi:10.1029/2010JB007631.

Simmons, N. A., S. C. Myers, and G. Johannesson, 2011, **Global-scale P wave tomography optimized for prediction of teleseismic and regional travel times for Middle East events: 2. Tomographic inversion**, *Journal of Geophysical Research: Solid Earth*, *116, no. B4*, doi:10.1029/2010JB007969.

Simmons, N. A., S. C. Myers, G. Johannesson, and E. Matzel, 2012, **LLNL-G3Dv3: Global P-wave tomography model for improved regional and teleseismic travel time prediction**, *Journal of Geophysical Research: Solid Earth*, *117, no. B10*, doi:10.1029/2012JB009525.

Simmons, N. A., S. C. Myers, G. Johannesson, E. Matzel, and S. P. Grand, 2015, **Evidence for long-lived subduction of an ancient tectonic plate beneath the southern Indian Ocean**, *Geophysical Research Letters*, *42*, doi:10.1002/ 2015GL066237.

Slinkard, M. E., D. B. Carr, and C. J. Young, 2013, **Applying waveform correlation to three aftershock sequences**, *Bulletin of the Seismological Society of America*, *103*, *no. 2A*, *675-693*, doi:10.1785/0120120058.

Slinkard, M., D. Schaff, N. Mikhailova, S. Heck, C. Young, and P. Richards, 2014, **Multistation validation of waveform correlation techniques as applied to broad regional monitoring**, *Bulletin of the Seismological Society of America*, *104*, *no. 6*, *2768-2781*, doi:10.1785/0120140140.

Slinkard, M., S. Ballard, A.V. Encarnacao, S. Heck, T. Draelos, E. P. Chael, C. J. Young, and R. Brogan, 2015, **Improved bulletin generation using an iterative processing framework**, *American Geophysical Union*, https://agu.confex.com/agu/fm15/webprogram/Paper84833.html.

Slinkard, M., S. Heck, D. Schaff, N. Bonal, D. Daily, C. Young, and P. Richards, 2016, **Detection of the Wenchuan aftershock sequence using waveform correlation with a composite regional network**, *Bulletin of the Seismological Society of America*, *106*, *no. 4*, *1371-1379*, doi:10.1785/0120150333.

Smith, W. H., and D. T. Sandwell, 1997, **Global sea floor topography from satellite altimetry and ship depth soundings**, *Science*, *277*, *no. 5334*, *1956–1962*, doi:10.1126/science.277.5334.1956.

Sneider, R., 2004, **Extracting the Green's function from the correlation of coda waves: A derivation based on stationary phase**, *Physical Review E*, *69*, *no. 4*, *046610*, doi:10.1103/PhysRevE.69.046610.

Snelson, C. M., R. E. Abbott, S. T. Broome, R. J. Mellors, H. J. Patton, A. J. Sussman, M. J. Townsend, and W. R. Walter, 2013, **Chemical explosion experiments to improve nuclear test monitoring**, *Eos, Transactions of the American Geophysical Union*, *94, no. 27, 237-239*, doi:10.1002/2013EO270002.

Steck, L. K., C. H. Thurber, M. Fehler, W. J. Lutter, P. M. Roberts, W. S. Baldridge, D. G. Stafford, and R. Sessions, 1998, **Crust and upper mantle P wave velocity structure beneath Valles caldera, New Mexico: results from the Jemez teleseismic tomography experiment**, *Journal of Geophysical Research: Solid Earth*, *103*, *24301–24320*, doi:10.1029/98JB00750.

Steck, L. K., C. A. Rowe, M. L. Begnaud, W. S. Phillips, V. L. Gee, and A. A. Velasco, 2004, **Advancing Seismic Event Location through Difference Constraints and Three-Dimensional Models**, *Los Alamos National Laboratory*, *1*, *346-355*, http://www.osti.gov/scitech/biblio/1027446.

Steck, L. K., W. S. Phillips, K. Mackey, M. L. Begnaud, R. J. Stead, and C. A. Rowe, 2009, **Seismic tomography of crustal P and S across Eurasia**, *Geophysical Journal International*, *177*, *no. 1*, *81-92*, doi:10.1111/j.1365-246X.2009.04109.x.

Steedman, D. W., C. R. Bradley, E. Rougier, and D. D. Coblentz, 2016, **Phenomenology and modeling of explosion-generated shear energy for the Source Physics Experiments**, *Bulletin of the Seismological Society of America*, *106*, *no. 1*, *42-53*, doi:10.1785/0120150011.

Stehly, L., M. Campillo, B. Froment, and R. L. Weaver, 2008, **Reconstructing Green's function by correlation of the coda of the correlation (C3) of ambient seismic noise**, *Journal of Geophysical Research: Solid Earth*, *113*, *no. B11306*, doi:10.1029/2008JB005693.

Stevens, J. L., and S. M. Day, 1985, **The physical basis of mb: MS and variable frequency magnitude methods for earthquake/explosion discrimination**, *Journal of Geophysical Research: Solid Earth*, *90*, *no. B4*, *3009-3020*, doi:10.1029/JB090iB04p03009.

Stevens, J. L., and J. R. Murphy, 2001, **Yield estimation from surface-wave amplitudes**, *Pure and Applied Geophysics*, *158*, *no. 11*, *2227-2251*, doi:10.1007/PL00001147.

Stevens, J. L., and K. L. McLaughlin, 2001, **Optimization of surface wave identification and measurement**, *Pure and Applied Geophysics*, *158*, *no. 8*, *1547-1582*, doi:10.1007/PL00001234.

Stevens, J. L., I. I. Divnov, D. A. Adams, J. R. Murphy, and V. N. Bourchik, 2002, **Constraints on infrasound scaling and attenuation relations from Soviet explosion data**, *Pure and Applied Geophysics*, *159*, *no. 5*, *1045–1062*, doi:10.1007/s00024-002-8672-4.

Stockwell, R. G., L. Mansinha, and R. P. Lowe, 1996, **Localization of the complex spectrum: the S transform,** *IEEE Transactions on Signal Processing, 44, no. 4, 998-1001,* doi:10.1109/78.492555.

Stohl, A., P. Seibert, and G. Wotawa, 2012, **The total release of xenon-133 from the Fukushima Dai-ichi nuclear power plant accident**, *Journal of Environmental Radioactivity*, *112*, *155-159*, doi:10.1016/j.jenvrad.2012.06.001.

Stokes, G. G., 1845, **On the theories of internal friction of fluids in motion, and of the equilibrium and motion of elastic solids**, *Cambridge University Press*, *8*, *Transactions of the Cambridge Philosophical Society*, *287-305*, http://www.chem.mtu.edu/~fmorriso/cm310/StokesLaw1845.pdf.

Stokes, G. G., 1849, **On some points in the received theory of sound**, *Philosophical Magazine*, *34*, *no. 226*, *Series 3*, *52-60*, doi:10.1080/14786444908646172.

Storchak, D.A., J. Schweitzer, and P. Bormann, 2003, **The IASPEI Standard Seismic Phase List**, *Seismological Research Letters*, *74*, *no. 6*, *761-772*, doi:10.1785/gssrl.74.6.761.

Stroujkova, A., J. L. Bonner, M. Leidig, P. Boyd, and R. J. Martin, 2012, **Shear waves from explosions in granite revisited: lessons learned from the New England Damage Experiment**, *Bulletin of the Seismological Society of America*, *102*, *no. 5*, *1913-1926*, doi:10.1785/0120110204.

Stroujkova, A., M. Leidig, and J. L. Bonner, 2015a, **Effect of the detonation velocity of explosives on seismic radiation**, *Bulletin of the Seismological Society of America*, *105*, *no. 2A*, *599-611*, doi:10.1785/0120140115.

Stroujkova, A., M. Leidig, and T. Rath, 2015b, **Seismic coupling of chemical explosions in intact and fractured granite in Barre, Vermont**, *Bulletin of the Seismological Society of America*, *105*, *no. 1*, *177-188*, doi:10.1785/0120130328.

Stroujkova, A., M. Carnevale, and O. Vorobiev, 2016, **Cavity radius scaling for underground explosions in hard rock**, *Bulletin of the Seismological Society of America*, *106*, *no. 6*, *2500-2510*, doi:10.1785/0120160122.

Stump, B. W., D. C. Pearson, and R. E. Reinke, 1999, **Source comparisons between nuclear and chemical explosions detonated at Rainier Mesa, Nevada Test Site**, *Bulletin of the Seismological Society of America*, *89*, *no. 2*, *409-422*, http://www.bssaonline.org/content/89/2/409.

Sykes, L. R., and D. M. Davis, 1987, **The yields of Soviet strategic weapons**, *Scientific American*, *256*, *no. 1*, *29-37*, doi:10.1038/scientificamerican0187-29.

Syracuse, E. M., M. Maceira, H. Zhang, and C. H. Thurber, 2015, **Seismicity and structure of Akutan and Makushin Volcanoes, Alaska, using joint body and surface wave tomography**, *Journal of Geophysical Research: Solid Earth*, *120*, doi:10.1002/2014JB011616.

Syracuse E. M., M. Maceira, G. A. Prieto, H. Zhang, and C. J. Ammon, 2016, **Multiple plates subducting beneath Colombia, as illuminated by seismicity and velocity from the joint inversion of seismic and gravity data**, *Earth and Planetary Science Letters*, *444*, *139-149*, doi:10.1016/j.epsl.2016.03.050.

Szuberla, C., K. Arnoult and J. Olson, 2006, **Performance of an infrasound source localization algorithm**, *Journal of the Acoustical Society of America*, *120*, *3179*, doi:10.1121/1.4787973.

Talandier, J., and E. A. Okal, 1998, **On the mechanism of conversion of seismic waves to and from T waves in the vicinity of island shores**, *Bulletin of the Seismological Society of America*, *88*, *no. 2*, *621-632*, http://www.bssaonline.org/content/88/2/621.

Tape, C., Q. Liu, A. Maggi, and J. Tromp, 2009, **Adjoint tomography of the southern California crust**, *Science*, *325*, *no. 5943*, *988-992*, doi:10.1126/science.1175298.

Tape, W., and C. Tape, 2012, **A geometric setting for moment tensors**, *Geophysical Journal International*, *190*, *no. 1*, *476-498*, doi:10.1111/j.1365-246X.2012.05491.x.

Taylor, S. R., 1996, **Analysis of high-frequency P-g/L(g) ratios from NTS explosions and western US earthquakes**, *Bulletin of the Seismological Society of America*, *86*, *no. 4*, *1042-1053*, http://www.bssaonline.org/content/86/4/1042.

Taylor, S. R., and H. E. Hartse, 1998, **A procedure for estimation and propagation amplitude corrections for regional seismic discriminants**, *Journal of Geophysical Research: Solid Earth*, *103*, *no. B2*, *2781-2789*, doi:10.1029/97JB03292.

Taylor, S. R., A. A. Velasco, H. E. Hartse, W. S. Phillips, W. R. Walter, and A. J. Rodgers, 2002, **Amplitude corrections for regional seismic discriminants**, *Pure and Applied Geophysics*, *159*, *no. 4*, *623-650*, doi:10.1007/s00024-002-8652-8.

Taylor, S. R., X. N. Yang, and W. S. Phillips, 2003, **Bayesian Lg attenuation tomography applied to eastern Asia**, *Bulletin of the Seismological Society of America*, *93*, *no. 2*, *795-803*, doi:10.1785/0120020010.

Thio, H. K., and H. Kanamori, 1995, **Moment-tensor inversions for local earthquakes using surface waves recorded at TERRAscope**, *Bulletin of the Seismological Society of America*, *1995*, *no. 85*, *1021-1038*, *4*, http://www.bssaonline.org/content/85/4/1021.

Thurber, C. H., 1983, **Earthquake locations and three-dimensional crustal structure in the Coyote Lake area, central California**, *Journal of Geophysical Research: Solid Earth*, *98*, *8226–8236*, doi:10.1029/JB088iB10p08226.

Tkalcic, H., M. Pasyanos, A. Rodgers, R. Gok, W. Walter, and A. Al-Amri, 2006, **A multi-step approach in joint modeling of surface wave dispersion and teleseismic receiver functions: Implications for lithospheric structure of the Arabian peninsula**, *Journal of Geophysical Research: Solid Earth*, *111, no. B11*, doi:10.1029/2005JB004130.

Tokam, A. K., C. T. Tabod, A. A. Nyblade, J. Julia, D. A. Wiens, and M. E. Pasyanos, 2010, **Structure of the crust beneath Cameroon, West Africa, from the joint inversion of Rayleigh wave group velocities and receiver functions**, *Geophysical Journal International*, *183*, *no. 2*, *1061-1076*, doi:10.1111/j.1365-246X.2010.04776.x.

Toksöz, M. N., A. Ben-Menahem, and D. G. Harkrider, 1964, **Determination of source parameters of explosions and earthquakes by amplitude equalization of seismic surface waves: 1. Underground nuclear explosions**, *Journal of Geophysical Research: Solid Earth*, *69*, *no. 20*, *4355–4366*, doi:10.1029/JZ069i020p04355.

Trampert, J., 1998, **Global seismic tomography: the inverse problem and beyond**, *Inverse Problems*, *14*, *no. 3*, *371-385*, doi:10.1088/0266-5611/14/3/002.

Trampert, J., and J. H. Woodhouse, 2001, **Assessment of global phase velocity models**, *Geophysical Journal International*, *144*, *no. 1*, *165-174*, doi:10.1046/j.1365-246x.2001.00307.x.

Tromp, J., C. Tape, and Q. Liu, 2005, **Seismic tomography, adjoint methods, time reversal and banana-doughnut kernels**, *Geophysical Journal International*, *160*, *195-216*, doi:10.1111/j.1365-246X.2004.02453.x.

TTBT, 1974, **Treaty Between The United States of America and The Union of Soviet Socialist Republics on the Limitation of Underground Nuclear Weapon Tests (and Protocol Thereto)**, *Department of State*, http://www.state.gov/t/isn/5204.htm.

Um, J., and C. Thurber, 1987, **A fast algorithm for two-point seismic ray tracing**, *Bulletin of the Seismological Society of America*, *77*, *972-986*.

Van der Lee, S., and G. Nolet, 1997, **Upper mantle S velocity structure of North America**, *Journal of Geophysical Research: Solid Earth, 102, no. B10, 22815-22838*, doi:10.1029/97JB01168.

Vincent, P., S. Larsen, D. Galloway, R. J. Laczniak, W. R. Walter, W. Foxall, and J. J. Zucca, 2003, **New signatures of underground nuclear tests revealed by satellite radar interferometry**, *Geophysical Research Letters*, *30*, *no. 22*, *2141*, doi:10.1029/2003GL018179.

Virieux, J., 1986, **P-SV-wave propagation in heterogeneous media—velocity-stress finite-difference method**, *Geophysics*, *51*, *889-901*, doi:10.1190/1.1442147.

von Seggern, D., and R. Blandford, 1972, **Source Time Functions and Spectra for Underground Nuclear Explosions**, *Geophysical Journal International*, *31*, *no. 1-3*, *83-97*, doi:10.1111/j.1365-246X.1972.tb02360.x.

Vorobiev, O., S. Ezzedine, T. Antoun, and L. Glenn, 2015, **On the generation of tangential ground motion by underground explosions in jointed rocks**, *Geophysical Journal International*, *200*, *1651-1661*, doi:10.1093/gji/ggu478.

Vortman, L. J., 1965, **Close-in air blast from a row charge in basalt**, *Sandia Corporation*, *PNE-608F*, doi:10.2172/4586141.

Wald, D. J., V. Quitoriano, C. B. Worden, M. Hopper, and J. W. Dewey, 2011, **USGS "Did You Feel It?" Internet-based macroseismic intensity maps**, *Annals of Geophysics*, *54*, *no. 6*, *688-707*, doi:10.4401/ag-5354.

Walter, W., 2009, **Sleuthing seismic signals**, *Lawrence Livermore National Laboratory*, *Science & Technology Review, March 2009*, *4-12*, https://str.llnl.gov/Mar09/pdfs/03.09.01.pdf.

Walter, W. R., and H. J. Patton, 1990, **Tectonic release from the Soviet Joint Verification Experiment**, *Geophysical Research Letters*, *17*, *no. 10*, *1517-1520*, doi:10.1029/GL017i010p01517.

Walter, W. R., and K. F. Priestley, 1991, **High frequency P wave spectra from explosions**, in *Explosion Source Phenomenology, American Geophysical Union, Geophysical Monograph 65*, *219-228*, doi:10.1029/GM065p0219.

Walter, W. R., K. M. Mayeda, and H. J. Patton, 1995, **Phase and spectral ratio discrimination between NTS earthquakes and explosions. Part I: Empirical observations**, *Bulletin of the Seismological Society of America*, *85*, *no. 4*, *1050-1067*, http://bssa.geoscienceworld.org/content/85/4/1050.

Walter, W. R., and S. R. Taylor, 2001, **A Revised Magnitude and Distance Amplitude Correction (MDAC2) Procedure for Regional Seismic Discriminants: Theory and Testing at NTS**, *Lawrence Livermore National Laboratory*, *UCRL-ID-146882*, *15 pp*, doi:10.2172/15013384.

Waltz, J., N. R. Morgan, T. R. Canfield, M. R. J. Charest, L. D. Risinger, and J. G. Wohlbier, 2014, **A three-dimensional finite element arbitrary Lagrangian–Eulerian method for shock hydrodynamics on unstructured grids**, *Computers & Fluids*, *92*, *172–187*, doi:10.1016/j.compfluid.2013.12.021.

Wang, Z., and F. A. Dahlen, 1995, **Spherical-spline parameterization of three-dimensional earth models**, *Geophysical Research Letters*, *22*, *3099–3102*, doi:10.1029/95GL03080.

Warburton, W.K., W. Hennig, J. A. Bertrand, S. M. George, and S. Biegalski, 2013, **Atomic layer deposition α-Al_2O_3 diffusion barriers to eliminate the memory effect in beta-gamma radioxenon detectors**, *Journal of Radioanalytical and Nuclear Chemistry*, *296*, *no. 1*, *541-549*, doi:10.1007/s10967-012-2061-y.

Waxler, R., L. G. Evers, J. Assink, and P. Blom, 2015, **The stratospheric arrival pair in infrasound propagation**, *Journal of the Acoustical Society of America*, *137*, *no. 4*, *1846-1856*, doi:10.1121/1.4916718.

Weaver, R. L., and O. I. Lobkis, 2001, **Ultrasonics without a source: thermal fluctuation correlations at MHz frequencies**, *Physical Review Letters*, *87*, *no. 13*, *134301*, doi:10.1103/PhysRevLett.87.134301.

Wei, M., 2017, **Location and source characteristics of the January 6, 2016 North Korean nuclear test constrained by InSAR**, *Geophysical Journal International*, doi:10.1093/gji/ggx053.

Weinberg, H., and R. Burridge, 1974, **Horizontal ray theory for ocean acoustics**, *Journal of the Acoustical Society of America*, *55*, *no. 1*, *63-79*, doi:10.1121/1.1919476.

Wen, L., and H. Long, 2010, **High-precision location of North Korea's 2009 nuclear test**, *Seismological Research Letters*, *81*, *no. 1*, *26-29*, doi:10.1785/gssrl.81.1.26.

Wetherill, G. W., 1953, **Spontaneous fission yields from uranium and thorium**, *Physical Review*, *92*, *no. 4*, *907-912*, doi:10.1103/PhysRev.92.907.

Whitaker, R. W., and J. P. Mutschlecner, 2008, **A comparison of infrasound signals refracted from stratospheric and thermospheric altitudes**, *Journal of Geophysical Research: Atmospheres*, *113*, *no. D8*, *D08117*, doi:10.1029/2007JD008852.

Williams, R., P. Humble, and J. Hayes, 2010, **Extraction of xenon using enriching reflux pressure swing adsorption**, *Los Alamos National Laboratory*, *Proceedings of the 2010 Monitoring Research Review, LA-UR-10-05578*, *619-626*, http://www.osti.gov/scitech/biblio/1027452.

Willis, D. E., J. DeNoyer, and J. T. Wilson, 1963, **Differentiation of earthquakes and underground nuclear explosions on the basis of amplitude characteristics**, *Bulletin of the Seismological Society of America*, *53*, *no. 5*, *979-987*.

Woodhouse, J. H., and A. M. Dziewonski, 1984, **Mapping the upper mantle: three-dimensional modeling of the earth structure by inversion of seismic waveforms**, *Journal of Geophysical Research: Solid Earth*, *89*, *5953-5986*, doi:10.1029/JB089iB07p05953.

Wotawa, G., L.-E. De Geer, P. Denier, M. Kalinowski, H. Toivonen, R. D'Amours, F. Desiato, J.-P. Issartel, M. Langer, P. Seibert, A. Frank, C. Sloan, and H. Yamazawa, 2003, **Atmospheric transport modelling in support of CTBT verification—overview and basic concepts**, *Atmospheric Environment*, *37*, *no. 18*, *2529-2537*, doi:10.1016/S1352-2310(03)00154-7.

Xiang, Y.-C., J. Gong, W. Li, Z.-S. Bian, F.-H. Hao, H.-X. Wang, Q. Wang, and Z.-H. Xiong, 2008, **Development of a system of measuring 37Ar by spectrum method**, *Acta Physica Sinica*, *57*, *no. 2*, *784-789*, http://wulixb.iphy.ac.cn/EN/Y2008/V57/I2/0784.

Xu, H., A. J. Rodgers, I. N. Lomov, and O. Y. Vorobiev, 2014, **Seismic source characteristics of nuclear and chemical explosions in granite from hydrodynamic simulations**, *Pure and Applied Geophysics*, *171*, *no. 3-5*, *507-521*, doi:10.1007/s00024-012-0623-0.

Yan, J., and K. K. Yen, 1995, **A derivation of three-dimensional ray equations in ellipsoidal coordinates**, *Journal of the Acoustical Society of America*, *97*, *no. 3*, *1538-1544*, doi:10.1121/1.412093.

Yang, X., T. Lay, X. Xie, and M. S. Thorne, 2007, **Geometric spreading of Pn and Sn in a spherical earth model**, *Bulletin of the Seismological Society of America*, *97*, *no. 6*, *2053-2065*, doi:10.1785/0120070031.

Yang, X., 2011, **A Pn spreading model constrained with observed amplitudes in Asia**, *Bulletin of the Seismological Society of America*, *101*, *no. 5*, *2201-2211*, doi:10.1785/0120100314.

Yang, X., 2016, **Source Spectra of the First Four Source Physics Experiments (SPE) Explosions from the Frequency-Domain Moment Tensor Inversion**, *Bulletin of the Seismological Society of America*, *106*, *no. 4*, *1637-1651*, doi:10.1785/0120150263.

Yang, Xiaoning, S. R. Taylor, and H. J. Patton, 2004a, **The 20-s Rayleigh wave attenuation tomography for central and southeastern Asia**, *Journal of Geophysical Research: Solid Earth*, *109*, *no. B12*, doi:10.1029/2004JB003193.

Yang, Xiaoping, I. Bondár, J. Bhattachryya, M. Ritzwoller, N. Shapiro, M. Antolik, G. Ekström, H. Israelsson, and K. McLaughlin, 2004b, **Validation of regional and teleseismic travel-time models by relocating GT events**, *Bulletin of the Seismological Society of America*, *94*, *897-919*.

Yao, H., G. Xu, L. Zhu, and X. Xiao, 2005, **Mantle structure from inter-station Rayleigh wave dispersion and its tectonic implication in western China and neighboring regions**, *Physics of the Earth and Planetary Interiors*, *148*, *no. 1*, *39-54*, doi:10.1016/j.pepi.2004.08.006.

Yoon, E. E., O. O'Reilly, K. J. Bergen, and G. C. Beroza, 2015, **Earthquake Detection through Computationally Efficient Similarity Search**, *Science Advances*, *1*, *no. 11*, *e1501057*, doi:10.1126/sciadv.1501057.

Young, C. J., J. Woodbridge, R. Shaw, and M. Slinkard, 2015, **Using KLSH to Rapidly Search Large Seismic Signal Archives on a Desktop Computer**, *American Geophysical Union*, https://agu.confex.com/agu/fm15/webprogram/Paper82067.html.

Zeiler, C., and A. A. Velasco, 2009, **Developing local to near-regional explosion and earthquake discriminants**, *Bulletin of the Seismological Society of America*, *99*, *no. 1*, *24-35*, doi:10.1785/0120080045.

Zhang, H., and C. Thurber, 2005, **Adaptive mesh seismic tomography based on tetrahedral and Voronoi diagrams: application to Parkfield, California**, *Journal of Geophysical Research: Solid Earth*, *110*, doi:10.1029/2004JB003186.

Zhang, H., M. Maceira, P. Roux, and C. Thurber, 2014, **Joint inversion of body-wave arrival times and surface-wave dispersion for three-dimensional seismic structure around SAFOD**, *Pure and Applied Geophysics*, *171*, *no. 11*, *Special edition on Crustal Fault Zones*, *3013-3022*, doi:10.1007/s00024-014-0806-y.

Zhang, J., and X. Yang, 2013, **Extracting surface wave attenuation from seismic noise using correlation of the coda of correlation**, *Journal of Geophysical Research: Solid Earth*, *118*, *no. 5*, *2191–2205*, doi:10.1002/jgrb.50186.

Zhang, W., Y. Shen, and L. Zhao, 2012, **Three-dimensional anisotropic seismic wave modeling in spherical coordinate by a collocated-grid finite difference method**, *Geophysical Journal International*, *188*, *1359-1381*, doi:10.1111/j.1365- 246X.2011.05331.x.

Zhang, Z., Y. Shen, and L. Zhao, 2007, **Finite-frequency sensitivity kernels for head waves**, *Geophysical Journal International*, *171*, *847-856*, doi:10.1111/j.1365-246X.2007.03575.x.

Zhang, Z., and Y. Shen, 2008, **Cross-dependence of finite-frequency compressional waveforms to shear seismic wave-speed**, *Geophysical Journal International*, *147*, *941-948*, doi:10.1111/j.1365-246X.2008.03840.x.

Zhao, D., A. Hasegawa, and S. Horiuchi, 1992, **Tomographic imaging of P and S wave velocity structure beneath Northeastern Japan**, *Journal of Geophysical Research: Solid Earth*, *97*, *19909-19928*, doi:10.1029/92JB00603.

Zhao, L., T. H. Jordan, K. B. Olsen, and P. Chen, 2005, **Fréchet kernels for imaging regional Earth structure based on three-dimensional reference models**, *Bulletin of the Seismological Society of America*, *95*, *2066-2080*, doi:10.1785/0120050081.

Zheng, S., X. Sun, X. Song, Y. Yang, and M. H. Ritzwoller, 2008, **Surface wave tomography of China from ambient seismic noise correlation**, *Geochemistry Geophysics Geosystems*, *9*, *no. 5*, *Q05020*, doi:10.1029/2008GC001981.

Zhu, H., E. Bozdag, D. Peter, and J. Tromp, 2012, **Structure of the European upper mantle revealed by adjoint tomography**, *Nature Geoscience*, *5*, *493-498*, doi:10.1038/NGEO1501.

Zhu, H., E. Bozdag, and J. Tromp, 2015, **Seismic structure of the European upper mantle based on adjoint tomography**, *Geophysical Journal International*, *201*, *no. 1*, *18-52*, doi:10.1093/gji/ggu492.

Zucca, J. J., W. R. Walter, A. J. Rodgers, P. Richards, M. E. Pasyanos, S. C. Myers, T. Lay, D. Harris, and T. Antoun, 2009, **The prospect of using three-dimensional Earth models to improve nuclear explosion monitoring and ground motion hazard assessment**, *Seismological Research Letters*, *80, no. 1, 31-39*, doi:10.1785/gssrl.80.1.31.

There have been significant technological and scientific revolutions in the fields of seismology, acoustics, and radionuclide sciences as they relate to nuclear explosion monitoring and the Comprehensive Nuclear-Test-Ban Treaty (CTBT), which opened for signature in 1996. It is valuable to pause from time to time and observe the arcs of progress evident in the research results reported in the literature related to improving monitoring capabilities. This document entitled "Trends in Nuclear Explosion Monitoring Research and Development – A Physics Perspective" reviews the accessible literature for four research areas: source physics (understanding signal generation), signal propagation (accounting for changes through physical media), sensors (recording the signals), and signal analysis (processing the signal). Over 40 trends are addressed, such as moving from 1D to 3D earth models, from pick-based seismic event processing to full waveform processing, and from separate treatment of mechanical waves in different media to combined analyses. Highlighted in the document for each trend are the value and benefit to the monitoring mission, key papers that advanced the science, and promising research and development for the future.